

**SOLAR FACADES  
FOR HEATING AND  
COOLING IN BUILDINGS**

**HOY YEN CHAN, MSc.**

**Thesis submitted to the University of Nottingham  
For the degree of Doctor of Philosophy  
DECEMBER 2011**

## Abstract

The aim of this thesis is to study the energy performance of a building integrated heating and cooling system. The research objectives are to investigate the system operating characters, to develop mathematical models for the heating and cooling systems, to demonstrate the technologies experimentally, to identify the best designs for a combined system and to investigate the cost effectiveness of the system. The main components of the systems are the aluminium plate façade and the building wall behind it, these form a plenum between them and the air is then heated or cooled as it flows through this plenum. Mathematical models were developed based on the energy balance equations and solved by matrix inversion method. These models were then validated with experimental results. The experiments were carried out in the laboratory with a facade area of 2m<sup>2</sup>. Two designs of facade were tested, i.e. flat and transpired plates. Results showed that the transpired design gave better thermal performance; the system efficiency for the flat plate was only about 30%, whereas it was about 85% for the transpired plate. On the other hand, a cooling system with double plenums was found to be better than a single plenum. Thus, a transpired plate with two plenums was identified as the best design for space heating and cooling. The cooling efficiency was nearly 2.0 even at low solar radiation intensity. A simulation study was carried out by assuming a 40m<sup>2</sup> of façade was installed on an office building in London. The yearly energy saving was estimated as 10,877kWh, which is equivalent to 5,874kgCO<sub>2</sub>/year of emission avoidance. The system is calculated to cost about £70/m<sup>2</sup>, and for a discount rate of 5% and 30 years of lifetime, the payback period for this system would be less than a years.

## **Acknowledgement**

I would like to express my utmost gratitude to my supervisors, Prof. Saffa Riffat and Dr. Jie Zhu for their guidance and supervisions throughout my research. Besides, I am grateful to have Dr. Shenyi Wu, Dr. Guoquan Qiu, Dr. Xiaoli Ma and Prof. Yuying Yan for their academic contributions in this research. Special thanks to Mr. John Rabone for the English consultation.

I would also like to thank the technicians at the Department of Architecture and Built Environment, especially Mr. David Oliver, Mr. David Taylor and Mr. Robert Clarke, without their helps the experiment would be impossible to carry out. Furthermore, I appreciate very much on the administration assistance of Ms. Zeny Amante-Roberts throughout these years.

My special gratitude goes to my parents, family and all my friends for their patience and support. Also, thanks to my colleagues at Universiti Kebangsaan Malaysia for their support and assistance.

Scholarship from the Ministry of Higher Education of Malaysia and the Innovation Fellowship awards from the East Midlands Development Agency are highly acknowledged.

## Table of contents

Abstract	ii
Acknowledgement	iii
Table of contents	iv
List of Figures	ix
List of Tables	xiv
Nomenclature	xvi
1. Introduction	
1.1 Background	1
1.2 Research problem	2
1.2.1 Building integration of solar thermal technology	2
1.2.2 System complication	3
1.3 Aim and objectives	4
1.4 Outline of thesis	6
2. Literature Review: Building Integrated Air heating and Cooling Designs	
2.1 Introduction	9
2.2 Existing designs of passive solar air heating and natural ventilation via buoyancy effect	9
2.2.1 Trombe Wall	12
2.2.2 Solar chimney	15
2.2.3 Solar air heater with jet plate	16
2.2.4 Solar air heater with transpired plate	17
2.2.4.1 Literature review on heat transfer coefficient for transpired solar collector	20
2.2.5 Solar Roof	23
2.3 Existing passive solar cooling via evaporative effect	24
2.3.1 Evaporative cooling	24
2.3.1.1 Direct evaporative cooling (DECC)	25
2.3.1.2 Indirect evaporative cooling (IEC)	25
2.3.2 Materials for evaporative cooling	26
2.3.3 Building Integration of Evaporative Cooling	27
2.3.3.1 Roof integration	27
2.3.3.2 Facades integration	28
2.4 Passive solar: Filling the gap of active solar technologies	29
	iv

2.5	Passive solar: Barriers	30
2.6	Conclusions: The need of a combined heating and cooling system	30
3.	Methodology	
3.1	Introduction	32
3.2	Overview of methodology approach	32
3.2.1	The heating systems	33
3.2.2	The cooling and the combined systems	33
3.3	Development of mathematical model	35
3.4	Experiment set up	37
3.4.1	The heating systems	37
3.4.2	The cooling systems	41
3.5	Parameter measurements	42
3.5.1	Air velocity	42
3.5.2	Mass flow rate	42
3.5.3	Solar radiation intensity	43
3.5.4	Temperatures	44
3.5.5	Water absorption and porosity studies of the sandtile	44
3.6	Calibrations of sensors	45
3.6.1	Thermocouples	45
3.6.2	Humidity sensors	48
3.7	Experimental percentage error	50
3.8	Heat transfer at insulated sandtile wall	51
3.9	Summary	52
4.	Solar façade for space heating	
4.1	Introduction	53
4.2	Heat transfer of flat plate solar façade	54
4.2.1	Assumptions of heating system with flat plate collector	54
4.2.2	Energy balance equations for flat plate collector	54
4.2.2.1	Heat flux equations	55
4.2.2.2	Mean temperature matrix	55
4.2.2.3	Heat transfer coefficient	56
4.2.3	Results and analysis of flat plate collector	58
4.2.3.1	Results comparison between the model and experiment for flat plate	59
4.2.3.2	Parametric analysis for the flat plate solar façade	63
4.3	Heat transfer of transpired solar façade	71
4.3.1	Assumptions of heating system with transpired plate collector	71

4.3.2	Energy balance equations for transpired plate collector	71
4.3.2.1	Heat flux and coefficient for transpired plate collector	73
4.3.3	Results and parametric analysis of transpired plate collector	74
4.3.3.1	Main parameters analysis	74
4.3.4	$Nu$ correlations for heat transfer involves vertical flow	84
4.3.4.1	The lack of non-uniform heat transfer coefficient for transpired solar collector	84
4.3.4.2	$Nu_{c,trans}$ correlation	85
4.3.4.3	$Nu_{f,trans}$ correlation	88
4.3.5	Development of mathematical modelling for transpired plate heating performance	89
4.3.5.1	Comparison of heat exchange effectiveness between modelling and experimental results	90
4.4	Thermal performance comparison between flat and transpired plates	93
4.4.1	Heat losses	93
4.4.2	Efficiency	99
4.5	System performance comparisons of solar air heaters	100
4.6	Summary	101
5.	Solar façade for space cooling	
5.1	Introduction	103
5.2	Results and analysis of cooling system with flat plate collector and single plenum	104
5.2.1	Parametric analysis cooling system with flat plate collector and single plenum	105
5.2.2	Cooling performance	108
5.2.3	Evaporation effect	113
5.3	Simulation results of cooling system with transpired plate solar collector and single plenum	114
5.4	Section summary	116
5.5	Heat transfer of cooling system with transpired plate and two plenums	117
5.5.1	Assumptions of cooling system with transpired plate collector	117
5.5.2	Energy balance equations for cooling system with transpired plate, two plenums and wet sandtile wall	117

5.5.2.1	Heat flux equations	119
5.5.2.2	Mean temperature matrix	120
5.5.2.3	Heat transfer coefficient equations	122
5.5.3	Results and analysis of cooling system with transpired plate and single plenum	124
5.5.3.1	Results comparison between the model and experiment	124
5.5.3.2	Parametric analysis	128
5.5.3.3	Cooling performance	134
5.5.3.4	Water evaporation	141
5.5.3.5	Performance analysis under the condition of no solar radiation	142
5.6	Summary and conclusions	143
6.	Solar facade for the combined heating and cooling system	
6.1	Introduction	145
6.1.1	The combined heating and cooling system with controlled dampers	145
6.2	Simulation on real building application	147
6.2.1	Building definition	147
6.2.2	Weather data of London	148
6.3	Heating and cooling performances	148
6.4	Energy and carbon savings	150
6.5	Economic analysis	151
6.6	Conclusions and recommendations	153
7.	Conclusions	
7.1	Overview of chapter	155
7.2	Summary and conclusions of the thesis	155
7.3	Contributions	159
7.4	Future works	160
	References	163
	Appendix I: Distribution of solar radiation intensities	173
	Appendix II: Matlab Programme	
II-1	Heating system with flat plate facade	174
II-2	Heating system with transpired plate facade	176
II-3	Heating system for transpired façade with Kutscher's model	178
II-4	Cooling system with flat plate and single plenum	180
II-5	Cooling system with transpired plate and single plenum	183
II-6	Cooling system with transpired plate and two plenums	186

Appendix III: Experiment and simulation results for heating systems	
III-1 Heating system with flat plate facade	189
III-2 Heating system with transpired plate facade	193
III-3 Cooling systems with flat plate and single plenum	197
III-4 Cooling systems with transpired plate and two plenums	199
Appendix IV: Power consumption of fan	202
Appendix V: List of publications	203

## List of figures

Figure 1-1. Configurations of (a) single and (b) double plenums of the systems.	5
Figure 2-1. Schematic diagram of classical Trombe wall (without dampers).	12
Figure 2-2. Schematic diagram of composite Trombe–Michel wall.	14
Figure 2-3. Solar chimney operation modes (Miyazaki, 2006).	16
Figure 2-4. Solar air heater with a glazed solar collector (Choudhury, 1991).	17
Figure 2-5. Schematic diagram of unglazed transpired solar facade.	18
Figure 2-6. The pipe network concept (Dymond, 1997).	22
Figure 2-7. Performance of roof materials on evaporative cooling effect.	26
Figure 2-8. Overcoming the limitations by combining heating and cooling systems, and the solar active and passive technologies.	31
Figure 3-1. The concept of the solar facades.	34
Figure 3-2. Development of a combined heating and cooling system.	34
Figure 3-3. Methodology overviews of heating systems with (a) flat and (b) transpired plates.	35
Figure 3-4. Matrix algorithm of the mathematical model.	36
Figure 3-5. Pictures of (a) the black painted aluminium transpired plate, (b) the front, and (c) side views of the sandtile.	38
Figure 3-6. Laboratory test rig.	39
Figure 3-7. Schematic view of experimental set up.	39
Figure 3-8. Thermocouples' location on the plate and sandtile wall.	40
Figure 3-9. Schematic diagram of cooling system with transpired plate and two plenums.	41
Figure 3-10. The hotwire anemometer.	41
Figure 3-11. The hotwire anemometer measurement positions (front view).	41
Figure 3-12. Pyranometer for solar radiation measurement.	43
Figure 3-13. Measurement points of solar radiation intensities.	43
Figure 3-14. Type-K Thermocouples.	44
Figure 3-15. Water absorption of the sandtile.	45
Figure 3-16. Calibration curve of thermocouples by using mercury thermometer as a reference.	46
Figure 3-17. The ISOTECH TTI-7-R PRT unit.	46
Figure 3-18. Calibration curves of (a) T25, (b) T26, (c) T27, (d) T28, (e)	47

T29 and (f) T30 by using ISOTECH TTI-7-R PRT as a reference.

Figure 3-19. Vaisala HMP45A sensor.	48
Figure 3-20. Calibration curves of P1 and P2 <i>RH</i> .	49
Figure 3-21. Calibration curves of P1 and P2 temperature.	49
Figure 3-22. Heat transfer diagram of insulated sandtile wall.	51
Figure 3-23. Percentage of heat loss to sandtile wall over total useful energy.	52
Figure 4-1. Side views of schematic diagrams of heating systems with unglazed a) flat and b) transpired plates as solar collector facades.	53
Figure 4-2. Heat transfer of flat plate solar façade.	54
Figure 4-3. Results comparison between the model and experiments over different solar radiation intensities for plenum depths of a) 0.20m, b) 0.25m and c) 0.30m.	61
Figure 4-4. Efficiency comparisons between the model and experiments over different solar radiation intensities at $V_{fan}=200\text{m}^3\text{hr}^{-1}$	61
Figure 4-5. Results comparison between the model and experiments over different airflow rates for plenum depths of a) 0.020m, b) 0.25m and c) 0.30m.	63
Figure 4-6. Efficiency comparisons between the model and experiments over different airflow rates at $I=307\text{W}^2\text{m}^{-2}$	64
Figure 4-7. Values of $T_p$ and $T_f$ at solar radiation intensity range from 307 to $820\text{Wm}^{-2}$ for plenum depth of (a) 0.20m, (b) 0.25m and (c) 0.30m.	66
Figure 4-8. Values of $T_p$ and $T_f$ at airflow rate range from 100 to $500\text{m}^3\text{hr}^{-1}$ for plenum depth of (a) 0.20m, (b) 0.25m and (c) 0.30m.	67
Figure 4-9. Effect of $T_a$ on the temperature change of $(T_{out}-T_a)$ for input parameters of $I=500\text{Wm}^{-2}$ , $V_{fan}=200\text{m}^3\text{hr}^{-1}$ and $D=0.20\text{m}$	68
Figure 4-10. Values of $(T_p-T_a)$ at various solar radiation intensities for plenum depths of 0.2m, 0.25m and 0.30m.	68
Figure 4-11. Values of $(T_{out}-T_a)$ at various solar radiation intensities for plenum depths of 0.2m, 0.25m and 0.30m.	69
Figure 4-12. Values of $(T_p-T_a)$ at various airflow rates for plenum depths of 0.2m, 0.25m and 0.30m.	70
Figure 4-13. Values of $(T_{out}-T_a)$ at various airflow rates for plenum depths of 0.2m, 0.25m and 0.30m.	70
Figure 4-14. Heat transfers of the unglazed transpired solar collector.	72

Figure 4-15. Values and percentages of air temperature rise for normal and vertical airflows for plenum depths of (a) 0.20m, (b) 0.25 and (c) 0.30m with various suction mass flow rates and at constant solar radiation intensity of $614\text{Wm}^{-2}$ .	77
Figure 4-16. Temperatures of the ambient, the plate and the air in the plenum for plenum depth of (a) 0.20, (b) 0.25 and (c) 0.30m at various solar radiation intensities.	79
Figure 4-17. Values and percentages of rise in air temperature for normal and vertical airflows for plenum depths of (a) 0.20m, (b) 0.25 and (c) 0.30m at various solar radiation intensities.	80
Figure 4-18. System efficiencies from experiment results at $614\text{Wm}^{-2}$ of solar radiation.	81
Figure 4-19. System efficiencies from experiment results at various solar intensities under a constant suction mass flow rate.	82
Figure 4-20. Air temperature rise of vertical flow in the plenum for plenum depth of 0.20m, 0.25m and 0.30m at various solar radiation intensities.	83
Figure 4-21. Air temperature rise of vertical flow in the plenum for plenum depth of 0.20m, 0.25m and 0.30m at various suction mass flow rates.	84
Figure 4-22. Correlations of $Nu_{c,trans}$ and $Re_{c,trans}$ for plenum depths of (a) 0.20m, (b) 0.25m and (c) 0.30m.	86
Figure 4-23. Average correlation of $Nu_{c,trans}$ and $Re_{c,trans}$ .	88
Figure 4-24. Correlation of $Nu_{f,trans}$ and $Re_{f,trans}$ for laminar flow.	89
Figure 4-25. Correlation of $Nu_{f,trans}$ and $Re_{f,trans}$ for turbulent flow.	89
Figure 4-26. Comparison of heat exchange effectiveness between modelling and experiment results	91
Figure 4-27. Comparisons of heat exchange effectiveness between Kutscher's model and experiment results for plenum depths of (a) 0.20m, (b) 0,25m and (c) 0.30m.	92
Figure 4-28. Simulated $T_{out}$ of flat and transpired plates for plenum depths of 0.20m, 0.25m and 0.30m at a constant $V_{fan}$ of $300\text{m}^3\text{hr}^{-1}$ and $T_a= 293\text{K}$ .	95
Figure 4-29. Simulated $T_p$ of flat and transpired plates for plenum depths of 0.20m, 0.25m and 0.30m at a constant $V_{fan}$ of $300\text{m}^3\text{hr}^{-1}$ and $T_a= 293\text{K}$ .	95
Figure 4-30. Heat fluxes of flat plate for $I=300$ to $I=800\text{Wm}^{-2}$ .	97
Figure 4-31. Heat fluxes of transpired plate for $I=300$ to $I=800\text{Wm}^{-2}$ .	97

Figure 4-32. Simulated $T_p$ of flat and transpired plates for plenum depths of 0.20m, 0.25m and 0.30m at a $I=500\text{Wm}^{-2}$ and $T_a= 293\text{K}$ .	98
Figure 4-33. Simulated $T_{out}$ of flat and transpired plates for plenum depths of 0.20m, 0.25m and 0.30m at a $I=500\text{Wm}^{-2}$ and $T_a= 293\text{K}$ .	98
Figure 4-34. Values of efficiency of flat and transpired plates at a constant $V_{fan}= 300\text{m}^3\text{hr}^{-1}$ .	99
Figure 4-35. Values of efficiency of flat and transpired plates at a constant $I= 500\text{Wm}^{-2}$ .	100
Figure 5-1. Schematic diagrams of cooling systems with flat plate as solar collector façade.	103
Figure 5-2. Schematic diagrams of cooling systems with transpired plate as solar collector façade.	104
Figure 5-3. Effects of $T_a$ and $T_w$ on $T_f$ over a range of solar radiation intensity at (a) low and (b) airflow rates.	106
Figure 5-4. Effects of $T_a$ and $T_w$ on $T_f$ over a range of airflow rate at (a) low and (b) high solar radiation intensities.	107
Figure 5-5. The effects of $T_a$ and $T_w$ on $(T_a-T_{out})$ .	108
Figure 5-6. Values of $(T_a-T_{out})$ at different airflow rates solar radiation intensities.	109
Figure 5-7. Values of plenum air temperatures of the systems with dry and wet sandtile wall.	110
Figure 5-8. Heat fluxes of the heat gain and removed by the system with flat plat and single plenum.	111
Figure 5-9. Cooling efficiency for system with flat plate and single plenum.	112
Figure 5-10. Values of $(\omega_{out}-\omega_{in})$ over different solar radiation intensities.	113
Figure 5-11. Values of the ratio of latent heat to energy input over different solar radiation intensities.	114
Figure 5-12. Values of $(T_a-T_{out})$ at suction velocity of $0.04\text{ms}^{-1}$ over different solar radiation intensities.	115
Figure 5-13. Values of $(T_a-T_{out})$ solar radiation intensity of $500\text{Wm}^{-2}$ over different suction velocities.	116
Figure 5-14. Heat transfer of cooling system with transpired plate solar façade and two plenums.	118
Figure 5-15. Temperature comparisons between the model and the experiments over solar radiation intensities.	126
Figure 5-16. Values of $T_p$ , $T_f$ and $T_w$ over different airflow rates at the Plenum 2, under a constant solar radiation intensity of $614\text{Wm}^{-2}$ .	127

Figure 5-17. Comparisons of the ratios of Exh_C to Exh_H between the model and experiment.	127
Figure 5-18. Values of outlet air humidity ratio from the experiments against the modelled results.	128
Figure 5-19. Values of $T_a$ , $T_{fi}$ , $T_r$ , $T_{s,in}$ and $T_{s,out}$ over solar radiation intensities.	129
Figure 5-20. Modelled results of the effects of $T_a$ , $T_{w,in}$ and $T_{s,in}$ on $(T_{in,s} - T_{s,out})$ .	132
Figure 5-21. Measured values of the water temperature throughout the experiments without cooling step.	132
Figure 5-22. Comparison of $(T_{s,in} - T_{s,out})$ for experiments with and without maintaining the water temperature.	133
Figure 5-23. Comparison of $(T_s - T_r)$ for experiments with and without maintaining the water temperature.	133
Figure 5-24. Measured results of $(T_{s,in} - T_r)$ and $(T_{s,in} - T_{s,out})$ .	135
Figure 5-25. Cooling effectiveness of the system over different solar radiation intensities.	136
Figure 5-26. Cooling effectiveness of the system over different airflow rates in plenum 2.	136
Figure 5-27. Simulation results of $(T_{s,in} - T_{s,out})$ for expanding the plate areas horizontally ( $H=2m$ ) and vertically ( $L=1m$ ).	137
Figure 5-28. Simulation results of large scale installation with $A_p=500m^2$ .	137
Figure 5-29. Plenum air temperatures of the systems with dry and wet sandtile wall.	138
Figure 5-30. Heat fluxes of the heat gain and removed, and values of cooling efficiency of the system with transpired plat and two plenums.	139
Figure 5-31. The difference of humidity ratio of the air in Plenum 1 over a range of solar radiation intensity.	141
Figure 5-32. Simulated values of $T_r$ and $(T_{s,in} - T_{s,out})$ during the day and night time.	143
Figure 6-1. (a) Heating and (b) cooling modes with controlled dampers.	146
Figure 6-2. Diagram of the building design for present simulation with total height of 14.8m, length of 40m and breadth of 25m.	147
Figure 6-3. Monthly average global solar irradiances and ambient temperatures of London (N51°9') (W0°10').	148
Figure 6-4. Outlet temperatures and temperature changes of the air throughout the year.	149

## List of tables

Table 1-1. Investigated system designs for present research.	5
Table 2-1. Summary of some of the selected previous researches.	10
Table 2-2. Summary of some case studies performance results of unglazed transpired solar wall for space heating.	19
Table 3-1. Physical properties of aluminium (Forsythe, 2003).	37
Table 3-2. Approximate corrosion rates of some selected metals in different atmosphere (Mattsson, 2001).	37
Table 3-3. Locations of thermocouples on the plate and santile wall.	40
Table 3-4. Specification of the CMP6 pyranometer.	43
Table 3-5. Specification of ISOTECH TTI-7-R PRT	47
Table 3-6. Technical data for Vaisala HMP45A sensor.	48
Table 3.7. The average percentage errors of the sensors and instruments	50
Table 4-1. Parameters for the experiments of flat plate for heating system.	57
Table 4-2. Parameters for the experiments of transpired plate for heating system.	75
Table 4-3. Heat fluxes of flat plate.	96
Table 4-4. Heat fluxes of transpired plate.	96
Table 4-5. System efficiency comparisons among some reported solar air heaters.	101
Table 5-1. Parameters for the experiments of cooling system with flat plate collector and single plenum.	105
Table 5-2. Input parameters of simulation studies for cooling system with transpired plate solar collector and single plenum.	115
Table 5-3. Parameters for the experiments of cooling system with two plenums.	125
Table 5-4. Input parameters for the model tests to investigate the effects of $T_a$ , $T_{w,in}$ and $T_{s,in}$ on $(T_{in,s} - T_{s,out})$ .	130
Table 5-5. Energy consumption comparisons for various types of cooling systems.	140
Table 5-6. Input parameters for the investigation on the cooling performance for $I=0Wm^{-2}$ .	142
Table 6-1. Values of maximum ambient air temperature of the day and air humidity throughout the year of London.	147
Table 6-2. Energy and CO <sub>2</sub> savings from present system.	150

Table 6-3. Initial installation and maintenance costs of the combined heating and cooling system.	151
Table 6-4. Comparisons of initial installation cost of solar glazed-covered flat plate air heater with present design.	152
Table 6-5. Payback period of the system investment with 5% discount rate and 30 year system lifetime.	153

## Nomenclature

$A_p$	Surface area of transpired plate, $m^2$
$c_p$	Heat capacity, $Jkg^{-1}K^{-1}$
$COP$	Coefficient of performance, %
$d$	Hole diameter, m
$d_h$	Hydraulic diameter, m
$D$	Plenum depth, m
$g$	Acceleration of gravity, $ms^{-2}$
$g_{heat}^*$	Reynolds flux
$G$	Suction mass flow rate per unit area, $kgs^{-1}m^{-2}$
$h$	Heat transfer coefficient, $Wm^{-2}K^{-1}$
$h_m$	mass transfer coefficient, $kgs^{-1}m^{-2}$
$H$	Plenum height, m
$H_{fg}$	Latent heat, $kJ/kg$
$H_{pw}$	Specific enthalpy of water vapour, $kJ/kg$
$I$	Solar irradiance, $Wm^{-2}$
$k$	Thermal conductivity, $Wm^{-1}K^{-1}$
$k_1$	Thermal conductivity of sandtile wall, $Wm^{-1}K^{-1}$
$k_2$	Thermal conductivity of insulation layer, $Wm^{-1}K^{-1}$
$k_H$	Weighted harmonic mean thermal conductivity, $Wm^{-1}K^{-1}$
$k_w$	Thermal conductivity of water, $Wm^{-1}K^{-1}$
$L$	Width of aluminium plate, m
$L_1$	Thickness of sandtile wall, m
$L_2$	Thickness of insulation layer, m
$Le$	Lewis number
$\dot{m}$	Mass flow rate, $kgs^{-1}$
$Nu$	Nusselt number
$p$	Vapour pressure, Pa
$ps$	Saturation vapour pressure, Pa
$P$	Plate porosity
$P_{pump}$	Power for water pump, kW
$Pit$	Pitch, m
$Pr$	Prandtl number
$q$	Heat flux, $Wm^{-2}$
$q_d$	Useful energy heat flux, $Wm^{-2}$
$Q$	Heat, W

$Ra$	Rayleigh number
$RH$	Relative humidity, %
$S$	Solar radiation heat flux absorbed by the aluminium plate, $Wm^{-2}$
$T$	Temperature, K
$U_L$	Overall heat transfer coefficient between sandtile wall and insulation layer
$U_o$	U-value of plate material, $Wm^{-2}K^{-1}$
$U_s$	Conductance of sandtile wall, $Wm^{-2}K^{-1}$
$U_w$	Wind velocity, $ms^{-1}$
$v_f$	Plenum velocity, $ms^{-1}$
$v_s$	Suction velocity, $ms^{-1}$
$V_{fan}$	Volume airflow rate, $m^3hr^{-1}$
$V_{water}$	Water flow rate, $m^3hr^{-1}$
$V_{st}$	Volume of the sandtile, $m^3$
$W_{dry}$	Weight of dry sandtile, kg
$W_{sat}$	Weight of sandtile that saturated with water, kg

### Greek symbols

$\alpha_p$	Absorptivity
$\beta$	Coefficient of volumetric expansion, $m^{-1}$
$\rho$	Air density ( $kgm^{-3}$ )
$\sigma$	Stefan–Boltzmann constant, $5.67 \times 10^{-8} Wm^{-2}K^{-4}$
$\varepsilon_p$	Emissivity of black painted plate
$\kappa$	Thermal diffusivity ( $m^2s^{-1}$ )
$\nu$	Kinematic viscosity ( $m^2s^{-1}$ )
$\varepsilon_{HX}$	Heat exchange effectiveness, %
$\varepsilon_p$	Emissivity
$\eta; Eff$	Efficiency, %
$\mu$	Dynamic viscosity ( $Nsm^{-1}$ )
$\omega$	Humidity ratio, kg/kg
$\phi$	Sandtile porosity

### Subscription

$a$	Ambient air
$air-wall$	Between plenum air and sandtile wall
$bp-air$	Between back-of-plate of transpired plate and plenum air

<i>c; conv</i>	Convection
<i>c,flat</i>	Convection between flat plate and ambient air
<i>c,trans</i>	Convection between transpired plate and ambient air, normal flow heat transfer of transpired plate
<i>f</i>	Air in Plenum 1; convection between back-of-plate and plenum air
<i>flat</i>	Flat plate
<i>f,flat</i>	Convection between back-of-plate of flat plate and plenum air
<i>free</i>	Free convection
<i>forced</i>	Forced convection
<i>f,trans</i>	Convection between back-of-plate of transpired plate and plenum air, vertical flow heat transfer of transpired plate
<i>i</i>	Air entering into plenum, air temperature at the bottom of plenum, K (transpired plate)
<i>in</i>	Inlet
<i>loss,wall-room</i>	Heat loss from sandtile wall to wall attached to the room
<i>L</i>	Laminar; latent heat
<i>out</i>	Outlet
<i>p</i>	Plate
<i>p-air</i>	Between transpired plate and ambient air
<i>p-sur</i>	Between plate and surrounding
<i>p-wall</i>	Between back-of-plate and sandtile wall
<i>r</i>	Wall attached to room (single plenum); backside of sandtile wall (2 plenums); radiation heat transfer from plate to surrounding
<i>rad; r1</i>	Radiation heat transfer from plate to surrounding
<i>r2</i>	Radiation heat transfer from plate to sandtile wall
<i>s</i>	Air in Plenum 2
<i>sand</i>	Sandtile wall
<i>trans</i>	Transpired plate
<i>T</i>	Turbulent
<i>v</i>	vapour
<i>w</i>	Sandtile wall; water; convection between wet surface and air in Plenum 1
<i>w1</i>	Heat transfer between the plenum air and the falling film
<i>w2</i>	Heat transfer between the plenum air and the wet surface

# 1. Introduction

## 1.1 Background

Heating, ventilating, and air-conditioning (HVAC) are indoor climate controls that regulate humidity and temperature to provide thermal comfort and indoor air quality. Hence, HVAC is part of the major energy consumption in buildings. Generally, energy use in residential, commercial and public buildings account for 35% of total global final energy consumption (IEA, 2008a), which is equivalent to about 2,754Mtonnes of CO<sub>2</sub> emissions (IEA, 2009). Space heating is the most important building energy user in cold countries, whereas, air conditioning is a major contributor to peak electricity demand in hot countries or during summer. For instance, in the United Kingdom, energy used for space heating was about 50% of the service sector energy consumption in 2004 (IEA, 2007a, 2008b). On the other hand, air-conditioning accounts for 40% of peak load during the summer in Shanghai. These heating and cooling loads are having an impact on CO<sub>2</sub> emissions, as well as on security of supply (IEA, 2007a, b). In addition, CO<sub>2</sub> emissions could raise global temperatures by up to 6°C by the end of this century and UK will have 3°C hotter summers by 2080 (HM Government, 2009). Thus, the air-conditioning demand in the UK is expected to increase, especially in urban areas such as London due to urban heat island effects (Kolokotroni, 2010). Apart from the impact on CO<sub>2</sub> emissions, the working fluids of conventional air-conditioning system such as CFCs and HCFCs are potentially causing ozone depletion too.

The International Energy Agency (IEA) has identified the building sector as one of the most cost-effective sectors for reducing energy consumption, with estimated possible energy savings of 1,509 million tonnes of oil equivalent (Mtoe) by 2050. Moreover, by reducing overall energy demand, improving energy efficiency in buildings can significantly reduce CO<sub>2</sub> emissions from the building

sector by 12Gtonnes of CO<sub>2</sub> emissions by 2050 (IEA, 2010). For example, energy efficient space heating could potentially save energy up to 50% in the residential sector and 40% in the commercial sector; whereas energy efficient air-conditioning systems would be able to save 13% of the energy consumption in the commercial sector and 6% in the residential sector (IEA, 2008a). Therefore, environmental friendly and low energy technologies are crucial in achieving energy and carbon saving targets. In this regard, renewable energy has become vital for heating and cooling; for instance, solar energy that utilises cost-free solar radiation from the sun. Our research aims to develop a combined heating and cooling system in buildings by using the façade as the solar collector.

## **1.2 Research problem**

### **1.2.1 Building integration of solar thermal technology**

Integrating the solar heating and cooling systems in the building envelope is a necessity if the systems are to be economically feasible. Typically, it can be roof or façade integrations such as wall, balcony, awning or shade of the building. The integration is only possible if the design of the solar technology is included in the design of the building. The major component of any such technology is the solar collector. Solar thermal collectors are often considered as separate elements and thus building integration is still relatively rare (Orel, 2005; Tripanagnostopoulos, 2000). They are usually installed separately from the building or confined to the roof top so that they are less visible, to minimise the building aesthetic impact (Matuska, 2006; Probst, 2007). Consequently, the installation cost of an active solar heating or cooling system might be considered as an additional initial cost of the building.

Generally, architects and engineers have the greatest influence on linkage between the thermal shell of building and the HVAC system size. Two elements need to be considered when establishing the architectural thermal design: 1) significant effect on the thermal response of the building; 2) parameters that are

directly influenced by architectural design decisions. In most cases architects design a building shell that meets with the client's requirements. The thermal characteristics of a building are largely influenced by design decisions during the preliminary design phase. With regard to low energy consumption, architects usually consider solar passive or energy efficiency features rather than solar active technology. These designs are then passed on to HVAC engineers to perform a thermal analysis and design the appropriate heating and/or cooling systems. Nevertheless, as the major building design decisions have already been made, it is often too late and difficult for the architect to change the design based on the thermal analysis results. Consequently, this limits building integrated with solar energy systems (Ellis, 2002, 2001; Hestnes, 1999).

According to a survey reported by Probst et al. (2007), solar systems should be integrated within the composition logic of the whole building with the following criteria:

- 1) The use of the solar energy system as a construction element (facade cladding, roof covering etc.) should greatly ease the integration design work;
- 2) The position and the dimension of the collector field should be defined considering the building as a whole (not just within a facade or the roof);
- 3) The colours and materials of the system should be chosen together with the colours and materials characterizing the building and the context and finally
- 4) Module size and shape should be chosen considering the building and the facades/roof composition grids (or vice versa).

It short, the collector should be conceived as part of a construction system which provides active and non active components, flexible enough to interface with the other building elements and able to adapt to different buildings.

### **1.2.2 System complication**

The technologies that use solar energy as an alternative energy source for heating and cooling are being intensively developed. However, the existing active

solar heating and cooling systems are usually separated. It is not only difficult to add solar air-conditioning to an air heating system, it also produces higher costs and noisier operation (Soteris, 2009).

Some of the solar active heating systems do not allow direct heating from a solar collector to heat the building but always transfer heat from the collector to storage, then to the load. Such systems are designed for total building thermal load requirements during cold months; they would be oversized for most of the year in moderate climate countries and thus not economically viable. While passive solar designs can function as heating and cooling systems, the cooling part in most of these designs is usually due to natural air ventilation rather than the production of cold air, like in an air-conditioning system. Research is needed on development of a user-friendly operating prototype of a combined system which is able to provide heat during the cold days and produce cold during hot days and that fully utilises solar energy throughout the year.

### **1.3 Aim and objectives**

Due to the above mentioned problems, a simple, environmentally friendly, low cost and building integrated system that can be used for heating and cooling throughout the year is needed to reduce the energy consumption and CO<sub>2</sub> emissions. Our system will use the same concept of an active solar air heater whereby solar heat is collected by an absorber and used to heat the air that passing through it. However, instead of confining it to the roof top as a separated element of the building, it will utilise the building facade as a solar collector to warm the air for heating in the winter, and cool the air in the summer. The system design is similar to the Trombe wall and vertical solar chimney, where the heat transfer of the air occurs between the façade and the building's wall. The differences of the present system and these two systems are:

- 1) The façade is made of black painted aluminium plate, instead of glazed materials. Black colour is selected to maximise the absorptivity of the plate

and aluminium is because of better corrosion resistant characteristic (See Section 3.4.1).

- 2) It is a fan-driven system instead of natural ventilation.
- 3) The cooling effects are not only because of air movement but also by the use of a wetted wall.

The overall objectives of the study are as follows:

**1. To investigate the solar facades performance for heating and cooling**

Five system designs were tested and two types of facades were investigated, i.e. flat (without holes) and transpired aluminium plates. For the heating, the systems consisted of a single plenum, whereas the cooling systems involved single and double plenums (Table 1-1). Configurations of the systems are as shown in Figure 1-1.

Table 1-1. Investigated system designs for present research.

	Flat plate	Transpired plate
Heating	1) Single plenum, dry wall	2) Single plenum, dry wall
Cooling	3) Single plenum, wet wall	4) Two plenums, dry wall 5) Two plenums, wet wall

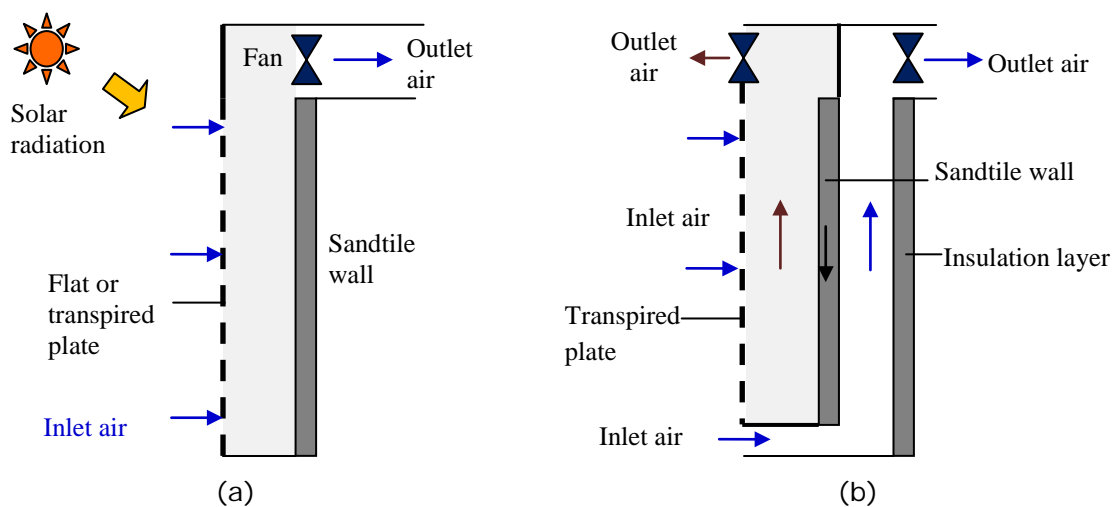


Figure 1-1. Configurations of (a) single and (b) double plenums of the systems.

**2. To develop mathematical models for the heating and cooling performances**

Models were developed for each system design. The models were developed by establishing energy balance equations and solved by matrix inversion method. The models were then validated with experiments results.

**3. To demonstrate the systems experimentally**

Experiments were carried out for all the system designs. A chamber was built in the laboratory to serve as a building, and the aluminium plate was installed on one of the side walls of the chamber as the façade. The experiments were carried out under different operation conditions, e.g. solar radiation intensities, airflow rates and plenum depths.

**4. To investigate the best system design for a combined heating and cooling system**

The heating and cooling performances of different designs were compared, and thus a design with combined system was developed. Apart from the small scale experiments, the performance of this combined system was simulated by using the UK weather data and assuming it was installed as the south-facing façade of an office building.

**5. To investigate the cost effectiveness of the combined system**

The initial cost for a 40m<sup>2</sup> of solar façade was estimated and compared to the active solar system. Energy and CO<sub>2</sub> savings from the combined system were estimated, too. Finally the total system cost and the payback period of the investment were calculated.

**1.4 Outline of thesis**

This thesis consists of seven chapters and the contents of the remaining chapters are summarised as follows:

## ***Chapter 2: Literature Review: Building Integrated Air heating and Cooling Designs***

This chapter reviews the existing building integrated systems for heating and cooling in buildings. The review focuses on system designs and performances. In addition, the advantages and barriers of these technologies are addressed. Finally, the chapter concludes by identifying the need for combined heating and cooling with the hybrid of active and passive solar technologies.

## ***Chapter 3: Methodology***

This chapter illustrates the concepts of system designs and outlines the research approach methods. The general development steps for the mathematical model are explained. In addition, experimental steps for heating and cooling systems are included and sensor calibration curves are provided, too.

## ***Chapter 4: Solar façade for space heating***

The working mechanisms of the heating systems are illustrated. This is followed by establishment of energy balance equations and hence the matrix inversions equations for the model. The simulation and experiment results are compared to validate the model accuracy. Moreover, the effects of operation parameters on the systems performance are discussed. Apart from that, for the transpired plate design, heat transfer coefficients are investigated too. Finally, the thermal performances of flat and transpired systems are compared and the heat losses are analysed.

## ***Chapter 5: Solar façade for space cooling***

This chapter illustrates the working mechanisms of the cooling systems and explains the approach for systems with one and two plenums. Energy balance equations are established for the mathematical models. Then, the accuracies of

the models are validated with the experiment results. This is followed by parametric analyses and discussions on system performances.

#### ***Chapter 6: Solar facade for the combined heating and cooling system***

The final design of a combined heating and cooling system is identified and the working mechanisms with dampers control for heating and cooling modes are explained. Simulation on real building installation is carried out by using the developed model from the previous chapter. The façade performance is modelled by assuming the façade is installed on an office building in London. Energy saving, CO<sub>2</sub> emission reduction and cost effectiveness of the system are analysed.

#### ***Chapter 7: Conclusions and future works***

This chapter includes the summary and conclusions of the thesis and contributions of the research work. It also provides some recommendations for future work.

## **2. Literature Review:**

### **Building Integrated Air heating and Cooling Designs**

#### **2.1 Introduction**

In order to make the technologies more economic feasible, building integrated designs are one of the focuses of present research. In this chapter, several passive solar designs and the performances are reviewed. Furthermore, the importance of passive solar designs in filling the gaps of active solar technologies is highlighted, and the barriers of passive solar are addressed. The chapter is concluded with identifying the need of a combined heating and cooling system, which integrates both passive and active solar technologies that can overcome each other limitations and benefit throughout the year.

#### **2.2 Existing designs of passive solar air heating and natural ventilation via buoyancy effect**

Solar passive heating and natural ventilation technologies share similar working mechanism. The driving force which controls the airflow rate is the buoyancy effect, whereby the airflow is due to the air temperature difference and so as the density difference at the inlet and outlet. Usually, the facades are designed in flexible functions basis whether to trap or store the heat; or create air movement that causes ventilation thus cooling effect. Table 2-1 summarises some of the selected literature reviews of passive solar facade and roof designs which includes the studies of collector performance, cost and energy analysis, main findings and recommendations.

Table 2-1. Summary of some of the selected previous researches.

Facade/ roof designs	Special Features	Performance			Cost and Energy analysis	Benefits/ findings	Limitations/ recommendations	Ref.
		Given conditions	Temperatures (Instantaneous efficiency, %)	Flow rate				
Solar chimney	Vertical, similar to Trombe wall	I= 650W/m <sup>2</sup> ; air gap depth= 0.1-0.3m	Exhaust air=38-40°C; Indoor air=30°C (40-41%)		N.A	<ul style="list-style-type: none"> <li>• Temperature rise and air velocity increased with solar radiation.</li> <li>• Temperature rise decreased with air gap depth.</li> <li>• No reverse air flow circulation was observed even at large gap of 0.3m</li> </ul>	N.A	(Ong, 2003)
Solar wall	Similar to Trombe wall, consists of glass cover, air gap, black metallic plate, insulator	I= 406W/m <sup>2</sup> ; T <sub>a</sub> = 30°C; height= 1m; air gap depth= 0.145m	Exhaust air =42°C; Indoor air=28°C	Mass flow rate= 0.016kg/s	N.A	<ul style="list-style-type: none"> <li>• Temperatures increased with increased wall height and decreased gap.</li> </ul>	<ul style="list-style-type: none"> <li>• In very hot season, providing residents' comfort is insufficient by natural ventilation but it is able to reduce the heat gain which in turn reduces the cooling load.</li> </ul>	(Hirunlabh, 1999)
Double facades	i) Outer skin: glaze; inner skin: glaze ii) Outer skin: PV panel; inner skin: glaze	Cavity width= 0.8m; inlet area= outlet area	N.A	i) Airflow rate=0.27m <sup>3</sup> /m-s ii) Airflow rate= 0.36m <sup>3</sup> /m-s	PV facade increased electricity conversion efficiency by reducing the cell temperature.	<ul style="list-style-type: none"> <li>• PV facade increased the efficiency of PV cells when outdoor air temperature is higher than the indoor.</li> </ul>	<ul style="list-style-type: none"> <li>• The outer skin temperature of PV panel increased depending on the degree of transparency.</li> </ul>	(Gan, 2006)
Single- sided heated solar chimney	Adjacent walls are insulated	Length= 1m; breath/height= 0.1; inlet temperature= 20°C	Exhaust air=33°C	Airflow rate= 0.5kg/s	N.A	<ul style="list-style-type: none"> <li>• The airflow rate reaches maximum when breath/height=0.1</li> </ul>	<ul style="list-style-type: none"> <li>• The optimised height can be determined according to the optimised section ratio of breath to height and available practical field conditions.</li> </ul>	(Li, 2004)

Solar chimney	Under hot and humid climate conditions, studies included during clear sky, partly cloudy and cloudy days	<ul style="list-style-type: none"> <li>i) Clear sky: <math>T_a = 35^\circ\text{C}</math>; <math>I = 800\text{W}/\text{m}^2</math>; wind velocity= 2.6m/s</li> <li>ii) Partly cloudy: <math>T_a = 34^\circ\text{C}</math>; <math>I = 594\text{W}/\text{m}^2</math>; wind velocity= 2.5m/s</li> <li>iii) Cloudy day: <math>T_a = 32^\circ\text{C}</math>; <math>I = 509\text{W}/\text{m}^2</math>; wind velocity= 1.8m/s</li> </ul>	<ul style="list-style-type: none"> <li>i) Exhaust air=<math>38^\circ\text{C}</math>; Indoor air=<math>33^\circ\text{C}</math>;</li> <li>ii) Exhaust air=<math>36^\circ\text{C}</math>; Indoor air=<math>32^\circ\text{C}</math>;</li> <li>iii) Exhaust air=<math>33^\circ\text{C}</math>; Indoor air=<math>32^\circ\text{C}</math></li> </ul>	N.A		N.A	<ul style="list-style-type: none"> <li>• Solar chimney can reduce indoor temperature by 1.0-3.5<math>^\circ\text{C}</math> compared to the ambient temperature of 32-40<math>^\circ\text{C}</math>.</li> </ul>	<ul style="list-style-type: none"> <li>• Indoor temperature (Chungloo, 2007) can be further reduced by 2.0-6.2<math>^\circ\text{C}</math> with combination of spraying of water on the roof.</li> </ul>
Roof solar collector	Air gap and openings of roof solar collector	N.A	N.A	10-100m <sup>3</sup> /hr	Insignificant extra cost of construction	<ul style="list-style-type: none"> <li>• Larger air gap larger and equal size of openings induced higher rate of airflow rate.</li> </ul>	<ul style="list-style-type: none"> <li>• Insufficient natural ventilation to satisfy residents' comfort.</li> <li>• Another device such as Trombe wall might be needed to improve comfort performance.</li> </ul>	(Khedari, 2000)
Roof-integrated water solar collector	Roof integrated, combining the conventional roof and flat plat solar collector by replacing water-coil and internal insulation with water pond and metallic sheet.	N.A	N.A	N.A	150-200 USD /m <sup>2</sup> compare to 160-220USD/m <sup>2</sup> of conventional air-conditioner; taking one-third of construction time that represents 15USD/m <sup>2</sup> ; Average daily energy absorbed= 0.68GJ; Annual energy= 247GJ	<ul style="list-style-type: none"> <li>• Able to control heat delivery to adapt with the environmental conditions.</li> <li>• Able to create heating or cooling effects</li> <li>• Provide hot domestic hot water during winter</li> </ul>	<ul style="list-style-type: none"> <li>• Large area of roof is needed</li> </ul>	(Juanico, 2008)
Roof solar collector	Single and double pass designs	$I = 500\text{W}/\text{m}^2$ ; $T_a = 0^\circ\text{C}$ ; mass flow rate 2000kg/h;	<ul style="list-style-type: none"> <li>i) Single pass: Supply air=<math>12^\circ\text{C}</math>; Indoor air=<math>8^\circ\text{C}</math>; (27%)</li> <li>ii) Double pass: Supply air=<math>18^\circ\text{C}</math>; Indoor air=<math>13^\circ\text{C}</math> (39%)</li> </ul>	N.A	Choosing suitable fan is important to reduce initial investment and operating cost.	<ul style="list-style-type: none"> <li>• Instantaneous efficiency of double pass was 10% higher than single pass collector whether spacing heating or natural ventilation.</li> </ul>	<ul style="list-style-type: none"> <li>• Two or more shorter collectors (Zhai, 2005) in parallel are recommended instead of one longer collector.</li> </ul>	

I= solar intensity;  $T_a$  = ambient air temperature; N.A= Not applicable; Ref. = references

### 2.2.1 Trombe Wall

The classical Trombe wall is a massive wall that covered by an exterior glazing with an air channel in between (without Dampers A and B in Figure 2-1). The massive wall absorbs and stores the solar energy through the glazing. Part of the energy is transferred into the indoor of the building (the room) through the wall by conduction. Meanwhile, the lower temperature air enters the channel from the room through the lower vent of the wall, heated up by the wall and flows upward due to buoyancy effect. The heated air then returns to the room through the upper vent of the wall.

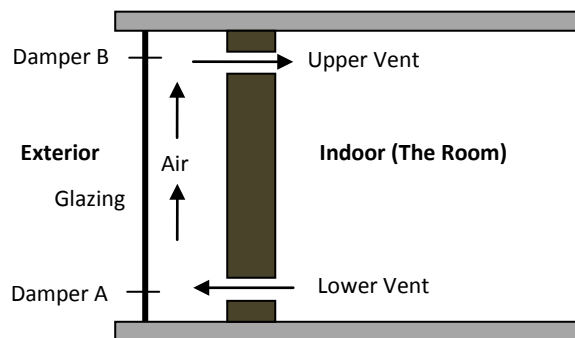


Figure 2-1. Schematic diagram of classical Trombe wall (without dampers).

Some of the challenges with this classical Trombe wall design are as follows:

- 1) Low thermal resistance. When small amount of the solar energy absorbed by the wall, e.g. during the night or prolonged cloudy periods, some heat flux is transferred from the inside to the outside, which results in excessive heat loss from the building (Shen, 2007).
- 2) Inverse thermo-siphon phenomena occur during winter, at night or non-sunny day. When the wall is colder than the indoor temperature, reverse air circulation from the upper vent to the lower vent causes the air being cooled and hence decrease the room temperature (Onbasioglu, 2002; Shen, 2007).
- 3) The uncertainty of heat transfer due to air movement in enclosures that heated by solar energy. The solar intensity is not constant and periodical. Any

change in solar intensity could cause temperature fluctuations of the wall (Onbasioglu, 2002).

- 4) The influences of channel width and the dimensions of the inlet and outlet openings affect the convection process and hence affect the overall heating performance (Gan, 2006; Onbasioglu, 2002).
- 5) Low aesthetic value (Jie, 2007).

Studies have been carried out to improve the classical Trombe wall design. The improvement can be classified into three aspects, i.e. inlet and outlet air openings control, thermal insulation designs, and air channel designs.

By installing adjustable dampers at the glazing and adjustable vents of the wall, the classical Trombe wall can be beneficial for winter heating and summer cooling (Gan, 1998; Jie, 2007). By referring to the Figure 2-1, in winter, Damper B is closed while Damper A, lower and upper vents are left open to circulate the heated air return to the room. Whereas during summer, Damper A and upper vent are closed. The buoyancy forces generated by the solar heated air between the warm wall and glazing draws room air from the lower vent and the heated air is then exhausted to the ambient through Damper B. Thus, during summer, the Trombe wall facilitates room air movement for summer cooling. Alternatively, in the case of Trombe wall that without adjustable damper at the glazing, the upper and lower vents are closed when the outdoor temperature is lower than the indoor (Shen, 2007).

Insulation levels of glazing and storage wall influence the surface temperatures and thereby the fluid flow rate. These two thermal insulation methods have their own strengths for different climate conditions. For winter heating, increasing the thermal resistance of glazing is generally more advantageous as this reduces the heat loss through glazing while making use of conductive heat transfer from the storage wall to the room. Richman and Pressnail (2009) introduced a low-e coating on a spandrel glass to minimize the radioactive losses to the exterior. Gan (1998) proposed that using double glazing

could increase the flow rate by 11 to 17%. Jie et. al (2007) introduced the PV-Trombe wall concept that not only improve the aesthetical aspect but also able to capture the heats and simultaneously reduce the PV cells temperature. On the other hand, insulating the interior surface of the storage wall for summer cooling can avoid excessive overheating due to south-facing glazing (Gan, 1998). Matuska and Sourek (2006) found that there was no effect on indoor comfort when sufficient insulation layers were applied on the storage wall.

In addition, composite Trombe–Michel wall has also been studied to overcome the heat loss from the inside to the outside of building (Shen, 2007). The concept of composite Trombe–Michel wall is similar to the traditional Trombe wall except there is an insulating wall at the back of the massive wall (Figure 2-2). The thermal energy can be transferred from outside to the interior air layer by conduction through the massive wall. Then it can be transferred by convection while using the thermo-circulation phenomenon of air between the massive wall and the insulating wall. During non-sunny days, winter or at nights, the vents in the insulating wall are closed. Hence, due to greater thermal resistance of this design, the thermal flux that going from indoor to outdoor is reduced.

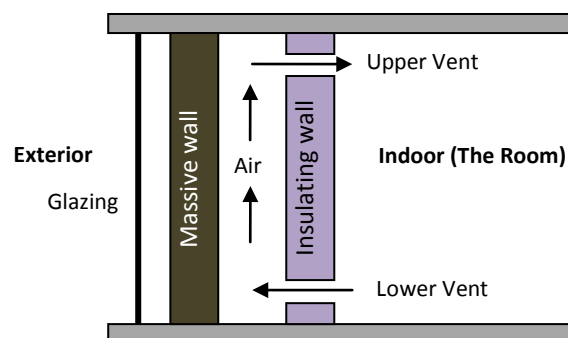


Figure 2-2. Schematic diagram of composite Trombe–Michel wall.

Typically, Trombe wall is a sensible heat storage wall. Another innovative design of Trombe wall is filling phase change materials (PCM) into the masonry wall to store the latent heat. For a given amount of heat storage, the phase change units require less space and are lighter in weight compared to mass wall

(Tyagi, 2007). Therefore, it is convenient for building retrofitting. Studies indicated that concrete-PCM combination Trombe wall can be used to develop low energy house as it is an effective energy storage wall (Onishi, 2001; Stritih, 2003). Nwachukwu and Okonkwo (Nwachukwu, 2008) had found that by applying a coating of superior absorption vigour on the exterior of storage wall could enhance the heat absorption and heat transfer across a Trombe wall. However studies on PCM properties for Trombe wall are yet to be developed to get the optimum results.

Apart from that, energy and air movement in the channel of a Trombe wall are induced by natural convection. Thus, the design parameters of Trombe wall channel are also factors that might affect the convection process (Onbasioglu, 2002). A parametric study has shown that airflow rate was almost unaffected by channel width, however airflow rate was increased with the height of the wall (Gan, 1998).

### **2.2.2 Solar chimney**

The function of a solar chimney is to generate airflow through a building, converting thermal energy into kinetic energy of air movement. The driving force which controls the airflow rate through the solar chimney is the density difference of air at inlet and outlet of the chimney. It provides ventilation not only for cooling but also heating if fan is used to direct the heated air into the building. When solar chimney is attached to wall, the working mechanism is similar to Trombe wall. It operates as passive heating by supplying warm air that heated up by the solar collector into the room. For cold or moderate climate, when the outdoor temperature is lower than the indoor temperature, solar chimney is functioned as passive cooling where natural ventilation is applied. However for hot climate, when the outdoor temperature is higher than the indoor, it operates as thermal insulation to reduce heat gain of the room. These three different modes are as illustrated in Figure 2-3 (Miyazaki, 2006). The simplest and most obvious layout is

to have a vertical chimney. Nonetheless, this may not be architectural attractive in term of aesthetics aspect. So a cheaper and less visually obtrusive format is to lay the collector along the roof slope while for greater height, a combination of both types may be used (Harris, 2007; Raman, 2001).

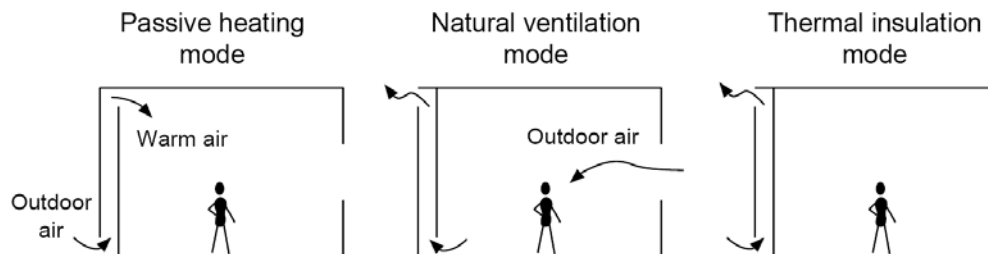


Figure 2-3. Solar chimney operation modes (Miyazaki, 2006).

### 2.2.3 Solar air heater with jet plate

Jet impingement technology is an effective tool in controlling the fluid flow for high energy transfer, which directs a jet flow from a nozzle of a given configuration to a target surface. Due to the thin thermal and hydrodynamic boundary layers formed on the impingement surface, the heat transfer coefficients associated with jet impingement are large. The convective heat transfer configuration is used for its high local transfer coefficients nearby the stagnation point. The wall impinging jet flows are widely used in engineering applications such as turbomachinery, food processing, drying, cooling and heating (Angioletti, 2003; Joshi, 2003; Na-pompet, 2011; Sagot, 2008). Some researches on solar air heater have applied this technology to enhance the heat transfer between the air and the absorber. Choudhury and Garg (1991) evaluated the thermal performance of solar air heaters with a glazed solar collector (Figure 2-4) where the metallic jet plate was placed in between the absorber and the back plate, whereas Belusko et al. (2008) examined the performance of jet impingement in an unglazed roof. Both studies have found that the jet designs give better thermal efficiency compared to the conventional parallel plate.

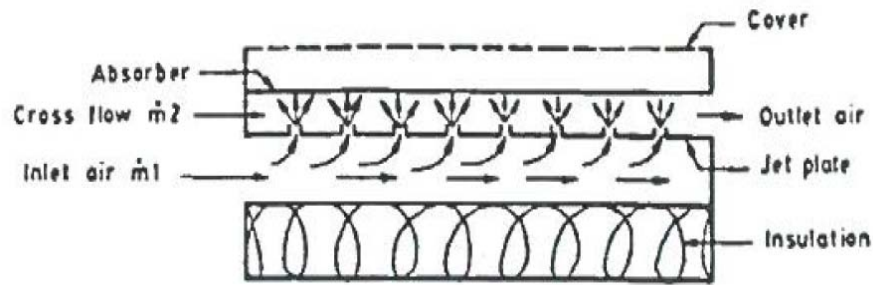


Figure 2-4. Solar air heater with a glazed solar collector (Choudhury, 1991).

#### 2.2.4 Solar air heater with transpired plate

Another façade design that able to serve as heating system without additional heat storage facility is the wall made of metal sheet with holes that operates as absorber to heat up the air. The schematic diagram of this type of solar collector is as illustrated in Figure 2-5. This collector is known as unglazed perforated-absorber collector by the Air System Working Group of International Energy Agency (IEA) Solar Heating and Cooling (SHC) Task 14. Other researchers have named it as unglazed transpired solar collector, whereas the Conserval Engineering Inc. refers the product as Solarwall. The metal cladding is heated by solar radiation. With the help of ventilation fans, the solar heated air is drawn through the holes of the transpired metal sheet. The heated air is then ducted into the building via a connection to the HVAC intake. This technology has been installed on a large number of sites in Canada. Table 2-2 summarises some of the case studies performance results for space heating, and more detail descriptions and installations around the world can be found in references (Cali, 1999; SolarWall). As compared to Trombe wall that using glazing, this elimination glazing design is able to reduce cost, and it is suitable for retrofitting.

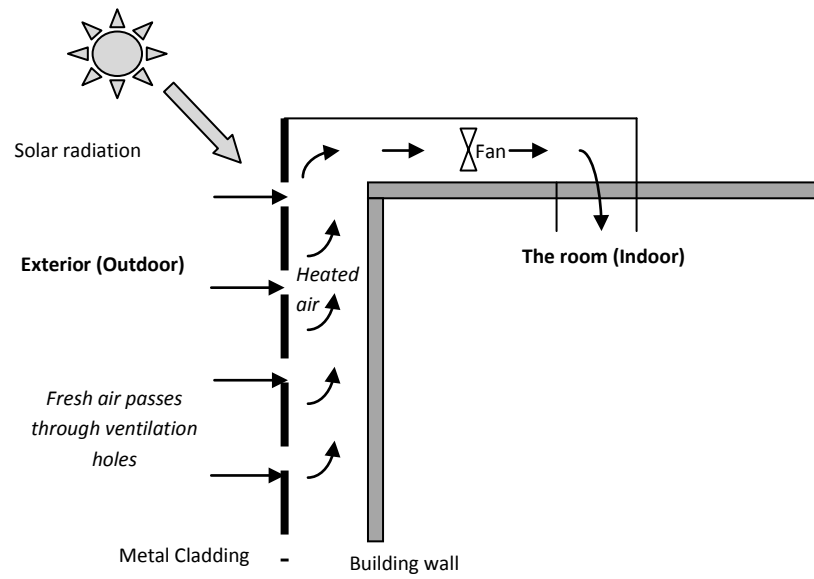


Figure 2-5. Schematic diagram of unglazed transpired solar facade.

Table 2-2. Summary of some case studies performance results of unglazed transpired solar wall for space heating.

Case study	Collector area and type	Airflow rate (m <sup>3</sup> /h/m <sup>2</sup> )	Temperature rise	Efficiency	Energy saving	Cost analysis (reference year)	Reference
Ford Canada	1877m <sup>2</sup> ; vertical wall; 2% porosity with 1% canopy	125	12°C (Sunny day)	57%	917kWh/m <sup>2</sup> /year	Cost of delivered energy =25USD/GJ/year (1990)	(Cali, 1999)
GM, Oshawa	420m <sup>2</sup> gross; 2% porosity on wall, 1% on canopy	72	13°C (Solar radiation: 500W/m <sup>2</sup> )	52%	754 kWh/m <sup>2</sup> /year	Cost of delivered energy =59USD/GJ/year (1991)	(Cali, 1999)
NREL Waste Handling Facility	27.9m <sup>2</sup> ; 2% porosity	N.A	N.A	63-68%	N.A	N.A	(Cali, 1999)
Windsor Housing Authority	335m <sup>2</sup> ; corrugated dark brown aluminium	N.A	N.A	N.A	195,700 kWh/year (estimated)	Estimated Saving: 4,184 USD/year (2.2 cents/kWh of natural gas)	(Hollick, 1996)
Combined PV/solarwall panel	Solarwall panel area= 1.1664m <sup>2</sup> ; PV cells covered 24% of solarwall surface	100	N.A	(Solar radiation: 600W/m <sup>2</sup> ) Thermal efficiency=48%; combined efficiency=51%	Energy saving= 500-1,000kWh/m <sup>2</sup> /year; PV power=18.5W; estimated 50-100kWh/m <sup>2</sup> /year of electricity generated	N.A	(Hollick, 1998)

#### **2.2.4.1 Literature review on heat transfer coefficient for transpired solar collector**

Due to present study involves investigation on heat transfer coefficients for the transpired solar collector, this section is included to review the previous researches and to address the research problem which related to current study.

Correlations of coefficient heat transfer between the air and the plate have been developed since 1980s. The study carried out by Sparrow and Carranco (Sparrow, 1982) examined the heat and mass transfer of the plate with different holes design by using naphthalene sublimation technique. They developed the  $Nu-Re-Pr$  relation for the heat transfer coefficient. However, the pitch-to-diameter ratios ( $Pit/d$ ) in their study are too small ( $\leq 2.5$ ) compared to a typical transpired plate solar collector where the ratio of  $Pit/d$  is close to 10 (Kutscher, 1994). In addition, the porosity and the Reynolds numbers in their study were very high and hence the correlation for the Nusselt number is not appropriate to be extrapolated for a transpired solar collector.

Andrews and Bazdidi-Tehrani (Andrews, 1989) found that the heat transfer coefficient agreed with Sparrow. They developed the  $Nu$  correlation for square arrays of holes and  $1.9 < Pit/d < 22$ . However the mass flow rate of  $0.1 < G < 1.7 \text{ kgm}^{-2}\text{s}^{-1}$  is very high for air heating purposes. Kutsher (Kutscher, 1992) has developed an empirical correlation of Nusselt number which is appropriate for thin transpired plates with porosity less than 2%, low suction flow rates and triangular hole arrays. To-date, this is the only study considering the porosity, hole diameter and crosswind conditions to reach the empirical correlation  $Nu$ . The correlation covers heat transfers from the front-of-plate, hole and back-of-plate but excludes the vertical airflow in the plenum. The author ignore heat transfer between the back surface and the vertical airflow because it is believed that the flow in plenum has little effect due to the injection effect on the back-of-plate side and the air laminarization induced by acceleration. The numerical results show that the heat transfer that occurs at the front surface

dominates heat transfer in the hole and on the back surface at suction flow rates of 0.02 to 0.07 kgm<sup>-2</sup>s<sup>-1</sup>. The crosswind data for the narrow transverse spacing are correlated as  $Nu=2.75[(Pit/d)^{-1.2}Re^{0.43}+0.011PRe(U_w/V_s)^{0.48}]$  with  $0.001 \leq P \leq 0.05$  and  $100 \leq Re \leq 200$  (Kutscher, 1994).

Arulanandam et.al (Arulanandam, 1999) study the  $Nu$  correlation for transpired plate with circular holes on a square pitch arrangement by using CFD (Computational Fluid Dynamics) simulations. The correlation of  $Nu$  is developed with assumptions including no-wind conditions and the exclusion of the effect of the heat transfer on the back-of-plate, too.

Apart from the development of the heat transfer coefficient correlation, Augustus and Kumar (Augustus, 2007) use the  $Nu$  developed by Kutscher (Kutscher, 1992) in their mathematical modelling to investigate the transpired solar collector thermal performance. The simulation study is also based on uniform airflow condition.

The above are the  $Nu$  correlations and thermal performance analysis that applicable to uniform flow. However, poor flow distribution occur in large building applications and this has been shown by infrared photographs (Dymond, 1997). The non-uniform airflow could result in two possibilities effects, e.g. heat transfer from the back-of-plate to the vertical flow in the plenum and the energy collected by the plate. in Gunnewiek et.al' study (Gunnewiek, 1996), results show that the former effect is significant while only modest effect on the latter case. The investigation has been carried out by using 2D CFD model to study the vertical direction airflow in the plenum. The transpiration of air through the plate is modelled as a process occurring through discrete holes. The collector height range is  $3.0 \leq H \leq 6.0$  m, and the plenum aspect ratio range is  $10 \leq H/D \leq 50$ . The range of  $U$ -value for the plate material is  $1.0 \leq U_o \leq 9.0$  Wm<sup>-2</sup>K<sup>-1</sup>. This represents the range from a non-selective surface plate to a selective surface. The range of volumetric flow rate drawn out of the top of the plenum by the fan is given in terms of the average suction velocity  $0.005 \leq v_s \leq 0.08$ m/s. The results show that different

settings of parameters yield different airflow profiles. The nature of the profile depends on whether the flow is dominated by buoyancy or by the forced-flow produced by the fan. When the flow is non-uniform, the code predicts that an important amount of heat transfer can take place from the back-of-plate to the vertical air in the plenum.

A computer program has been developed by Dymond and Kutscher (Dymond, 1997) to predict flow uniformity and efficiency on the basis of pipe networks concept (Figure 2-6). The studied range of plenum depth,  $D$  is between 5 and 30cm. A collector with single exit at the top center shows that the face velocity in front of the exit is the highest and decreases dramatically when it is further away from the exit. This is due to the areas of the top left and right corners of the collector have higher pressure drop and hence result in flow starvation. Area where the face velocity is higher shows lower surface temperature because of better heat transferred away from the collector to the air, which also gives higher efficiency. Though the results show the non-uniform of the airflow over the collector surface is possible, the effects of the non-uniformity flow on the vertical airflow are not included in this study due to the absence of the heat transfer correlation between the back-of-plate and the vertical airflow.

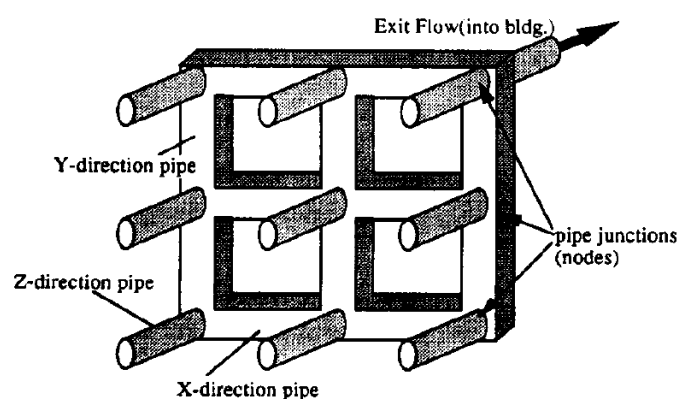


Figure 2-6. The pipe network concept (Dymond, 1997).

In summary,  $Nu$  correlations have been developed by researchers based on uniform flow distribution (Andrews, 1989; Arulanandam, 1999; Kutscher,

1992; Sparrow, 1982). However, research by Dymond and Kutscher (Dymond, 1997) has shown that non-uniformity flow might occur, and Gunnewiek et. al (Gunnewiek, 1996) simulated that for non-uniform flow, heat transfer from the back-of-plate to the plenum air could occur if the buoyancy flow is dominated. Both findings indicate that the effects of the airflow uniformity on the transpired plate thermal performance are crucial. If the flow is non-uniform, the air temperature in the plenum might not constant throughout the plenum and hence the correlation developed by Kutshcer (Kutscher, 1992), which is based on uniform flow might inappropriate to apply in this regards. Furthermore, in practice it is a challenge to maintain a very uniform flow distribution. Local pressure drops need to be measured to ensure the uniformity of the flow distribution. In present study, an alternative way to establish the heat transfer concept was developed and it is further discussed in Chapter 4.

#### **2.2.5 Solar Roof**

Methods of passive cooling by roof are such as water firm, roof pond, roof garden and thermal insulation. Solar roof ventilation may perform better than Trombe wall design in climates where the solar altitude is large. This is because roof collectors provide larger surface area to collect the solar energy and hence higher air exit temperature (Awbi, 1998). Nevertheless, Khedari et al. (2000) observed that with only roof solar collector system, there is little potential to satisfy room thermal comfort. Additional device such as Trombe wall to be used together with roof solar collector would provide better cooling effect especially in hot climate. Dimoudi et al. (2006a, b) studied the thermal performance of the ventilated roof during summer and winter. The ventilated roof component consisted of reinforced concrete slab and insulation layer as the typical component but with an air gap between the insulation and the upper prefabricated slab. Results show that there is no clear improvement of the thermal performance during the winter period but during the summer period, the building is protected from the solar gains due to

the insulation properties. On the other hand, Zhai et al. (2005) reported that the efficiency of double pass of air gap is able to induce more air change rate and hence is generally 10% higher than that of single pass roof solar collector. Roof-integrated water solar collector that made of several layers of glass followed by water chamber and metallic sheet at the bottom was developed by Juanico (2008) and could be used for domestic heating and cooling systems.

### **2.3 Existing passive solar cooling via evaporative effect**

Evaporative cooling is the oldest technique of cooling and may be applied in both active and passive systems. Conventional mechanical cooling systems that require high energy cost and harm the environmental have prompted the researchers to begin looking back at the evaporative technique and trying to improve its efficiency (Henning, 2007a). Hence it has been intensively used as evaporative cooler or heat exchanger in air-conditioning system. However, building integration of evaporative cooling is a potential field yet to be developed.

#### **2.3.1 Evaporative cooling**

Amer (2006) has found that among the passive cooling systems, evaporative cooling gives the best cooling effect, followed by solar chimney, which reduced inside air temperature by 9.6°C and 8.5°C respectively. Evaporative cooling process uses the evaporation of water to cool an air stream. Basically water absorbs heat from the air (surrounding) to evaporate into vapour. Thus, reduce the temperature of the air or surrounding. In Middle East wind towers were developed to scoop the cool wind into the building, which was made to pass over water cisterns to produce evaporative cooling and a feeling of freshness (Miyazaki, 2006). Evaporative cooling can be classified into direct and indirect evaporating cooling.

### **2.3.1.1 Direct evaporative cooling (DECC)**

The principle underlying direct evaporative cooling is the conversion of sensible heat to latent heat. The air is cooled when water in the air stream is evaporated. The water in the air stream is supplied and recirculated continuously so that the water is removed by the air and yield the cooling effect. Some of the sensible heat of the air is transferred to the water and becomes latent heat by evaporating some of the water. The latent heat follows the water vapor and diffuses into the air. Thus, the moisture of the supply air is increased after the process. During the intermediate seasons in hot dry climates, direct evaporative cooling can offer energy conservation opportunities. However, the increase of moisture into the air stream during the process reduces the cooling system efficiency. Cooling effect might not sufficient especially during the summertime and in region with very humid climate. Therefore, the incoming air is usually dehumidified by forcing it through a desiccant to improve the cooling efficiency (Daou, 2006; Fan, 2007; Florides, 2002; Henning, 2007b). Joudi and Mehdi (2000) introduced combination of membrane air-drying and evaporative cooling systems. The membrane constituted of hollow fibres, i.e. cellulose acetate and polysulfone. The selective membrane allowed for efficient separation of the water vapour from the air. The air was pre-treated (dried) by passing through the membrane before entering the evaporative cooling system and hence operated in drier air stream.

### **2.3.1.2 Indirect evaporative cooling (IEC)**

IEC involves heat exchange with another air stream. These two air streams are separated by a heat exchanging wall, where one side of the wall is wet and another is dry. The working air passes through the wet side, while the product air passes through the dry side. The wet side absorbs heat from the dry side by water evaporation and hence cools the dry side. The wet air stream involves latent heat while the dry air stream involves sensible heat. Therefore, no additional moisture is introduced into the product air.

### 2.3.2 Materials for evaporative cooling

Zhao et al. (2008) compared several heat and mass exchange materials for indirect evaporative cooling system. The materials included metals, fibres, ceramics, zeolite and carbon. It is found that, though fibre materials are relatively cheaper, wick attained metal materials are the most adequate for evaporative cooling; not only higher thermal conductivity but also easier to be cleaned and sterilised to avoid bacteria growth. On the other hand, Wanphen & Nagano (2009) studied the performance of roof materials on evaporative cooling effect and the results are summarised in Fig 2-7. Among the studied materials, siliceous shale which comprises of a high number of mesopores is found to have the greatest evaporation performance and it is the most effective material for keeping surface moisture from vapour adsorption. Due to the high absorption rate, this material is able to absorb more vapour during night time. The precipitation water that stored inside the porous layers of siliceous shale material evaporates and relatively releases more latent heat to the atmosphere during sunlight hours. In contrast, silica sand, volcanic ash and pebbles yield more sensible heat. Moreover, high evaporation rate of siliceous shale tends to cool down the surface temperature. As a result, siliceous shale is able to reduce the roof surface temperature up to 8.63°C as compared to mortar concrete.

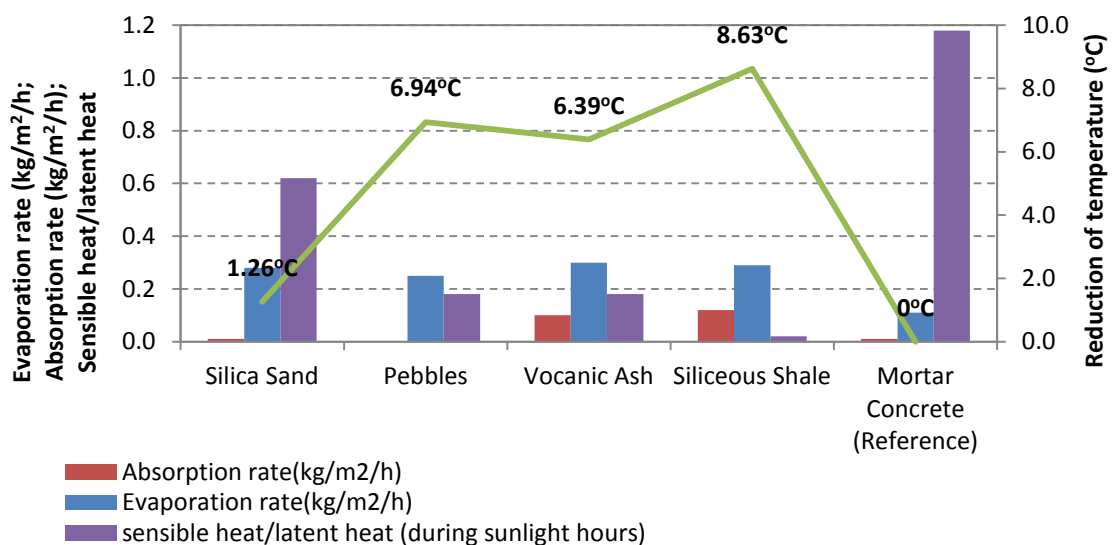


Figure 2-7. Performance of roof materials on evaporative cooling effect.

### **2.3.3 Building Integration of Evaporative Cooling**

#### **2.3.3.1 Roof integration**

One of the building integration applications of evaporative cooling is porous roof. During periods of precipitation, rainwater penetrates through the porous layer and is stored within the layer. The porous layer retains a significant amount of rainwater, which is released back into the atmosphere via evaporation during sunlight hours. When evaporation takes place, the surface temperature of the porous layer decreases due to the release of latent heat. Therefore, heat flux from the roof slab, which could raise the room temperature of the building, would also be reduced. When the air is at high humidity during night time or on cloudy days, the porous layer adsorbs moisture from the air and continues to cool the roof materials (Wanphen, 2009).

Raman et al. (2001) developed solar air heaters for solar passive designs that cooperated with evaporation for summer cooling. The system consisted of two solar air heaters with natural flow, i.e. on the roof and the ground. The roof air heater acted as an exhaust fan, venting out the air from the room during sunshine whereas the air heater on the ground was functioned as air heater during winter and as an indirect evaporative cooler during summer. However, the system performs well during winter but not for summer cooling. As a result, modifications were made whereby the south wall collector and a roof duct were wetted on the top side by an evaporative cooled surface were constructed. The results show that the modified system is able to give better thermal comfort for both seasons. On the other hand, Chungloo and Limmeechokchai (2007) carried out the studies by spraying water on the roof during partly and cloudy days under hot and humid climate in Thailand. They found that water spraying on metal ceiling is able to decrease indoor temperature. When the water is evaporated, the surface temperature of the roof is decreased and hence reduces the indoor temperature. The average ambient air temperature during the experiment period ranged from 33.7 to 35.0°C and the maximum temperature difference between

the ambient and the indoor air temperatures is 6°C. Furthermore, higher solar radiation and ambient temperature gives better performance.

Other researchers found that the reduction of heat flux by evaporation of a water film maintained over a roof has been found that it is more effective than a roof pond system in reducing cooling loads of the buildings (Sodha, 1980). A similar design, evapo-reflective roof for passive cooling for hot dry climates was studied by Cheikh and Bouchair (Cheikh, 2004). The roof was composed of a concrete ceiling and a flat aluminium plate separated by an air space partially filled with high thermal capacity rocks placed in a small quantity of water. Results show that this system manages to improve the cooling effect in buildings and the cooling can be enhanced by combining the system with night ventilation. For instance, at the hottest hour of the day, the cooling roof managed to reduce the room air temperature for about 6.8°C compared to the bare roof, and further reduced for nearly 1°C with night ventilation.

### **2.3.3.2 Facades integration**

Giabaklou and Ballinger (1996) demonstrated a passive evaporative cooling system by natural ventilation which can be installed on the facades, e.g. balcony for multi-storey residential buildings. The water falls vertically over filaments to form as a curtain, while the air flows through this water film horizontally and hence the evaporation. The cooling effect is able to satisfy the thermal comfort of the majority of the building's occupants (Ghiabaklou, 2003). Apart from that, passive evaporative cooling wall that was developed by He and Hoyano (He, 2010) was able to achieve the cooling efficiency at the maximum of 0.7. On the other hand, Maerefat and Haghghi (Maerefat, 2010) developed a natural ventilation system that combined solar chimney with evaporative cooling. The evaporative cooling effects took place in a cooling cavity, where the circulating water was sprayed at the top of the wall and hence formed a thin film on the wall surface. The air that passing through the cavity is then cooled by direct

evaporation process. The results show that this ventilation system is able to improve the indoor thermal comfort and it is suitable for countries with moderate and arid climates.

#### **2.4 Passive solar: Filling the gap of active solar technologies**

Proper design of orientation, structure, envelope, construction materials of a building is important to control the thermal loads from the solar heat gain, hence reduce the HVAC size, which in turn enhancing the feasibility of solar cooling technologies. Solar passive features might add 0 to 15% to design and construction costs (Cooperative Extension Service, 2006). However paying this initial cost in return is long life energy saving. For instance, the solar H.P. Co-operative Bank building in India demonstrated that solar passive designs with double glazing are able to reduce the total heat loss by about 35% (Chandel, 2008).

Apart from energy savings, passive solar designs are building integrated whereby facades or roofs are part of the heating or cooling system components. This in turn reduces initial cost. For instance, the unglazed transpired solar facade cost about 7 to 10 USD/ft<sup>2</sup>, plus installation (Specht); whereas a typical active solar water heater cost about 134 USD/ft<sup>2</sup> or 59 USD/ft<sup>2</sup> after incentives (Dymond, 2007).

Another advantage of passive solar designs is the function flexibility. Designs such as Trombe wall and solar chimney are able to provide warm air or create cooling effect depend on the climate needs by damper controllers. As compared to the active solar thermal technologies, the solar collectors are only meant for collecting heat. The heated air or water is either directly used by building occupants or to be used as heat source for heating or cooling systems. The combined heating and cooling systems require an additional system that not as simple as shifting the damper controllers.

## **2.5 Passive solar: Barriers**

Most of the passive solar technologies are natural air driven systems which are relatively more complex in predicting and guaranteeing the behaviour in actual climate conditions, compared to the active technologies (Abreu, 2011). The building owners hence may perceive that long-term benefits are uncertain if the additional investment is not reflected in re-sale values (IEA, 2008). Therefore, passive technologies need to be demonstrated through commercial or public buildings to promote the technologies and raise awareness of these technologies more widely.

## **2.6 Conclusions: The need of a combined heating and cooling system**

As pointed out by Abreu et al. (2011), there are great potential of future research and development in solar heating and cooling, which include overcoming the barriers of the technologies. Even though a lot of active and passive solar designs for heating and cooling have been developed, they generally have their own limitations. Active solar technologies need developments of smaller capacity, simpler, low cost and more maintenance and operational friendly systems (IEA, 2008). Whereas passive solar designs might not sufficient to provide indoor thermal comfort, particularly regions that have extreme climates.

The research areas that need to be carried out to improve the existing solar technologies performance and market acceptance are the system efficiency, architectural aesthetic, and cost effectiveness aspects. They in fact have been carried out intensively. Otherwise, research on development of a combination system could be an alternative. Studied done by Probst et al. (2007) suggested that solar collector should be conceived as part of a construction system which is providing active and passive solar benefits, flexible enough to interface with the other building elements and able to adapt to different buildings. As illustrated in Figure 2-8, combination of heating and cooling systems is able to harness the solar energy throughout the year in countries with hot and cold seasons, whereas

hybrid of solar active and passive technologies would improve the system efficiency and cost effectiveness. Hence, limitations of the technologies are overcome by each other's advantages and making the overall solar heating and cooling system feasible, more marketable and increase the public acceptance.

Therefore, the aim of present research is to develop a combined heating and cooling system that integrates the active and passive solar features. The design of present research adopts the passive solar features in heating and cooling the air through building facades and cavities that similar to Trombe wall design. In contrast, the active features are the low cost unglazed aluminium plate to be used as the solar collector and fan-driven system is chosen instead of fully natural ventilation.

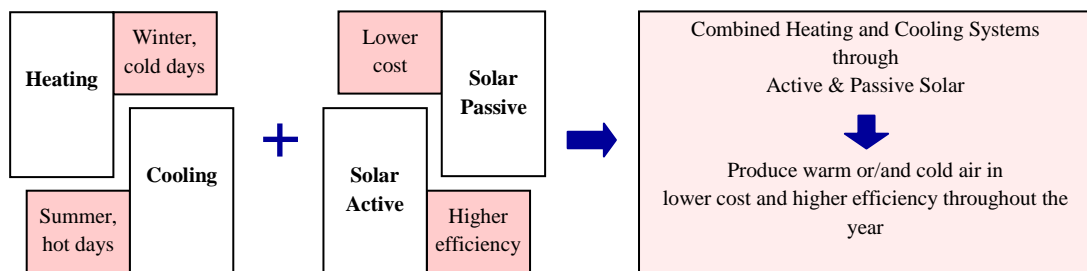


Figure 2-8. Overcoming the limitations by combining heating and cooling systems, and the solar active and passive technologies.

## **3. Methodology**

### **3.1 Introduction**

This chapter describes the methodologies for the research investigations. Contents include the general concepts, modelling and experimental steps. Methods and sensor calibrations for the parameters measurement are explained, too. However, the detailed explanations of concept and model equations for the specific system design will not be included until the following Chapters, i.e. 4 and 5.

### **3.2 Overview of methodology approach**

The solar façade for a combined heating and cooling system is based on the concept of heating or cooling the plenum air through heat transfer (Figure 3-1), whereby the outlet air can be supplied as either warm or cold air into the building. The research development is as shown in Figure 3-2. The research investigations can be divided into two systems, i.e. the heating and the cooling. The investigations began with a heating system where two types of plate were used: flat and transpired plates. These heating systems both consist of a single plenum (Plenum 1 in Figure 3-1) and a dry sandtile wall. On the other hand, two different designs for the cooling systems were investigated: one with a single plenum and the other with two plenums. Both systems were operated with a wet sandtile wall. The façade of the former system was a flat plate, while the latter was the transpired type. For the system using two plenums, Plenum 1 was the earlier examined heating system and the Plenum 2 was mainly used to cool the air supply (Figure 3-1). All the investigations on the heating and cooling system performance were carried out by establishing mathematical models and then by conducting experimental examinations.

For the cooling system, investigation on flat plate with single plenum was carried out experimentally and because of its adverse results, only simulation study was carried out for the transpired plate with single plenum. This simulation results showed adverse results too. Thus the investigation was then followed by cooling system with two plenums. Due to the heating system with a transpired plate and cooling system with two plenums were found to have better performance, they were selected to be the combined heating and cooling system for the final investigation. The final investigation aimed to simulate the system performance by using London weather conditions for an office building. Therefore, by taking account that the UK climate needs more space heating than cooling, combination of flat plate with two plenums were not included in this study.

### **3.2.1 The heating systems**

The research methodologies for the investigation on the heating systems performance are as shown in Figure 3-3. The flat plate system started with establishment of a mathematical model and this was followed by experiments; while the transpired plate system started with experiments to develop the heat transfer correlation and these were adopted into the mathematical model. Next, parameter analyses were carried out for both systems and finally the thermal performances were compared with each other.

### **3.2.2 The cooling and the combined systems**

The methodology approaches for the cooling systems were the same as the heating system with flat plate (Figure 3-2). The investigations started with flat plate collector and single plenum. However, due to this design giving adverse results, the system design was modified to transpired plate with two plenums. This modified design was also the combined system that was used for the economical analysis.

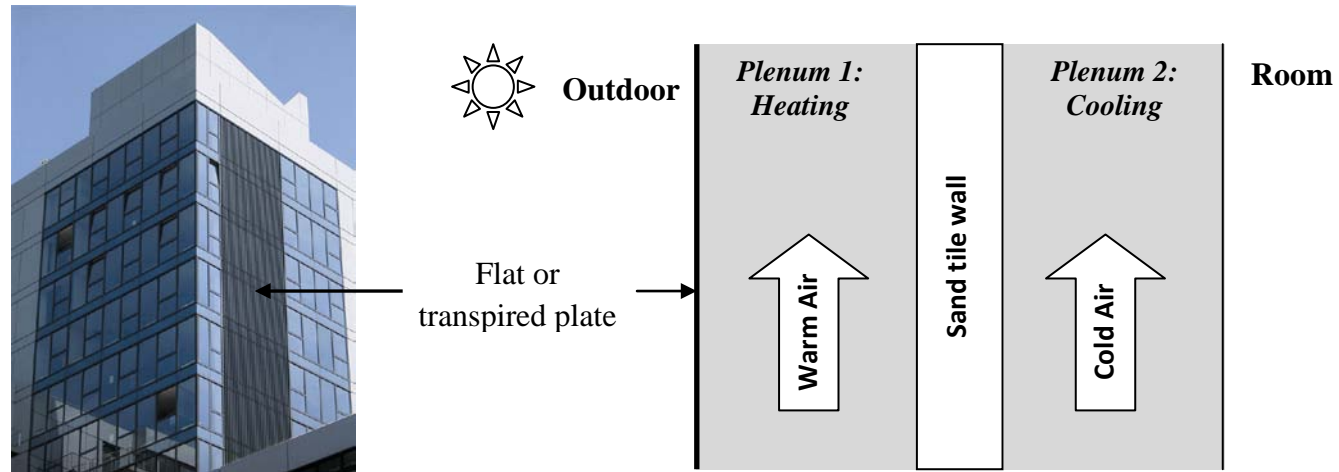


Figure 3-1. The concept of the solar facades.

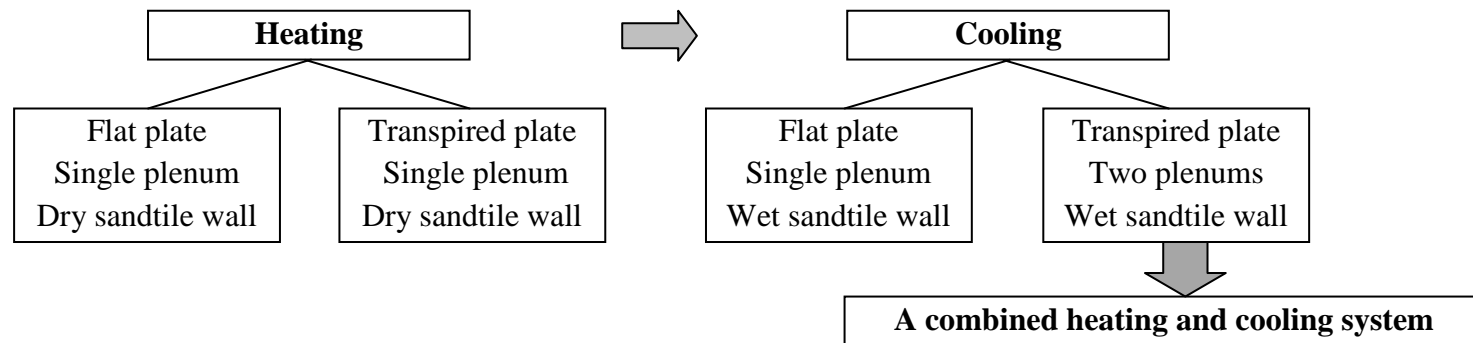


Figure 3-2. Development of a combined heating and cooling system.

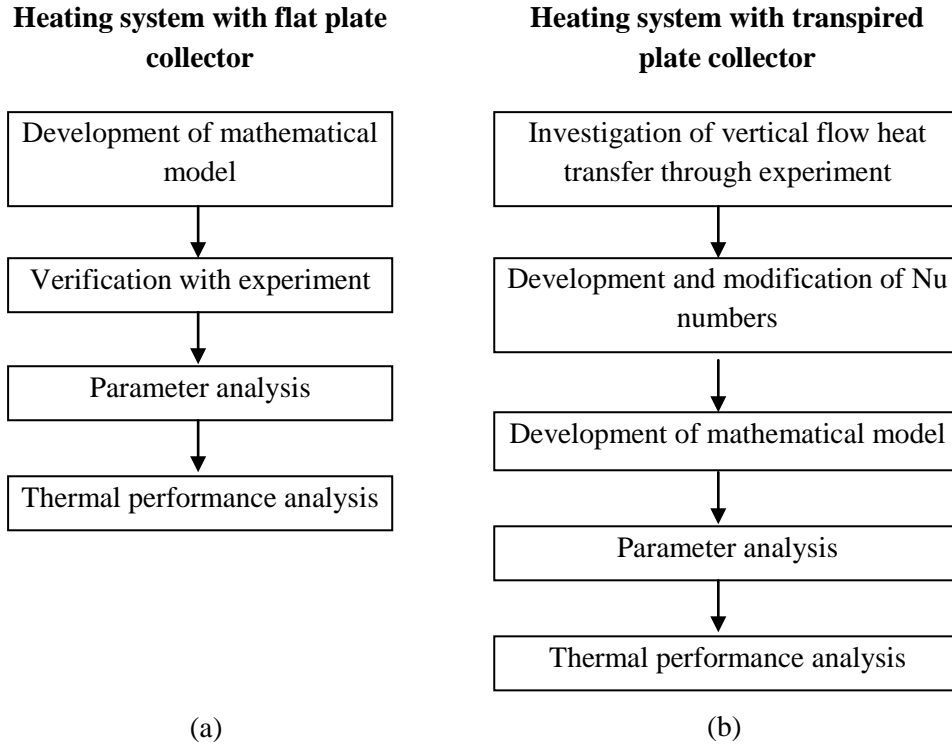


Figure 3-3. Methodology overviews of heating systems with (a) flat and (b) transpired plates.

### 3.3. Development of mathematical model

Both heating and cooling systems share common steps in this section. The models were developed from the establishment of energy balance equations. The detail descriptions of the energy balance equations are as discussed in Chapters 4 and 5 for heating and cooling respectively, however the heated and cooled air equations are as shown below:

i) Heated air with flat plate:

$$\dot{m}c_p(T_{out} - T_{in}) = I \alpha_p A_p - Q_c - Q_r$$

ii) Heated air with transpired plate:

$$\sum \dot{m}c_p(T_i - T_a) + \sum \dot{m}c_p(T_{out} - T_i) = I \alpha_p A_p - Q_{rad,p-sur}$$

iii) Cooled air:

$$\dot{m}_s c_{p,s} (T_{in,s} - T_{out,s}) = Q_{conv,s,air-wall}$$

The main purpose of the models was to investigate the temperature of the plates and air, and hence the system efficiencies. Therefore, the temperature equations were obtained by rewriting the energy balance equations in a matrix form, and solved by the matrix inversion method. The matrix algorithm was carried out using the MATLAB programme, the commands of which are as attached in Appendix II. Figure 3-4 shows the flow chart of the algorithm process, whereby the temperatures were solved iteratively. The process started with initiating the values of the variables i.e. the temperatures. The determined temperatures were then used for repeating the calculation cycle. This step was repeated until a convergence was reached, i.e. temperature difference between successive iterative was less than  $10^{-6}$ . Then, the calculated temperatures were substituted into the energy balance equations. The differences between the left and right hand sides of the equations should give values less than  $10^{-3}$ . This step was to check the accuracy of both the calculated temperatures and the matrix equations.

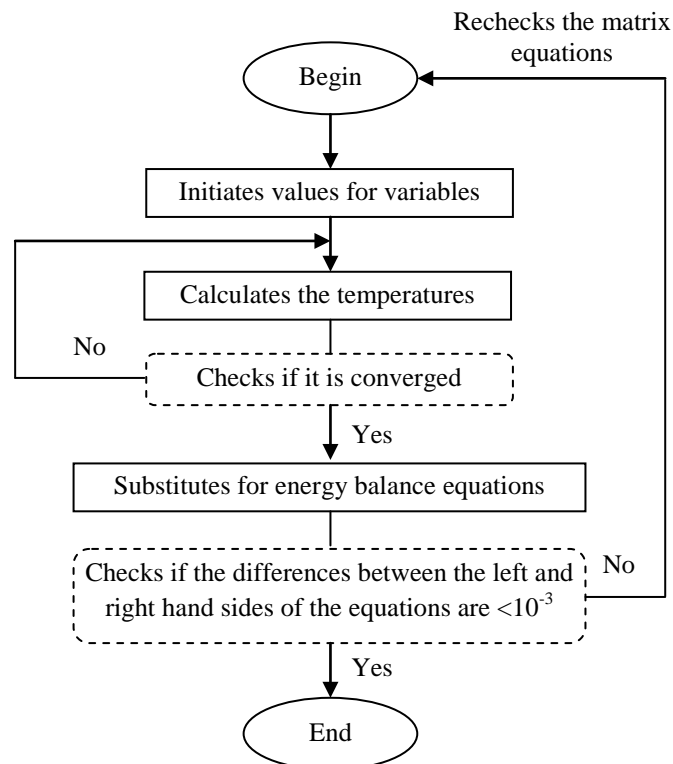


Figure 3-4. Matrix algorithm of the mathematical model.

### 3.4 Experiment set up

#### 3.4.1 The heating systems

The main materials of the solar façades were the aluminium plates and the sandtiles, and they are as shown in Figure 3-5. The physical properties of the aluminium are as shown in Table 3-1. Although the thermal conductivity of aluminium is only about 55% of copper (Forsythe, 2003), it has better corrosion-resistant characteristic. Table 3-2 shows the corrosion rates of some selected metals in different types of atmosphere.

Table 3-1. Physical properties of aluminium (Forsythe, 2003).

Density at 20°C (gcm <sup>-3</sup> )	Melting point (°C)	Latent heat of fusion (calg <sup>-1</sup> )	Coefficient of linear thermal expansion (°C x 10 <sup>6</sup> )	Thermal conductivity (Wcm <sup>-2</sup> )	Modulus of elasticity (kgmm <sup>-2</sup> )	Tensile strength (kgmm <sup>-2</sup> )
2.70	660.1	93	22.9	2.18	7250	6.3

Table 3-2. Approximate corrosion rates of some selected metals in different atmosphere (Mattsson, 2001).

Type of atmosphere	Corrosion rate (µm/year)			
	Aluminium	Copper	Steel	Zinc
Rural	<0.1	<1	5-10	0.5-1
Marine	0.4-0.6	1-2	10-30	0.5-2
Urban or industrial	~1	1-3	10-60	1-10

For the experiment set up, a chamber was built inside a laboratory (Figure 3-6). Both flat and transpired plate collectors shared the same set up. Figure 3-7 illustrates the schematic view of the experimental set up. The plate was attached with three other solid walls to form a plenum. Both plates were made from a black painted aluminium sheet with 2m in height, 1m in width, and 0.001m in thickness. The flat plate was a plate without hole, while the transpired plate had holes. The porosity (ratio of hole area to total surface area) of the transpired plate was 0.84%, with a circular hole diameter of 0.0012m, a pitch distance of 0.012m in triangular geometry. Due to the availability constraint of the plate

porosity in the market, 0.84% is selected based on the justification of it falls between the study range of previous study (Kutscher, 1994). The sandtile wall was made of eight sandtile blocks with dimensions of 0.25m x 0.25m x 0.055m for each single block. The thermal conductivity of the sandtile material is  $1.07\text{Wm}^{-1}\text{K}^{-1}$ , with porosity of 10.7% and density of  $204\text{kgm}^{-3}$ . Whereas the other two adjunction walls attached to both aluminium plate and sandtile wall were rigid polyisocyanurate foam boards with glassfibre 0.07m in thickness and with a conductivity of  $0.023\text{Wm}^{-1}\text{K}^{-1}$ . The dimensions of openings at the bottom and the top of the plenum were 0.167m x 1.0m and 0.23m x 1.0m respectively. In addition, two fans were installed at the air outlet., The ratio of height to depth of the cavity (H/D) that were chosen in studies which had the similar design to present study ranged from 1 to 200 (Gunnewiek, 1996, Gunnewiek, 2002, Gan, 2006, Zamora, 2006, Gan, 2011). Furthermore, Zamora and Kaiser (2009) found that the mass flow rate of the air increased with the values of H/D between 5 to 10 and reach the maximum point near to 10. Hence, the ratios of H/D ranged from 6 to 10 were chosen in this study, and the depth of the channel (D) was adjusted accordingly from 0.20m to 0.30m. In terms of sensors, nine K-type calibrated thermocouples (see section 3.6.1) were placed on each aluminium plate, the plenum and the sandtile wall, as shown in Figure 3-8 and Table 3-3. The locations of thermocouples between the wall and the plate (the plenum) were in line with the thermocouples on the sandtile wall. The thermocouples were then connected to a computer-controlled data logger.

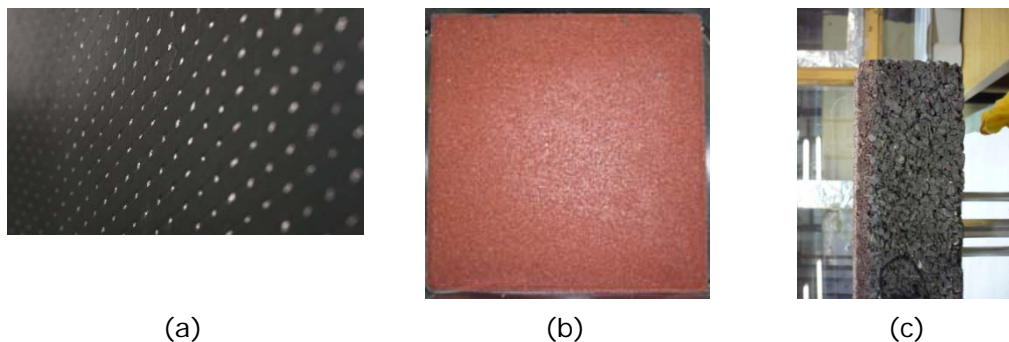


Figure 3-5. Pictures of (a) the black painted aluminium transpired plate, (b) the front, and (c) side views of the sandtile.



Figure 3-6. Laboratory test rig.

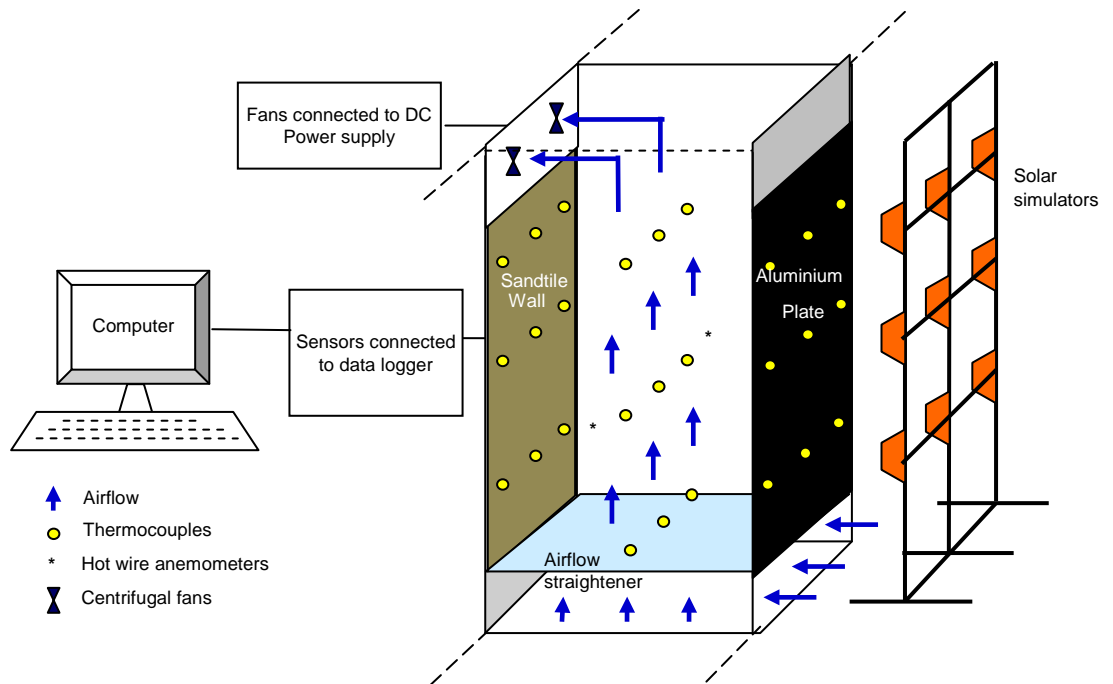


Figure 3-7. Schematic view of experimental set up.

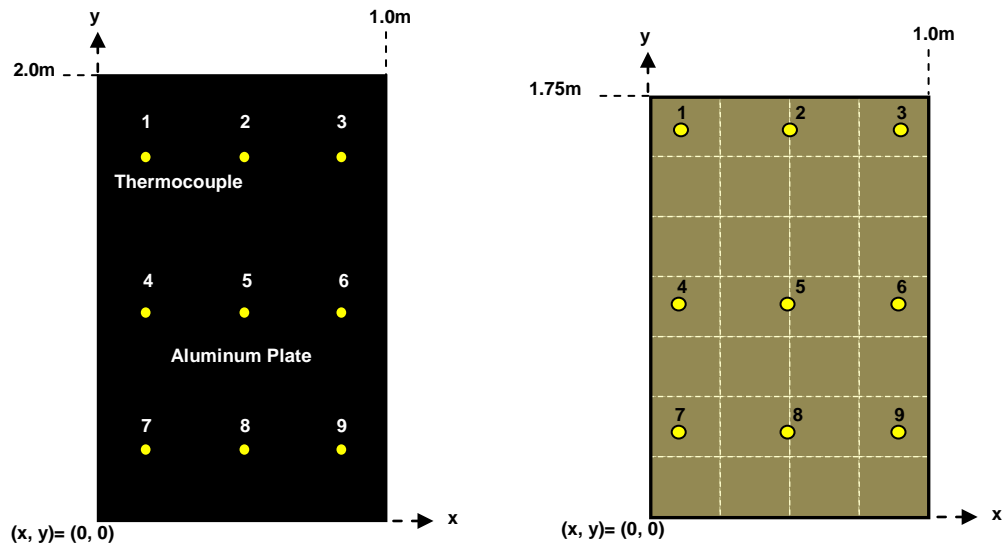


Figure 3-8. Thermocouples' location on the plate and sandtile wall.

Table 3-3. Locations of thermocouples on the plate and sandtile wall.

Thermocouple	Aluminium plate (x, y)	Sandtile wall (x,y)
1	(0.12, 1.85)	(0.12, 1.65)
2	(0.50, 1.85)	(0.50, 1.65)
3	(0.88, 1.85)	(0.88, 1.65)
4	(0.12, 1.00)	(0.12, 0.90)
5	(0.50, 1.00)	(0.50, 0.90)
6	(0.88, 1.00)	(0.88, 0.90)
7	(0.12, 0.15)	(0.12, 0.20)
8	(0.50, 0.15)	(0.50, 0.20)
9	(0.88, 0.15)	(0.88, 0.20)

The heating system with flat plate collector drew air from the opening at the bottom of the plenum and delivered the air into the room through the opening at the top of the plenum. In order to reach a steady state, temperatures were not recorded until two hours after the test began, when the constant temperatures were achieved. Temperatures were then taken every minute for the next 30 minutes. Air velocities were measured by hot wire anemometers at the centreline of the plenum and at the outlet of the plenum. Experiments were repeated for heating system with transpired plate collector by replacing the flat plate. In this case, the opening at the bottom was closed so that the air was

drawn through the holes and delivered into the room through the opening at the top of the plenum.

### 3.4.2 The cooling systems

The experiment set up and the testing steps were similar to the heating systems with. From the heating tests, it was found that the plenum depth of 0.20m gave the best performance for the flat plate system while 0.25m for the transpired plate (See Chapter 4). Thus, the plenum depths for the cooling systems were fixed at these optimum distances. In addition, for the cooling tests, water was pumped from a tank at the bottom of the plenum to the sandtile wall. This was a preliminary step in order to ensure the wall was saturated with water before the experiments were started. Nonetheless, for the cooling system with transpired plate, the experiment set up was modified from single plenum to two plenums and the schematic diagram is as shown in Figure 3-9. The depth of plenum 2 is set to be 0.20m. The air in the Plenum 1 was ducted out as exhaust air at the top whilst the air in plenum 2 was ducted into the chamber.

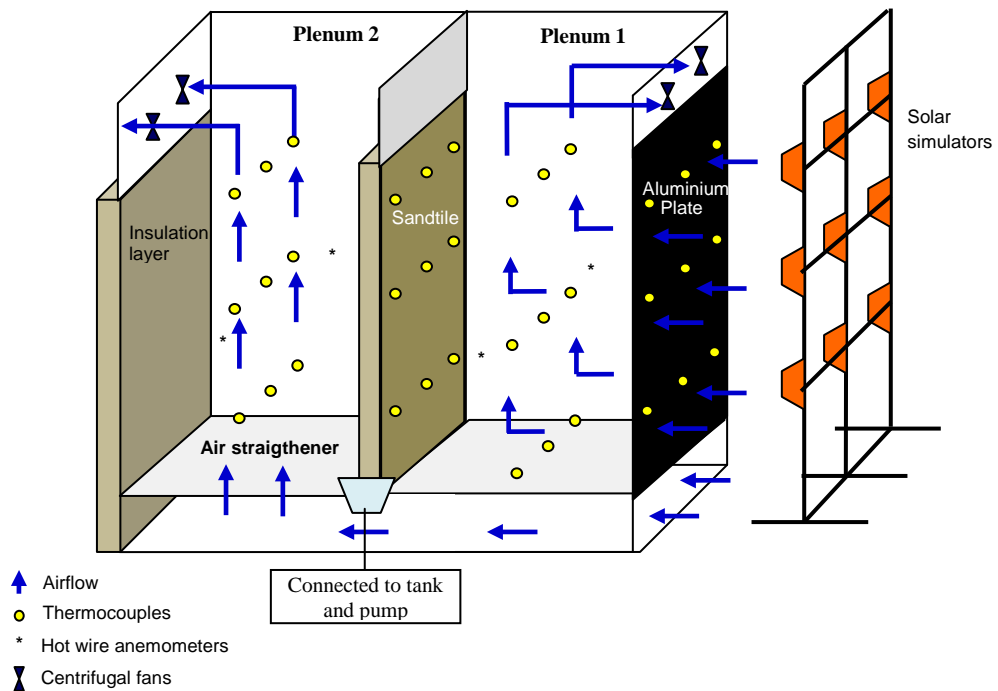


Figure 3-9. Schematic diagram of cooling system with transpired plate and two plenums.

### 3.5. Parameter measurements

#### 3.5.1 Air velocity

The hotwire anemometers that were used in this study are TSI 8455-300-1 as shown in Figure 3-10. The measuring range of the meters is between  $0.13$  to  $50.80\text{ms}^{-1}$  with accuracy of  $\pm 2\%$  at operating temperature of  $0$  to  $93^\circ\text{C}$ . The vertical airflow velocity in the plenum was measured at the centreline of the plenum with two hotwire anemometers, i.e. each  $0.30\text{m}$  from the left and the right of the plenum sidewalls (Figure 3-11).



Figure 3-10. The hotwire anemometer.

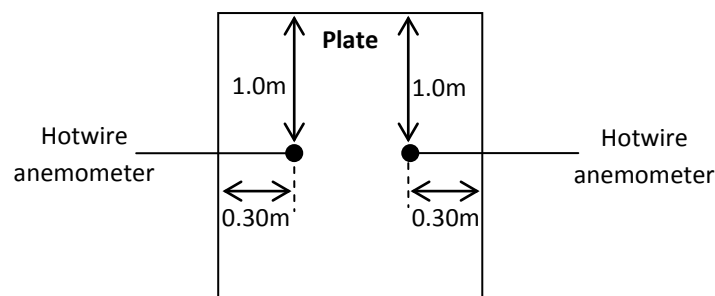


Figure 3-11. The hotwire anemometer measurement positions (front view).

#### 3.5.2 Mass flow rate

The mass flow rates of the systems were calculated by:

$$\dot{m} = vA_c\rho , \quad (3-1)$$

where  $v$  is airflow velocity in the outlet duct and  $A_c$  is the cross section area of the duct.

### 3.5.3. Solar radiation intensity

The solar radiation intensity was measured by using a CMP 6 pyranometer (Figure 3-12) and the specification is as stated in Table 3-4. The value of the intensity that was used for discussions was the average of intensities of eight points on the plate (Figure 3-13). The radiation intensities at each point were included in Appendix I.



Figure 3-12. Pyranometer for solar radiation measurement.

Table 3-4. Specification of the CMP6 pyranometer.

Spectral range	285 to 2800 nm
Sensitivity	12.09 $\mu\text{V}/\text{W}/\text{m}^2$
Temperature dependence of sensitivity (-10 °C to +40 °C)	< 4 %
Operating temperature range	-40 °C to +80 °C
Maximum solar irradiance	2000 $\text{W}/\text{m}^2$

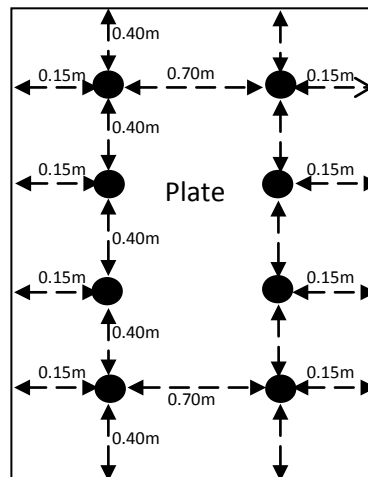


Figure 3-13. Measurement points of solar radiation intensities.

#### **3.5.4. Temperatures**

The value of surfaces and temperatures that were used for the discussions in future chapters were the mean temperatures of nine thermocouples on each surface or in the plenum. They are type-K thermocouples as shown in Figure 3-14.



Figure 3-14. Type-K Thermocouples.

#### **3.5.5. Water absorption and porosity studies of the sandtile**

The water absorption study was carried out to investigate the ability of the sandtile material in retaining the water. The sandtile was soaked in water and weighted for every 15 minutes until a constant weigh was achieved, when it was saturated. Figure 3-15 shows that the sandtile is saturated with water at 90min with cumulative inflow of about  $6.1\text{kgm}^{-2}$ . Thus, for the sandtile wall area of  $2\text{m}^2$  in present experiment set up would need about 12L of water to reach a saturation condition.

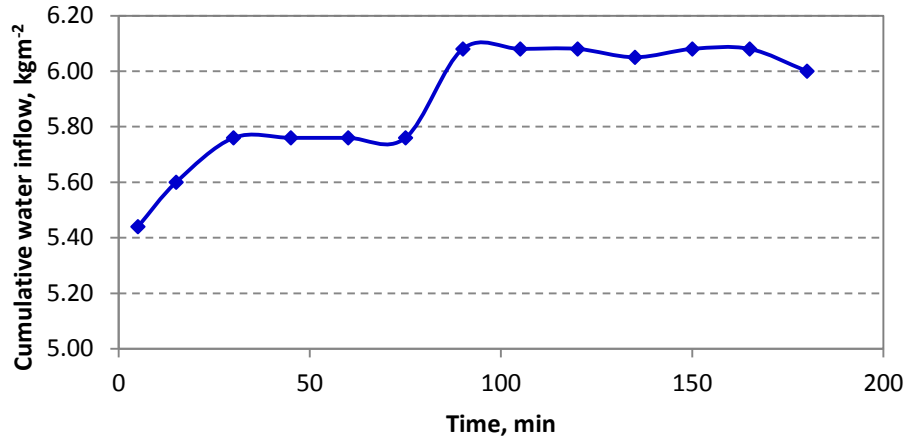


Figure 3-15. Water absorption of the sandtile.

On the other hand, the porosity of the sandtile was investigated by using the equation 3-2. It was found that the porosity of this sandtile material is about 10.67%.

$$\phi = (1/V_{st}) [(w_{sat} - w_{dry})/\rho_{water}]x100\% , \quad (3-2)$$

where  $w_{sat}$  and  $w_{dry}$  are the weighs of the sandtile when it is saturated with water and dry respectively,  $\rho_{water}$  is the water density, and  $V_{st}$  is the volume of the sandtile.

### 3.6. Calibrations of sensors

The sensors that were used in the heating and cooling experiments include thermocouples and humidity sensors. They were calibrated before the experiments are carried out.

#### 3.6.1. Thermocouples

The operating temperature range for the K-type thermocouples is -50 to 250 °C. They were calibrated with a mercury thermometer with accuracy of  $\pm 0.2^\circ\text{C}$ . The range of the calibration is 10 to 70 °C and the average readings are plotted in Figure 3-16. However, due to the temperature change in Plenum 2 for the cooling system is less than 1°C, six thermocouples i.e. T25 to T30 that were measuring

the air temperature were calibrated with a standard platinum resistance thermometer (PRT) which gives accuracy of  $\pm 0.001^{\circ}\text{C}$ . The TTI-7-R PRT from ISOTECH (Figure 3-17) is a precision thermometer that has high accuracy which is designed for laboratory and industrial temperature measurement and calibration applications. Table 3-5 describes the specifications of the PRT whereas Figures 3-18(a) to (f) show the calibration curves for the thermocouples.

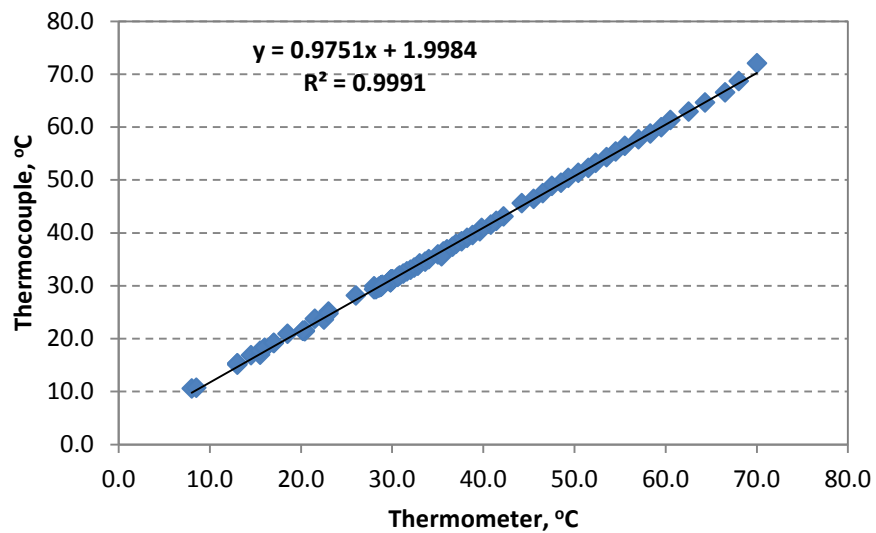


Figure 3-16. Calibration curve of thermocouples by using mercury thermometer as a reference.



Figure 3-17. The ISOTECH TTI-7-R PRT unit.

Table 3-5. Specification of ISOTECH TTI-7-R PRT.

Resistance measurement range	10 to 460 $\Omega$
Display resolution	0.001 $^{\circ}\text{C}$
Resistance measurement uncertainty	$\pm 2.5\text{m}\Omega @ +20^{\circ}\text{C} \pm 2^{\circ}\text{C}$
Temperature coefficient (resistance measurement)	$\pm (3\text{ppm of reading}/^{\circ}\text{C} + 0.5\text{m}\Omega / ^{\circ}\text{C})$
Long term stability (resistance measurement)	$\pm 10\text{ppm of reading} / \text{year}$
Temperature measurement uncertainty	Over - 190 to + 660 $^{\circ}\text{C} \pm 0.01^{\circ}\text{C}$
Measurement configuration	3 and 4 wire selectable
Sense current	0.5 mA (DC) polarity switchable
User selectable measurement display units	$^{\circ}\text{C} / ^{\circ}\text{F} / \text{K}$
Front panel connection	2 sets, 5 terminals
Input impedance	$>10\text{M}\Omega$
Max common and differential mode input voltage	$\pm 40\text{VDC}, 28\text{Vrms}$

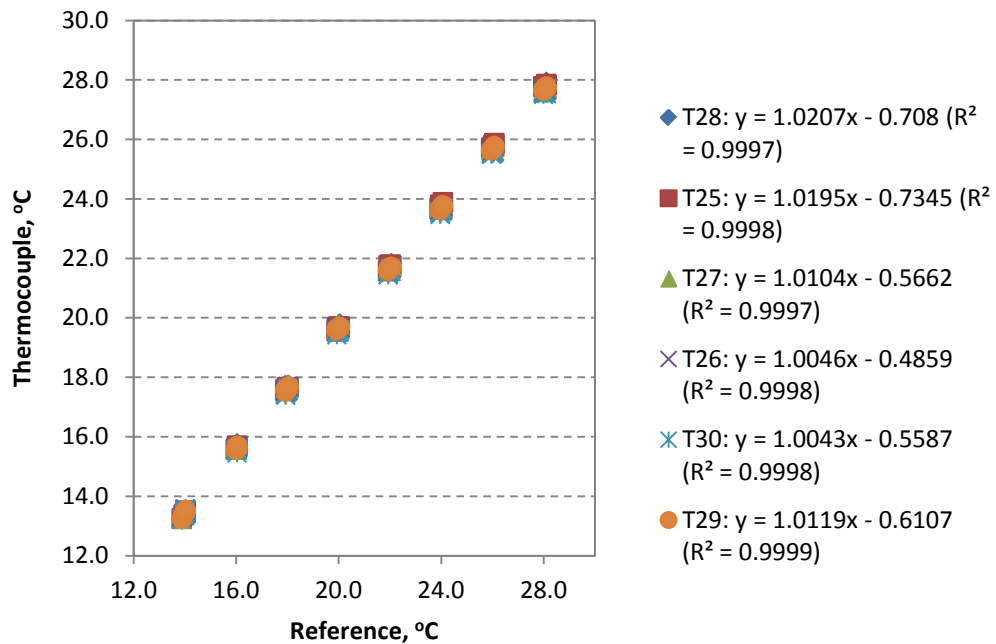


Figure 3-18. Calibration curves of T25, T26, T27, T28, T29 and T30 by using ISOTECH TTI-7-R PRT as a reference.

### 3.6.2. Humidity sensors

Two Vaisala HMP45A sensors (Figure 3-19) were used in the experiments, i.e. P1 and P2. The probes gave outputs of relative humidity (*RH*) and temperature. The technical data for the sensor is as described in Table 3-6. These two probes were calibrated separately. The probes together with dry and wet bulb thermometers were placed in an air-conditioner. Readings were taken by altering the volume of water intake of the air-conditioning system. Then, the reference *RH* values are read from a psychometric chart by using the dry and wet bulb temperatures from the thermometers. The *RH* and temperature values from the probes are compared with the reference *RH* values and dry bulb thermometer. The calibration curves of *RH* and temperature for each of the probes are as shown in Figures 3-20 and 3-21.



Figure 3-19. Vaisala HMP45A sensor.

Table 3-6. Technical data for Vaisala HMP45A sensor.

Technical parameters	Range
Operating temperature range, K	-313 to 333
Measurement range for relative humidity, %	0.8 to 100
Output scale of relative humidity	0 to 100 %RH equals 0 to 1VDC
Accuracy of relative humidity measurement	$\pm 2$ %RH (for 0 to 90 %RH) $\pm 3$ %RH (for 90 to 100 %RH)
Measurement range for temperature, K	-312.2 to 333
Output scale of temperature	-313 to 333K equals 0 to 1VDC
Accuracy of relative humidity measurement	$\pm 0.2$ K

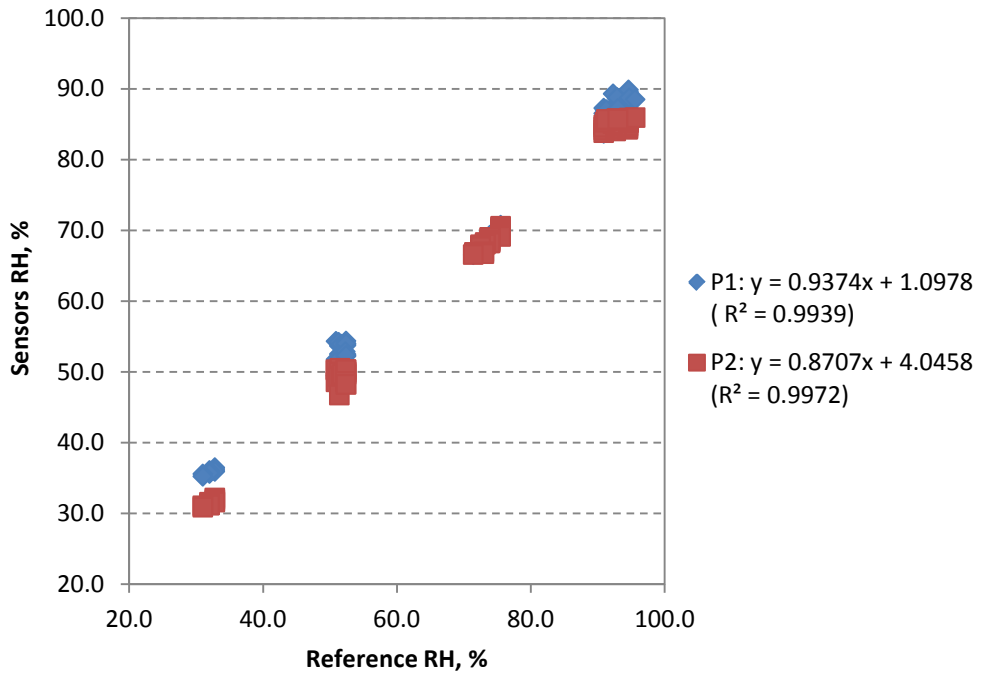


Figure 3-20. Calibration curves of P1 and P2 RH.

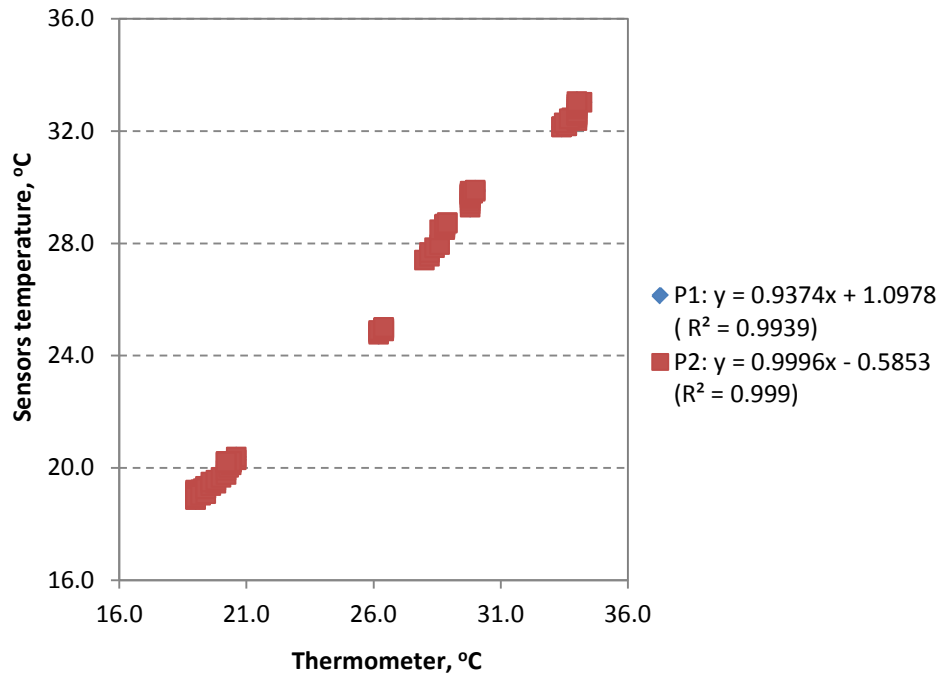


Figure 3-21. Calibration curves of P1 and P2 temperature.

### 3.7 Experimental percentage error

The values of system efficiency ( $\eta$ ) (Section 4.2.3.1) and ratio of heating to cooling effectiveness ( $Exh\_C/Exh\_H$ ) (Section 5.5.3.1) are chosen to validate the mathematical models for the heating and cooling systems respectively. The validations were done by comparing the results between the simulated and the measured. The average percentage errors of the sensors and instruments can be summarised in Table 3-7.

Table 3.7. The average percentage errors of the sensors and instruments.

Parameter (Study range)	Average percentage error (%)
Velocity (0.14-0.69ms <sup>-1</sup> )	±2.0
Length (0.2-1.0m) <sup>a</sup>	±0.5
Air temperature difference for heating system (2.0-4.0K) <sup>b</sup>	±13.3
Temperature difference for cooling system in Plenum 1 (4-18K) <sup>b</sup>	±3.6
Air temperature difference for cooling system in Plenum 2 (0.4-0.7K) <sup>c</sup>	±0.4
Temperature difference of ( $T_p - T_a$ ), (9.5-30.0K) <sup>b</sup>	±2.0
Temperature difference of ( $T_r - T_s$ ), (1.3-3.0K) <sup>d</sup>	±9.3
Solar radiation intensity (307-820Wm <sup>-2</sup> )	±0.2

<sup>a</sup>Cross section area of the measured velocity.

<sup>b</sup>The error of thermocouple is ±0.2°C. The percentage error of air temperature difference =  $\frac{\delta(T_1 - T_2)}{T_1 - T_2}$ , which the numerator is the total error of ( $T_1 - T_2$ ) = 0.2+0.2=0.4°C

<sup>c</sup>The error of thermocouple is ±0.001°C. The percentage error of air temperature difference =  $\frac{\delta(T_1 - T_2)}{T_2 - T_2}$ , which the numerator is the total error of ( $T_2 - T_2$ ) = 0.001+0.001=0.002°C

<sup>d</sup>The errors of thermocouples for  $T_r$  and  $T_s$  are ±0.2°C and ±0.001°C respectively. The percentage error of air temperature difference =  $\frac{\delta(T_1 - T_2)}{T_2 - T_2}$ , which the numerator is the total error of ( $T_2 - T_2$ ) = 0.2+0.001=0.201°C

According to Nelkon and Ogborn (1962), the values of percentage error of  $\eta$  and ( $Exh\_C/Exh\_H$ ) can be calculated by using Equations 3-3 and 3-4 respectively:

$$\eta = \frac{\sum \dot{m} c_p (T_{out} - T_a)}{IA_p}$$

Where  $\dot{m} = v * \text{cross section area} * \rho$

By neglecting the errors from the values of air properties and  $A_p$  (which were measured by the plate suppliers), the percentage error (multiplied by 100) for the heating system is hence:

$$\frac{\delta\eta}{\eta} = \pm \frac{\delta v}{v} \pm \frac{\delta(T_{out}-T_a)}{T_{out}-T_a} \mp \frac{\delta l}{l} \quad (3-3)$$

The maximum percentage error of heating system efficiency = +2.0+0.5+13.3+0.2=16.0%

Thus, the  $\eta = \eta_{measured} \pm 16.0\%$

For the cooling system,

$$\frac{Exh_c}{Exh_H} = \frac{(T_{s,in}-T_{s,out})/(T_r-T_{s,in})}{(T_{out}-T_a)/(T_p-T_a)}$$

Hence, 
$$\frac{\delta\left(\frac{Exh_c}{Exh_H}\right)}{\left(\frac{Exh_c}{Exh_H}\right)} = \pm \frac{\delta(T_{s,in}-T_{s,out})}{(T_{s,in}-T_{s,out})} \mp \frac{\delta(T_r-T_{s,in})}{(T_r-T_{s,in})} \mp \frac{\delta(T_{out}-T_a)}{(T_{out}-T_a)} \pm \frac{\delta(T_p-T_a)}{(T_p-T_a)} \quad (3-4)$$

The maximum percentage error of cooling system = +0.4+9.3+3.6+2.0=15.3%

Thus, the  $\frac{Exh_c}{Exh_H} = \left(\frac{Exh_c}{Exh_H}\right)_{measured} \pm 15.3\%$

### 3.8. Heat transfer at insulated sandtile wall

This section is to verify that the heat loss from the sandtile wall to the surface of the room is negligible. Figure 3-22 is the diagram of heat transfer of the wall from  $T_w$  to  $T_r$ . Thickness of sandtile wall ( $L_1$ ) and insulation layer ( $L_2$ ) were 0.055 and 0.070m respectively; and conductivity of sandtile wall ( $k_1$ ) and insulation layer ( $k_2$ ) were 1.07 and 0.023Wm<sup>-1</sup>K<sup>-1</sup> respectively (Bejan, 1993). The heat flux equation is as follows:

$$q_{loss,wall-room} = U_L(T_w - T_r) , \quad (3-5)$$

where  $U_L = 1/(L_1/k_1 + L_2/k_2)$

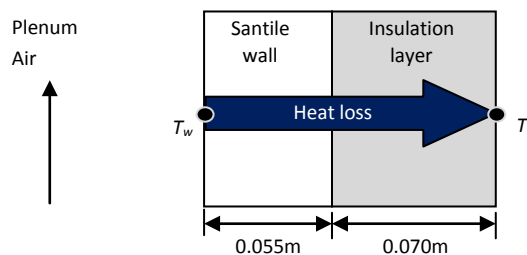


Figure 3-22. Heat transfer diagram of insulated sandtile wall.

Temperatures of  $T_w$  and  $T_r$  were measured through experiments and the heat losses were calculated. Results show that for all the experiments that were carried out, the heat losses were less than 0.5% of the total useful energy delivered for plenum depth of 0.20m, 0.25m and 0.30m (Figure 3-23). Thus, heat transfer at insulated sandtile wall is negligible. Therefore, here after, all the energy balance equations that involved with insulated sandtile wall will be ignored in the future chapters.

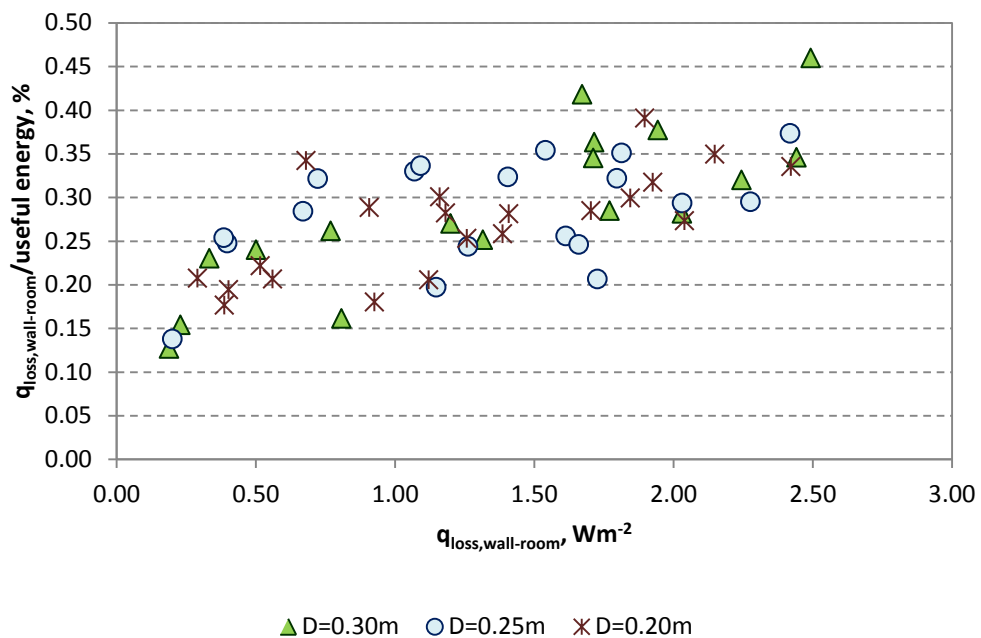


Figure 3-23. Percentage of heat loss to sandtile wall over total useful energy.

### 3.9 Summary

The general concepts, model and experiment steps for the heating and cooling systems are discussed. Methods and sensors calibrations for the parameters measurement are also been shown. Furthermore the heat transfer at the sandtile wall with the insulation layer has also been proved to be negligible.

## 4. Solar façade for space heating

### 4.1 Introduction

Two types of solar façades were selected in this study, i.e. flat and transpired plates. Figure 4-1 illustrates the side views of the heating systems. The plates were made of black painted aluminium sheets. They were used as solar collectors that absorb heat from the solar radiation. Thermal performances of these systems were investigated through mathematical models and experiment. The energy balance equations were established based on steady state one-dimensional heat transfer. In addition, heat transfer mechanisms including the thermal performance analyses for both designs were discussed separately in the sections 4.2 and 4.3. Besides the thermal performances, vertical flow heat transfer between the back-of-plate and the air in the plenum for the system with transpired plate was investigated, too. Finally in the section 4.4, the thermal performances between these two designs are compared.

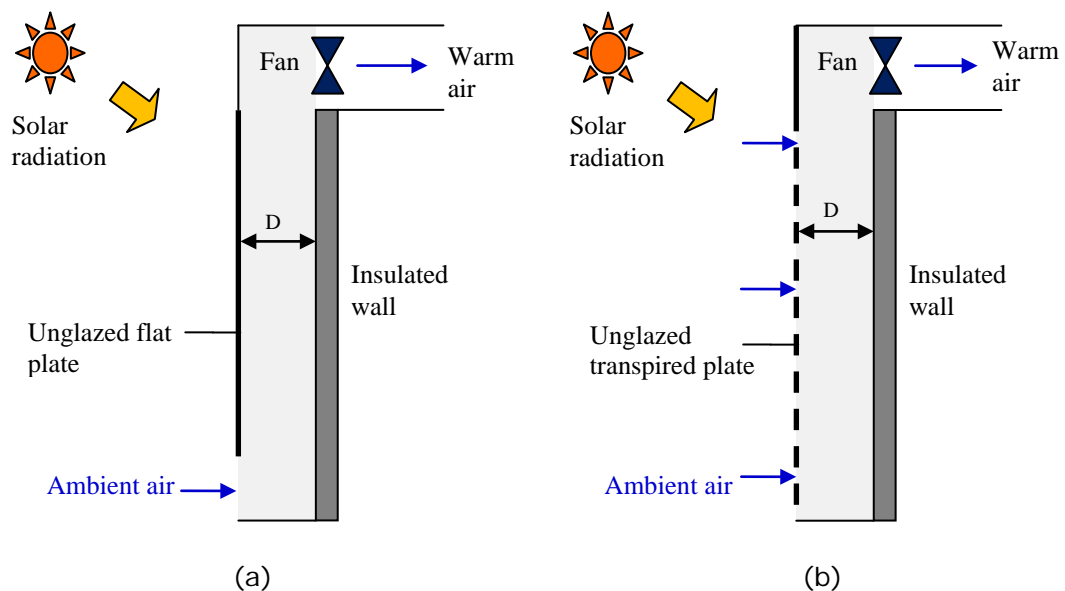


Figure 4-1. Side views of schematic diagrams of heating systems with unglazed a) flat and b) transpired plates as solar collector facades.

## 4.2 Heat transfer of flat plate solar façade

### 4.2.1 Assumptions of heating system with flat plate collector

Some assumptions have been made while developing the mathematical model.

They are as follows:

- i) The airflow rate is assumed to be constant throughout the plenum.
- ii) There is no heat loss through the sandtile wall and side walls that attached with the aluminium plate (Chapter 3).
- iii) All the measured temperatures that were used in the energy balance equations were assumed to be the constant temperatures after reaching the steady stage.

### 4.2.2 Energy balance equations for flat plate collector

Equation 4-1 shows the energy balance equations for the system under a steady state and the related parameters are as shown in Figure 4-2:

$$\dot{m}c_p(T_{out} - T_{in}) = I \alpha_p A_p - Q_c - Q_r \quad (4-1)$$

The left-hand side of this equation represents the useful energy collected. The first term on the right-hand side is the solar energy absorbed by the aluminium black plate. The second and third terms are the heat losses to the surrounding via radiation and convection respectively.

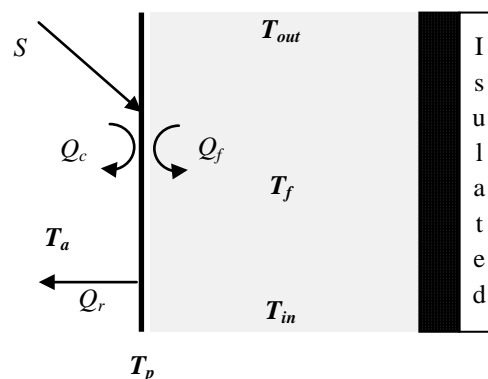


Figure 4-2. Heat transfer of flat plate solar façade.

**The flat plate:**

The fans-assisted system draws the ambient air through the opening at the bottom into the plenum. Energy balance equation of the plate is as shown in Equation 4-2.

$$I \propto_p A_p = Q_c + Q_f + Q_r \quad (4-2)$$

**The plenum air:**

The ambient air is heated by the back-of-plate while the air is flowing throughout the plenum. The energy balance equation of the air inside the plenum is shown in Equation 4-3.

$$\sum \dot{m} c_p (T_{out} - T_{in}) = Q_f \quad (4-3)$$

**4.2.2.1 Heat flux equations**

From the above equations, heat flux equations for the plate and plenum can be rewritten as:

**The flat plate:**

$$S = h_c(T_p - T_a) + h_f(T_p - T_f) + h_r(T_p - T_a), \quad (4-4)$$

where  $T_a = T_{in}$ , and  $S = I \propto_p$

**The plenum air:**

$$M(T_{out} - T_a) = h_f(T_p - T_f) , \quad (4-5)$$

where  $M = (\sum \dot{m} c_p) / A_p$  ;  $A_p = HL$ ;  $\dot{m} = \rho_f v_f DL$  ; and  $v_f = V_{fan} / DL$ ;  $T_f = (T_{out} + T_{in}) / 2$

**4.2.2.2. Mean temperature matrix**

Equations 4-4 and 4-5 can be simplified to Equations 4-6 and 4-7 respectively, and form a 2x2 matrix equation (4-8) as follows:

$$(h_c + h_f + h_r)T_p - h_f T_f = S + h_c T_a + h_r T_a \quad (4-6)$$

$$h_f T_p - (h_f + 2M) T_f = -2MT_a \quad (4-7)$$

$$\begin{bmatrix} h_c + h_f + h_r & -h_f \\ h_f & -(h_f + 2M) \end{bmatrix} \begin{bmatrix} T_p \\ T_f \end{bmatrix} = \begin{bmatrix} S + h_c T_a + h_r T_a \\ -2MT_a \end{bmatrix} \quad (4-8)$$

Hence, rewrite the Equation 4-8 by using matrix inversion method,

$$\begin{bmatrix} T_p \\ T_f \end{bmatrix} = \begin{bmatrix} h_c + h_f + h_r & -h_f \\ h_f & -(h_f + 2M) \end{bmatrix}^{-1} \begin{bmatrix} S + h_c T_a + h_r T_a \\ -2MT_a \end{bmatrix} \quad (4-9)$$

Equation 4-9 is then solved by iteration method and the iteration process is continued until the convergence value is smaller than  $10^{-6}$ .

#### 4.2.2.3. Heat transfer coefficients

##### ***The radiation heat transfer coefficient***

The radiation coefficient is given in Equation 4-11 where the emissivity ( $\epsilon_p$ ) of black paint is taken as 0.95 (Incropera, 2002).

$$q_r = h_r (T_p - T_a) = \sigma \epsilon_p (T_p^4 - T_a^4) \quad (4-10)$$

$$h_r = \sigma \epsilon_p (T_p + T_a) (T_p^2 + T_a^2) \quad (4-11)$$

##### ***The convection heat transfer coefficient from the plate to the ambient***

The natural convection heat transfer coefficient from the plate to the ambient air is as shown in Equations 4-12, where for turbulent flow and  $Pr$  values near to 1.0, correlation between the average  $Nu_{c,flat}$  and the  $Ra > 10^9$  are given as Equation 4-13 (Jaluria, 2003):

$$h_c = Nu_{c,flat} k_f / H \quad (4-12)$$

$$Nu_{c,flat} = \left\{ 0.825 + \frac{0.387 Ra^{1/6}}{\left[ 1 + \left( \frac{0.492}{Pr} \right)^{9/16} \right]^{8/27}} \right\}^2 \quad (4-13)$$

and 
$$Ra = 9.807 \beta H^3 (T_p - T_a) / \kappa_f \nu_f \quad (4-14)$$

##### ***The heat transfer coefficient from back-of-plate to the air in the plenum***

The coefficient is correlated with the  $Nu_{f,flat}$  as follows:

$$h_{f,flat} = Nu_{f,flat} k_f / H \quad (4-15)$$

Where

$$Nu_{f,flat} = 0.664 Re_{f,flat}^{1/2} Pr^{1/3}$$

Plenum geometry with air gap dimension (D) over 10 cm and air velocity lower than  $0.5\text{ms}^{-1}$ , the free convection proportion cannot be neglected even with fan-driven forced ventilation. It should be treated as mixed convection condition, which the  $Re_{f,flat}$  should consist both from free and forced convections (Equation 4-16) (Eicker, 2003).

$$Re_{f,flat} = \sqrt{Re_{free}^2 + Re_{forced}^2} \quad (4-16)$$

where  $Re_{free} = \sqrt{Gr/2.5}$ ,  $Gr = g\beta H^3(T_f - (T_p + T_w)/2)/\nu_f$ , and  $Re_{forced} = v_f \rho_f H / \mu_f$ .

Due to the fact that the maximum air velocity for present study was  $0.69\text{ms}^{-1}$ , the flows are treated as laminar modes ( $Re < 2 \times 10^5$ ) for all the operation conditions of experiments. In addition, the air velocity in the plenum was measured at  $D/2$  and hence the measured velocity was the maximum velocity for laminar flow. The mean plenum air velocity can be calculated by using Equation 4-17. For flow between two parallel plates (Nakayama, 2000),

$$v_f = (1/1.5)v_{max} \quad (4-17)$$

### **Solar radiation**

The solar radiation intensity that absorbed by the plate is given as below where the absorptivity ( $\alpha_p$ ) for black paint is taken as 0.95 (ASHRAE, 2009):

$$S = I\alpha_p \quad (4-18)$$

### **System efficiency**

The efficiency of the heating system is the ratio of the useful energy delivered to the total solar energy input on the plate, and it is given as:

$$\eta = \sum \dot{m} c_p (T_{out} - T_a) / (IA_p) \quad (4-19)$$

### **Percent difference**

Let  $x_1$  and  $x_2$  be the values taken from the model and experiment respectively, and the percent difference is calculated as:

$$\text{Percent difference} = \left| \frac{x_1 - x_2}{(x_1 + x_2)/2} \right| \times 100\% \quad (4-20)$$

### **Physical properties of air**

The physical properties of air are calculated by using linear interpolation for air properties between 300K and 350K (Incropera, 2002).

$$k_f = (0.0782T_f + 2.64) \times 10^{-3} \text{ W/mK}$$

$$\kappa_f = (0.14T_f - 18.62) \times 10^{-6} \text{ m}^2/\text{s}$$

$$\nu_f = (0.0942T_f - 11.822) \times 10^{-6} \text{ m}^2/\text{s}$$

$$\mu_f = (0.4876T_f + 36.72) \times 10^{-7} \text{ Ns/m}^2$$

$$\rho_f = (-0.0047T_f + 2.5612) \text{ kg/m}^3$$

$$c_{p_f} = (2 \times 10^{-5}T_f + 1.001) \times 10^3 \text{ J/kgK}$$

$$Pr = 0.72$$

### **4.2.3. Results and analysis of flat plate collector**

The experiment set up is as described in Chapter 3. The experiments were carried out with operation conditions as described in Table 4-1. In this section, the modelling results are compared to the experiments and followed by parametric analysis. Parts of the results are selected for discussions, however the complete sets of measured data can be found in Appendix III-1.

Table 4-1 Parameters for the experiments of flat plate for heating system.

Parameter	Value/ range
Solar radiation intensity ( $I$ ), $\text{Wm}^{-2}$	300-800
Volume airflow rate ( $V_{fan}$ ), $\text{m}^3\text{hr}^{-1}$	67-331
Plenum depth ( $D$ ), m	0.20-0.30
Height of the flat plate ( $H$ ), m	2.0
Width of the flat plate ( $L$ ), m	1.0
Area of the flat plate ( $A_p$ ), $\text{m}^2$	2.0
Plate thickness, m	0.001

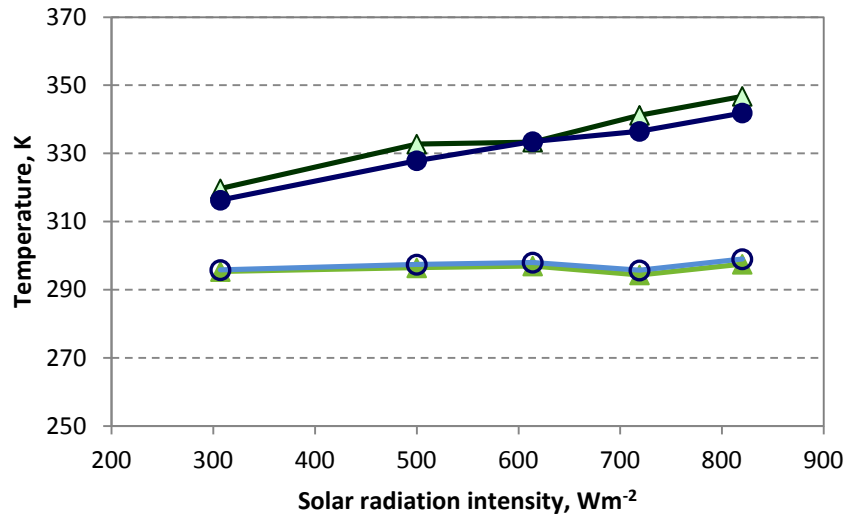
#### 4.2.3.1 Results comparison between the model and experiment for the flat plate

The purpose in this section is to validate the mathematical model by comparing the results with the experiment measurements. Thus, the discussion is focused on the differences of temperatures between the simulated and measured; and arguments related to parametric analysis are discussed in next sections.

##### ***Comparison over different solar radiation intensities***

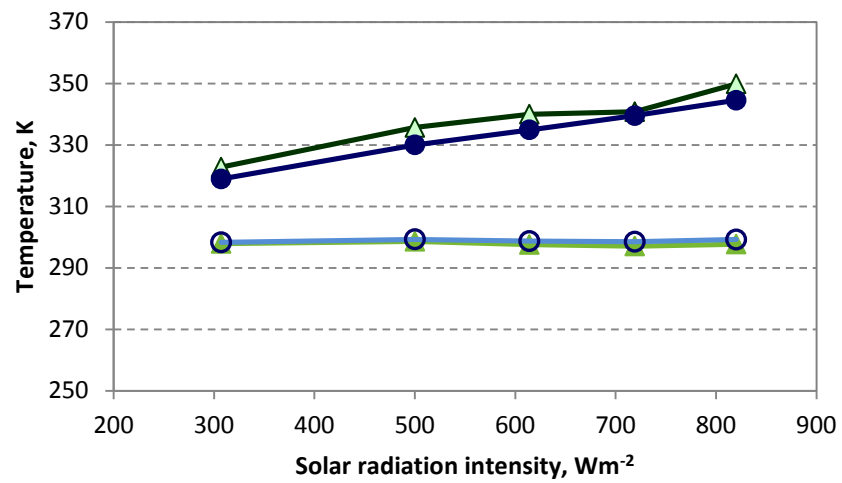
Figure 4-3(a), (b) and (c) are temperature comparisons between the model and the experiments for plenum depths of 0.20m, 0.25m and 0.30m respectively. The tests were carried out at a constant airflow rate of  $200\text{m}^3\text{hr}^{-1}$  over solar radiation intensity ranged from 307 to  $820\text{Wm}^{-2}$ . Both the modelled and experiment results show the same temperature patterns of plate and air temperatures. The plate temperature difference between the model and measured ranges from 0.1 to 5.6K with an average value of 3.7K. Whereas for the  $T_f$ , the temperature difference ranges from 0.2 to 1.5K with an average value of 0.3K. Nonetheless, in terms of system efficiency (Figure 4-4), they show close results with the maximum difference of efficiency at the point of  $719\text{Wm}^{-2}$  with plenum depth of 0.25m. The modelled and measured efficiencies are 0.17 and 0.15 respectively. As the experimental percentage error is calculated as  $\pm 16\%$  of

the measured efficiency (Section 3.7), the modelled results fall between the acceptance range (0.13 to 0.17).



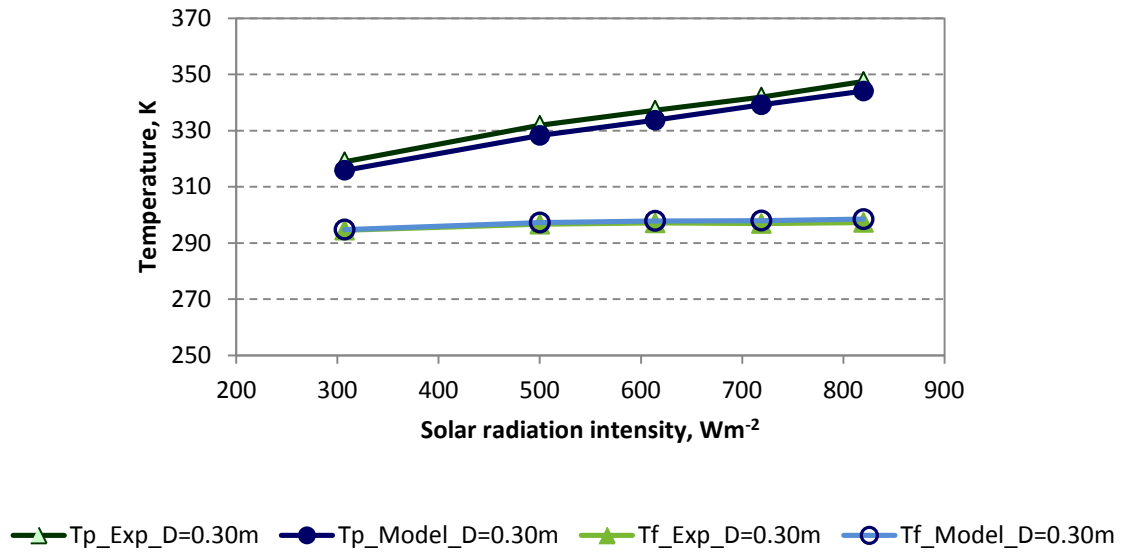
▲  $T_{p\_Exp\_D=0.20m}$    
 ●  $T_{p\_Model\_D=0.20m}$    
 ▲  $T_{f\_Exp\_D=0.20m}$    
 ○  $T_{f\_Model\_D=0.20m}$

(a)



▲  $T_{p\_Exp\_D=0.25m}$    
 ●  $T_{p\_Model\_D=0.25m}$    
 ▲  $T_{f\_Exp\_D=0.25m}$    
 ○  $T_{f\_Model\_D=0.25m}$

(b)



(c)

Figure 4-3. Results comparison between the model and experiments over different solar radiation intensities for plenum depths of a) 0.20m, b) 0.25m and c) 0.30m.

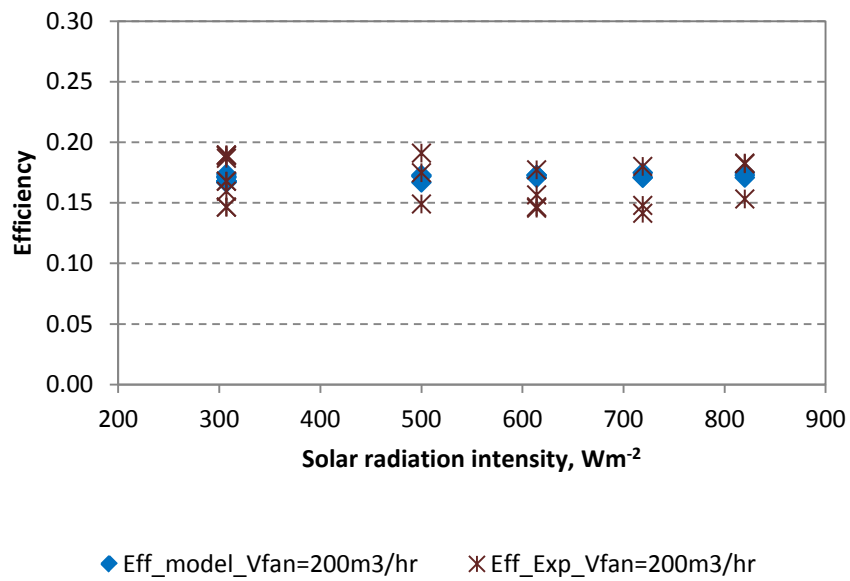
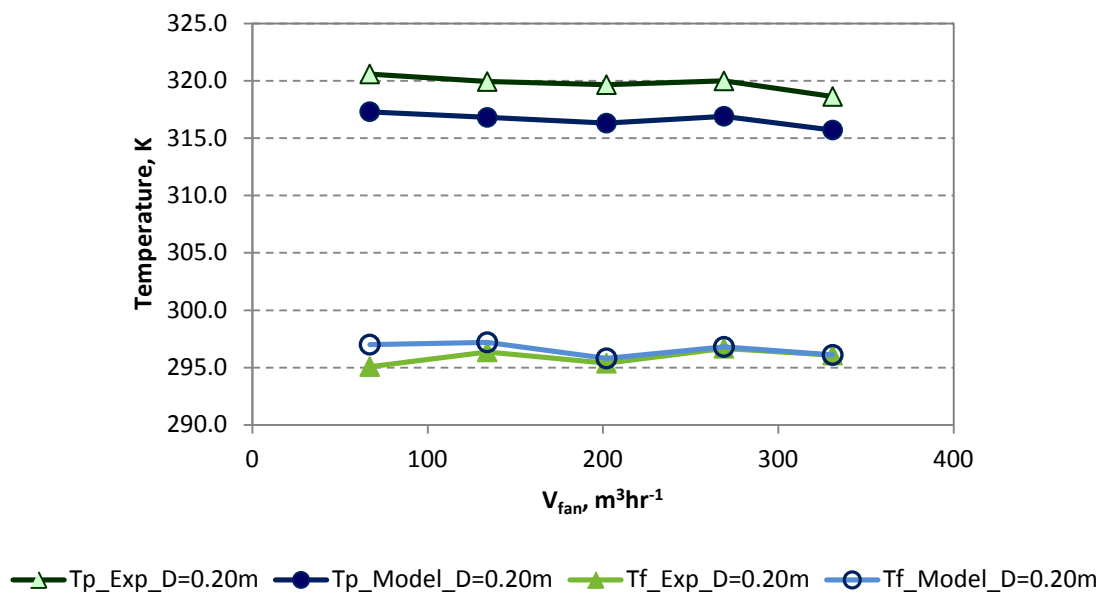


Figure 4-4. Efficiency comparisons between the model and experiments over different solar radiation intensities at  $V_{fan}=200m^3hr^{-1}$

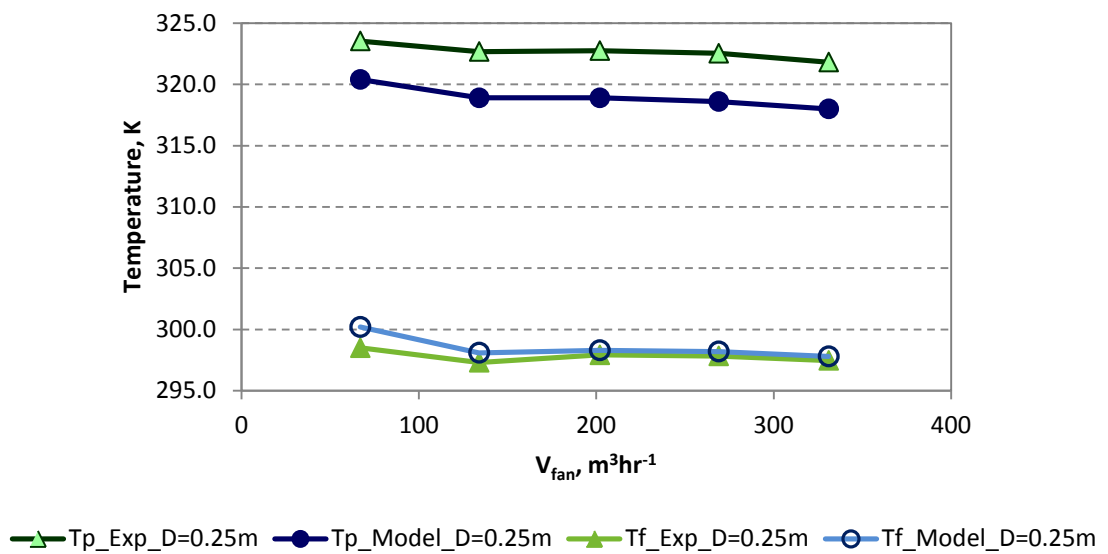
**Comparison over different airflow rates**

Figure 4-5(a), (b) and (c) are temperature comparisons between the model and the experiments for plenum depths of 0.20m, 0.25m and 0.30m respectively, at a

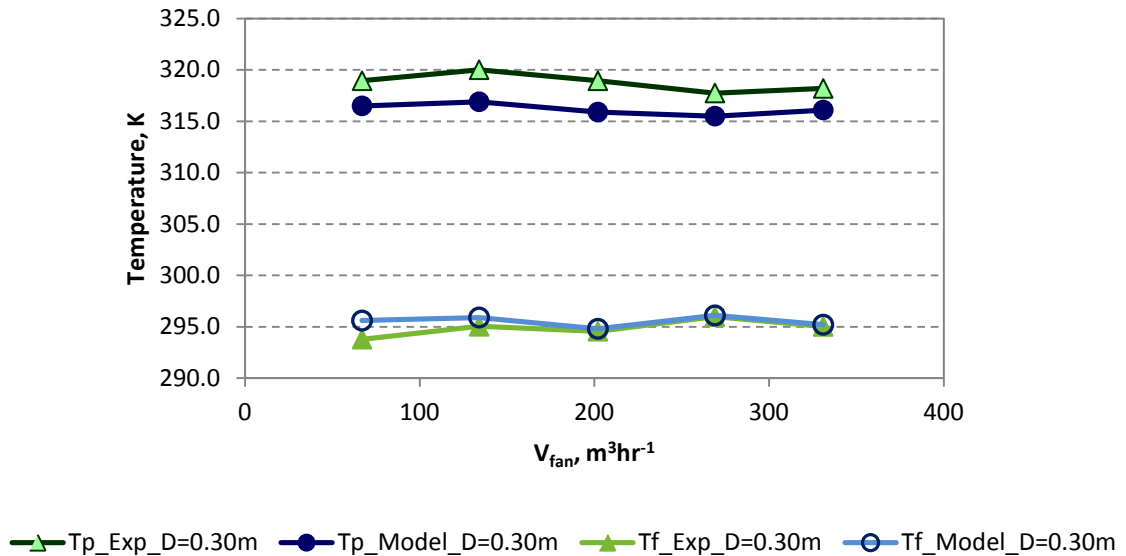
constant solar radiation intensity of  $307\text{Wm}^{-2}$  over airflow rate ranges from 67 to  $331\text{m}^3\text{hr}^{-1}$ . Both the model and experiment show the same temperature patterns of plate and air. The temperature difference of  $T_p$  between the modelled and measured ranges from 1 to 4K, with most of them falls within 3.0-4.0K that give an average value of 3.2K. Whereas for the  $T_f$ , the temperature difference ranges from 0.1 to 1.9K, with most of them smaller than 0.4K and give an average value of 0.2K.



(a)



(b)



(c)

Figure 4-5. Results comparison between the model and experiments over different airflow rates for plenum depths of a) 0.020m, b) 0.25m and c) 0.30m.

Apart from the temperature comparisons, Figure 4-6 shows the efficiency comparisons between the model and the experiments at a constant solar radiation intensity of  $307Wm^{-2}$ . The maximum difference of efficiency values is at  $331m^3hr^{-1}$  with plenum depth of 0.3m where the modelled and measured efficiencies are 0.18 and 0.22 respectively. As the percentage error from the experiment is  $\pm 16.0\%$  (Section 3.7) of the measured efficiency, the acceptable efficiency ranges from 0.18 to 0.26, which also the modelled efficiency fall between.

#### 4.2.3.2. Parametric analysis for the flat plate solar façade

The parameters that are included in discussions are the ambient temperature, solar radiation intensity, airflow rate and plenum depth. All the temperatures are measured from experiments unless mentioned.

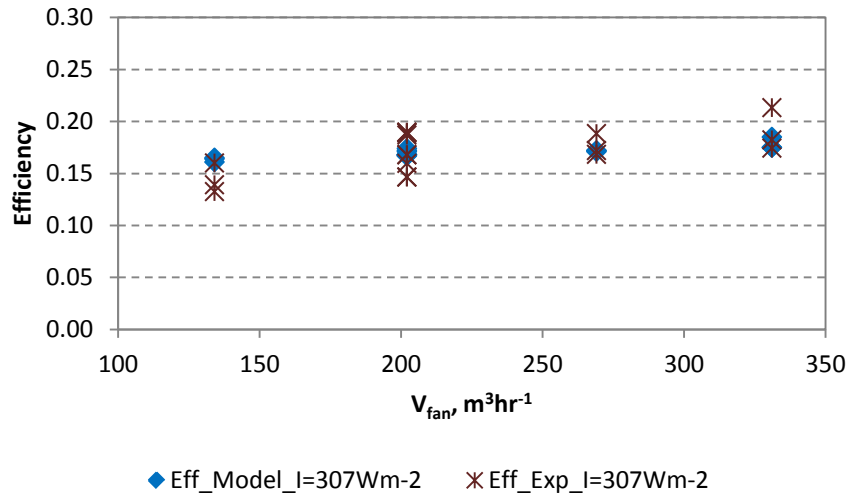
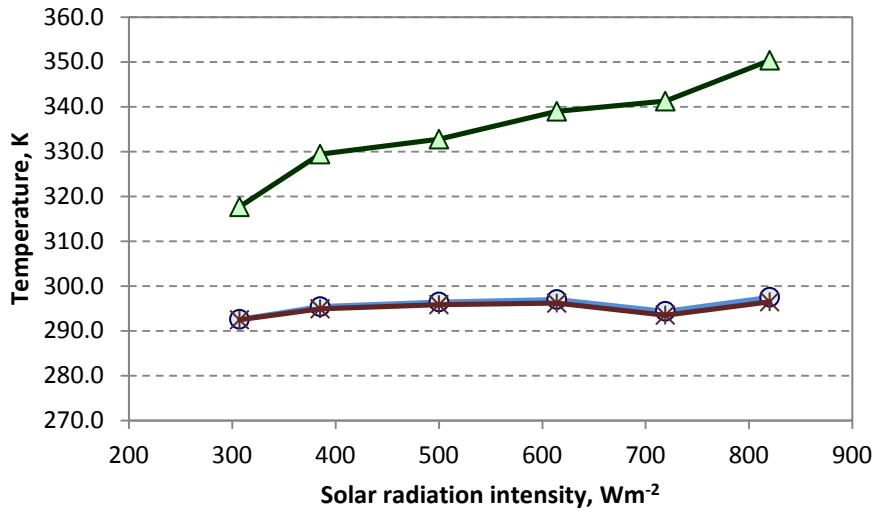


Figure 4-6. Efficiency comparisons between the model and experiments over different airflow rates at  $I=307W^2m^{-2}$

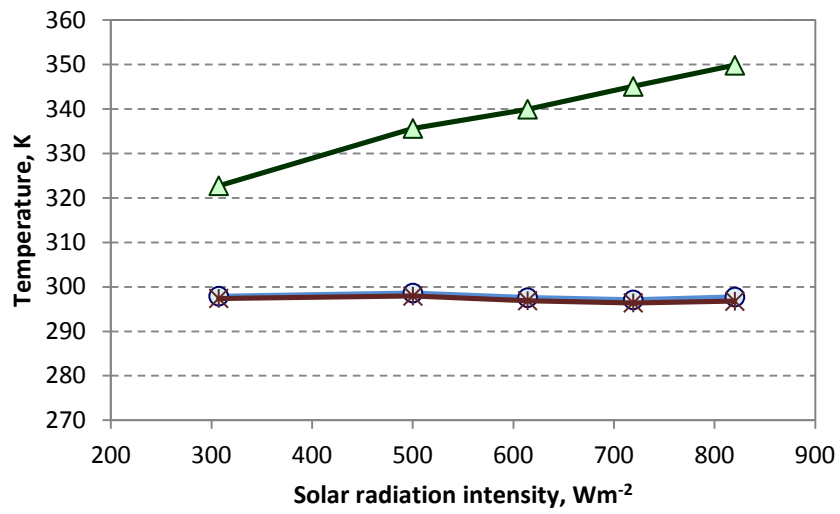
#### ***Effect of ambient air temperature***

The influence of  $T_a$  on  $T_p$  and  $T_f$  is investigated by studying the patterns of  $T_p$  and  $T_f$  values compared to the  $T_a$  values. Figure 4-7 shows that the values of  $T_f$  are influenced by the  $T_a$  where they have the same patterns as  $T_a$ , from low to high solar radiation intensity. In contrast, for  $T_p$  the solar radiation intensity has stronger effect than  $T_a$ , whereby the values of  $T_p$  increase with solar radiation intensity. On the other hand, under a constant solar radiation intensity both  $T_p$  and  $T_f$  are influenced by the values of  $T_a$  over a range of airflow rates (Figure 4-8). To further investigate the  $T_a$  effect on the rise in air temperature ( $T_{out}-T_a$ ), Figure 4-9 is plotted by using the simulation results from the developed model. The input parameters are  $I=500Wm^{-2}$ ,  $V_{fan}=200m^3hr^{-1}$  and  $T_a=275$  to  $300K$  for plenum depth of  $0.20m$ . It is found that the effect of  $T_a$  can be concluded as higher  $T_a$  gives higher  $T_f$  but no significant effect on overall ( $T_{out}-T_a$ ) due to the fact that increasing  $20K$  of  $T_a$  is only  $0.05K$  of difference in air temperature change. In fact, it is also found that the air temperature change of ( $T_{out}-T_a$ ) decreases with  $T_a$ , though in very small value.



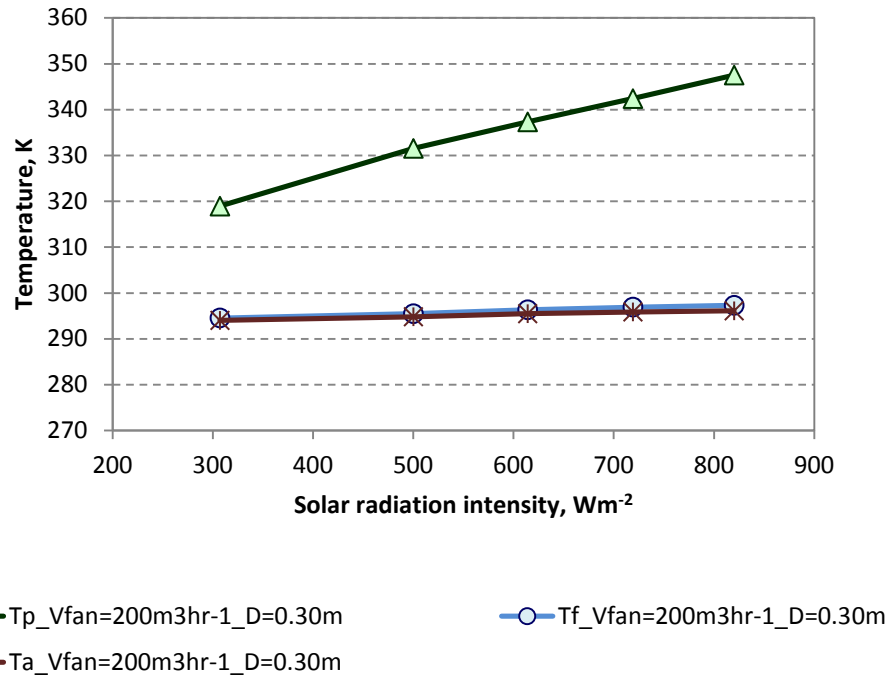
—▲  $T_p$ \_Vfan=200m3hr-1\_D=0.20m      —○  $T_f$ \_Vfan=200m3hr-1\_D=0.20m  
—\*  $T_a$ \_Vfan=200m3hr-1\_D=0.20m

(a)



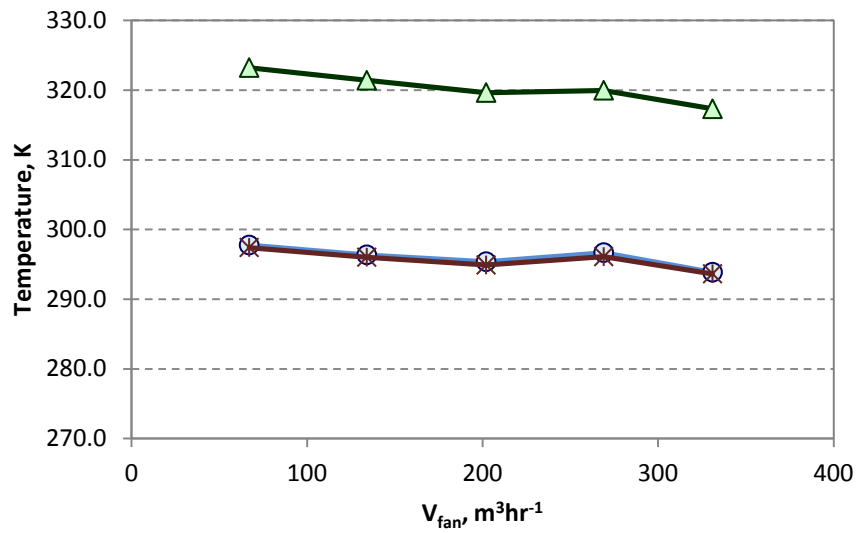
—▲  $T_p$ \_Vfan=200m3hr-1\_D=0.25m      —○  $T_f$ \_Vfan=200m3hr-1\_D=0.25m  
—\*  $T_a$ \_Vfan=200m3hr-1\_D=0.25m

(b)



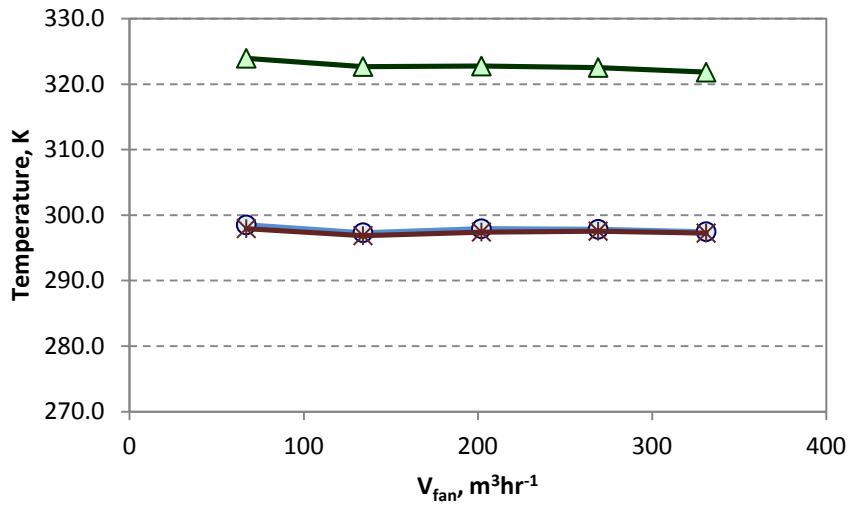
(c)

Figure 4-7. Values of  $T_p$  and  $T_f$  at solar radiation intensity range from 307 to  $820Wm^{-2}$  for plenum depth of (a) 0.20m, (b) 0.25m and (c) 0.30m.



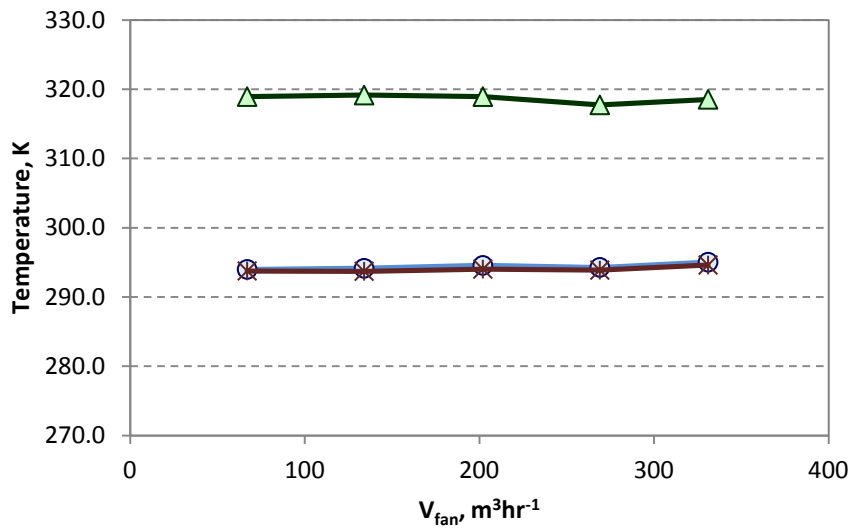
—△—  $T_p$ ,  $I=307Wm^{-2}$ ,  $D=0.20m$     —○—  $T_f$ ,  $I=307Wm^{-2}$ ,  $D=0.20m$     —\*—  $T_a$ ,  $I=307Wm^{-2}$ ,  $D=0.20m$

(a)



—△  $T_p$ \_I=307Wm-2\_D=0.25m   
 —○  $T_f$ \_I=307Wm-2\_D=0.25m   
 —\*  $T_a$ \_I=307Wm-2\_D=0.25m

(b)



—△  $T_p$ \_I=307Wm-2\_D=0.30m   
 —○  $T_f$ \_I=307Wm-2\_D=0.30m   
 —\*  $T_a$ \_I=307Wm-2\_D=0.30m

(c)

Figure 4-8. Values of  $T_p$  and  $T_f$  at airflow rate range from 100 to 500  $m^3hr^{-1}$  for plenum depth of (a) 0.20m, (b) 0.25m and (c) 0.30m.

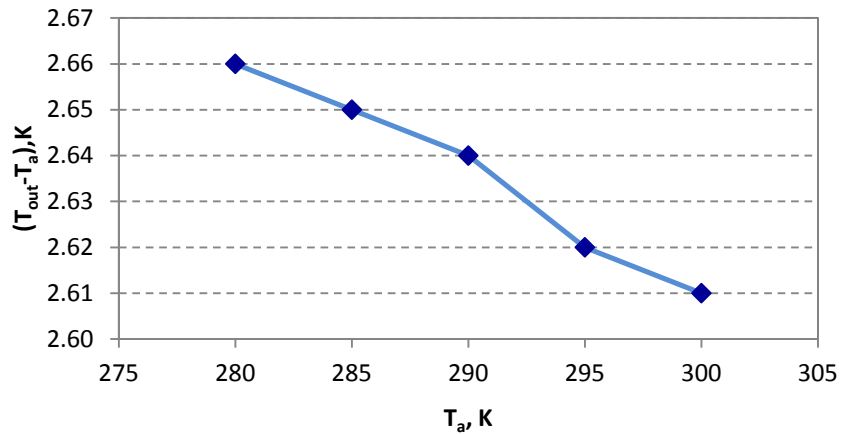


Figure 4-9. Effect of  $T_a$  on the temperature change of  $(T_{out} - T_a)$  for input parameters of  $I=500Wm^{-2}$ ,  $V_{fan}=200m^3hr^{-1}$  and  $D=0.20m$

### Effect of solar radiation

In order to avoid the misleading trends that could be affected by the values of  $T_a$ , the effects of solar radiation on plenum air temperatures are investigated by plotting  $(T_p - T_a)$  and  $(T_{out} - T_a)$  instead of  $T_p$  and  $T_f$ . As shown in Figures 4-10 and 4-11, both  $T_p$  and  $T_f$  increase with solar radiation intensity. When the solar radiation intensity increases from  $307Wm^{-2}$  to  $820Wm^{-2}$ ,  $T_p$  increases about 27 to 28K but only about 2 to 3K rise in air temperature. This indicates that heat transfer between the flat plate and the air in the plenum are poor.

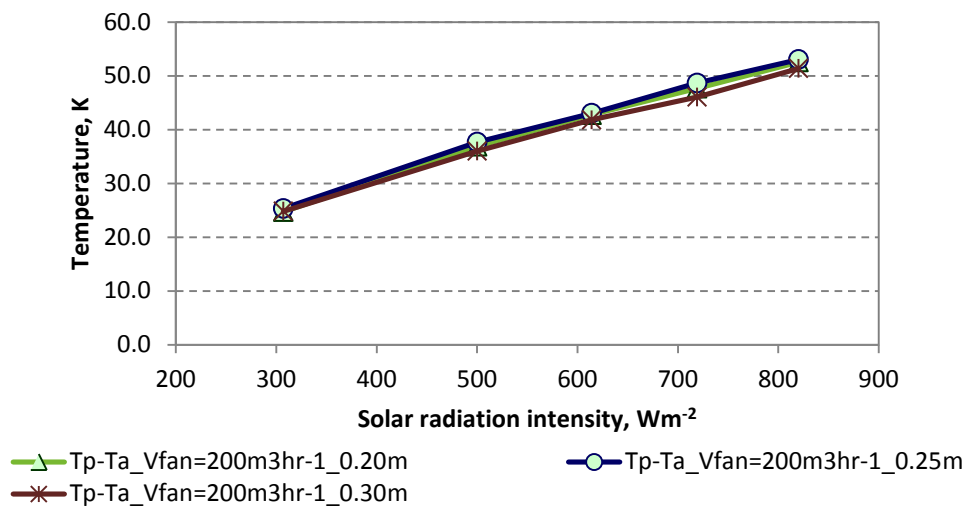


Figure 4-10. Values of  $(T_p - T_a)$  at various solar radiation intensities for plenum depths of 0.2m, 0.25m and 0.30m.

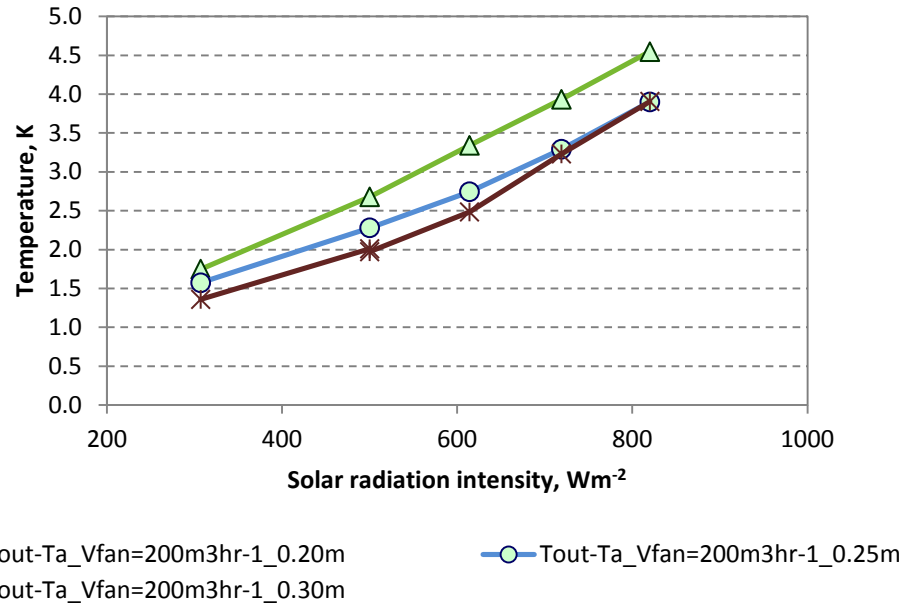


Figure 4-11. Values of  $(T_{out}-T_a)$  at various solar radiation intensities for plenum depths of 0.2m, 0.25m and 0.30m.

#### **Effect of airflow rate**

Figures 4-12 and 4-13 show that plate and air temperatures decrease with airflow rate. However, in relative to the effect of solar radiation (Figure 4-10), airflow rate does not have obvious effect on the  $T_p$  (Figure 4-12). Over the range of 67 to  $331m3hr^{-1}$ , values of  $(T_p-T_a)$  drop from 26K to 22K, which give only about 2K of temperature difference in  $(T_{out}-T_a)$ . On the other hand, higher air speed will have shorter interaction time of heat transfer with the heated plate. Results show reductions of about 1.0 to 1.4K in air temperature from low to high airflow rate. So, as long as the outlet air meets the desired mass flow rate, lower airflow rate is preferable in order to obtain higher rise in air temperature and avoid energy waste of the fan.

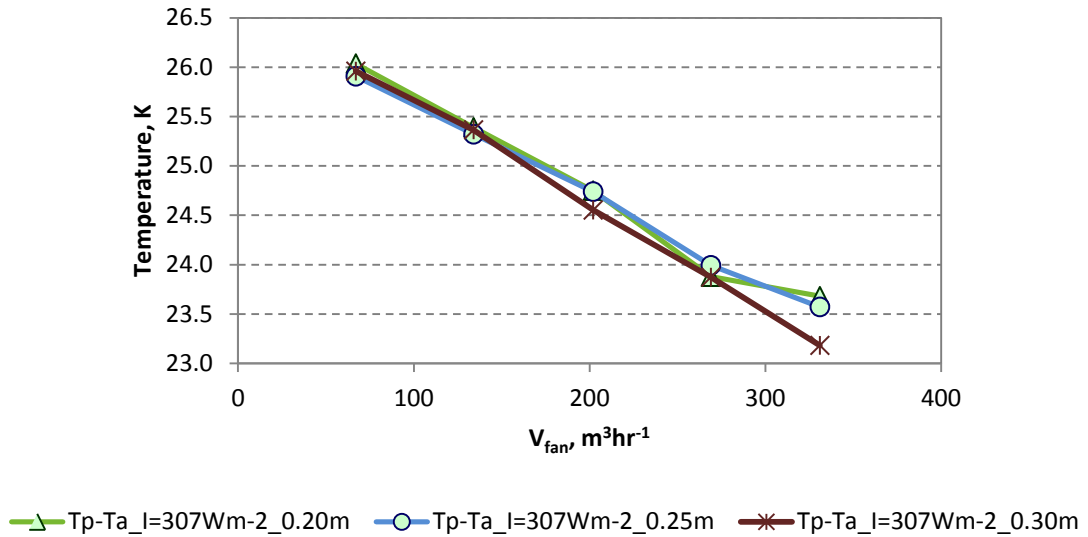


Figure 4-12. Values of  $(T_p - T_a)$  at various airflow rates for plenum depths of 0.2m, 0.25m and 0.30m.

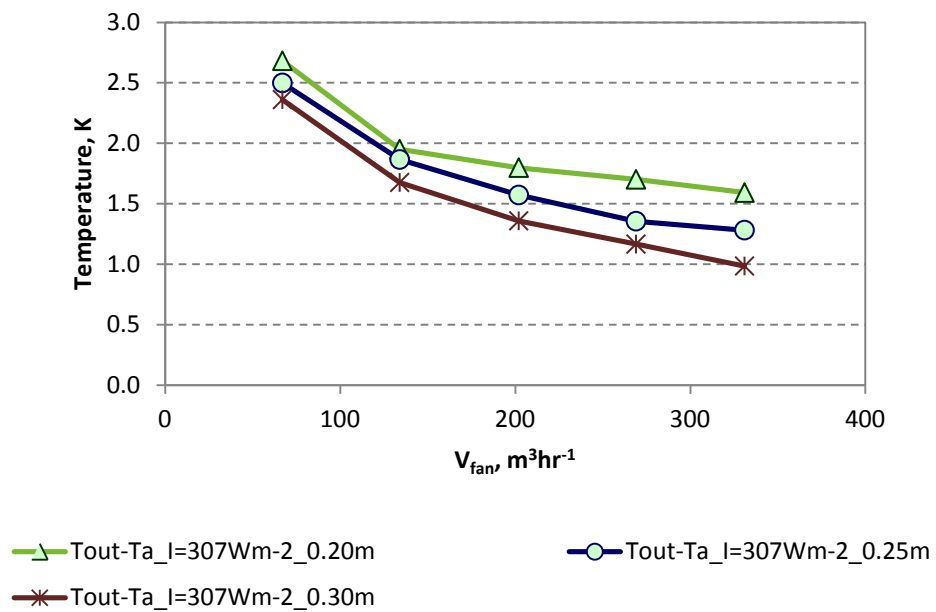


Figure 4-13. Values of  $(T_{out} - T_a)$  at various airflow rates for plenum depths of 0.2m, 0.25m and 0.30m.

### Effect of plenum depth

Figures 4-11 and 4-13 show that smaller gap of the plenum gives higher rise in air temperature. However, the rise in air temperature show differences of only about 0.5K or less as compared  $D=0.20m$  to  $D=0.30m$ .

### **4.3. Heat transfer of transpired solar façade**

#### **4.3.1. Assumptions of heating system with transpired plate collector**

Due to the complication of heat transfer process of the unglazed transpired plate, some assumptions have been made as follows:

- i) The radiation heat loss over the surface of the transpired plate is everywhere constant as this has been proved that it has a modest effect on the flow distribution (Gunnewiek, 1996).
- ii) There is no heat loss through the sandtile wall and side walls that attached with the aluminium plate (Chapter 3).
- iii) In addition to experimental tests were carried out in a close laboratory, the convection losses to the ambient are negligible and have been verified by previous study (Kutscher, 1994).
- iv) No reverse flow over the plate as the face velocities in this study are higher than  $0.0125\text{ms}^{-1}$  (Gunnewiek, 1996).
- v) The temperatures that are measured by the thermocouples which have the same height with the first row of holes from the bottom are taken as air temperatures reach the plenum after passing through the holes.
- vi) The air properties maintain the same throughout the plenum (the maximum air temperature difference between the inlet and outlet is about 10K in this study).

#### **4.3.2. Energy balance equations for transpired plate collector**

Energy balance equations are established for two components of the system, i.e. unglazed transpired plate and the air in the plenum. The heat transfers of the system are as shown in Figure 4-14.

##### ***The unglazed transpired collector:***

The fans-assisted system draws the ambient air through the holes so that heat, which would otherwise be lost by convection, is captured by the airflow into the

plenum. Thus, there will have very small amount of convection heat loss to the ambient which indeed can be neglected (Augustus, 2007, Dymond, 1997, Kutscher, 1993). Energy balance equation on an unglazed transpired plate is as shown in Equation 4-21.

$$I \alpha_p A_p = Q_{conv,p-air} + Q_{conv,bp-air} + Q_{rad,p-sur} \quad (4-21)$$

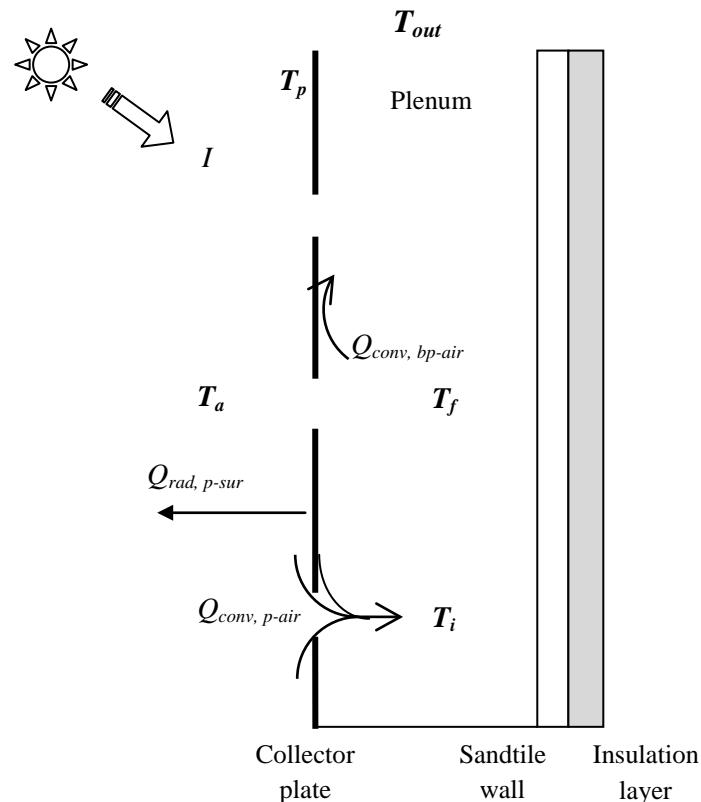


Figure 4-14. Heat transfers of the unglazed transpired solar collector.

### **The plenum air:**

The ambient air which heated by the front and hole of the transpired plate is further heated by the back-of-plate when flowing throughout the plenum. Energy balance equation of the air in the plenum is shown in Equation 4-22.

$$\sum \dot{m} c_p (T_{out} - T_i) = Q_{conv,bp-air} \quad (4-22)$$

#### 4.3.2.1. Heat flux and coefficient of heat transfer for transpired plate collector

##### ***Convection heat transfer from the front and hole of transpired plate to the ambient air***

The convection heat transfer equations can be written in term of mass flow rate and heat flux as shown in Equations 4-23 and 4-24 respectively.

$$q_{conv,p-air} = \sum \dot{m} c_p (T_i - T_a) / A_p \quad (4-23)$$

$$q_{conv,p-air} = h_{c,trans} (T_p - T_i) \quad (4-24)$$

The convection coefficient is defined as Equation 4-25 where the  $Nu_{c,trans}$  correlation is discussed in section 4.3.4.2.

$$h_{c,trans} = Nu_{c,trans} * k_a / d \quad (4-25)$$

##### ***Convection heat transfer from the back of the transpired plate to the air in the plenum***

The coefficient is shown in Equation 4-26 and the  $Nu_{f,trans}$  correlation (Equation 4-27) will be further discussed in the section 4.3.4.3.

$$q_{conv,bp-air} = h_{f,trans} (T_p - T_f) , \quad (4-26)$$

where  $T_f = (T_i + T_{out})/2$

$$h_{f,trans} = Nu_{f,trans} * k_f / H \quad (4-27)$$

##### ***Radiation heat transfer from the front of transpired plate to the surrounding***

The radiation coefficient is the same as discussed in earlier section (Equation 4-11).

##### ***Solar radiation***

The solar radiation intensity that absorbed by the transpired plate is given as Equation 4-18.

### ***System efficiency***

The efficiency of the heating system is given as in Equation 4-19.

### ***Heat exchange effectiveness***

The heat exchange effectiveness of the solar collector is defined as the ratio of the actual temperature rise of air to the maximum possible temperature rise (Kutscher, 1994):

$$\varepsilon_{HX} = (T_{out} - T_a) / (T_p - T_a) \quad (4-28)$$

### **4.3.3. Results and parametric analysis of transpired plate collector**

The experiment set up is as described in Chapter 3. The experiments were carried out with operation conditions as described in Table 4-2. The parametric analysis includes investigations on factors that would affect the thermal performance of the system. In addition, vertical flow heat transfer is also been highlighted within the section. Discussion on the efficiency is also included in this section. Parts of the results are selected for discussions, however the complete sets of measured data can be found in Appendix III-2.

#### **4.3.3.1 Parametric analysis for the transpired solar facades**

The main parameters of the collector include ambient air temperature, suction mass flow rate, solar radiation intensity, and the plenum depth.

Table 4-2. Parameters for the experiments of transpired plate for heating system.

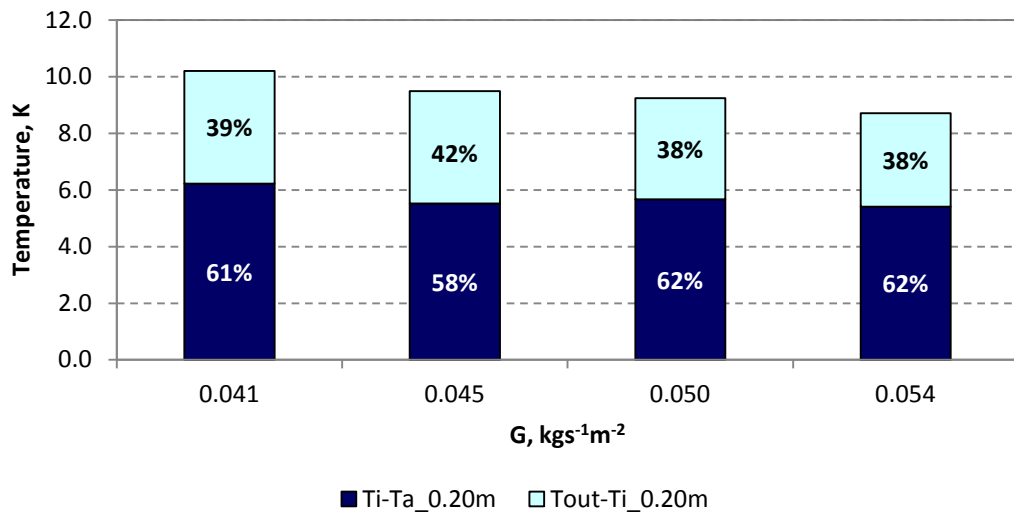
Parameter	Value/ range
Solar radiation intensity, $Wm^{-2}$	300-800
Suction velocity, $ms^{-1}$	0.03-0.05 <sup>a</sup>
Plenum depth, m	0.20-0.30
Porosity (ratio of hole area to total surface area), %	0.84
Pitch, m	0.012
Hole diameter, m	0.0012
Holes array geometry	Triangular
Height of the transpired plate, m	2.0
Width of the transpired plate, m	1.0
Area of the transpired plate, $m^2$	2.0
Plate thickness, m	0.001

<sup>a</sup> The supply airflow rate= air changes per hour \* interior room volume. The requirement of air changes per hour (ACH) for office room is about  $2.0h^{-1}$  (ASHRAE, 2009); the room volume for the heating study is  $15.7m^3$ , hence the required minimum airflow rate and suction velocity are  $31.4m^3hr^{-1}$  and  $0.0044ms^{-1}$  respectively. However to avoid the reverse flow, suction velocity should be higher than  $0.0125ms^{-1}$ . Thus, the above range was chosen in this study. The total volume airflow rate was measured at the outlet and hence the suction velocity is calculated as the measured volume airflow rate per plate area (Augustus, 2007).

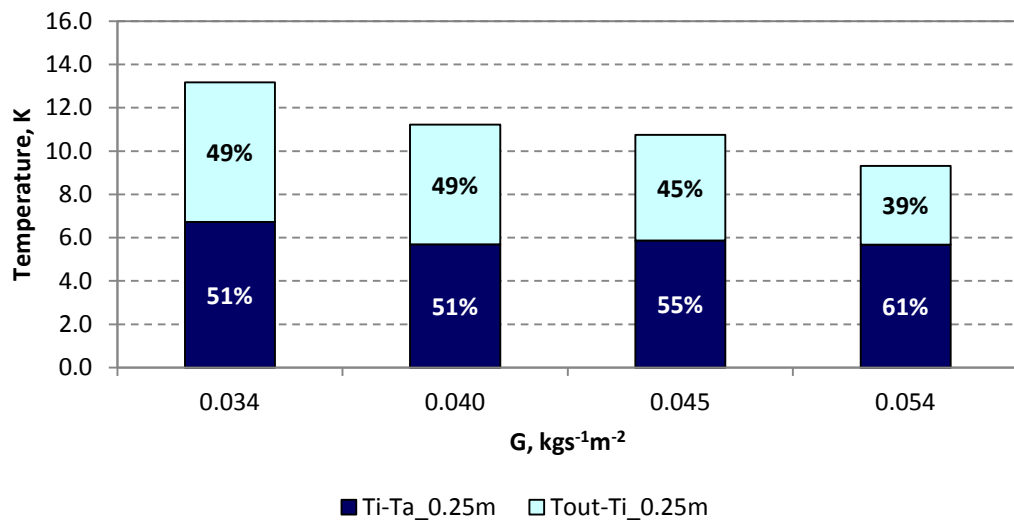
### ***Suction mass flow rate***

Figure 4-15 shows the temperature rise for different depths of the plenum at different suction mass flow rates with a solar radiation intensity of  $614Wm^{-2}$ . The temperature rise of  $(T_{out}-T_a)$  is the overall temperature rise for the system, which is the temperature difference between the outlet air and the ambient air. The temperature rise of  $(T_i-T_a)$  is the temperature difference between the ambient air and the heated air after passing through the holes (normal flow). Whereas the  $(T_{out}-T_i)$  is temperature change of the vertical flow from the bottom to the top of plenum. The values of  $(T_i-T_a)$  and  $(T_{out}-T_i)$  decrease with the suction mass flow rate. Increasing the suction mass flow rate by about  $0.02kgs^{-1}m^{-2}$ ,  $(T_{out}-T_a)$  decreases nearly 2 to 4K, while  $(T_i-T_a)$  and  $(T_{out}-T_i)$  decrease nearly 1-2K. The share of temperature rises contributed from normal and vertical flows are about the same between  $0.03$  and  $0.05kgs^{-1}m^{-2}$  (Figure 4-15) (The degrees of temperature decrease for the normal and vertical flows are about the same). Nonetheless, results shows that in terms of percentage, the vertical flow  $(T_{out}-T_i)$

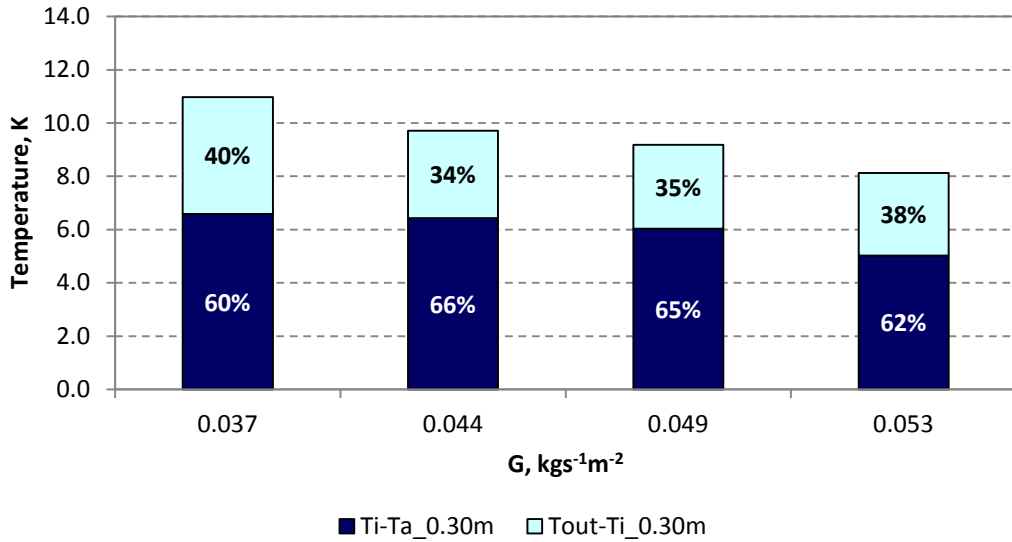
contributes about 38-49% of the total air temperature rise ( $T_{out}-T_a$ ), which disagrees with previous study (Kutscher, 1992) that ignoring the vertical direction of heat transfer in the plenum.



(a)



(b)



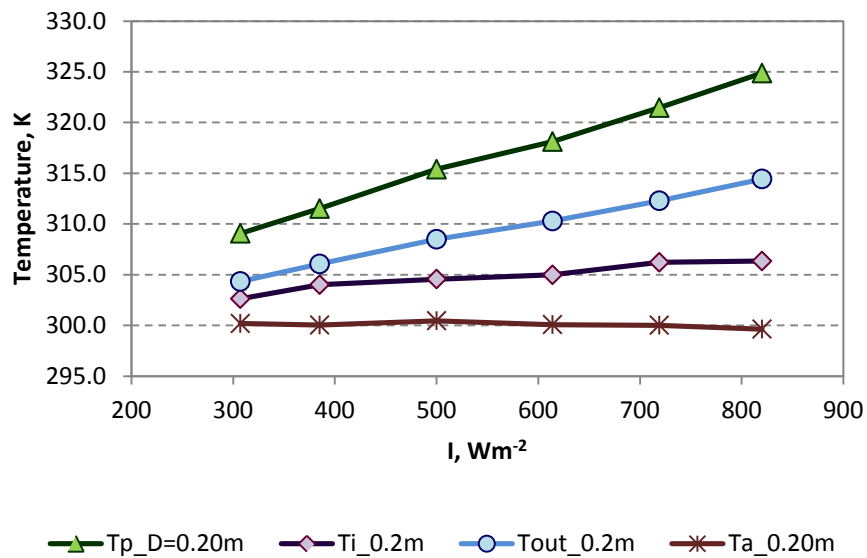
(c)

Figure 4-15. Values and percentages of air temperature rise for normal and vertical airflows for plenum depths of (a) 0.20m, (b) 0.25 and (c) 0.30m with various suction mass flow rates and at constant solar radiation intensity of  $614\text{Wm}^{-2}$ .

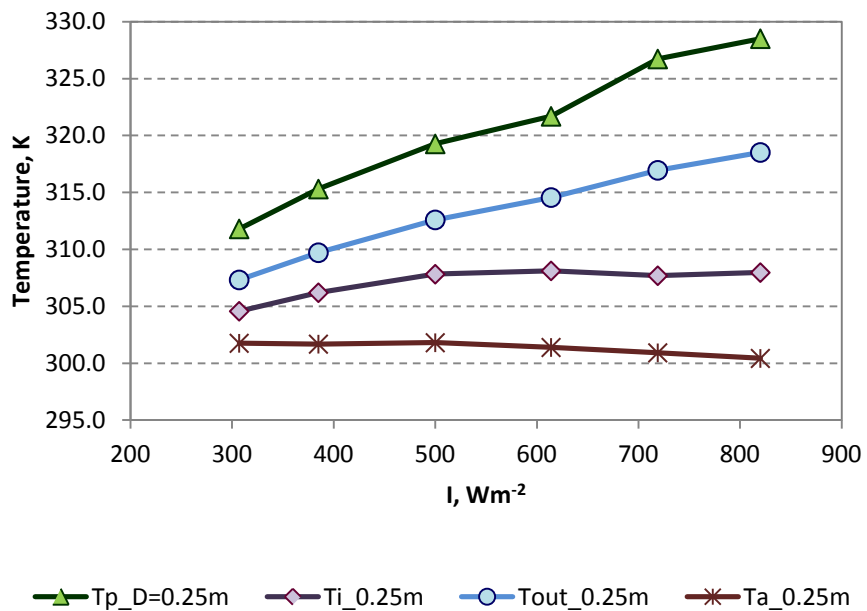
### **Solar radiation intensity**

Figure 4-16 shows the temperatures of the ambient, the plate and the air in the plenum for plenum depth of 0.20, 0.25 and 0.30m respectively, at a constant suction mass flow rate. The values of the temperatures increase with the solar radiation intensity and they are influenced by the  $T_a$ . For example (Figure 4-16c), due to lower  $T_a$  at  $600\text{Wm}^{-2}$  the  $T_i$  has lower value compared to  $T_i$  at  $500\text{Wm}^{-2}$ , however the total collected energy is higher for  $600\text{Wm}^{-2}$ . Figure 4-17 shows the share of rise in air temperature contributed by the normal ( $T_i - T_a$ ) and vertical ( $T_{out} - T_i$ ) flows. In terms of percentage, vertical flow contributes 41% of total temperature rise at  $307\text{Wm}^{-2}$  and increases to 51% at  $820\text{Wm}^{-2}$  for the plenum depth of 0.20m. As for plenum depth of 0.25 and 0.30m, they increase from 34% and 44% to 58% and 52% respectively. Both plenum depths with 0.20 and 0.25m show that normal and vertical flows contribute equally at  $719\text{Wm}^{-2}$ , whereas for plenum depth of 0.30m, this occurs at  $614\text{Wm}^{-2}$ . Even at low solar radiation intensity, the contributions of vertical flows are above 30% of the total

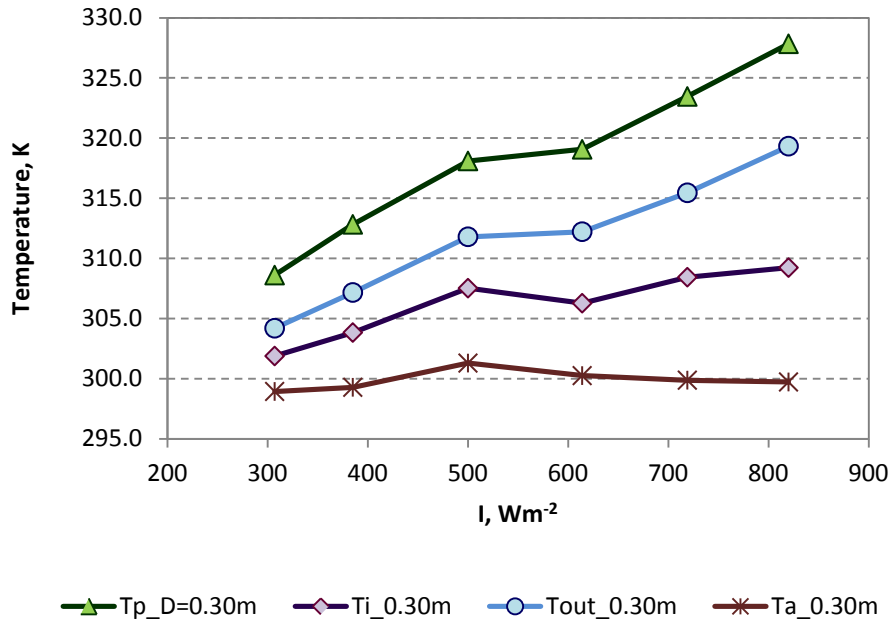
rise in temperature. Hence, the vertical heat transfer is inappropriate to be ignored. Moreover, the overall rise in temperature ( $T_{out}-T_a$ ) from 307 to 820Wm<sup>-2</sup> is about 6 to 18K, which approximately increases 3K for every increase of 100Wm<sup>-2</sup>. Thus, the solar radiation intensity plays an important role in the thermal performance of the system.



(a)

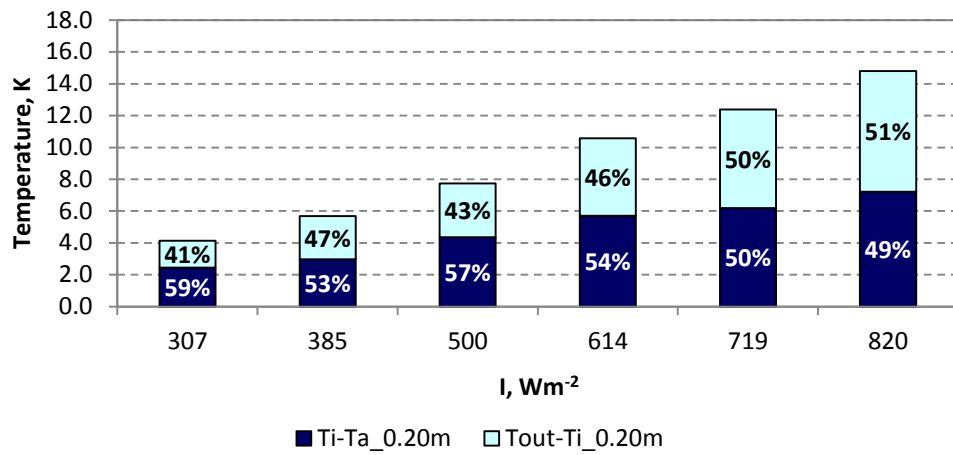


(b)

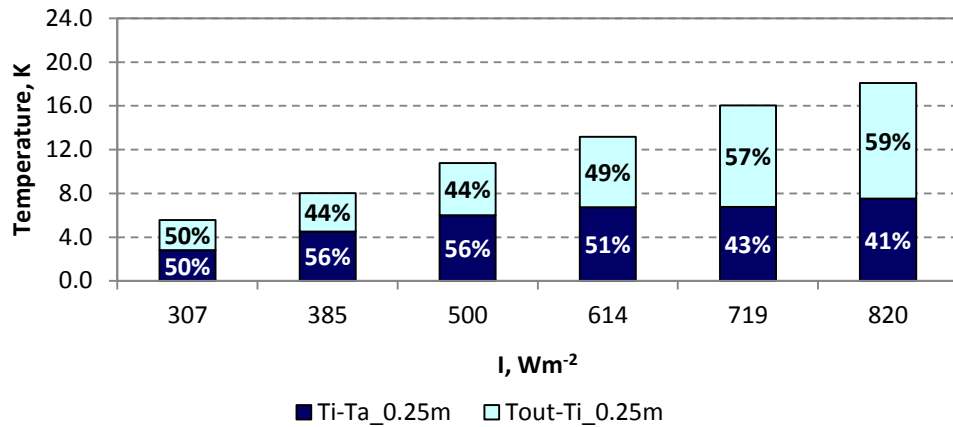


(c)

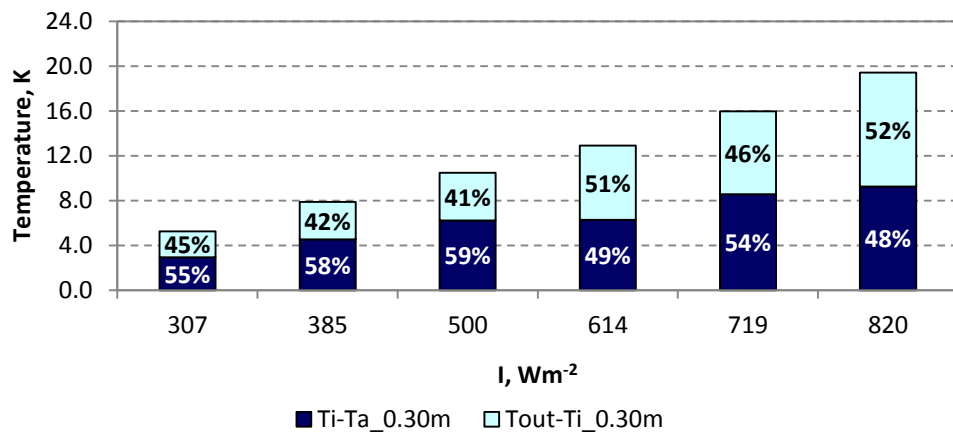
Figure 4-16. Temperatures of the ambient, the plate and the air in the plenum for plenum depth of (a) 0.20, (b) 0.25 and (c) 0.30m at various solar radiation intensities.



(a)



(b)



(c)

Figure 4-17. Values and percentages of rise in air temperature for normal and vertical airflows for plenum depths of (a) 0.20m, (b) 0.25 and (c) 0.30m at various solar radiation intensities.

### System efficiency

For solar collector applications, system efficiency is crucial in terms of heating performance. The efficiency for suction mass flow rate between 0.034 to 0.054  $\text{kgs}^{-1}\text{m}^{-2}$  at solar intensity of  $614\text{Wm}^{-2}$  is as shown in Figures 4-18. Results show that higher suction mass flow rate gives higher system efficiency. For the system design in this study, the efficiency of the system is between 67 to 83% which are equivalent to temperature rise of 9-13K. For the practical applications, operating parameters would very much depend on the application purpose of the heating system. Typical suction velocities range from  $0.01\text{ms}^{-1}$  for desiccant

regeneration to  $0.05 \text{ ms}^{-1}$  for preheating ventilation air. Since the system efficiency is high, applications that require a lower rise in air temperature, the solar collector can be painted with variety choices of colours by choosing the appropriate absorptivity and emissivity values of the plate. In terms of aesthetics, this is one of the most important aspects for building integration technologies.

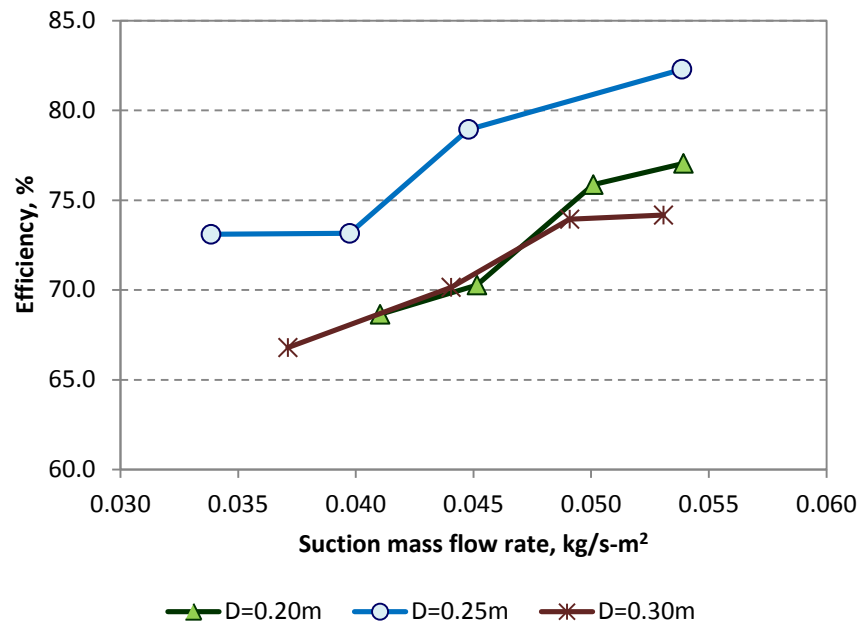


Figure 4-18. System efficiencies from experiment results at  $614 \text{ Wm}^{-2}$  of solar radiation

On the other hand, Figures 4-19 show the efficiency at various solar radiation intensities with a constant suction mass flow rate. The efficiency increases with the solar radiation intensity, ranging from 68 to 96%. These account for rises in air temperature of 4-5K at  $307 \text{ Wm}^{-2}$  and 16K at  $820 \text{ Wm}^{-2}$ . Thus local weather conditions might affect the thermal performance. However, countries with low solar radiation availability, the performance can be improved by using lower airflow rate and this will be discussed in sections 4.4.1 and 4.4.2.

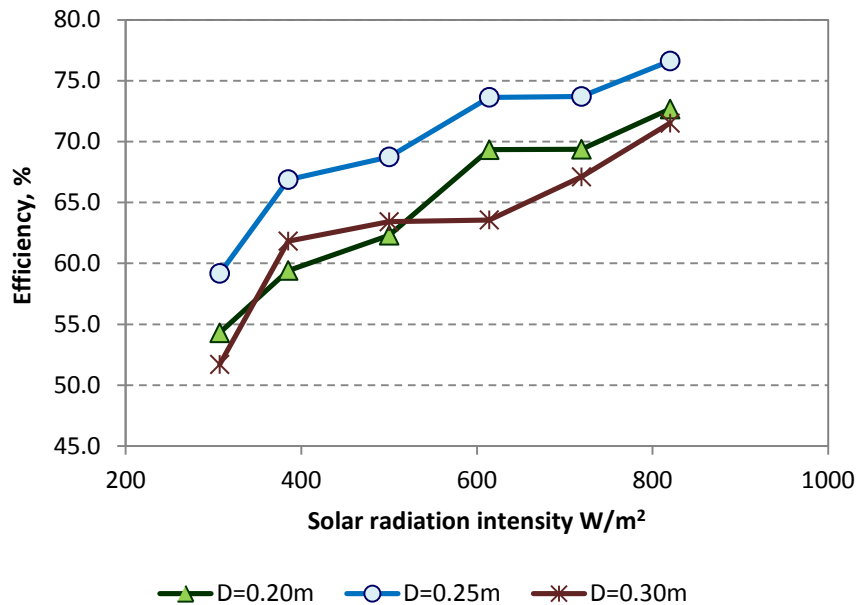


Figure 4-19. System efficiencies from experiment results at various solar intensities under a constant suction mass flow rate of  $0.04 \text{ kg s}^{-1} \text{ m}^{-2}$ .

### ***Plenum depth***

The plenum depths that have been studied are 0.20, 0.25 and 0.30m. Their ratios of height to depth of the plenum ( $H/D$ ) are 10, 8 and 6.7, respectively. Figure 4-20 shows the values of temperature rise for vertical flows over different solar radiation intensities. Whereas temperature rises for vertical flow over different suction mass flow rates are as shown in Figure 4-21. The temperature rise of vertical flow is increases with solar radiation and decreases with suction mass flow rate. Plenum depth of 0.25m not only gives the highest temperature rise for both cases but also higher efficiencies (Figures 18 and 19). One of the possibilities for 0.25m having the best performance is the flow pattern. In the plenum, there are two types of flows, i.e. buoyant flow driven by temperature differences and forced flow developed by the fans. The buoyant flow causes the air flows from the bottom to the top while the forced flow draws more air at the top than the bottom. If the flow distribution over the plate is uniform, the forced flow is dominant, and the tendency of the flow in vertical direction is decreased. This is

especially when the plenum depth is narrow (high value of  $H/D$ ) and it is because of high acceleration and wall friction. This phenomena is clearly shown in Gunnewiek et al.' study when the  $H/D$  is higher than 40 (Gunnewiek, 1996). In contrast, if the flow distribution is non-uniform, buoyant flow might take place and hence the heat transfer of back-of plate to the air. Also, results from Gunnewiek et al.' study show higher efficiency when the flow is buoyancy dominated. Therefore, flow throughout the plenum depth of 0.25 and 0.30m might be dominated by buoyant flow while 0.20m is dominated by forced flow. In addition, 0.25m might be the optimum depth ( $H/D=8$ ) for the studied range of flow rate compared to 0.30m; and when forced flow is dominant in 0.20m, the performance tends to decrease.

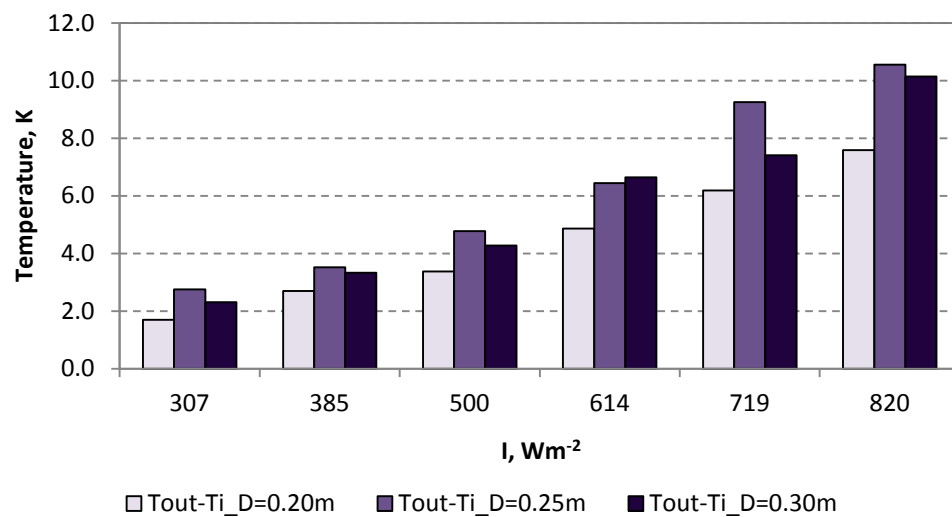


Figure 4-20. Air temperature rise of vertical flow in the plenum for plenum depth of 0.20m, 0.25m and 0.30m at various solar radiation intensities.

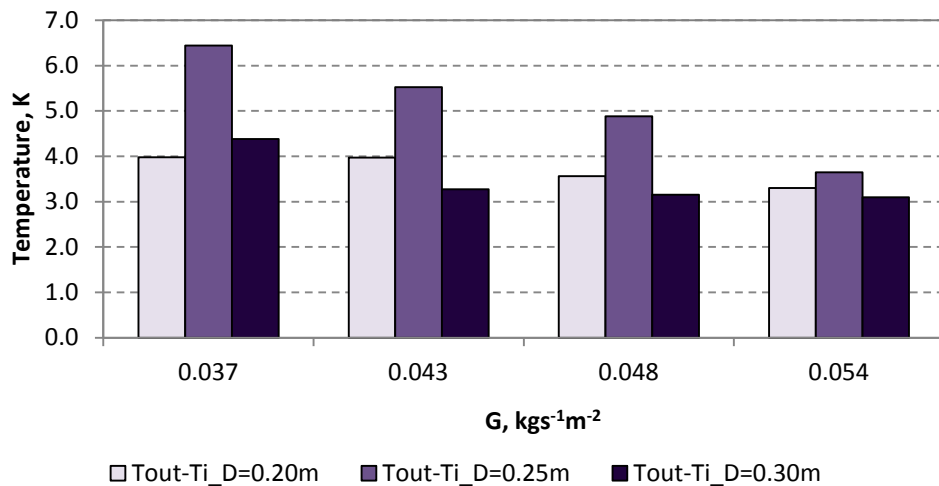


Figure 4-21. Air temperature rise of vertical flow in the plenum for plenum depth of 0.20m, 0.25m and 0.30m at various suction mass flow rates.

#### 4.3.4. *Nu* correlations for heat transfer involves vertical flow

In this section, the research problems related to vertical flow heat transfer are addressed and *Nu* correlations are developed for both normal and vertical flows in respect to present plate design.

##### 4.3.4.1. The lack of non-uniform heat transfer coefficient for transpired solar collector

Literature review on the development of *Nu* correlations for transpired plate is detailed in Chapter 2. Following is the summary of the research problems related to vertical flow.

There were studies related to *Nu* correlations for jet plate heat transfer. The investigations include influences of number of holes (porosity), diameter, pitch and shape of the hole, and the hole array geometry (Andrews G.E., 1986, Andrews G.E., 1989, Andrews G.E., 1987, Bazdidi-Tehrani F. , 1994, Dabagh A.M., 1990, Hollworth B.R., 1987, Sparrow, 1982). However, due to the high porosity and *Re*, these empirical correlations are not appropriate for solar

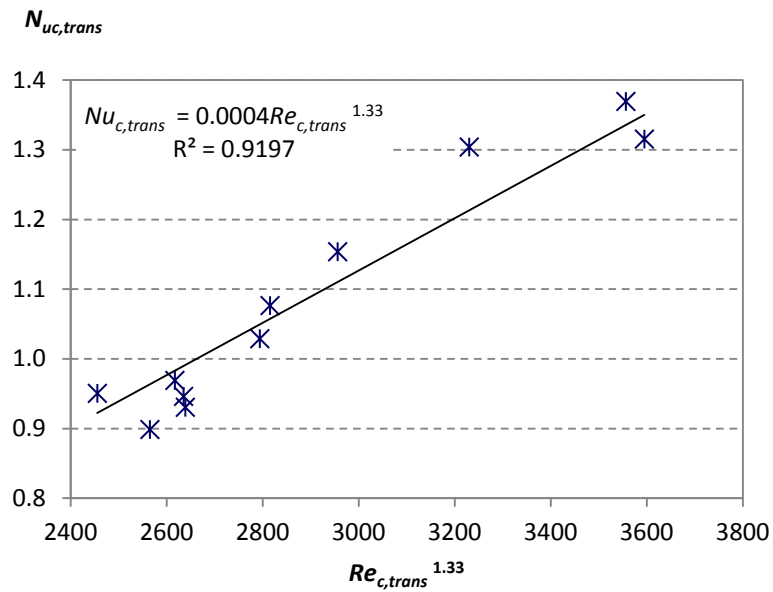
collector application. Therefore researches on empirical correlations (Arulanandam, 1999, Kutscher, 1993, Kutscher, 1994, Kutscher, 1992, Van Decker G. W. E., 2001) for this application were then carried out, followed by studies related to flow distribution (Dymond, 1997, Gunnewiek, 1996), wind effects (Fleck, 2002) and conductivity of the plate (Gawlik, 2005). Nonetheless, taking the account of the porosity, the hole diameter and the hole array geometry of present plate design, the closest empirical correlation can be applied is the Kutscher's model (Kutscher, 1992) . In Kutscher's study, the flow distribution was monitored in such condition of uniform flow and hence the effect of back-of-plate heat transfer in the plenum (vertical flow) was ignored. Pressure drop of the air in present study was not measured and thus the uniformity is uncertain. Gunnewiek and his team (Gunnewiek, 1996) had demonstrated that the vertical heat transfer is possible if the flow is non-uniform. However, to-date, there is no correlations that relate to non-uniform flow. In regard to this, heat transfer coefficients for the normal and vertical flows are developed in present work.

#### 4.3.4.2. $Nu_{c,trans}$ correlation

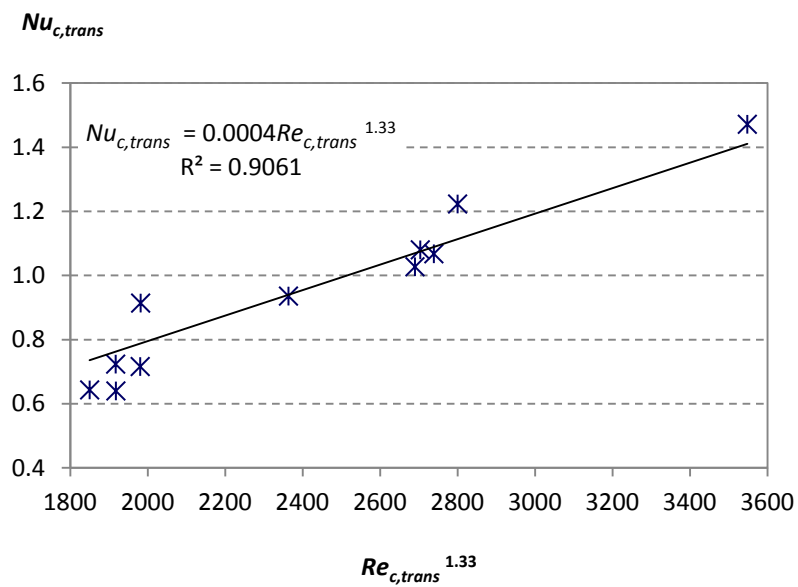
The correlation is developed from the Equations 4-23 to 4-25, and  $Re_{c,trans} = (v_s d) / (\rho \nu)$  where both  $Nu_{c,trans}$  and  $Re_{c,trans}$  are based on hole diameter ( $d$ ) as the characteristic length and ambient air properties. Figure 4-22 shows the correlations for plenum depth of 0.20, 0.25 and 0.30m respectively, while Figure 4-23 shows the average correlation of these three distances. The R-squared for the individual correlations are about 0.91 and the average is 0.93. The constant values for the correlations are the same, i.e. 0.0004, with exception of the plenum depth of 0.30m with a constant value of 0.0005. However, the small value (0.0001) of difference is insignificant and hence the depths of plenum in this study are unlikely to affect the heat transfer rate from the plate to the air. Thus, the suggested correlation for  $Nu_{c,trans}$  is:

$$Nu_{c,trans} = 0.0004 Re_{c,trans}^{1.33} \quad \text{for } 260 \leq Re_{c,trans} \leq 470 \quad (4-29)$$

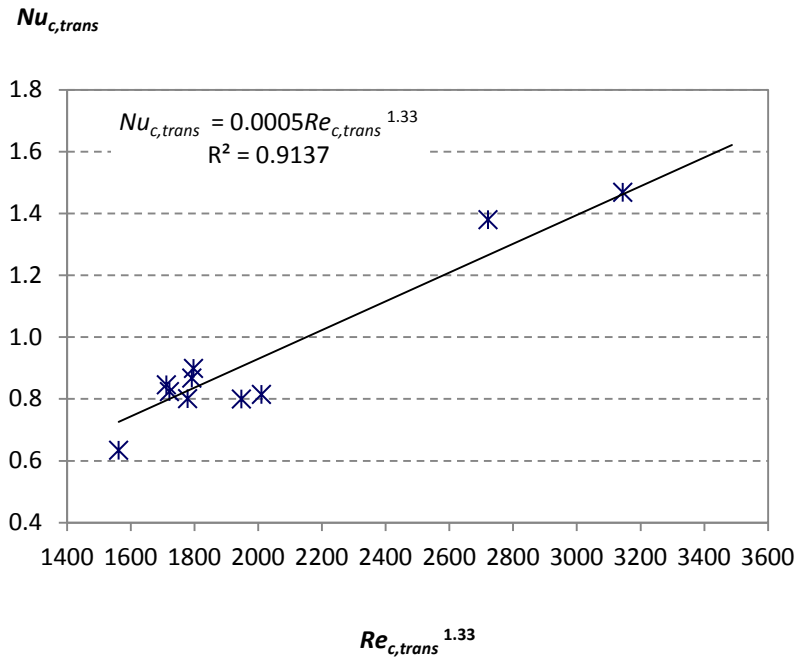
The heat transfer from the back-of-plate will be discussed in next section. Nonetheless, even though Kutscher's study (Kutscher, 1992, Kutscher, 1994) found the correlation that includes pitch and hole diameter, the effects of pitch and hole diameter in the present study remain conservative on account of the fact that one design of hole distribution has been studied.



(a)



(b)



(c)

Figure 4-22. Correlations of  $Nu_{c,trans}$  and  $Re_{c,trans}$  for plenum depths of (a) 0.20m, (b) 0.25m and (c) 0.30m.

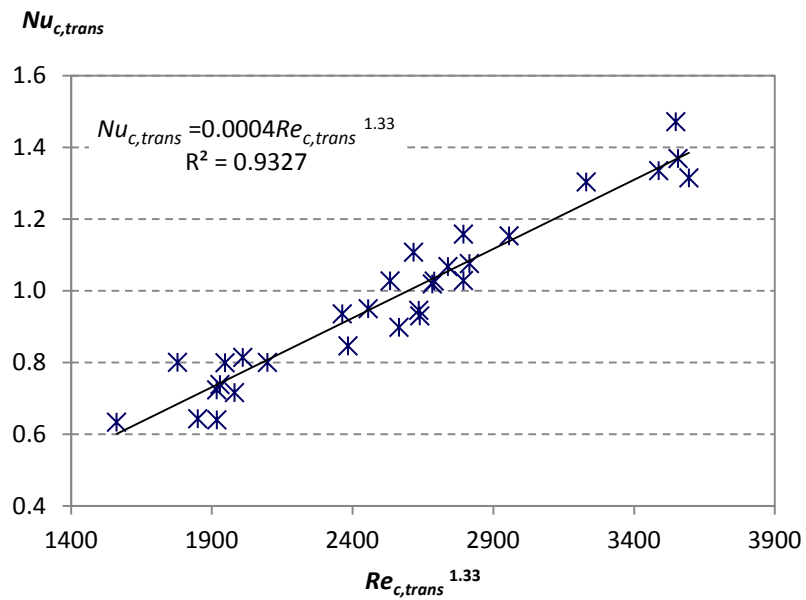


Figure 4-23. Average correlation of  $Nu_{c,trans}$  and  $Re_{c,trans}$ .

#### 4.3.4.3. $Nu_{f,trans}$ correlation

$h_f$  from experiments are calculated by using Equation 4-22 and 4-26, and substituted for Equation 4-27. Correlation of  $Nu_{f,trans}$  and  $Re_{f,trans}$  is then developed, where  $Re_{f,trans} = (v_f d_h) / (\nu)$ .  $Re_{f,trans}$  for the plenum depth of 0.25 and 0.30m are less than 2300. This indicates that the air in these plenum depths is in laminar flow mode. However, plenum depth with 0.20m shows turbulent flow for all the operation conditions. Figure 4-24 shows the correlation of  $Nu_{f,trans}$  for laminar flow, whereas Figure 4-25 is for turbulent flow with R-squared of 0.90 and 0.93 respectively. The  $Nu_{f,trans}$  correlations are suggested to be:

Laminar flow:

$$Nu_{f,L,trans} = 0.158 Re_{f,trans}^{1.25} \quad \text{for } 1100 < Re_{f,trans} < 2000 \quad (4-30)$$

Turbulent flow:

$$Nu_{f,T,trans} = 0.0023 Re_{f,trans}^{1.7} \quad \text{for } Re_{f,trans} \geq 2300 \quad (4-31)$$

Though the studies show that plenum depth affects the flow profile and hence the heat transfer rate, it is inappropriate to define the correlation, which involves the depth of plenum, because only three distances have been carried out. However, the present study found that plenum with  $H/D \geq 10$  would have turbulence profile for the vertical flow in the plenum. This information is crucial for designers to decide which flow profile would fit best for their purposes.

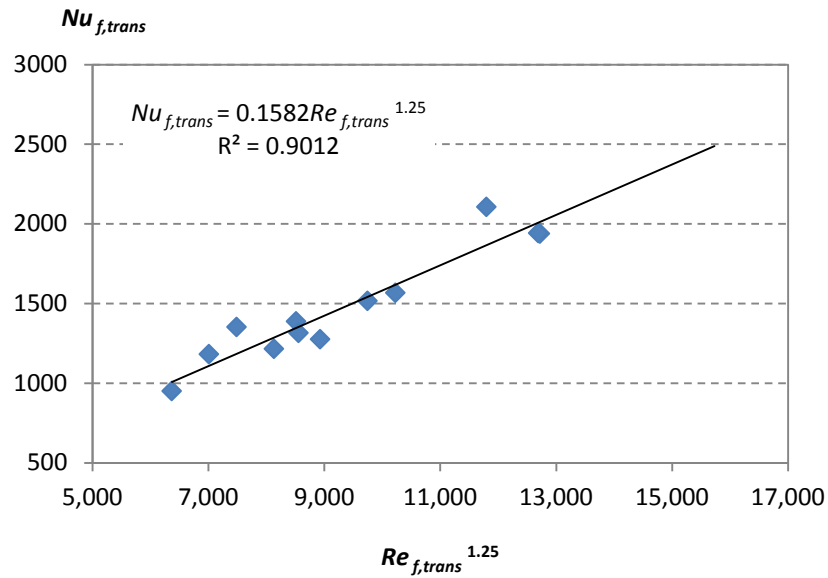


Figure 4-24. Correlation of  $Nu_{f,trans}$  and  $Re_{f,trans}$  for laminar flow.

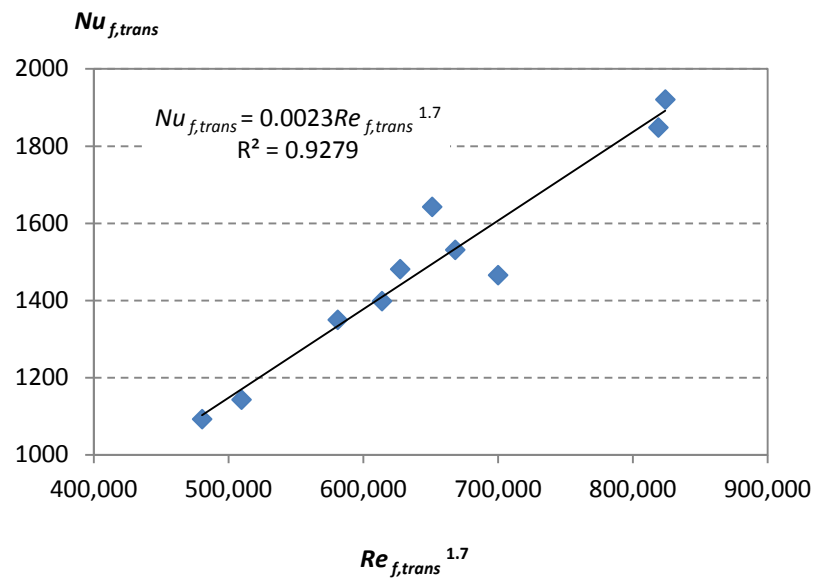


Figure 4-25. Correlation of  $Nu_{f,trans}$  and  $Re_{f,trans}$  for turbulent flow.

#### 4.3.5. Development of mathematical modelling for transpired plate heating performance

The model is developed based on the findings in the previous section. Hence, the energy balance equations in terms of heat fluxes are simplified and rewritten. By

substituting Equations 4-11, 4-24 and 4-26 for equation 4-21, the heat balance equation for the unglazed transpired collector gives:

$$(h_{c,trans} + h_{f,trans} + h_r)T_p - (h_{c,trans} + h_{f,trans}/2)T_i - (h_{f,trans}/2)T_{out} = I \alpha_p + h_r T_a \quad (4-32)$$

For the plenum air, substituting Equation 4-25 for Equation 4-22 gives:

$$h_{f,trans}T_p + (Gc_p - h_{f,trans}/2)T_i - (Gc_p + h_{f,trans}/2)T_{out} = 0 \quad (4-33)$$

Where  $G = \sum \dot{m}/A_p$ ; and  $T_f = (T_i + T_{out})/2$

Finally, Equations 4-23 and 4-24 are combined and give:

$$h_{c,trans}T_p - (Gc_p + h_{c,trans})T_i = -Gc_p T_a \quad (4-34)$$

Thus, Equations 4-32 to 4-34 can be written in a 3x3 matrix form:

$$\begin{bmatrix} (h_{c,trans} + h_{f,trans} + h_r) & -(h_{c,trans} + h_{f,trans}/2) & -(h_{f,trans}/2) \\ h_{f,trans} & (Gc_p - h_{f,trans}/2) & -(Gc_p + h_{f,trans}/2) \\ h_{c,trans} & -(Gc_p + h_c) & 0 \end{bmatrix} \begin{bmatrix} T_p \\ T_i \\ T_{out} \end{bmatrix} = \begin{bmatrix} I \alpha_p + h_r T_a \\ 0 \\ -Gc_p T_a \end{bmatrix} \quad (4-35)$$

#### 4.3.5.1. Comparison of heat exchange effectiveness between modelling and experimental results

Due to the Kutscher's study (Kutscher, 1992) developed the heat transfer coefficient through heat exchange effectiveness ( $\epsilon_{HX}$ ) and hence in this section  $\epsilon_{HX}$  is used for the comparisons purposes. From Figure 4-26, the values of  $\epsilon_{HX}$  which are calculated from both experiment and model methods give close results with the highest percent difference of 7.9% for three different plenum depths at various solar intensities and suction mass flow rate values. Whereas simulation results by using Kutscher's model, are as shown in Figure 4-27. Though Kutscher's study assumed that the temperature of the vertical flow is constant and has the same value of the outlet air temperature, which is contrast to present study that the vertical flow temperature is increasing gradually throughout the plenum; Kutscher's model gives the values of outlet air temperature that are close to the experiments. Hence, the results of the heat exchange effectiveness are comparable with the present study. However, they are only limited to solar

radiation intensity above  $400\text{Wm}^{-2}$  for all different depths. Moreover, by comparing to the experiment results, Kutscher's model gives the percent differences as 22%, 14% and 16% for  $D=0.20\text{m}$ ,  $D=0.25\text{m}$  and  $D=0.30\text{m}$  respectively, at  $307\text{Wm}^{-2}$ . On the other hand, if the main concern is the total rise in air temperature ( $T_{out}-T_a$ ), present model is comparable with Kutscher's. Therefore, the simplified heat transfer concept and experiment measurements can be used as alternative method to evaluate the thermal performance of the transpired plate solar collector even when the uniformity of the flow is uncertain. Furthermore, present model is able to simulate the mean air temperature in the plenum besides the plate temperature. This provides an idea of plenum air temperature when the uniformity of the flow is not perfectly monitored.

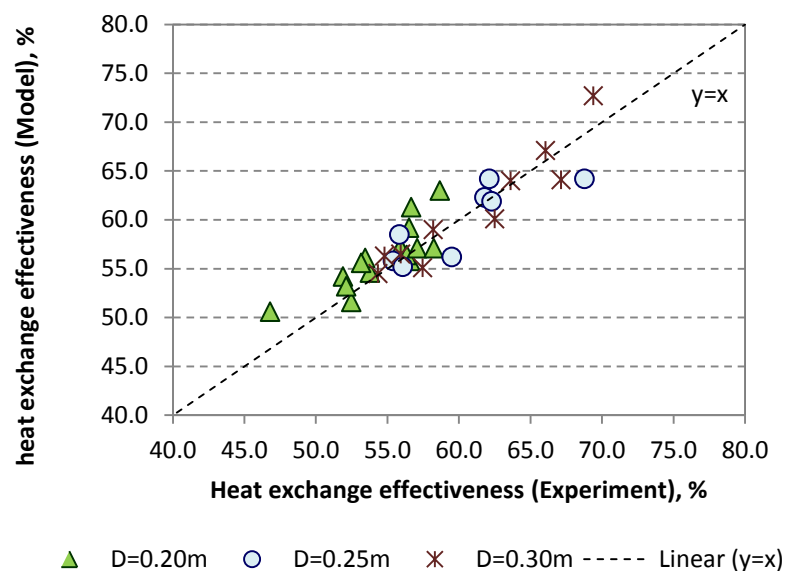
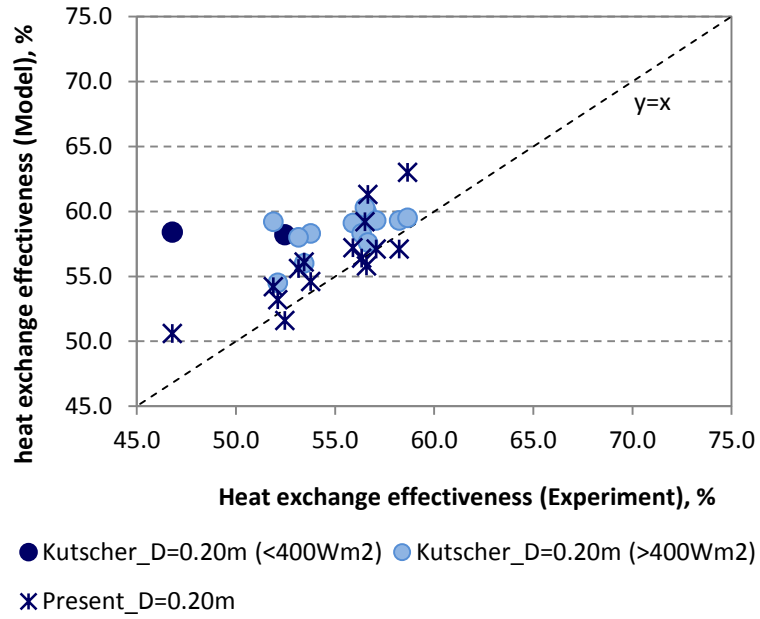
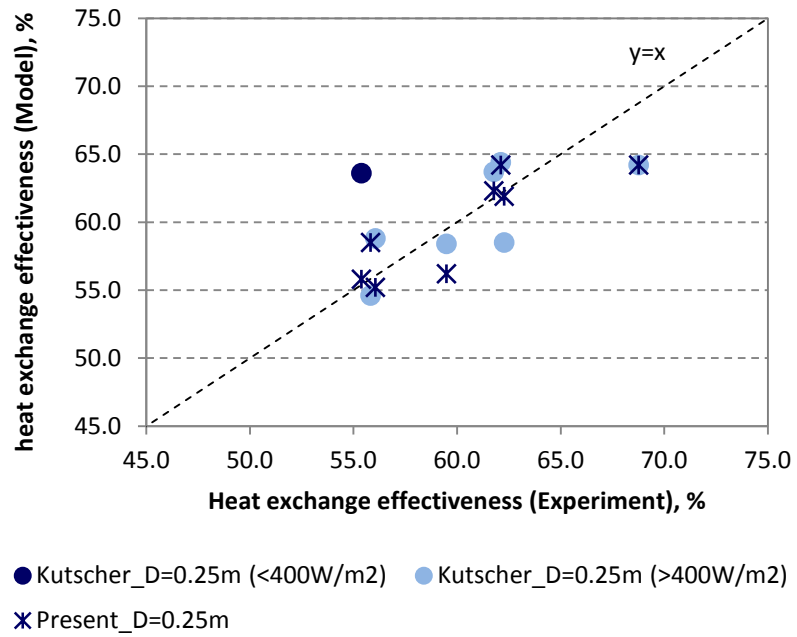


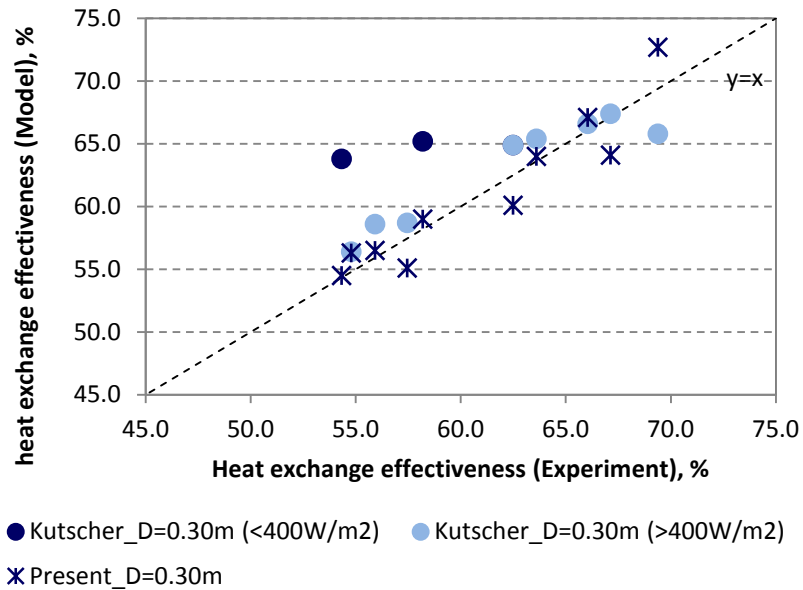
Figure 4-26. Comparison of heat exchange effectiveness between modelling and experiment results.



(a)



(b)



(c)

Figure 4-27. Comparisons of heat exchange effectiveness between Kutscher's model and experiment results for plenum depths of (a) 0.20m, (b) 0,25m and (c) 0.30m.

#### 4.4. Thermal performance comparison between flat and transpired plates

In this section, the thermal performances of both flat and transpired plates are evaluated by using the models that have been developed. The input parameters for both plates are the same, i.e. solar radiation intensity, ambient air temperature, airflow rate, plate area and plenum depth.

##### 4.4.1. Heat losses

As shown in Figure 4-4, great increase in flat plate temperatures are observed while increasing the solar radiation intensity. However, the values of  $T_f$  are just slightly increased. In contrast to the flat plate, transpired type gives higher rise in air temperature (Figure 4-28) though the values of  $T_p$  are lower than the flat type (Figure 4-29). This indicates that the transpired plate has better heat transfer compared to the flat plate. In order to further investigate the heat losses of the plates, Tables 4-3 and 4-4 show the fractions of heat fluxes of the plates. The useful heat flux that delivered by the system with flat plate is only about 30%

of total solar heat flux that been absorb by the plate while for the transpired plate it is about 84%. These represent the total heat losses for flat plate is about 70% while for transpired plate is only 20% of total energy absorbed. Figures 4-30 show the rises in heat fluxes of flat plate when the solar radiation intensity is increased from 300 to 800Wm<sup>-2</sup> at a constant airflow rate of 300m<sup>3</sup>hr<sup>-1</sup>. The losses to the ambient are increased and particularly the  $q_r$  has the greatest increase. As for the  $q_f$ , though it is increased with the solar radiation intensity, the amount of rise is smaller than the losses (sum of  $q_r$  and  $q_c$ ). These explain why the values of flat plate temperature increase greatly but only small rise in air temperature. On the other hand, for transpired plate, the rise in  $q_c$  and  $q_f$  are greater than the  $q_r$  (Figure 4-31). This results in great increase of  $q_d$  (sum of  $q_c$  and  $q_f$ ). The heat losses to ambient of flat plate are partly caused by convection heat loss while for transpired plate, the ambient convection heat loss can be ignored, whereby most of the heat which indeed would loss to the ambient has been sucked into the plenum through the small holes. This reduces the total heat losses and hence has better heat transfer with transpired design.

The values of temperatures decrease with airflow rates, where flat plate has higher plate temperature (Figure 4-32) and lower air temperature (Figure 4-34) compared to the transpired plate. Though Figure 4-29 shows that  $T_{out}$  relies on the local solar radiation availability, it can be improved by controlling the airflow rate. For instance, a heating system with transpired plate is installed at location with solar radiation availability of 500Wm<sup>-2</sup> and operated at airflow rate of 200m<sup>3</sup>hr<sup>-1</sup> (Figure 4-33) is able to achieve almost the same value of  $T_{out}$  at location with solar radiation intensity of 800Wm<sup>-2</sup> that operates at 300m<sup>3</sup>hr<sup>-1</sup> (Figure 4-28). Thus, lower airflow rate should be used if the heating demand requires higher value of  $T_{out}$  especially if the heating systems are installed at location with low intensity of solar radiation.

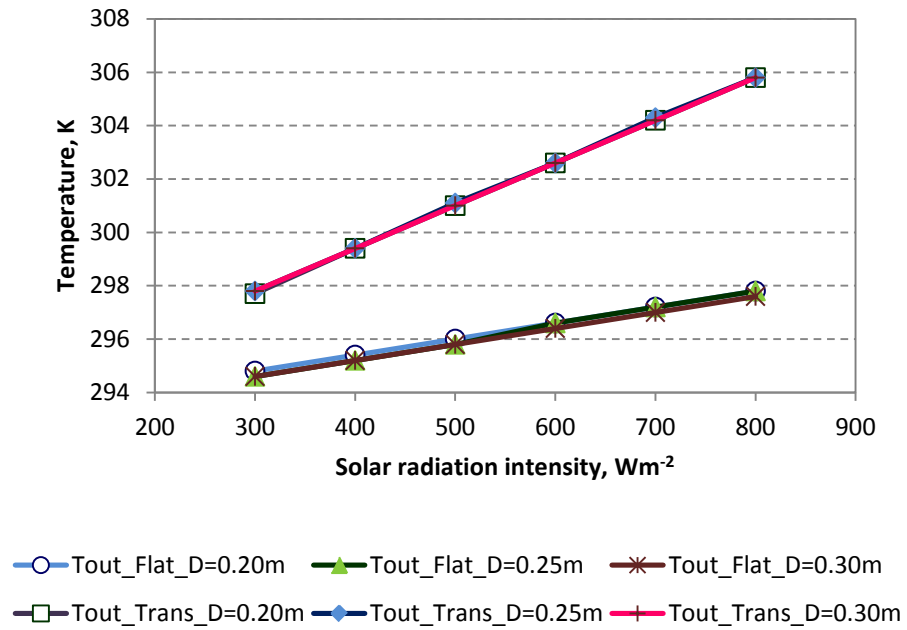


Figure 4-28. Simulated  $T_{out}$  of flat and transpired plates for plenum depths of 0.20m, 0.25m and 0.30m at a constant  $V_{fan}$  of  $300m^3hr^{-1}$  and  $T_a= 293K$ .

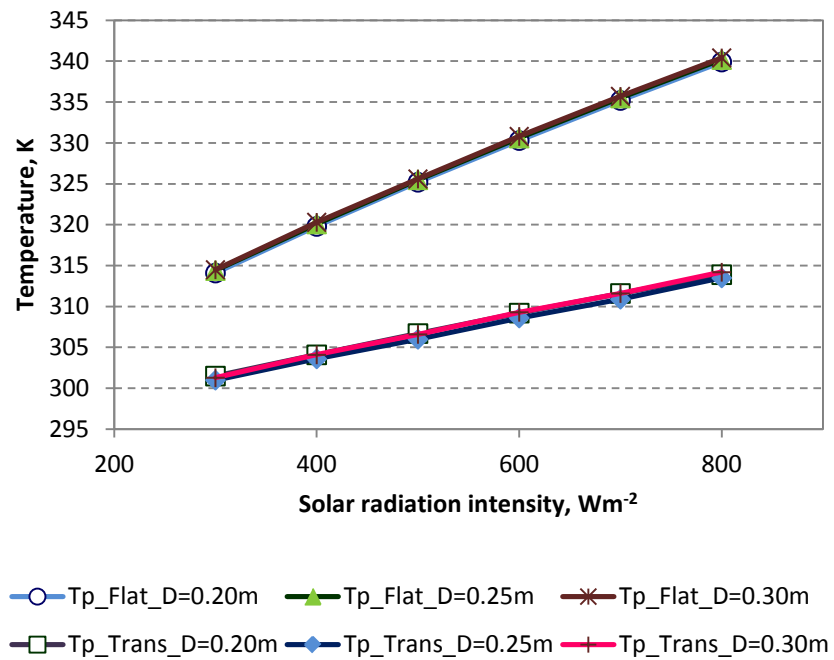


Figure 4-29. Simulated  $T_p$  of flat and transpired plates for plenum depths of 0.20m, 0.25m and 0.30m at a constant  $V_{fan}$  of  $300m^3hr^{-1}$  and  $T_a= 293K$ .

Table 4-3. Heat fluxes of flat plate.

$I, \text{Wm}^{-2}$	$V_{fan}, \text{m}^3\text{hr}^{-1}$	$T_a, \text{K}$	$D, \text{m}$	$S^*$ (%)	$q_r^*$ (%)	$q_c^*$ (%)	$q_f=q_d^*$ (%)
300	300	293	0.20	291.7 (100)	123.3 (42.3)	79.6 (27.3)	88.7 (30.4)
800	300	293	0.20	779.0 (100)	312.1 (40.1)	222.8 (28.6)	244.1 (31.3)
300	300	293	0.25	291.7 (100)	125.0 (42.9)	80.9 (27.7)	85.7 (29.4)
800	300	293	0.25	779.0 (100)	314.7 (40.4)	224.7 (28.8)	239.6 (30.8)
300	300	293	0.30	291.7 (100)	126.0 (43.2)	81.7 (28.0)	83.9 (28.8)
800	300	293	0.30	779.0 (100)	316.2 (40.6)	225.8 (29.0)	237.0 (30.4)

\* They are heat fluxes that based on Equation 4-2 in unit of  $\text{Wm}^{-2}$ , where  $S$  is the total solar heat flux absorb by the plate,  $q_r$  is and  $q_c$  are the losses to ambient through radiation and convection respectively.  $q_f$  is the convection of back-of-plate which is also the useful heat flux that delivered by this heating system.

Table 4-4. Heat fluxes of transpired plate.

$I, \text{Wm}^{-2}$	$V_{fan}, \text{m}^3\text{hr}^{-1}$	$T_a, \text{K}$	$D, \text{m}$	$S^*$ (%)	$q_r^*$ (%)	$q_c^*$ (%)	$q_f^*$ (%)	$q_d^*$ (%)
300	300	293	0.20	291.7 (100)	46.6 (16.0)	136.8 (46.9)	108.3 (37.1)	245.1 (84.0)
800	300	293	0.20	779.0 (100)	122.6 (15.7)	337.5 (43.3)	318.9 (40.9)	656.4 (84.3)
300	300	293	0.25	291.7 (100)	43.7 (15.7)	128.8 (46.0)	119.1 (38.3)	247.9 (84.3)
800	300	293	0.25	779.0 (100)	120.0 (16.0)	330.4 (44.0)	328.8 (39.9)	659.2 (84.0)
300	300	293	0.30	291.7 (100)	43.7 (15.0)	128.8 (44.2)	119.1 (40.8)	247.9 (85.0)
800	300	293	0.30	779.0 (100)	119.7 (15.4)	330.4 (42.4)	328.8 (42.2)	659.2 (84.6)

\* They are heat fluxes that based on Equation 4-25 in unit of  $\text{Wm}^{-2}$ , where  $S$  is the total solar heat flux absorb by the plate,  $q_r$  is radiation heat loss;  $q_d$  is the sum of  $q_c$  and  $q_f$ , also the useful heat flux that delivered by this heating system.

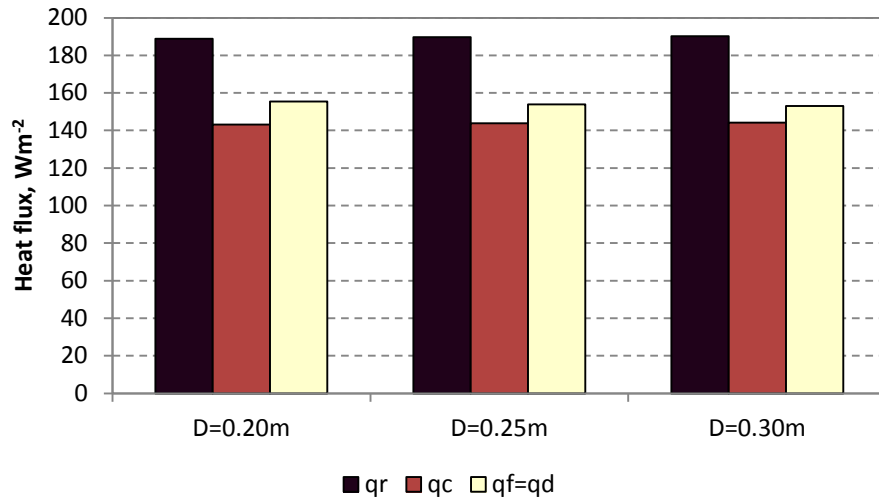


Figure 4-30. Heat fluxes of flat plate for  $I=300$  to  $I=800\text{Wm}^{-2}$ .

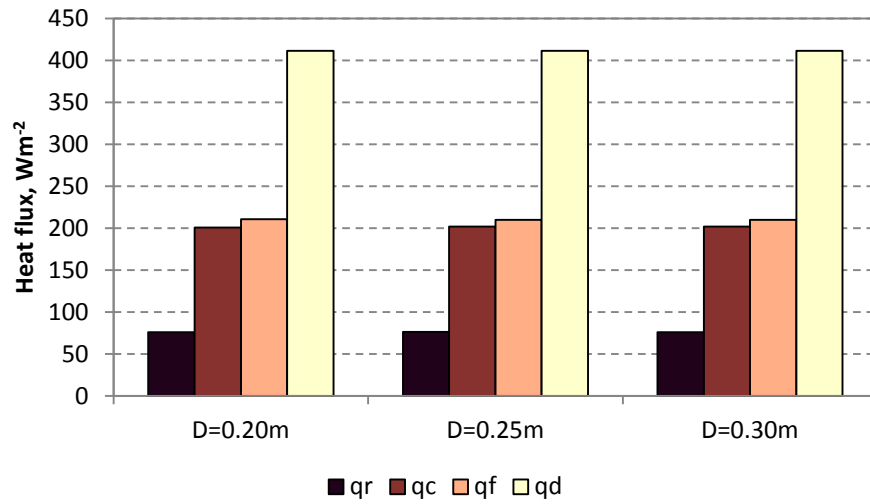


Figure 4-31. Heat fluxes of transpired plate for  $I=300$  to  $I=800\text{Wm}^{-2}$ .

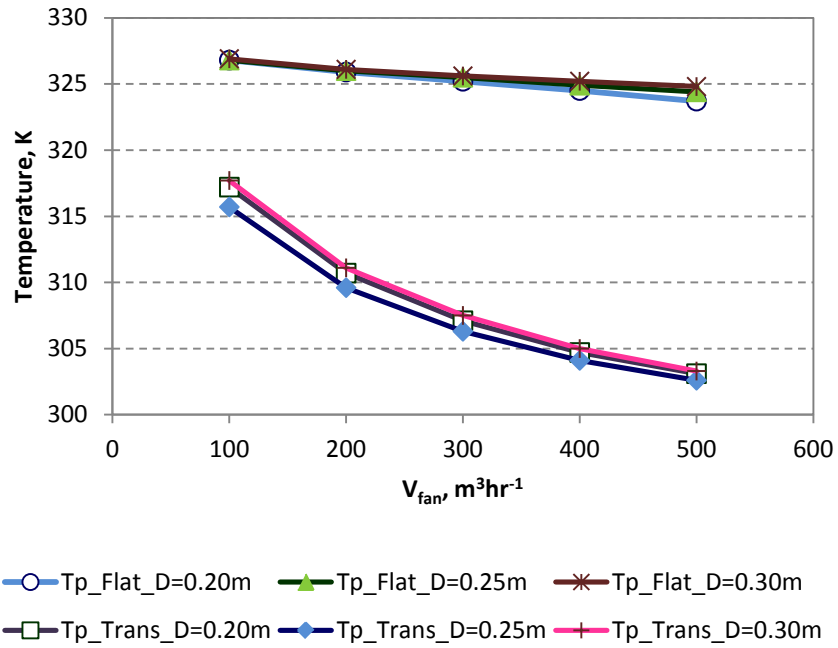


Figure 4-32. Simulated  $T_p$  of flat and transpired plates for plenum depths of 0.20m, 0.25m and 0.30m at a  $I=500Wm^{-2}$  and  $T_a= 293K$ .

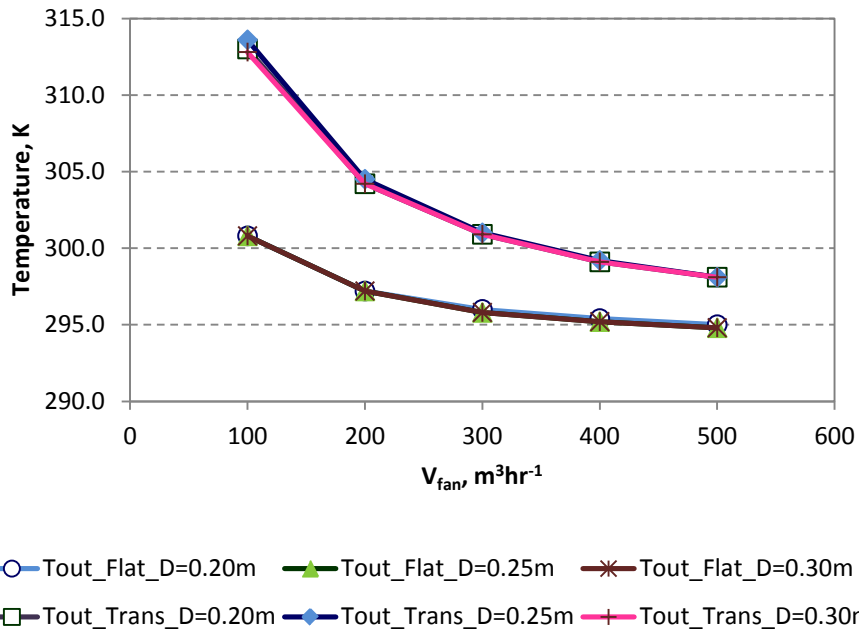


Figure 4-33. Simulated  $T_{out}$  of flat and transpired plates for plenum depths of 0.20m, 0.25m and 0.30m at a  $I=500Wm^{-2}$  and  $T_a= 293K$ .

#### 4.4.2. Efficiency

The system efficiencies are plotted over a range of solar radiation (Figure 4-34) and over a range of airflow rate (Figure 4-35). Efficiency is relatively more sensitive to airflow rate than solar radiation intensity. From the lowest to the highest intensity of solar radiation, the efficiencies for both plates are almost constant (Figure 4-34). On the other hand, increasing the airflow rate from 100 to  $500\text{m}^3\text{hr}^{-1}$  would increase the system efficiencies by about 6% and 17% with flat and transpired plates respectively (Figure 4-35). These results show that the thermal performance in terms of efficiency is not hindered by the local solar radiation availability and can be improved by controlling the airflow rate. Higher efficiency gives higher output mass flow rate but lower rise in air temperature. Thus, the airflow rate need to be adjusted depend on the heating demand to satisfy the thermal comfort as well as the air mass flow rate requirements.

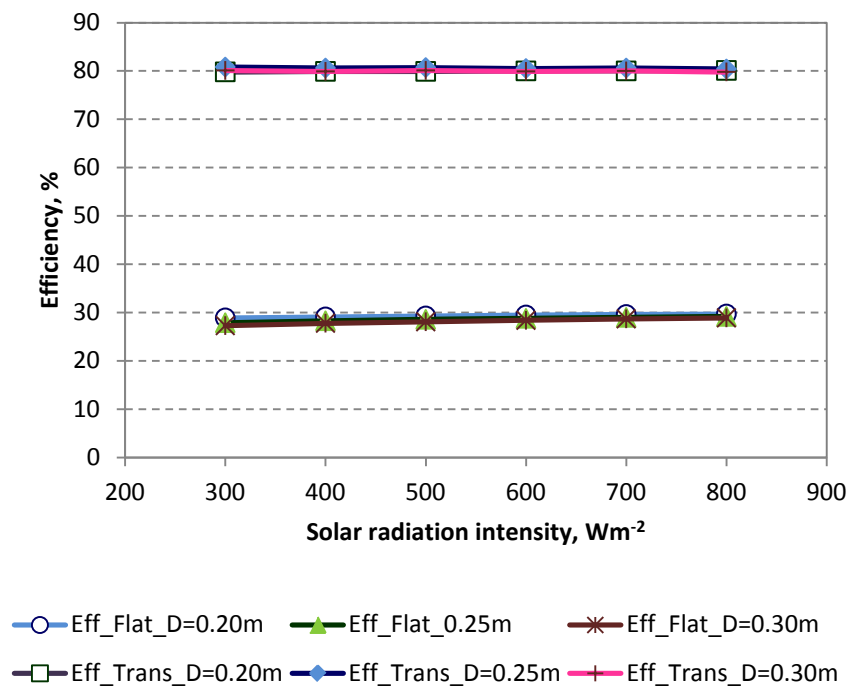


Figure 4-34. Values of efficiency of flat and transpired plates at a constant  $V_{fan}=300\text{m}^3\text{hr}^{-1}$ .

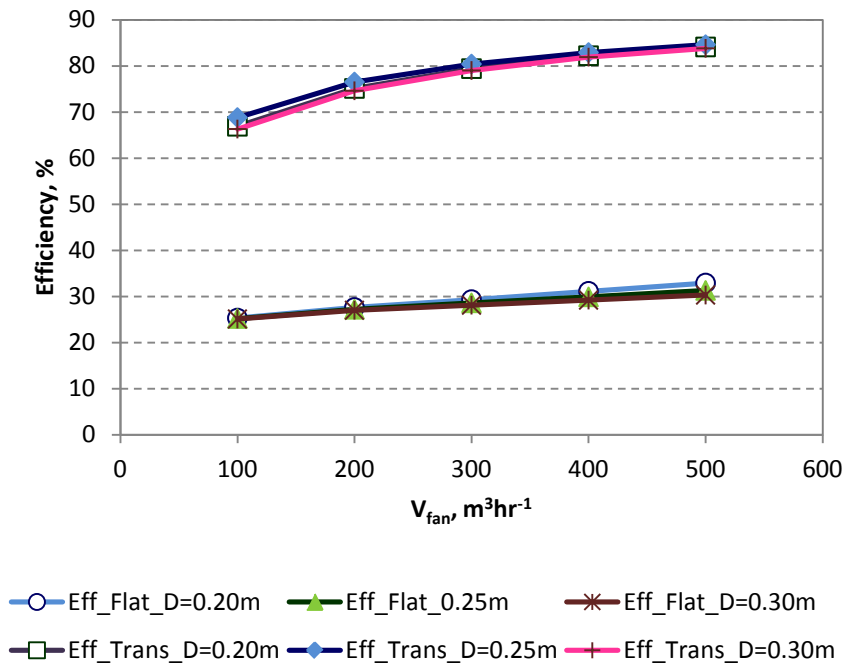


Figure 4-35. Values of efficiency of flat and transpired plates at a constant  $I=500Wm^{-2}$ .

#### 4.5 System performance comparisons of solar air heaters

The system efficiency of present system is compared to various designs of solar air heaters and they are as shown in Table 4-5. Present design gives the highest efficiency among all the reported maximum values of efficiency. Besides the benefit of low convection heat loss to the ambient of present design, all the active solar air heaters are glass covered to form a channel between the glass and absorber for the air passing through it, whereas present design is the unglazed type, hence gives higher thermal performance. Present design not only manages to achieve higher system efficiency, but also benefit in terms of system simplicity and lower cost (Chapter 6). Moreover, because of the high efficiency, it is more aesthetical flexible in choosing the façade colours.

Table 4-5. System efficiency comparisons among some reported solar air heaters.

Solar air heater	System efficiency	References
Present (maximum)	0.82	
Transpired solar collector	0.78	(Kutscher, 1993)
Vertical flat plate	0.50	(Hatami, 2008)
Flat plate	0.49	(Gao, 2007)
Cross-corrugated plate	0.60	(Gao, 2007)
Single pass with double ducts	0.70	(Forson, 2003)
Double pass-finned plate	0.55	(El-Sebaili, 2011)
Double pass v-corrugated plate	0.65	(El-Sebaili, 2011)
Double pass with aluminium cans	0.70	(Ozgen, 2009)
Wire-mesh packing	0.46-0.68	(Prasad, 2009)
	0.80	(Aldabbagh, 2010)
Cylindrical absorber with conical concentrator	0.12	(Togrul, 2004)

#### 4.6. Summary

In this chapter the experiment results of heating systems with flat and transpired plate are discussed. Mathematical models for the thermal performances have also been developed. The main findings can be summarised as follows:

- 1) The heat transfer between the flat plate and the air in the plenum are poor, e.g.  $T_p$  increases about 27 to 28K, but only about 2 to 3K rise in air temperature when solar radiation intensity increases from  $307\text{Wm}^{-2}$  to  $820\text{Wm}^{-2}$ .
- 2) Vertical flow heat transfer of transpired plate accounts for about 40 to 50% of total useful energy delivered, and thus should not be ignored.
- 3) Normal flow Nu correlation for transpired plate with 0.84% of porosity with triangular array of holes and 2m of height has been modified as follows:

$$Nu_{c,trans} = 0.0004Re_{c,trans}^{1.33} \quad \text{for } 260 \leq Re_{c,trans} \leq 470$$

- 4) Vertical flow Nu correlation for transpired plate with 0.84% of porosity with triangular array of holes and 2m of height has been developed as follows:

Laminar flow:

$$Nu_{f,L,trans} = 0.158Re_{f,trans}^{1.25} \quad \text{for } 1100 < Re_{f,trans} < 2000$$

Turbulent flow:

$$Nu_{f,T,trans} = 0.0023Re_{f,trans}^{1.7} \quad \text{for } Re_{f,trans} \geq 2300$$

- 5) Though present study has simplified the heat transfer concept between the back-of-plate and the vertical airflow, the values of simulated heat exchange effectiveness of the system are close to the previous study model. Hence, this simplified method in terms of theoretical calculation and experiment measurements can be used as alternative methods to evaluate the thermal performance of transpired plate solar collector even when the uniformity of the flow is uncertain.
- 6) Transpired type is a better design in terms of heat transfer. For instance, systems that operate at  $500\text{Wm}^{-2}$  of solar radiation intensity,  $300\text{m}^3\text{hr}^{-1}$  of airflow rate and air temperature of  $293\text{K}$  give  $3\text{K}$  and  $8\text{K}$  in air temperature rise for flat and transpired plates respectively.
- 7) System efficiency is relatively more sensitive to airflow rate compared to solar radiation intensity. At various solar radiation intensities, the efficiencies for both plates are almost constant. On the other hand, increasing the airflow rate would increase the system efficiencies for about  $6\%$  and  $17\%$  with flat and transpired plates respectively.
- 8) Installations of these heating systems at location with low solar radiation intensity, the thermal performance in terms of air temperature rise can be increased by using lower airflow rate.
- 9) Present design shows the highest system efficiency among various types of solar air heaters.

## 5. Solar façade for space cooling

### 5.1 Introduction

In view of the system simplicity, the system designs for space heating (Chapter 4) were adopted for cooling test with water flowing over the sandtile wall. The flat and transpired plate façades were used to collect the heat for water evaporation on the wet sandtile wall. The design is as shown in Figure 5-1. Experimental works were carried out for the flat plate façade and due to the fact that the results showed that water evaporation was too low to provide cooling effect, a simple simulation study was carried out for the transpired plat with this design. Simulation results showed that replacing the flat plate with transpired type was insufficient to give the cooling effect, too. In addition, the water evaporation process increased the air humidity. Thus, the air that directly supply into the building might not suitable for space ventilation, especially in the regions with humid climate.

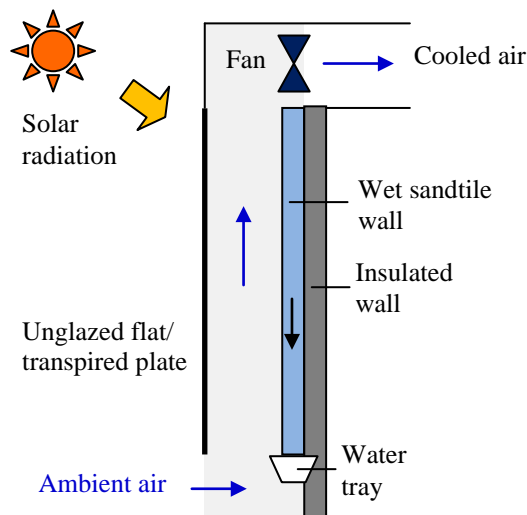


Figure 5-1. Schematic diagrams of cooling systems with flat plate as solar collector façade.

Therefore, the design was hence modified and the façade was replaced by a transpired plate as shown in Figure 5-2. This concept is similar to a counter flow heat exchanger whereby the heat from the second plenum (flowing from the bottom) is absorbed by the water (flowing from the top). The results for single plenum systems are summarised, and the mathematical model, experimental results as well as parametric analysis are discussed within this chapter.

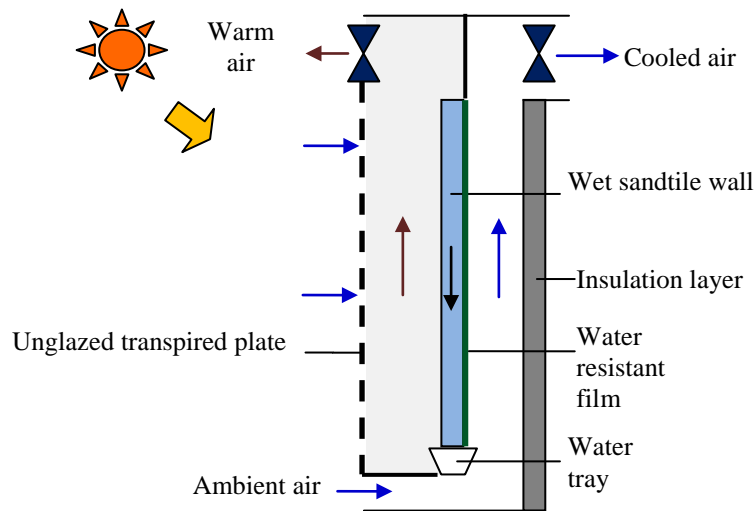


Figure 5-2. Schematic diagrams of cooling systems with transpired plate as solar collector façade.

## 5.2. Results and analysis of cooling system with flat plate collector and single plenum

Parts of the results are selected for discussions, however the complete sets of measured data can be found in Appendix III-3. Parameters for the experiments of cooling system with flat plate collector and single plenum are as described in Table 5-1.

Table 5-1 Parameters for the experiments of cooling system with flat plate collector and single plenum.

Parameter	Value/ range
Solar radiation intensity, $Wm^{-2}$	300-800
Volume airflow rate, $m^3hr^{-1}$	67-331
Plenum depth, m	0.20
Height of the flat plate, m	2.0
Width of the flat plate, m	1.0
Area of the flat plate, $m^2$	2.0
Plate thickness, m	0.001
Water flow rate per unit area of sandtile wall, $kgs^{-1}m^{-2}$	0.01

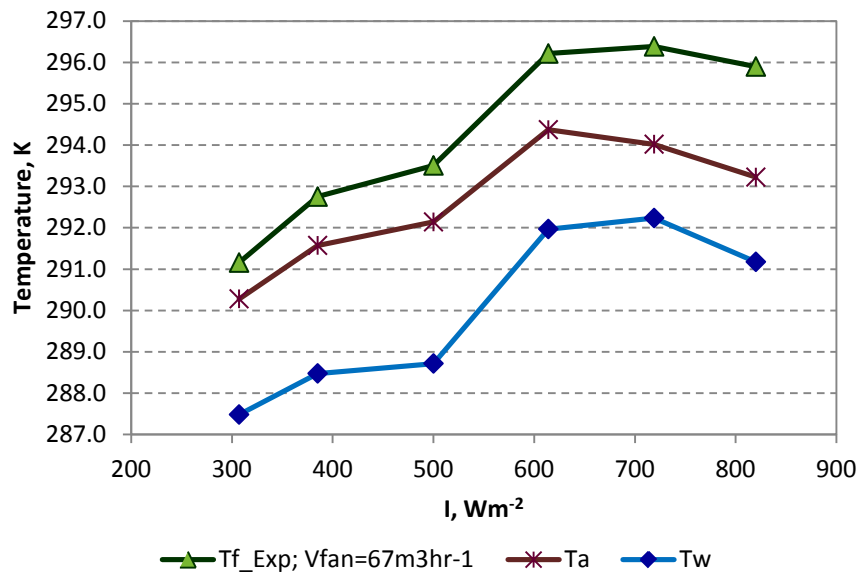
### 5.2.1. Parametric analysis cooling system with flat plate collector and single plenum

The parameters that are discussed include ambient air temperature, solar radiation intensity, airflow rate and humidity.

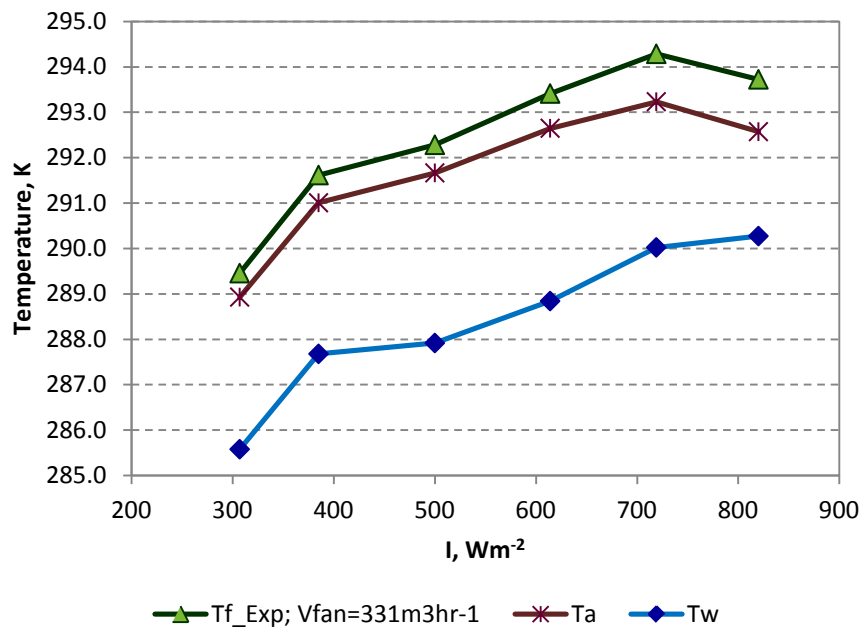
#### ***Effects of ambient air and inlet water temperatures***

The influence of  $T_a$  on  $T_p$  has been discussed in the section 4.2.4.2. In this section the discussions involves only the effects of  $T_a$  and  $T_w$  on the  $T_f$ . Figure 5-3 shows the effects of  $T_a$  and  $T_w$  on  $T_f$  at various radiation intensities. As the values of  $T_f$  follow the patterns of  $T_a$  and  $T_w$ ,  $T_f$  is either influenced by any of them or both. Similarly, the values of  $T_f$  follow the patterns of  $T_a$  and  $T_w$  over a range of airflow rates (Figure 5-4). In order to further investigate the effect of  $T_a$  and  $T_w$  on the plenum air,  $(T_a - T_{out})$  is plotted based on simulation results from the corrected model. To investigate the effect of  $T_a$ , the input parameters were  $I=500Wm^{-2}$ ,  $V_{fan}=200m^3hr^{-1}$ ,  $RH=50\%$ , and  $T_a=275$  to  $315K$ . The input water temperatures were set to be 3K lower than  $T_a$ . Whereas to investigate the effect of  $T_w$ , the parameters were the same as above mentioned except the  $T_a$  is set to be a constant value of 300K and the  $T_w$  is ranging from 277 to 310K. The results are plotted in Figure 5-5. Results show that the values of  $(T_a - T_{out})$  are almost constant

even though  $T_a$  has increased 40K; whilst decreasing the temperatures of the inlet water would result in colder outlet air. Though the patterns of temperature rise in  $T_f$  follows the patterns of  $T_a$  and  $T_w$ , the net temperature differences of  $(T_a - T_{out})$  are not affected by the  $T_a$  but give better cooling effect with lower temperature of  $T_w$ .

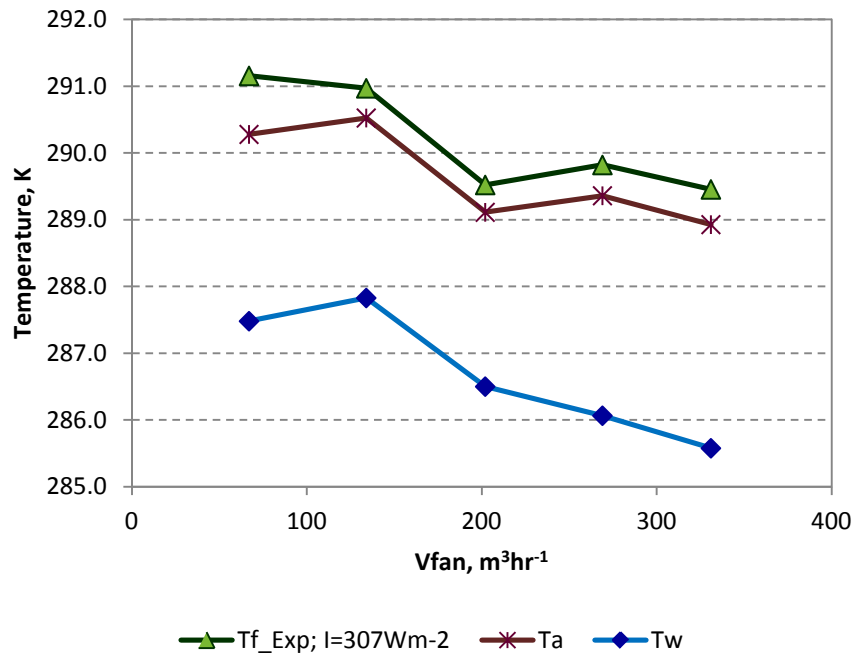


(a)

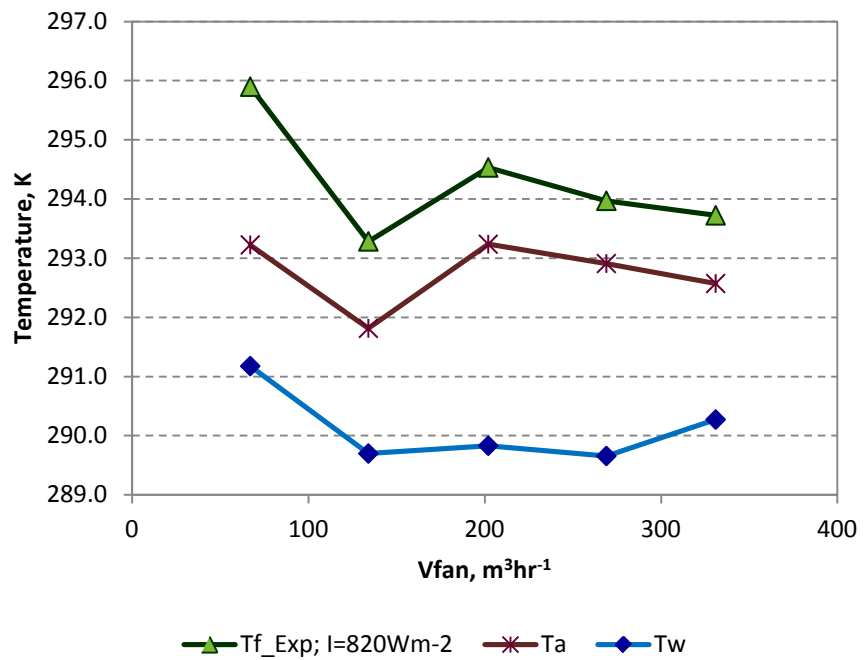


(b)

Figure 5-3. Effects of  $T_a$  and  $T_w$  on  $T_f$  over a range of solar radiation intensity at (a) low and (b) airflow rates.



(a)



(b)

Figure 5-4. Effects of  $T_a$  and  $T_w$  on  $T_f$  over a range of airflow rate at (a) low and (b) high solar radiation intensities.

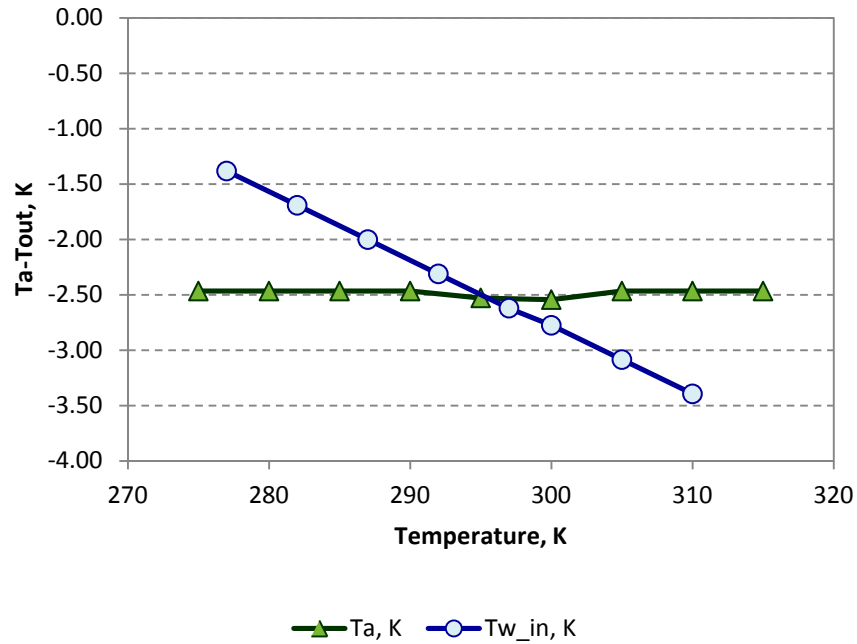


Figure 5-5. The effects of  $T_a$  and  $T_w$  on  $(T_a - T_{out})$ .

### 5.2.2. Cooling performance

The cooling performance of the system is investigated in terms of temperature difference between the outlet and the ambient  $(T_a - T_{out})$ , and cooling efficiency of the system.

#### **Temperature difference, $(T_a - T_{out})$**

As shown in Figure 5-6, the values of  $(T_a - T_{out})$  are negative over the studied ranges of solar radiation intensity and airflow rate. The negative values indicate that the inlet air from the ambient is not cooled by the system and in fact heat is added into the air and hence, adverse results. The cooling effect is far to achieve when the solar radiation intensity is high and the airflow rate is low. Nonetheless, further investigation was carried out to compare the plenum air temperature for the system with dry sandtile wall. This was done by using the model that has been developed in Chapter 4 with the same input parameters as the tests for wet sandtile wall. Figure 5-7 shows the plenum air temperatures of the systems with dry and wet sandtile wall. The air temperatures are lower when the wall is wet.

Thus, system with wet sandtile wall does remove the heat but due to the small amount (relative to the total heat gain of the air) of heat removal (Figure 5-8), the cooling effect is not significant enough to produce cold air.

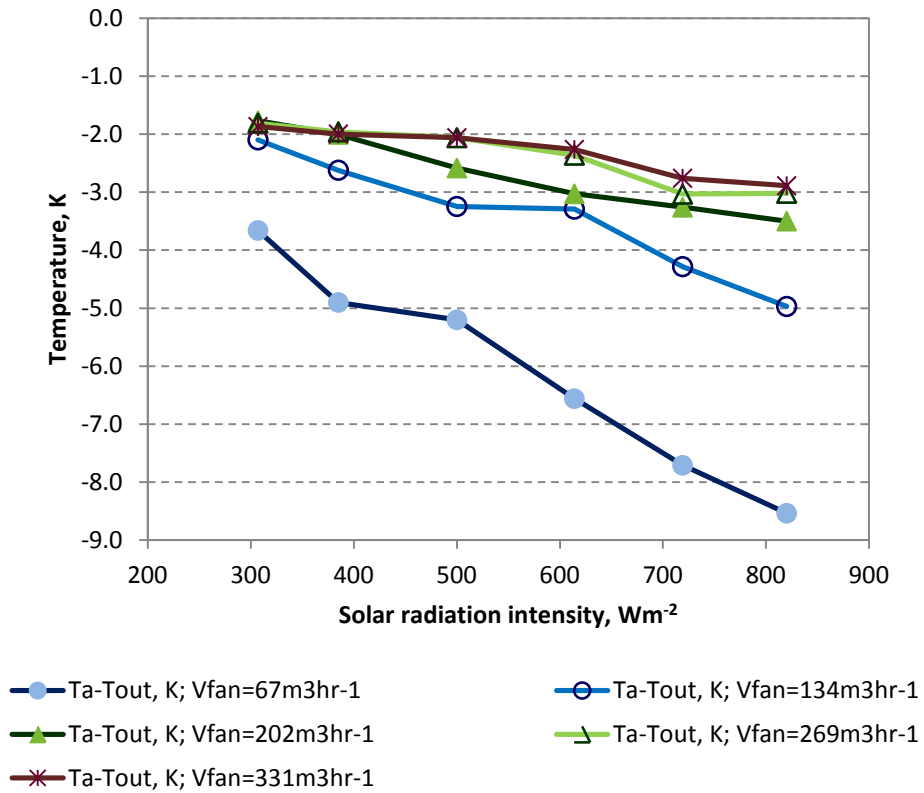


Figure 5-6. Values of  $(T_a - T_{out})$  at different airflow rates solar radiation intensities.

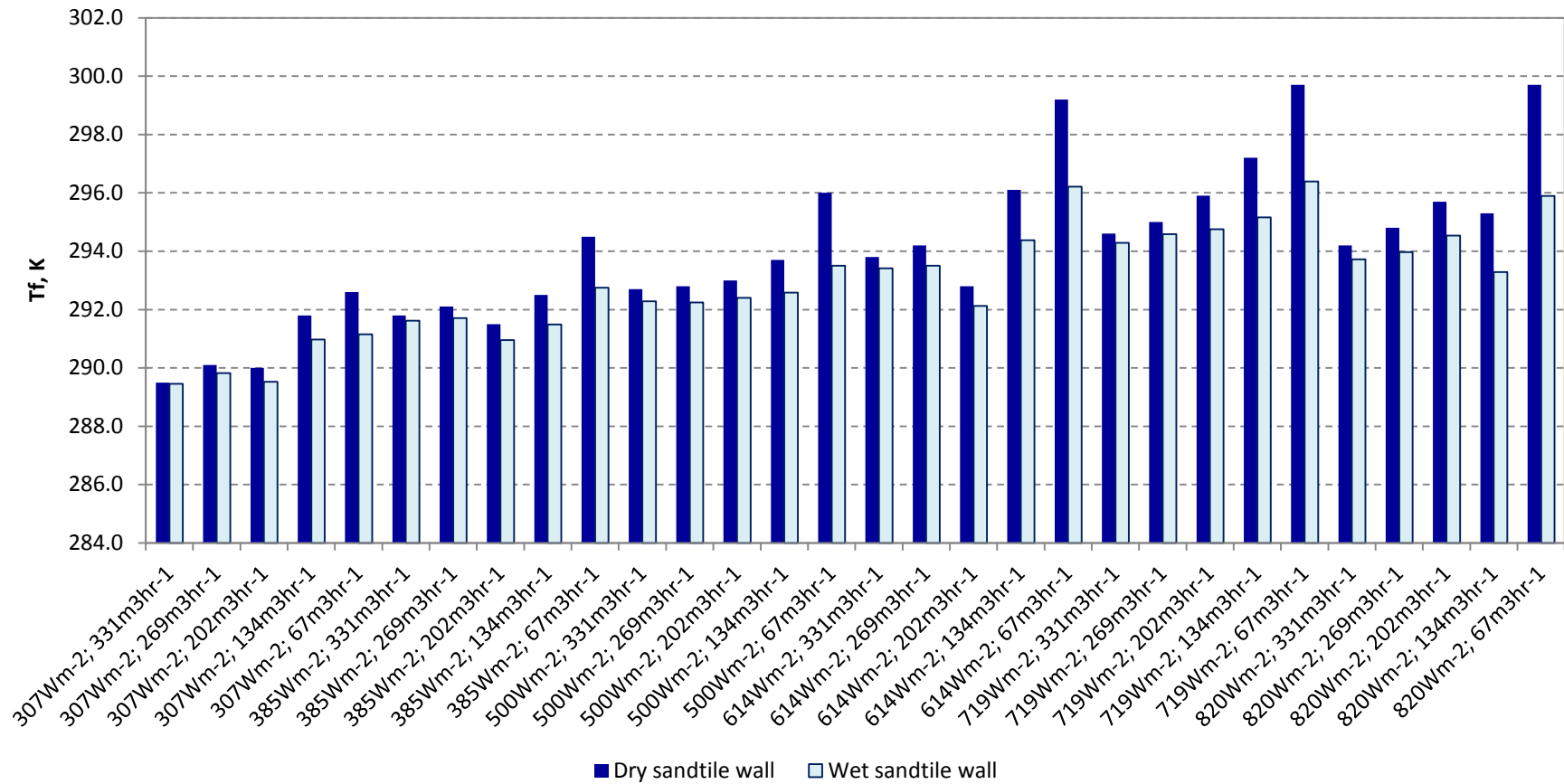


Figure 5-7. Values of plenum air temperatures of the systems with dry and wet sandtile wall.

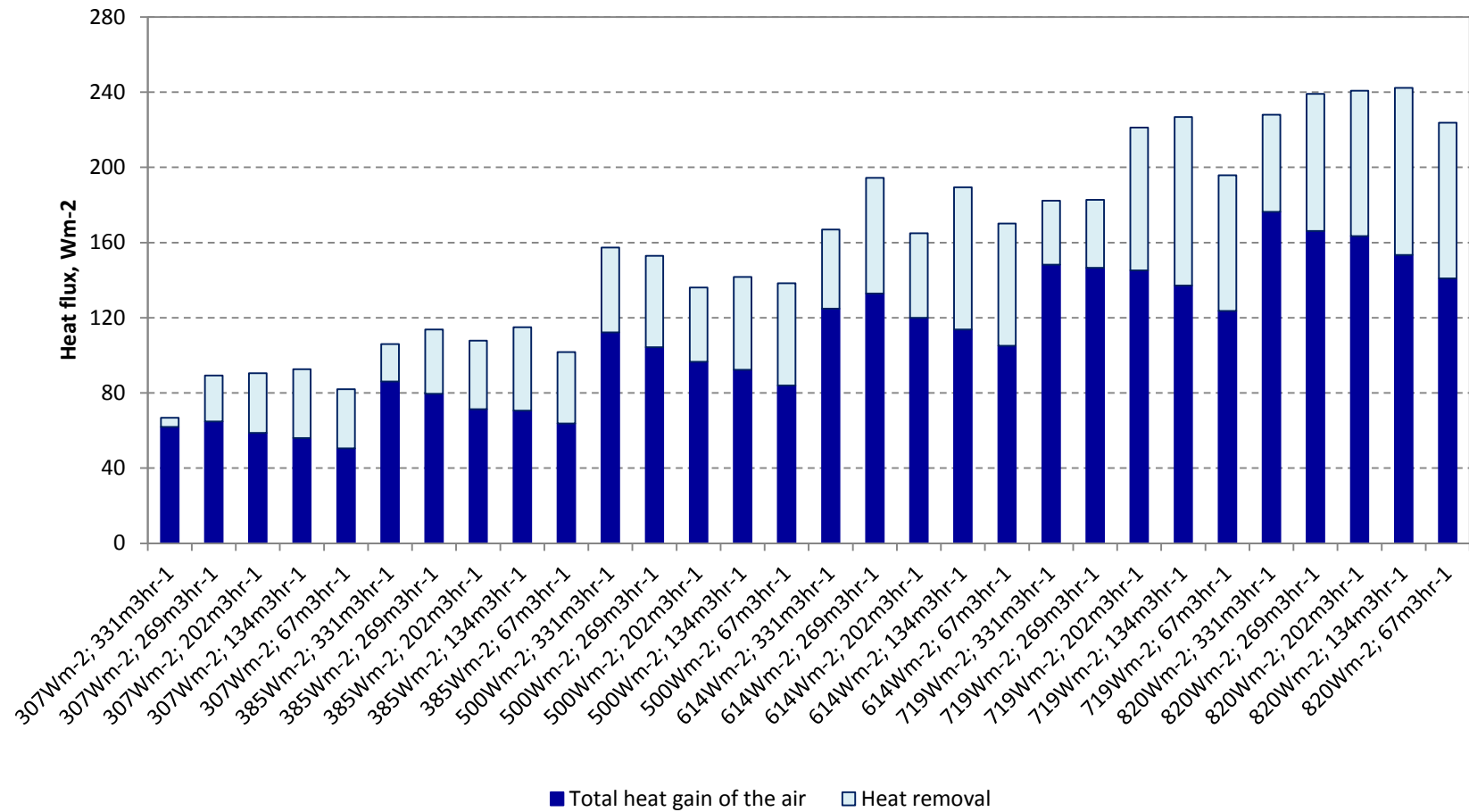


Figure 5-8. Heat fluxes of the heat gain and removed by the system with flat plat and single plenum.

### Cooling efficiency

The cooling efficiency is defined as the ratio of evaporation cooling capacity to the total energy consumption for the fans and pump ( $Q_{aux}$ ):

$$\eta_{cool,1 Plenum} = d\dot{m}_w H_{fg} / Q_{aux} \quad (5-1)$$

The power applied for the fans are calculated according to the power-airflow rate chart that provided by the supplier and it is included in Appendix IV. Whereas the water pump is assumed to have an efficiency of 0.6 and the approximate power consumption is calculated from Equation 5-2.

$$P_{pump} = [V_{water} \rho_{water} g H / (3.6 \times 10^6)] / \eta_{pump} \quad (5-2)$$

Figure 5-9 shows the cooling efficiency of the system. The efficiencies are above 1.0 with maximum close to 10.0. These indicate that the power consumption for the fans and pumps are a lot lower than the cooling capacity of the system, though the overall cooling effect of the air is insignificant ( $T_{out} > T_a$ ).

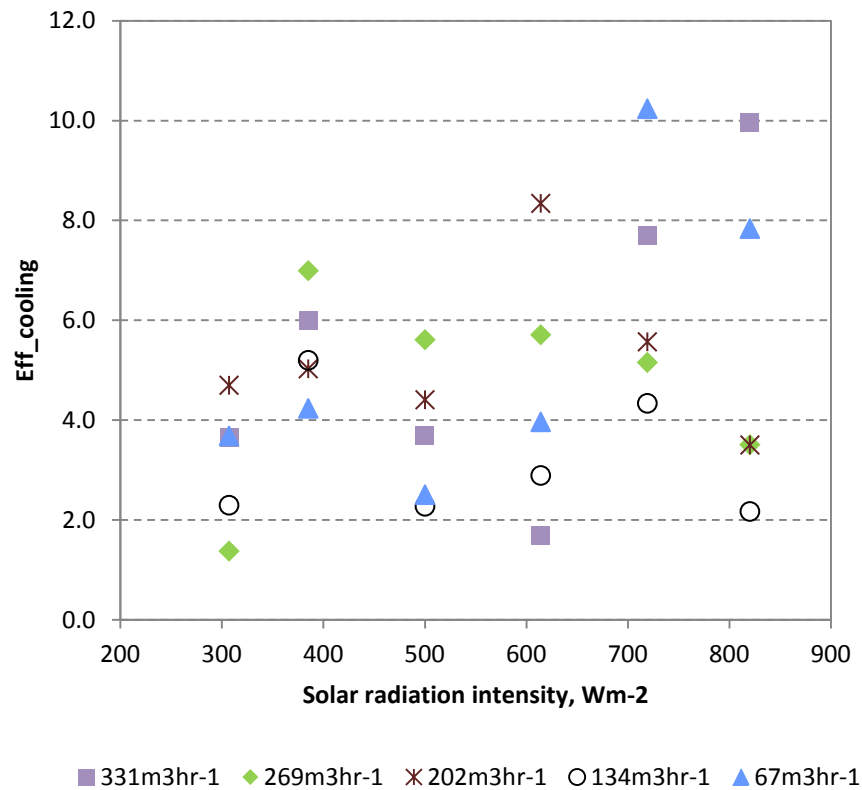


Figure 5-9. Cooling efficiency for system with flat plate and single plenum.

### 5.2.3. Evaporation effect

In Figure 5-10, the positive values of  $(\omega_{out}-\omega_{in})$  indicate that the humidity ratios of outlet air have increased throughout the operating process. Hence the water of the wet sandtile wall is evaporated and moist is added into the plenum air. However, the evaporation is low and this can be seen in Figure 5-11. For all the experiments that had been carried out, the maximum latent heat of evaporation is only about 23% and the lowest is only about 3% of the total heat that absorbed by the plate. These small amounts of heat that drawn by the water are not sufficient to cool the plenum air that heated by the plate.

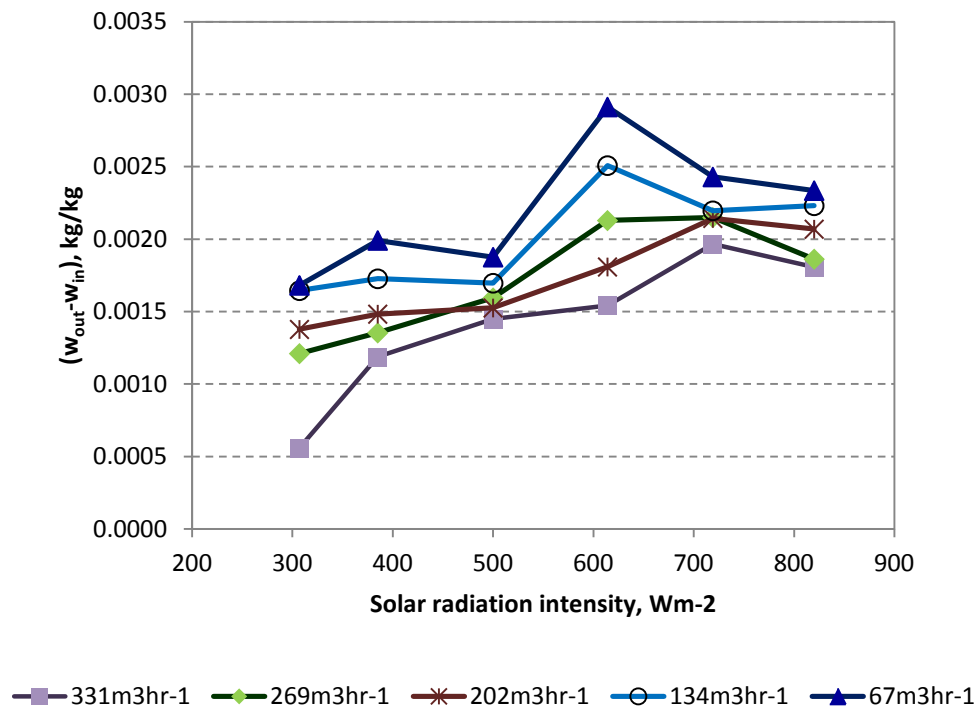


Figure 5-10. Values of  $(\omega_{out}-\omega_{in})$  over different solar radiation intensities.

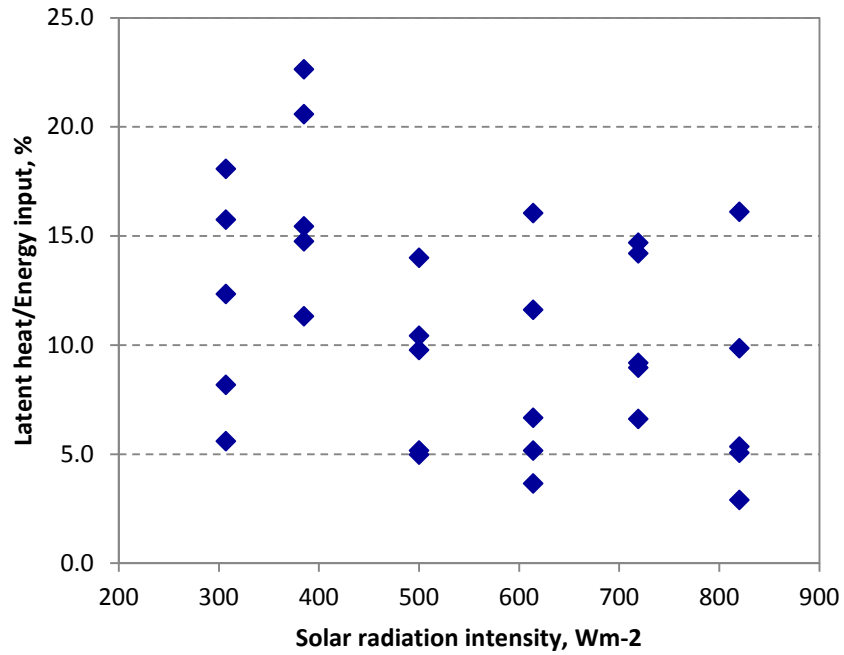


Figure 5-11. Values of the ratio of latent heat to energy input over different solar radiation intensities.

### 5.3. Simulation results of cooling system with transpired plate solar collector and single plenum

Simple simulation studies were carried out to investigate the cooling effect of this system design. The input parameters are as shown in Table 5-2. Figures 5-2 and 5-3 show the values of  $(T_{out}-T_a)$  over different solar radiation intensities and suction velocities. They give adverse cooling results whereby  $(T_a-T_{out})$  are in negative values. Therefore, the research was continued with the modified cooling design without carrying out the experiments.

Table 5-2. Input parameters of simulation studies for cooling system with transpired plate solar collector and single plenum.

$I$ , $Wm^{-2}$	$v_s$ , $ms^{-1}$	$T_a$ , K	Input water temperature, K	$RH$ , %
300	0.04	300	283	50
400	0.04	300	283	50
500	0.04	300	283	50
500	0.05	300	283	50
500	0.06	300	283	50
500	0.07	300	283	50
500	0.08	300	283	50
500	0.09	300	283	50
500	0.10	300	283	50
600	0.04	300	283	50
700	0.04	300	283	50
800	0.04	300	283	50

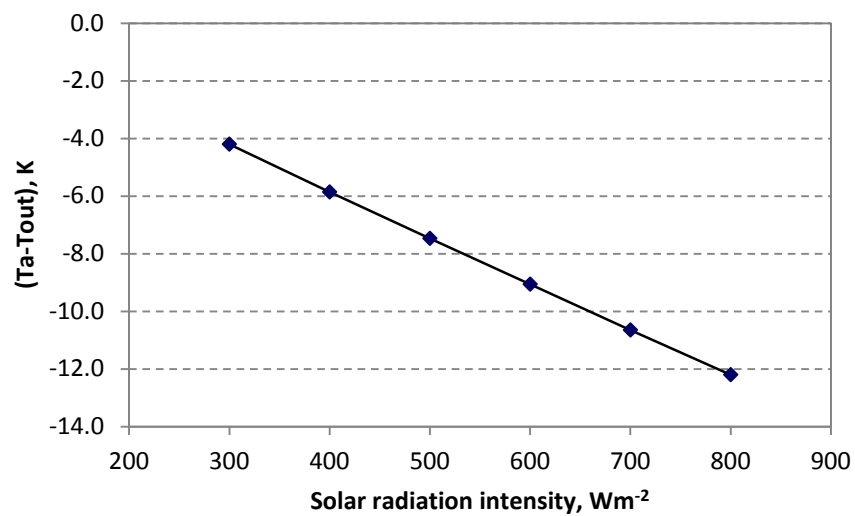


Figure 5-12. Values of  $(T_a - T_{out})$  at suction velocity of  $0.04ms^{-1}$  over different solar radiation intensities.

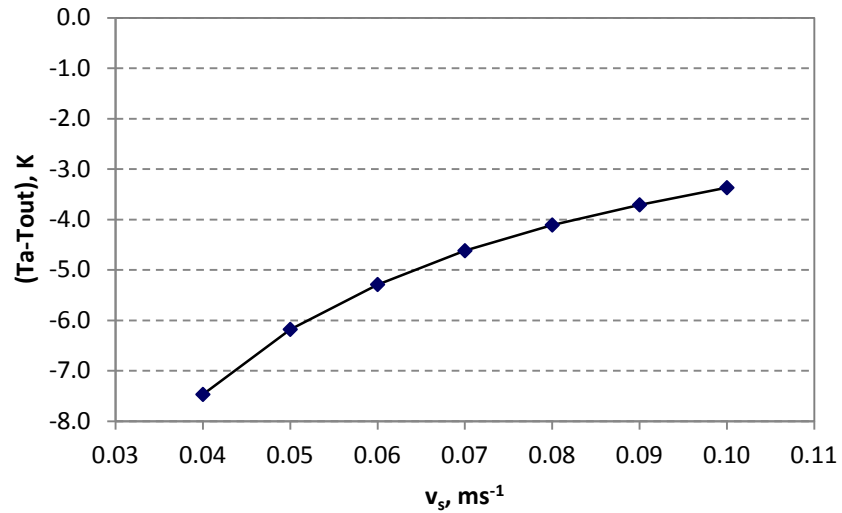


Figure 5-13. Values of  $(T_a - T_{out})$  solar radiation intensity of  $500\text{Wm}^{-2}$  over different suction velocities.

#### 5.4. Section summary

Though results shows that lower values of  $T_w$  are able to reduce the temperatures of outlet air (Figure 5-5), both systems with flat and transpired plates are still showing adverse results ( $T_{out} > T_a$ ) even if the wall is wetted with chilled water. Moreover, the rate of heat transfer from the hot plate to the air is greater than the air losses heat to the wet sandtile wall, whereby the evaporation of water is relatively low (Figure 5-11). Therefore, these system designs are not sufficient enough to provide cold air for space cooling. These results also bring the idea of cooling the air by the backside of cold sandtile wall which is also avoiding the direct contact of the supply air with the hot plate. This design is discussed in the next section.

## 5.5 Heat transfer of cooling system with transpired plate and two plenums

### 5.5.1 Assumptions of cooling system with transpired plate collector

Some assumptions have been made while developing the mathematical model and they are as mentioned in the sections 4.3.1. Additional assumptions are as follows:

- i) The sandtile wall is saturated with water before the experiment.
- ii) 70% of the wet surface of sandtile wall is covered by a thin water film.
- iii) The temperatures of the water film and sandtile wall are the same.
- iv) The areas of plate and sandtile wall surfaces are taken to be the same, i.e.  $A_p = 2\text{m}^2$ .
- v) The Lewis number that relates heat and mass transfer is taken as 1.0 (Maerefat, 2010)
- vi) The conduction heat transfer of the water resistant film on the sandtile wall is negligible due to the thickness is only about 0.0005m.
- vii) There is no heat transfer between the air and the insulation wall at the second plenum.

### 5.5.2 Energy balance equations for cooling system with transpired plate, two plenums and wet sandtile wall

The energy balance equations are established and the related parameters are as shown in Figure 5-14.

#### ***The transpired plate:***

The fans-assisted system draws the ambient air through the holes into the plenum and heated by the plate:

$$I \alpha_p A_p = Q_{conv,p-air} + Q_{conv,bp-air} + Q_{rad,p-sur} + Q_{rad,p-wall} \quad (5-3)$$

**The Plenum 1:**

The heated air transfers heat into the water film and wet surface of the sandtile wall. The water is then evaporated and moist is added to the air. Energy balance equation of the air in Plenum 1 is shown in Equation (5-4).

$$\sum \dot{m}_f c_{p,f} T_i + \sum \dot{m}_f \omega_{in} H_{in} + Q_{conv,bp-air} + Q_L - Q_w = \sum \dot{m}_f c_{p,f} T_{out} + \sum \dot{m}_f \omega_{out} H_{out} \quad (5-4)$$

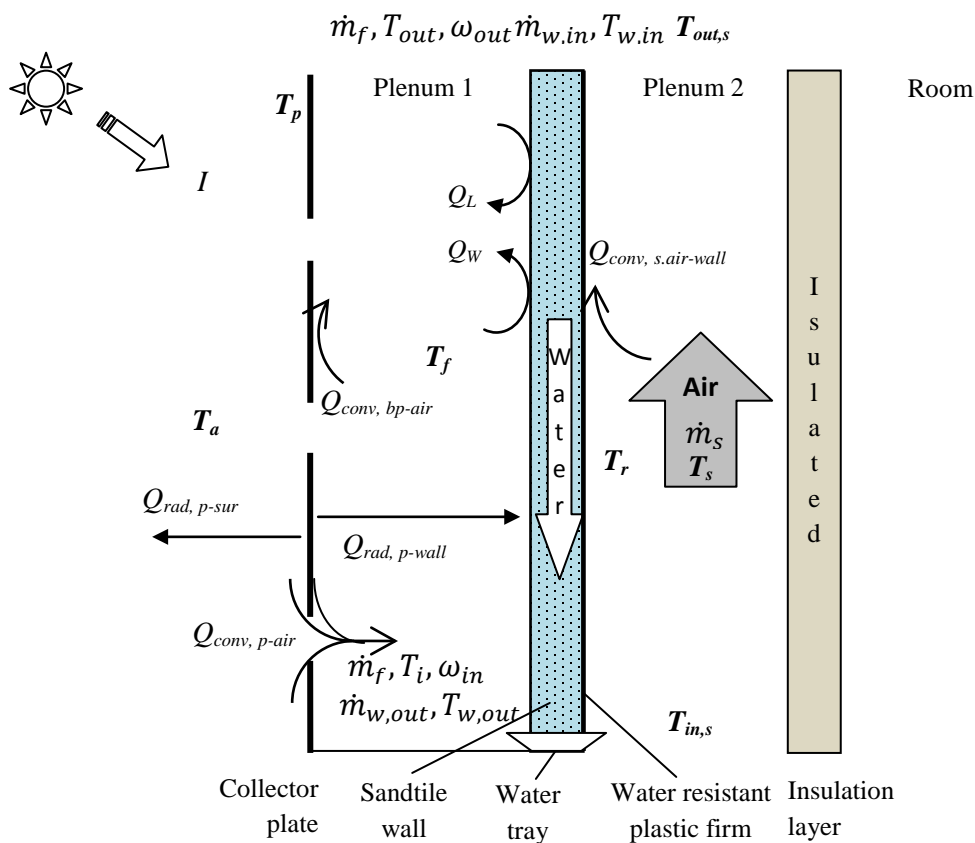


Figure 5-14. Heat transfer of cooling system with transpired plate solar façade and two plenums.

**The wet sandtile wall:**

The sandtile wall is cooled by the flowing water that has a lower temperature than the ambient. The water film and the wet surface of sandtile wall absorbed heat from the air in the plenum and also heat that is transferred from the surface of water resistant film at the other side of the wall. The energy equation balance equation gives:

$$Q_{rad,p-wall} + Q_w + Q_{conv,s.air-wall} - Q_L = \dot{m}_w dH_w + H_w d\dot{m}_w \quad (5-5)$$

**The Plenum 2:**

The air in the Plenum 2 is cooled by the cold surface of the sandtile wall and gives:

$$\dot{m}_s c_{p,s} (T_{in,s} - T_{out,s}) = Q_{conv,s.air-wall} \quad (5-6)$$

**5.5.2.1 Heat flux equations**

The heat flux equations are as below:

**The transpired plate:**

$$I \alpha_p = h_{c,trans} (T_p - T_i) + h_{f,trans} (T_p - T_f) + h_{r,trans-sur} (T_p - T_a) + h_{r,trans-wall} (T_p - T_w) \quad (5-7)$$

**The Plenum 1:**

$$\sum \frac{\dot{m}_f c_{p,f} (T_{out} - T_i)}{A_p} + \frac{\sum \dot{m}_f (\omega_{out} H_{out} - \omega_{in} H_{in})}{A_p} = \frac{d\dot{m}_w H_{pw}}{A_p} + h_{f,trans} (T_p - T_f) - h_w (T_f - T_w), \quad (5-8)$$

where  $T_{out} = 2T_f - T_i$ ; and the latent heat of vaporisation is as expressed in Equation (5-9).

$$Q_L = d\dot{m}_w H_{pw} \quad (5-9)$$

The specific enthalpy of water vapour is almost linear function of temperature (Maerefat, 2010):

$$H_{pw} = c_{p,v} T_w + H_{fg} \quad (5-10)$$

**The wet sandtile wall:**

$$\begin{aligned} & h_{r,trans-wall} (T_p - T_w) + h_w (T_f - T_w) + h_{f,s.air-wall} (T_s - T_r) - \frac{d\dot{m}_w H_{pw}}{A_p} \\ & = \frac{2\dot{m}_w (c_{p,w} T_w - c_{p,w} T_{w1})}{A_p} + \frac{c_{p,w} T_w d\dot{m}_w}{A_p}, \end{aligned} \quad (5-11)$$

where  $T_w = (T_{w1} + T_{w2})/2$  and

$$h_{f,s,air-wall}(T_s - T_r) = U_s(T_r - T_w) \quad (5-12)$$

where  $U_s = 1/(L_1/k_H)$  and for heat conduction takes place in series (Bejan, 2003),

$$1/k_H = [(1 - \phi)/k_1] + (\phi/k_w) \quad (5-13)$$

### The Plenum 2:

$$\dot{m}_s c_{p,s}(T_{in,s} - T_{out,s}) = h_{f,s,air-wall}(T_s - T_r) \quad (5-14)$$

### 5.5.2.2 Mean temperature matrix

The heat flux equations are then simplified and rewritten into Equations 5-15, and 5-17 to 5-20 respectively, and form a 5x5 matrix Equation 5-21 as follows:

$$\left( h_{c,trans} + h_{f,trans} + h_{r1} + h_{r2} - \frac{h_{c,trans}^2}{B} \right) T_p - h_{f,trans} T_f - h_{r2} T_w = S + \left( \frac{h_{c,trans} G c_{p,a}}{B} + h_r \right) T_a, \quad (5-15)$$

where Equation 5-16 is substituted for  $T_i$  in Equation 5-7, which is simplified from Equations 4-26 and 4-27:

$$T_i = (h_{c,trans}/B) T_p + (G c_{p,a}/B) T_a, \quad (5-16)$$

where  $B = G c_{p,a} + h_{c,trans}$

$$\left( h_{f,trans} + \frac{2G c_{p,f} h_{c,trans}}{B} \right) T_p - (2G c_{p,f} + h_{f,trans} + h_w) T_f + \left( \frac{d\dot{m}_w c_{p,v}}{A_p} + h_w \right) T_w = G(\omega_{out} H_{out} - \omega_{in} H_{in}) - \frac{2G^2 c_{p,a} c_{p,f} T_a}{B} - \frac{d\dot{m}_w H_{fg}}{A_p} \quad (5-17)$$

$$h_{r2} T_p + h_w T_f - \left( h_w + \frac{2\dot{m}_w c_{p,w}}{A_p} + \frac{d\dot{m}_w c_{p,v}}{A_p} + \frac{c_{p,w} d\dot{m}_w}{A_p} + h_{r2} + U_L \right) T_w = -\frac{2\dot{m}_w c_{p,w} T_{w1}}{A_p} + \frac{d\dot{m}_w H_{fg}}{A_p} \quad (5-18)$$

$$U_L T_w - (U_L + h_{f,s,air-wall}) T_r + h_{f,s,air-wall} T_s = -2\dot{m}_w c_{p,w} T_{w1}/A_p + d\dot{m}_w H_{fg}/A_p \quad (5-19)$$

$$-h_{f,s,air-wall} T_r + (2\dot{m}_s c_{p,s}/A_p + h_{f,s,air-wall}) T_s = (2\dot{m}_s c_{p,s}/A_p) T_{in,s} \quad (5-20)$$

$$\begin{bmatrix} AT & BT & CT & DT & ET \\ FT & GT & HT & JT & KT \\ LT & MT & NT & OT & PT \\ QT & RT & ST & TT & UT \\ VT & WT & XT & YT & ZT \end{bmatrix} \begin{bmatrix} T_p \\ T_f \\ T_w \\ T_r \\ T_s \end{bmatrix} = \begin{bmatrix} AAT \\ BBT \\ CCT \\ DDT \\ EET \end{bmatrix}, \quad (5-21)$$

Where

$$\begin{aligned} AT &= h_{c,trans} + h_{f,trans} + h_{r1} + h_{r2} - h_{c,trans}^2/B; & BT &= -h_{f,trans}; \\ CT &= -h_{r2}; & DT &= 0; \\ ET &= 0; & FT &= h_{f,trans} + 2Gc_{p,f}h_{c,trans}/B; \\ GT &= -(2Gc_{p,f} + h_{f,trans} + h_w); & HT &= d\dot{m}_w c_{p,v}/A_p + h_w; \\ JT &= 0; & KK &= 0; \\ LT &= h_{r2}; & MT &= h_w; \\ NT &= -\left(h_w + \frac{2\dot{m}_w c_{p,w}}{A_p} + \frac{d\dot{m}_w c_{p,v}}{A_p} + \frac{c_{p,w} d\dot{m}_w}{A_p} + h_{r2} + U_L\right); & OT &= 0; \\ PT &= 0; & QT &= 0; \\ RT &= 0; & ST &= U_s; \\ TT &= -(U_s + h_{f,s,air-wall}); & UT &= h_{f,s,air-wall}; \\ VT &= 0; & WT &= 0; \\ XT &= 0; & YT &= -h_{f,s,air-wall}; \\ ZT &= 2\dot{m}_s c_{p,s}/A_p + h_{f,s,air-wall}; & AAT &= S + (h_{c,trans} Gc_{p,a}/B + h_r)T_a; \\ BBT &= G(\omega_{out}H_{out} - \omega_{in}H_{in}) - \frac{2G^2 c_{p,a} c_{p,f} T_a}{B} - \frac{d\dot{m}_w H_{fg}}{A_p}; & CCT &= -\frac{2\dot{m}_w c_{p,w} T_{w1}}{A_p} + \frac{d\dot{m}_w H_{fg}}{A_p}; \\ DDT &= -2\dot{m}_w c_{p,w} T_{w1}/A_p + d\dot{m}_w H_{fg}/A_p; \text{ and} & EET &= (2\dot{m}_s c_{p,s}/A_p)T_{in,s} \end{aligned}$$

Hence, rewrite the Equation 5-21 by using matrix inversion method,

$$\begin{bmatrix} T_p \\ T_f \\ T_w \\ T_r \\ T_s \end{bmatrix} = \begin{bmatrix} AT & BT & CT & DT & ET \\ FT & GT & HT & JT & KT \\ LT & MT & NT & OT & PT \\ QT & RT & ST & TT & UT \\ VT & WT & XT & YT & ZT \end{bmatrix}^{-1} \begin{bmatrix} AAT \\ BBT \\ CCT \\ DDT \\ EET \end{bmatrix} \quad (5-22)$$

and Equation 5-22 is then solved by iteration method and the iteration process is continued until the convergence value is smaller than  $10^{-6}$ .

### 5.5.2.3 Heat transfer coefficient equations

The radiation heat transfer coefficient,  $h_{r,trans-wall}$  (Equation 4-11) and the convection heat transfer coefficients, i.e.  $h_{c,trans}$  (Equation 4-25),  $h_{f,trans}$  (Equation 4-27) and  $h_{f,s,air-wall}$  (Equation 4-15) and the solar radiation,  $S$  (Equation 4-18) are as discussed in section 4.2.2.3. The followings are the remaining heat transfer coefficients that involved in this system.

#### ***Heat transfer coefficient between the plenum air and the water***

The total heat transfer between the plenum air and water is the sum of heat transfer between the plenum air and the falling film and also the wet surface of the wall. Due to the uneven surface of the sandtile wall, it was observed that only about 70% of the area of the wall was covered by water film. The wall is assumed to be saturated with water before experiment is started, and so the overall coefficient is defined as:

$$h_w = 0.7h_{w1} + 0.3h_{w2} \quad (5-12)$$

Where  $h_{w1}$  is the convection heat transfer coefficient between the plenum air and the falling film, whereas  $h_{w2}$  is the coefficient between the air and the wet surface. For turbulent film ( $\dot{m}/(\mu H) > 500$ ), the Reynolds flux ( $g_{heat}^*$ ) is expressed as Equation 5-24 (Splading, 1963), where  $Nu_{w1}$  is correlated with  $g_{heat}^*$  as Equation 5-25 and thus the  $h_{w1}$  can be calculated through Equation 5-26.

$$g_{heat}^* = 2.156 \times 10^{-5} Pr^{-2/3} (\dot{m}_w \rho^2 g / H)^{1/3} \quad (5-24)$$

$$Nu_{w1} = g_{heat}^* H / (k c_p) \quad (5-25)$$

$$h_{w1} = Nu_{w1} k / H \quad (5-26)$$

Heat transfer between the air and the wet surface (not covered by water film) is included due to the temperature different between the plenum air and the wet surface is above 14K, and thus it is inappropriate to be ignored. The  $h_{w2}$  has the same correlation as  $h_{f,flat}$  (Equation 4-15) with exception that the air properties are evaluated at the mean of air and wall temperatures.

### **Humidity ratio of outlet air**

Equation 5-27 is the mass balance of the air and water, and thus the humidity ratio of the outlet air can be defined as equation 5-28.

$$d\dot{m}_w = \dot{m}_f(\omega_{out} - \omega_{in}) \quad (5-27)$$

$$\omega_{out} = h_m A_p (\omega_{Tw} - \omega_{in}) / \dot{m}_f + \omega_{in} \quad (5-28)$$

The mass flow rate of water that is evaporated into the air is given as:

$$d\dot{m}_w = h_m A_p (\omega_{Tw} - \omega_{in}) , \quad (5-29)$$

where  $h_m = h_w / (c_p Le)$

In addition, for the experiments, the measured *RH* values are converted into air humidity ratio by using Equation 5-30.

$$\omega_f = 0.622p / (101325 - p), \quad (5-30)$$

Where  $p = ps(RH/100)$  , and

$$ps = \exp(-6069.94T^{-1} + 21.24 - 2.71 \times 10^{-2}T + 1.67 \times 10^{-5}T^2 + 2.43 \ln T) \quad (5-31)$$

### **Cooling efficiency**

The cooling efficiency is defined as the ratio of net cooling capacity to the total power consumption for the fans and pump ( $Q_{aux}$ ):

$$\eta_{cool,2 Plenums} = \dot{m}_s c_{ps} (T_{s,in} - T_{s,out}) / Q_{aux} \quad (5-32)$$

The power consumed by the fans are calculated according to the power-airflow rate chart that provided by the supplier and it is included in Appendix IV. Whereas the power consumption for the water pump calculated from Equation 5-2.

### **Cooling effectiveness**

The cooling effectiveness is defined as the ratio of actual temperature drop to the maximum possible temperature drop. The lowest temperature that can be achieved in Plenum 2 is the temperature of  $T_r$ . Thus the equation for the effectiveness is as follows:

$$\varepsilon_{HX,cool} = (T_{s,in} - T_{s,out}) / (T_r - T_{s,in}) \quad (5-33)$$

### ***Thermophysical properties of vapour air and water***

The properties of dry air are calculated as discussed in section 4.2.2.3, whereas for the vapour air and water they are as follows (Forsythe, 2003; Incropera, 2002):

$$k_v = (0.0579T_f + 2.417) \times 10^{-3} \text{ W/mK}$$

$$\mu_v = (0.04T_f - 2.91) \times 10^{-6} \text{ Ns/m}^2$$

$$\rho_v = (0.0012T_f - 0.3281) \text{ kg/m}^3$$

$$c_{p_v} = (1 \times 10^{-5}T_f^2 - 0.0048T_f + 2.4615) \times 10^3 \text{ J/kgK}$$

$$H_{fg} = (-2.3571T_f + 3144.8) \times 10^3 \text{ J/kg}$$

$$H_f = (1.9118T_f + 1973.6) \times 10^3 \text{ J/kg}$$

$$p_w = 1.71.12T_w - 47427 \text{ Pa}$$

$$c_{p_w} = (3 \times 10^{-5}T_w^2 - 0.0195T_w + 7.1425) \times 10^3 \text{ J/kgK}$$

$$Pr_v = 0.0016T_f + 0.377$$

### **5.5.3 Results and analysis of cooling system with transpired plate and double plenum**

The experiment set up is as described in Chapter 3, with operation conditions as described in Table 5-3. In this section, the modelling results are compared to the experiments and followed by parametric analysis. Parts of the results are selected for discussions, however the complete sets of measured data can be found in Appendix III-4.

#### **5.5.3.1 Results comparison between the model and experiment**

The purpose in this section is to validate the mathematical model by comparing the results with the experiment measurements. Thus, the discussion is focused on the differences of temperatures between the simulated and measured; and arguments that related to parametric analysis are discussed in next sections.

Table 5-3. Parameters for the experiments of cooling system with two plenums.

Parameter	Value/ range
Solar radiation intensity, $Wm^{-2}$	300-800
Height of the transpired plate, m	2.0
Width of the transpired plate, m	1.0
Plate thickness, m	0.001
Plenum 1: suction air velocity, $ms^{-1}$	0.04
Plenum 1: depth, m	0.25
Water flow rate per unit area of sandtile wall, $kgs^{-1}m^{-2}$	0.01
Plenum 2: volume airflow rate, $m^3hr^{-1}$	67-331
Plenum 2: depth, m	0.20

### ***Temperatures comparison between the model and experiment***

Figure 5-15 shows temperature comparisons between the model and the experiments over solar radiation intensity ranges from 307 to  $820Wm^{-2}$ , with a constant suction mass flow rate of  $0.05kgs^{-1}m^{-2}$  ( $v_s=0.04ms^{-1}$ ) at Plenum 1 and airflow rate of  $67m^3hr^{-1}$  at Plenum 2. On the other hand, Figure 5-18 shows the temperature plots over different airflow rates at Plenum 2, under a constant solar radiation intensity of  $614Wm^{-2}$ . Both the model and experiment not only give the same patterns of temperature plots but also very close values. The maximum percent differences between the model and the measured temperatures for  $T_p$ ,  $T_r$ ,  $T_w$ ,  $T_r$  and  $T_s$  are 2.1%, 0.7%, 0.1%, 0.3% and 0.1% respectively. In addition, the heat exchange effectiveness (Exh\_H) at Plenum 1 and cooling effectiveness (Exh\_C) at plenum 2 are calculated from experiments and the model. The comparisons between the ratios of Exh\_C to Exh\_H from these two methods are as shown in Figure 5-17. They have similar results with maximum difference at  $I=614Wm^{-2}$  and  $V_{fan}=331m^3hr^{-1}$ . The modelled and measured results are 0.08 and 0.10 respectively. As the calculated experimental percentage error for the system is 15.3% (Section 3.7), the accepted range for the measured results is 0.08 to 0.12, where the modelled results fall between. These results verify the accuracy

of the model for this cooling system. Hence the model will be used for further analysis purposes where appropriate and necessary.

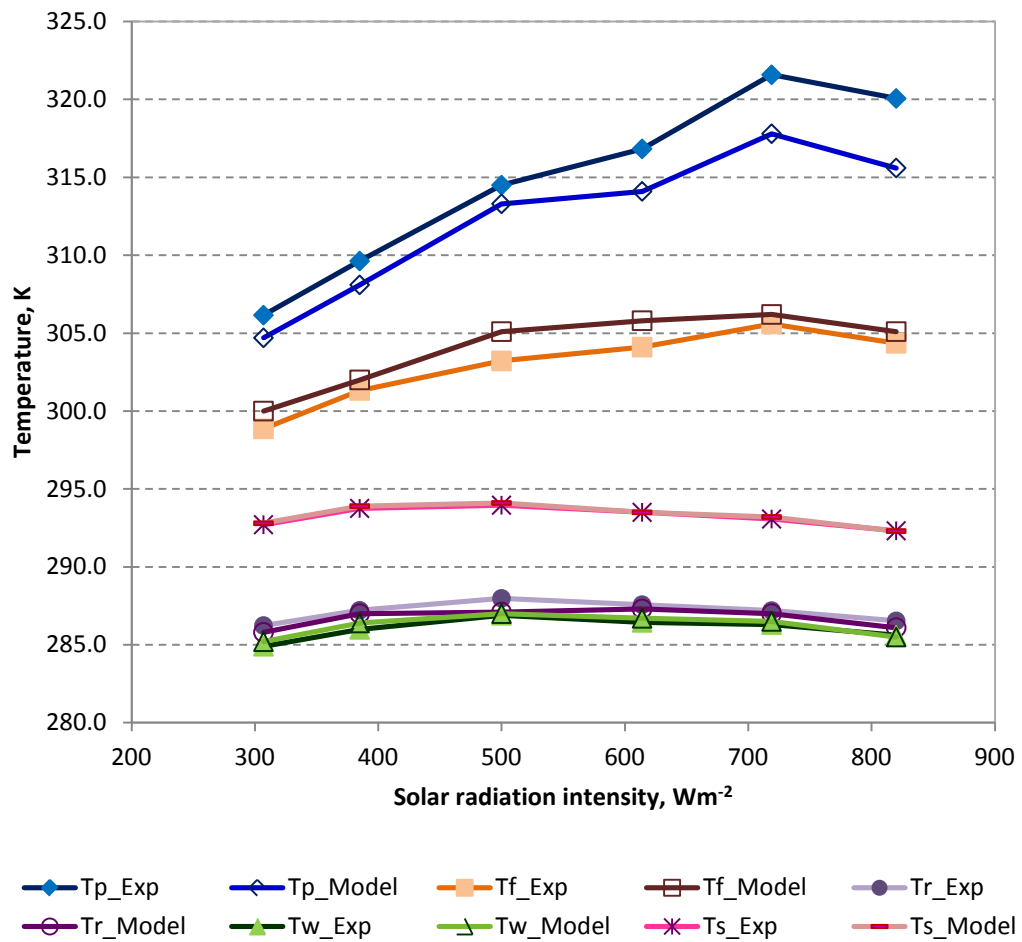


Figure 5-15. Temperature comparisons between the model and the experiments over solar radiation intensities.

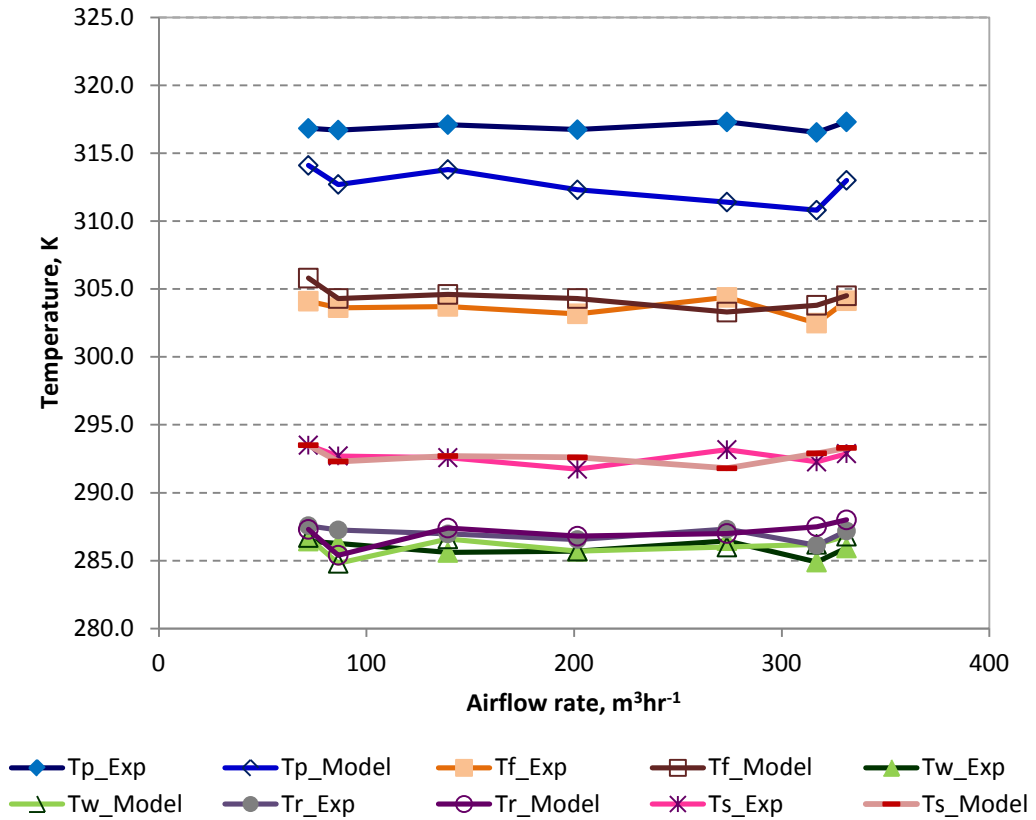


Figure 5-16. Values of  $T_p$ ,  $T_f$  and  $T_w$  over different airflow rates at the Plenum 2, under a constant solar radiation intensity of  $614\text{Wm}^{-2}$ .

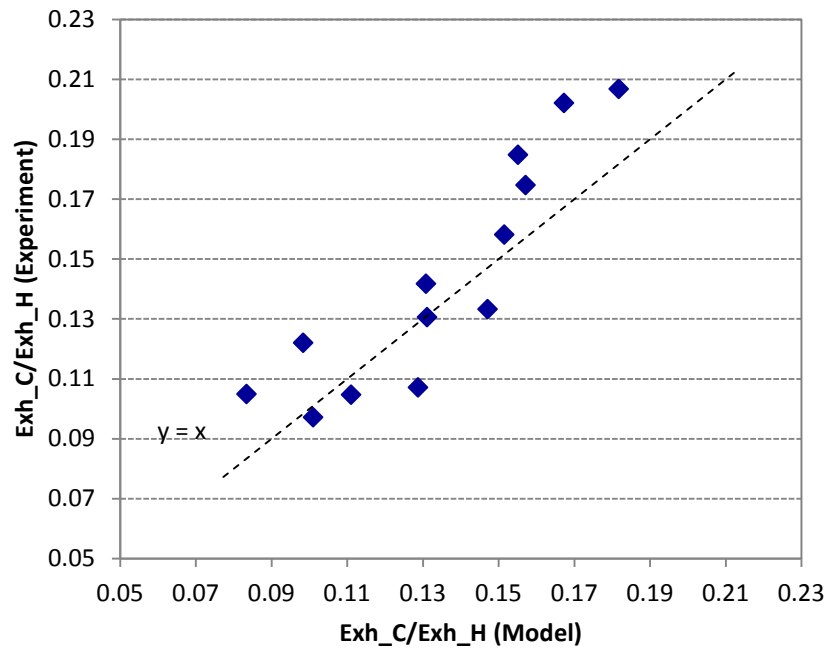


Figure 5-17. Comparisons of the ratios of Exh\_C to Exh\_H between the model and experiment.

### ***Comparison of humidity ratio of outlet air in Plenum 1 between the model and experiment***

The humidity ratios of the outlet air from the experiments are then compared with the results from the model, and they are as shown in Figure 5-18. Most of the modelled results are approximately 20% higher than the measured. However, in terms of the values of humidity ratio, this amount of difference is only about 0.003kg/kg. Moreover, the accuracy of model on outlet air humid ratio can be improved by using the corrected liner correlation as shown in the Figure 5-18.

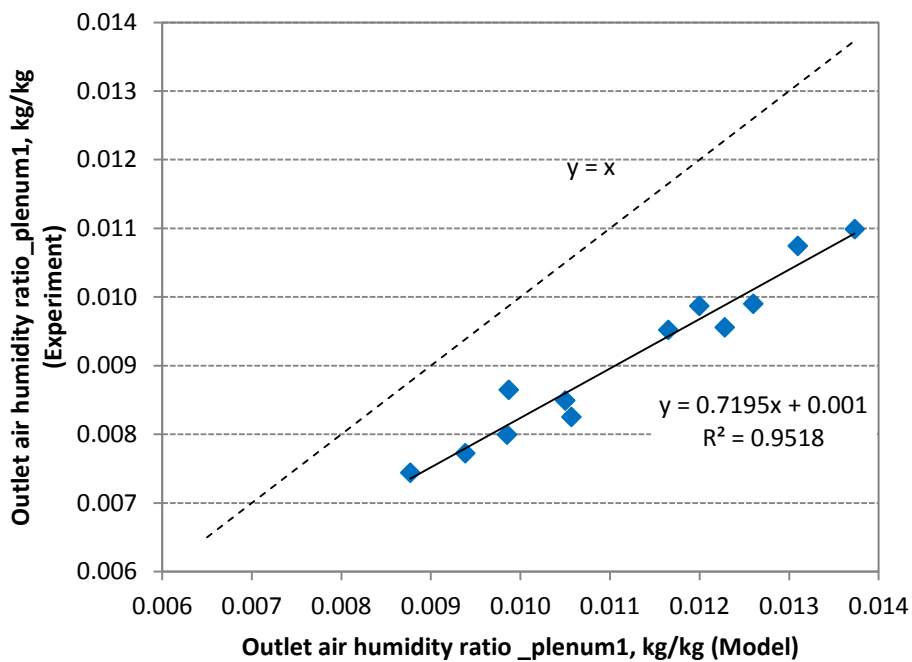


Figure 5-18. Values of outlet air humidity ratio from the experiments against the modelled results.

#### **5.5.3.2. Parametric analysis**

As the heating effects of Plenum 1 have been discussed in Chapter 3, this section is focused on the cooling effect of the system. The effects of ambient air, inlet air of the Plenum 2 and water temperatures on the cooling effect are discussed. The values of air temperature drop in the Plenum 2 ( $T_{s,in} - T_{s,out}$ ) are used to analyse the cooling effect.

Due to the operation parameters for the experiments e.g. ambient, water, sandtile wall and  $T_{s,in}$  temperatures are in the same patterns, the values of  $T_{s,out}$  that also follow these patterns (Figure 5-19) need to be further investigated by using the modelled results. The input parameters and the modelled results are as shown in Table 5-4 and Figure 5-20 respectively, whereby M1 to M6, M7 to M12 and M13 to M18 are to investigate the effects of  $T_a$ ,  $T_{w,in}$  and  $T_{s,in}$  correspondingly.

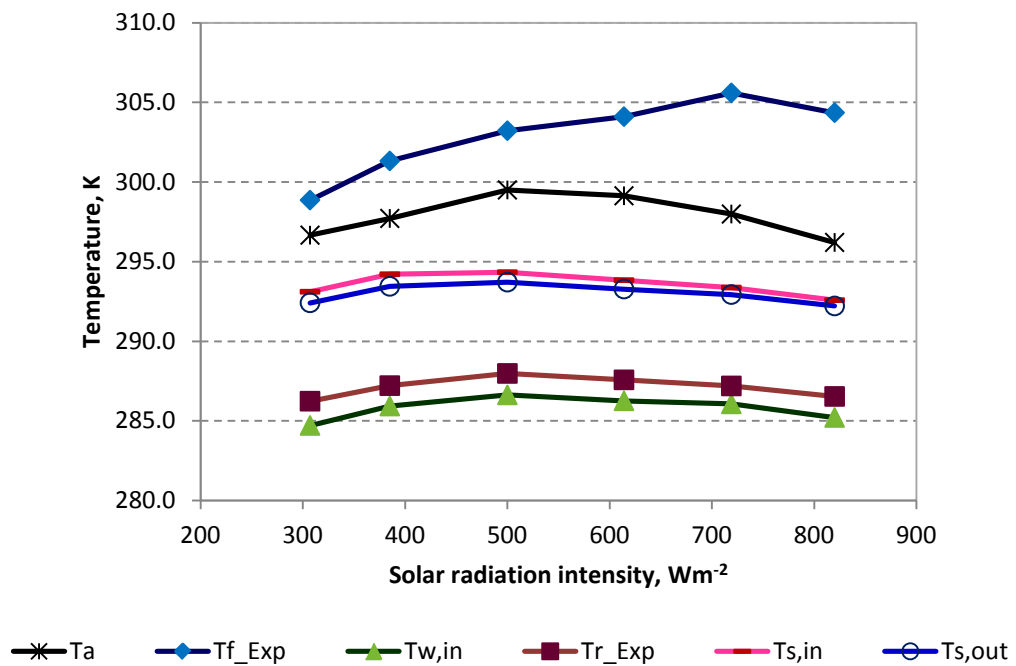


Figure 5-19. Values of  $T_a$ ,  $T_{f_i}$ ,  $T_{r_i}$ ,  $T_{s,in}$  and  $T_{s,out}$  over solar radiation intensities.

Table 5-4. Input parameters for the model tests to investigate the effects of  $T_{a,i}$ ,  $T_{w,in}$  and  $T_{s,in}$  on  $(T_{in,s}-T_{s,out})$ .

Model	$I_i$ , $Wm^{-2}$	$v_{s,i}$ , $ms^{-1}$ (Plenum 1)	$V_{fan,i}$ , $m^3hr^{-1}$ (Plenum 2)	$RH$ of $T_{a,i}$ %	$T_{a,i}$ , K	$T_{w,in,i}$ , K	$T_{s,in,i}$ , K
M1	500	0.046	67	50	283.0	288.0	295.0
M2	500	0.046	67	50	288.0	288.0	295.0
M3	500	0.046	67	50	293.0	288.0	295.0
M4	500	0.046	67	50	298.0	288.0	295.0
M5	500	0.046	67	50	303.0	288.0	295.0
M6	500	0.046	67	50	308.0	288.0	295.0
M7	500	0.046	67	50	298.0	280.0	295.0
M8	500	0.046	67	50	298.0	285.0	295.0
M9	500	0.046	67	50	298.0	290.0	295.0
M10	500	0.046	67	50	298.0	295.0	295.0
M11	500	0.046	67	50	298.0	300.0	295.0
M12	500	0.046	67	50	298.0	305.0	295.0
M13	500	0.046	67	50	298.0	288.0	288.0
M14	500	0.046	67	50	298.0	288.0	293.0
M15	500	0.046	67	50	298.0	288.0	298.0
M16	500	0.046	67	50	298.0	288.0	303.0
M17	500	0.046	67	50	298.0	288.0	308.0
M18	500	0.046	67	50	298.0	288.0	313.0

The ambient air temperatures ( $T_a$ ) do not show strong effect on the temperature drop of  $(T_{s,in}-T_{s,out})$  (Figure 5-20). However, the values of  $(T_{s,in}-T_{s,out})$  decrease with the temperature of inlet water ( $T_{w,in}$ ). When the inlet air temperature of Plenum 2 ( $T_{s,in}$ ) was set to be the same as the  $T_{w,in}$  (M10 and M13), there is almost no change in air temperature in Plenum 2. Moreover, the outlet air temperatures becomes higher than the inlet when the values of  $T_{w,in}$  are higher than the  $T_{s,in}$ . This is because the air Plenum 2 is convectively cooled by the back of the sandtile wall where the water resistant film is attached ( $T_r$ ), so higher value of  $T_{w,in}$  gives higher  $T_r$ , and reduces the cooling effect. The effect of inlet water temperature was also observed through experiments. By using a pump, the water that collected at the bottom of the sandtile wall is reused as inlet

water without any cooling step in between. While the water is flowing through the sandtile wall, it carries heat from the sandtile wall and hence the water temperature is increasing from a cycle to another. This can be seen in Figure 5-21, where the maximum rise in water temperature of nearly 5K at  $I=820\text{Wm}^{-2}$  was recorded. While in Figure 5-22, the values of  $(T_{s,in}-T_{s,out})$  are compared between the reuse water that was recycled back to the wall without any cooling step and water temperature that was monitored and maintained within 2K of difference throughout the experiment. When the water is recycled back to the wall from cycle to cycle,  $T_w$  is increased, hence the  $T_r$ . Figure 2-23 shows the values of temperature difference between  $T_s$  and  $T_r$  from the beginning (time=0min) to the end of the experiments (time=150min) at solar radiation intensity of  $500\text{Wm}^{-2}$ . Greater value of  $(T_s-T_r)$  results in greater heat transfer from the air to the wall. The values of  $(T_s-T_r)$  decrease over the experiments period when the inlet water temperature is not maintained, whereas the values remain constant if the inlet water temperature is maintained. As a result, at higher solar radiation intensities, i.e.  $719$  and  $820\text{Wm}^{-2}$ , the system gives adverse effect whereby the air is heated instead of cooled (Figure 5-22). In contrast, if the water temperature is maintained, the system gives greater values of  $(T_s-T_r)$  and hence  $(T_{s,in}-T_{s,out})$ , so even at higher solar radiation intensities cooling effects are achievable.

Apart from the effects of  $T_a$  and  $T_{w,in}$ , the effect of  $T_{s,in}$  on the cooling effect has been investigate through the model and it is as shown in Figure 5-20. Higher values of  $T_{s,in}$  give greater values of  $(T_{s,in}-T_{s,out})$  when the values of  $T_{w,in}$  are fixed. This is because in such circumstance the temperature difference between  $T_r$  and the air is also greater. Therefore, greater amount of heat is transferred from the air to the sandtile wall and cooled the air more. This suggests that the cooling effect is also depended on the temperature difference between the air and  $T_r$ . Nonetheless, in order to achieve the required cooling demand, water temperature is a crucial factor whereby higher  $T_{s,in}$  needs lower  $T_w$  to obtain lower  $T_r$  and finally lower  $T_{s,out}$ .

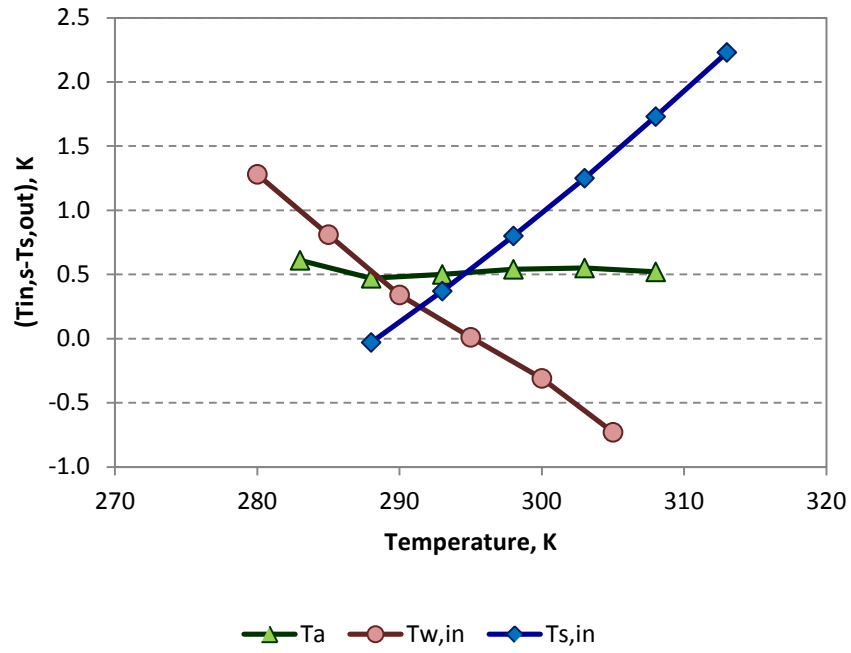


Figure 5-20. Modelled results of the effects of  $T_a$ ,  $T_{w,in}$  and  $T_{s,in}$  on  $(T_{in,s} - T_{s,out})$ .

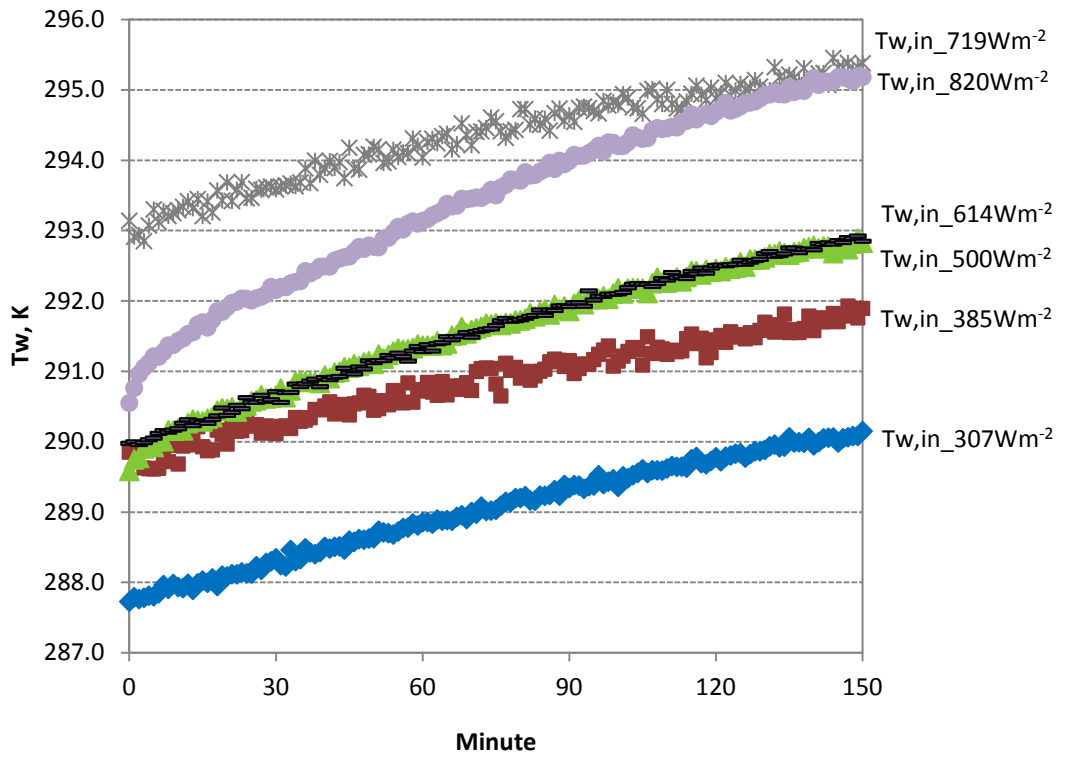


Figure 5-21. Measured values of the water temperature throughout the experiments without cooling step.

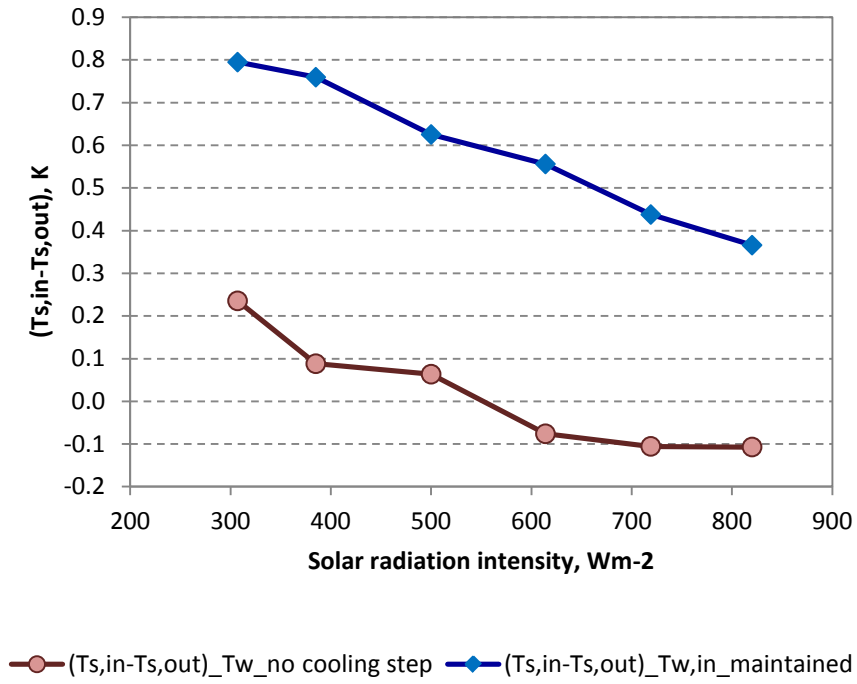


Figure 5-22. Comparison of  $(T_{s,in} - T_{s,out})$  for experiments with and without maintaining the water temperature.

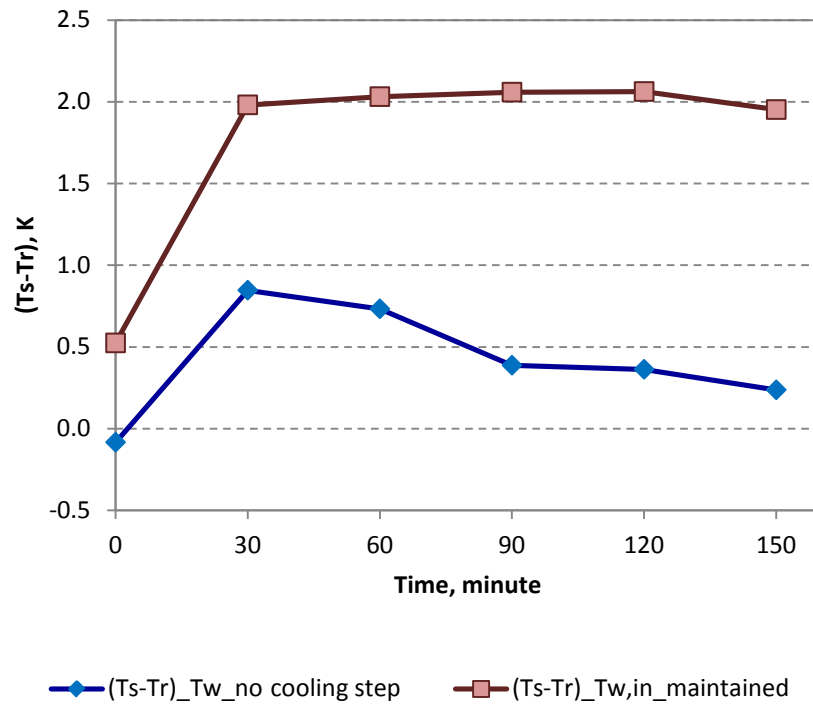


Figure 5-23. Comparison of  $(T_s - T_r)$  for experiments with and without maintaining the water temperature.

### 5.5.3.3 Cooling performance

The cooling performance of the system is investigated in terms of cooling effectiveness, and cooling efficiency.

#### *Cooling effectiveness*

The air in Plenum 2 is cooled by the sandtile wall. Hence, the more heat is conducted from the surface of sandtile wall at Plenum 2 to Plenum 1, the better cooling effect it would be. However in this study, this amount of heat is only about 25% of the total enthalpy change of the water on the sandtile wall. The water absorbs more heat from Plenum 1 than the Plenum 2. As a result, the system demonstrates low cooling effects, whereby the present design and operation conditions give a maximum drop in air temperature of only 0.7K, even though the temperature difference of  $(T_{s,in}-T_r)$  is at least 5K (Figure 5-24). Therefore, the cooling effectiveness of the system is low, which the maximum is only approximately 11% (Figure 5-25), at  $307\text{Wm}^{-2}$  and it drops gradually to 6.0% at  $820\text{Wm}^{-2}$ . Furthermore, the cooling effectiveness also decreases with the airflow rate at Plenum 2 (Figure 5-26). Thus, Plenum 2 needs to be maintained at low airflow rate in order to have better cooling effect.

Despite that, simulation studies were carried out to further investigate the cooling effectiveness for larger area of the façade. The studies assume that the plate and the sandtile wall are always in the same dimensions, and input parameters are  $T_a=305\text{K}$ ,  $T_{w,in}=293\text{K}$ ,  $v_s=0.046\text{ms}^{-1}$ ,  $V_{fan}=500\text{m}^3\text{hr}^{-1}$  per unit area of the plenum opening. The simulation tests were carried out for plate area ranges from 2 to  $12\text{m}^2$ .  $H$  was fixed to be 2.0m and increasing the  $L$  accordingly, and this step was repeated for a fix  $L$  of 1m and increasing the  $H$  accordingly. Figure 5-27 shows the simulation results. Expanding the plate area horizontally does not give obvious effect on the cooling performance, however increasing the area vertically manages to increase the value of  $(T_{s,in}-T_{s,out})$  gradually. In this case, façade with 12m height is able to reduce the air temperature of nearly 3K,

compared to façade with 2m height, the temperature drop is only 1K. This information is crucial for the building designers during the design process. However, taller façade may result in the higher installation cost and higher auxiliaries' electricity consumption. The façade need to be proper designed to reach the trade-off between the system cost and the net energy saving.

A simulation study on large scale installation was carried out. The results for 500m<sup>2</sup> installation are as show in Figure 5-28. When the ambient air temperature is 313K, the system is able to reduce the air temperature by 10.6K which is about 6.6kW of cooling capacity.

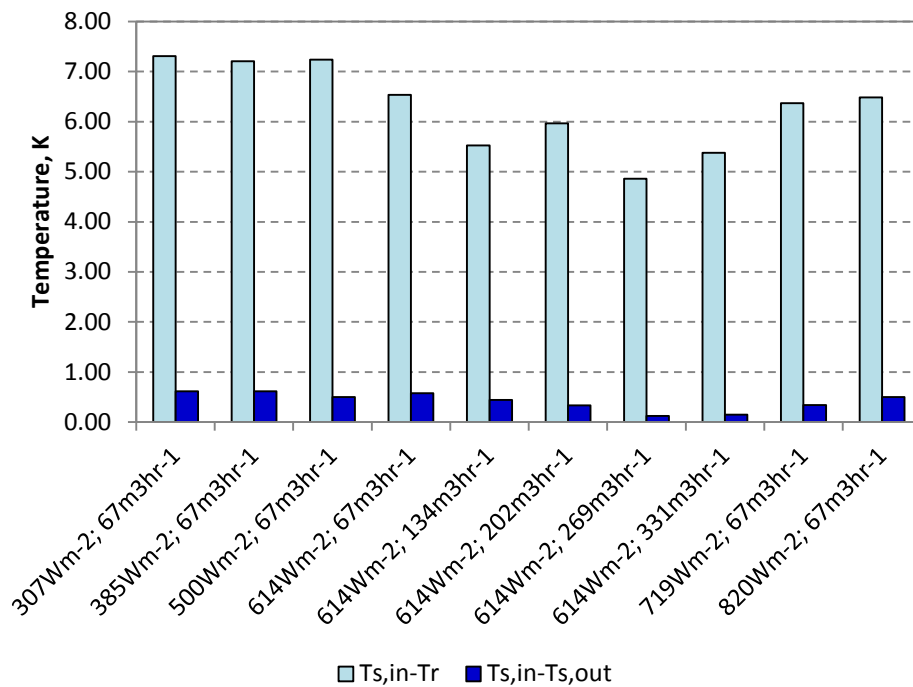


Figure 5-24. Measured results of  $(T_{s,in}-T_r)$  and  $(T_{s,in}-T_{s,out})$ .

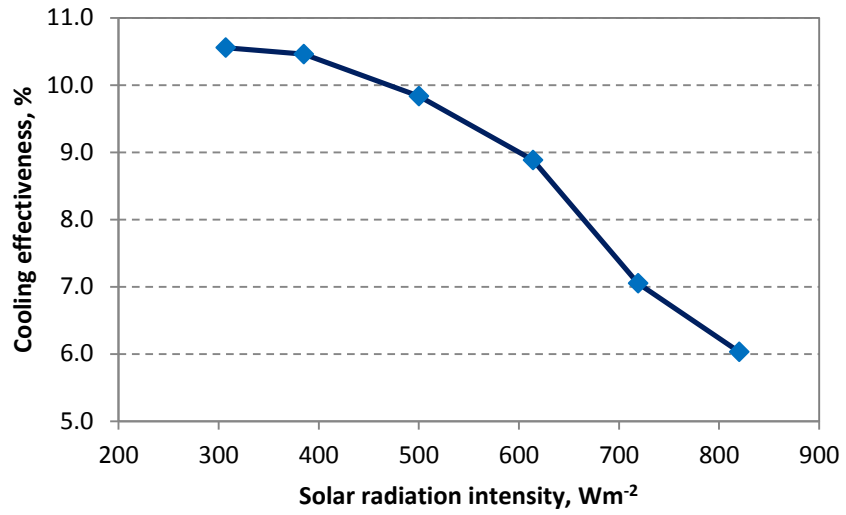


Figure 5-25. Cooling effectiveness of the system over different solar radiation intensities.

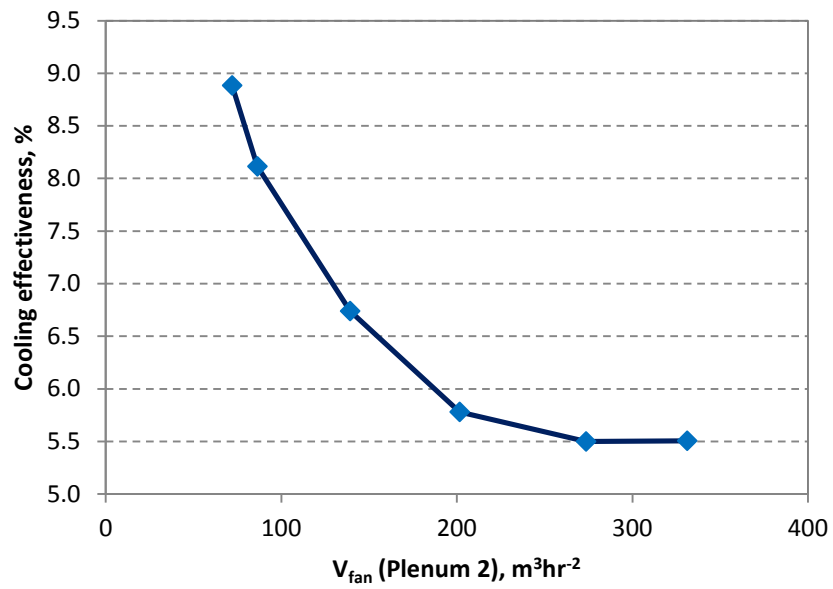


Figure 5-26. Cooling effectiveness of the system over different airflow rates in plenum 2.

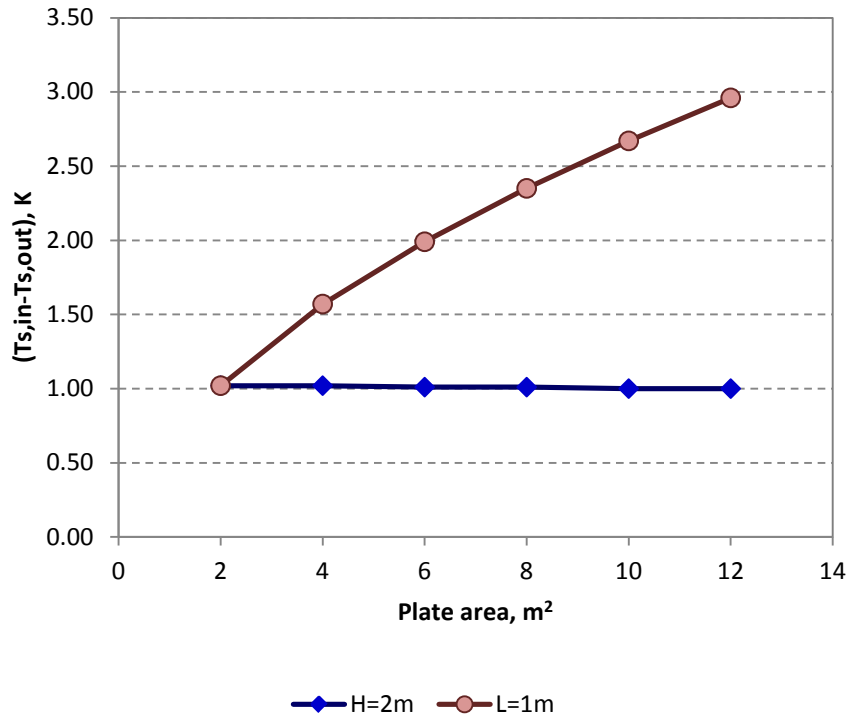


Figure 5-27. Simulation results of  $(T_{s,in}-T_{s,out})$  for expanding the plate areas horizontally ( $H=2m$ ) and vertically ( $L=1m$ ).

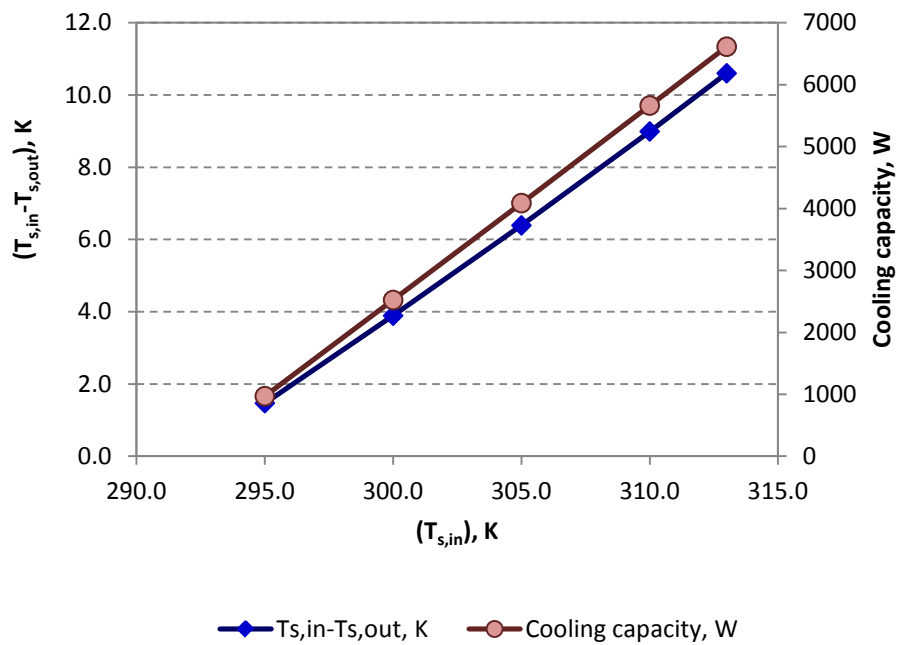


Figure 5-28. Simulation results of large scale installation with  $A_p=500m^2$ .

### Cooling efficiency

Further investigation was carried out to compare the air temperature of Plenum 2 when the sandtile wall is dry. Figure 5-29 shows the plenum air temperatures of the systems with dry and wet sandtile wall. The values of the air temperature ( $T_s$ ) are higher than the inlet air temperature ( $T_{s,in}$ ) when the wall is dry. In contrast, when the wall is wet, the values of  $T_s$  are not only lower than the values of  $T_s$  when the wall is dry, but also lower than the inlet. Hence, system with dry sandtile wall warms the air in Plenum 2 and cools the air when the wall is wet. In terms of the amount of total heat that has been removed by the system, it is the sum of the amounts that heat gain of the air in Plenum 2 when the wall is dry and the heat loss of the air when the wall is wet. They are as shown in Figure 5-30. Whereas in terms of the cooling efficiency, the system gives greater net cooling capacity than the power required by the auxiliaries (cooling efficiency  $>1.0$ ) for solar radiation intensity lower than  $719\text{Wm}^{-2}$ . Furthermore, it is also found that the cooling efficiency decreases with solar radiation intensity but increase with airflow rate.

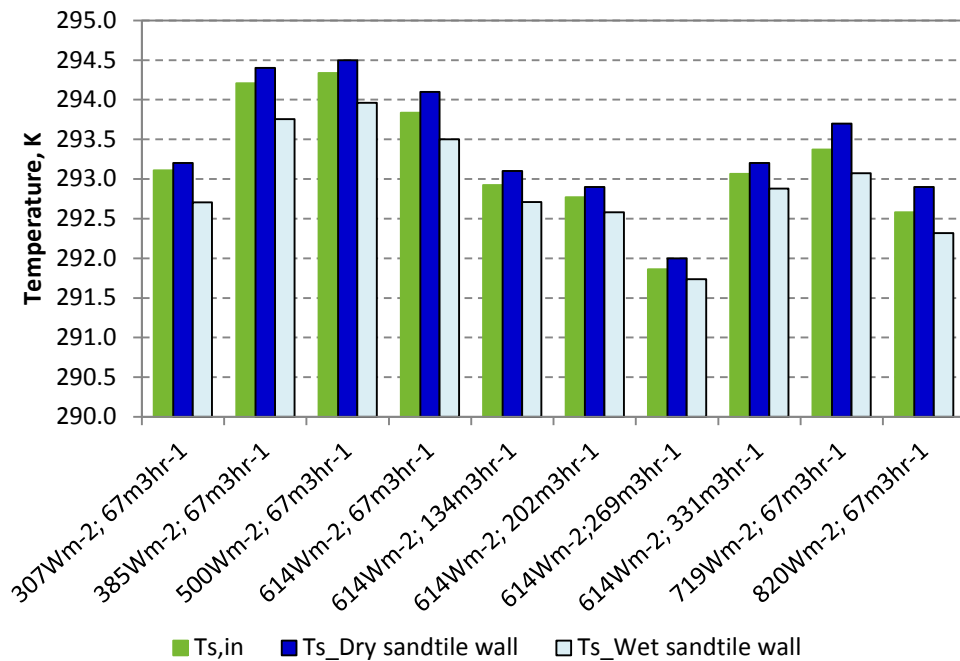


Figure 5-29. Plenum air temperatures of the systems with dry and wet sandtile wall.

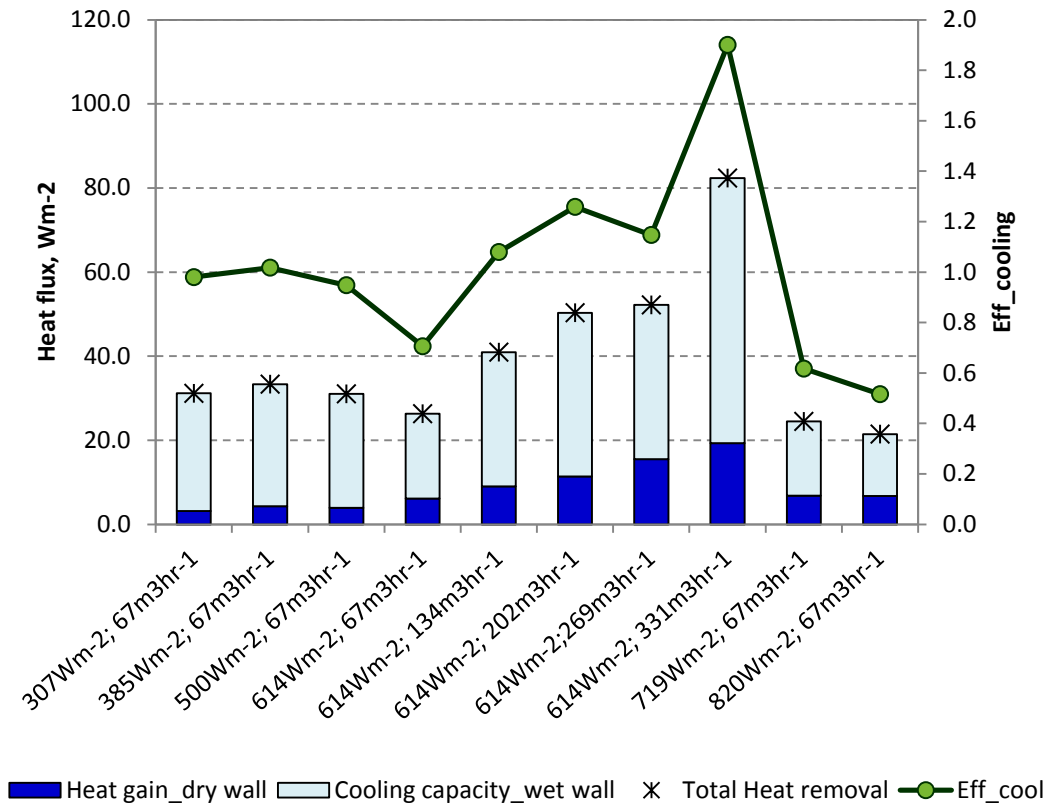


Figure 5-30. Heat fluxes of the heat gain and removed, and values of cooling efficiency of the system with transpired plat and two plenums.

### ***Energy consumption comparisons of reported cooling systems***

Table 5-5 shows the energy consumption of various types of cooling systems in order to produce 1kW of cooling load. The selected systems are the conventional refrigerators and some solar cooling technologies. In addition, the values of the energy consumption are calculated based on the highest COP that have been reported and the values only represent the energy from fossil fuels and electricity. Present system shows similar amount of energy required to solar indirect evaporative cooling and desiccant cooling systems that reported by Bourdoukan (2009) and Enteria (2009) respectively. Though present design consumes more energy to produce the same amount of cooling loads than the conventional refrigerators and absorption systems, lower installation cost and building integrated features should be seen as advantages of the system.

Table 5-5. Energy consumption comparisons for various types of cooling systems.

System	Auxiliary energy consumption to produce 1kWh of cooling load*, kWh	References
Present	0.52	
Vapour-compression refrigerators with different types of refrigerants	0.25-0.40	(Devotta, 2001; Park, 2007)
Air-conditioner with air condenser	0.22	(Hajidavalloo, 2010)
Air-conditioner with evaporative condenser	0.16-0.39	(Hajidavalloo, 2010; Nasr, 2009)
Desiccant integrated refrigerator	0.26	(Elsayed, 2006)
Evaporative cooling with solid desiccant	1.11	(Jain, 1995)
Indirect evaporative cooling	0.06-0.5 0.04	(Joudi, 2000) (El-Dessouky, 2000)
Solar -assisted absorption cooling	0.19 (solar fraction=0.75) 0.29 (solar fraction=0.80) 1.50 (solar fraction=0.25) 0.26 (solar fraction=0.34) 0.10 (solar fraction=0.74)	(Nasr, 2009) (Eicker, 2009) (Casals, 2006) (Tsoutsos, 2010) (Tsoutsos, 2010)
Hybrid solar-assisted ejector cooling/heating	0.20	(Huang, 2010)
Solar indirect evaporative cooling	0.50	(Bourdoukan, 2009)
Solar desiccant cooling	0.20 0.58 0.42 0.22	(Bourdoukan, 2009) (Enteria, 2009) (Fong, 2010) (Eicker, 2010)

\*Represent energy consumption from non-solar energy.

### 5.5.3.4 Water evaporation

Figure 5-31 shows the difference of humidity ratio of the air in Plenum 1, over a range of solar radiation intensity. The positive values of  $(\omega_{out}-\omega_{in})$  indicate that the humidity ratio of outlet air is increased and hence suggest that the water of the wet sandtile wall is evaporated and moist is added into the air. In addition, the pattern of the  $(\omega_{out}-\omega_{in})$  and  $T_i$  follow the value of  $T_a$ , whereby higher temperatures give greater values of  $(\omega_{out}-\omega_{in})$ . At  $600\text{Wm}^{-2}$ , the  $T_a$  is lower than the  $T_a$  at  $500\text{Wm}^{-2}$ , and hence the  $(\omega_{out}-\omega_{in})$  is also lower than that at the  $500\text{Wm}^{-2}$ . The total amount of the water that is evaporated ( $V_{water,eva}$ ) is calculated from the Equation 5-16.

Although present investigation on water consumption is not studied in depth, optimisation on water consumption by using sandtile wall can be done as future research. If the optimisation is able to produce an even wet surface and no additional water drops at the bottom of the wall, this would have dual benefits, i.e. power saving in auxiliaries due to no pump is needed to recycle the water, and also because of the water is not recycled back, cooling step to maintain the inlet water temperature can be avoided. Such idea was applied in other evaporative cooling design by using porous ceramic (He, 2010).

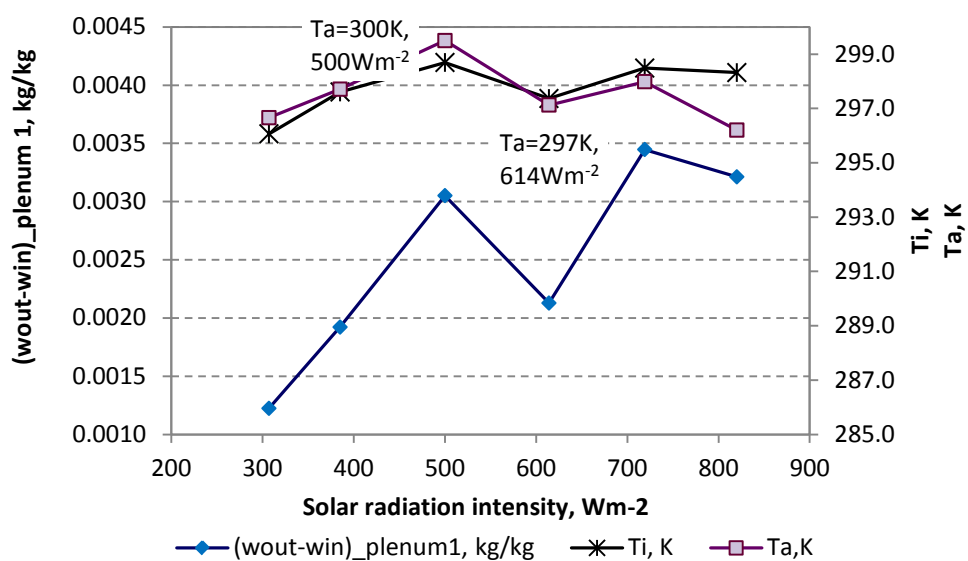


Figure 5-31. The difference of humidity ratio of the air in Plenum 1 over a range of solar radiation intensity.

### 5.5.3.5 Performance analysis under the condition of no solar radiation

The sandtile wall absorbs heat from the air in Plenum 1 that heated by the solar radiation and so the wall temperature is increased; and this reduces the capability of cooling in Plenum 2. Thus, further investigation was carried out to study the cooling performance when there is no solar heat gain. The investigation was carried out by using the model and the input parameters are as shown in Table 5-6. The tests were repeated for solar radiation intensity of  $500\text{Wm}^{-2}$  and both set of results were then compared.

Table 5-6. Input parameters for the investigation on the cooling performance for  $I=0\text{Wm}^{-2}$ .

Input parameters	Value/ Range
$I$ , $\text{Wm}^{-2}$	0 and 500
$RH$	50%
$T_{a,i}$ , $\text{K} = T_{s,in,i}$ , $\text{K}$	296 to 304
$T_{w,in,i}$ , $\text{K}$	5K lower than $T_a$
$v_s$ (Plenum 1), $\text{ms}^{-1}$	0.046
$V_{fan}$ (Plenum 2), $\text{m}^3\text{hr}^{-1}$	67
$H$ , $\text{m}$	2.0
$L$ , $\text{m}$	6.0

As shown in Figure 5-32, the sandtile wall temperatures ( $T_r$ ) for  $I=0\text{Wm}^{-2}$  are relatively lower than  $I=500\text{Wm}^{-2}$ , and hence better cooling effect (greater values of  $(T_{s,in}-T_{s,out})$ ). This indicates that this system is applicable at night. Moreover, if the ambient air temperature is not too high, the cooled outlet air during the night might be cold enough to satisfy the thermal comfort and air-conditioner can be avoided. For instance, the system is able to cool the air to  $22^\circ\text{C}$  when the ambient air temperature is  $25^\circ\text{C}$ . Besides, this also suggests that the cooling performance can be improved by reducing the solar heat gain during the daytime. This can be done by using plate colour with low absorptivity.

Alternatively, controlled insulation curtain can be installed behind the plate and used it during hot seasons. For buildings that have high cooling demand, both attempts might be needed to reduce more heat gain.

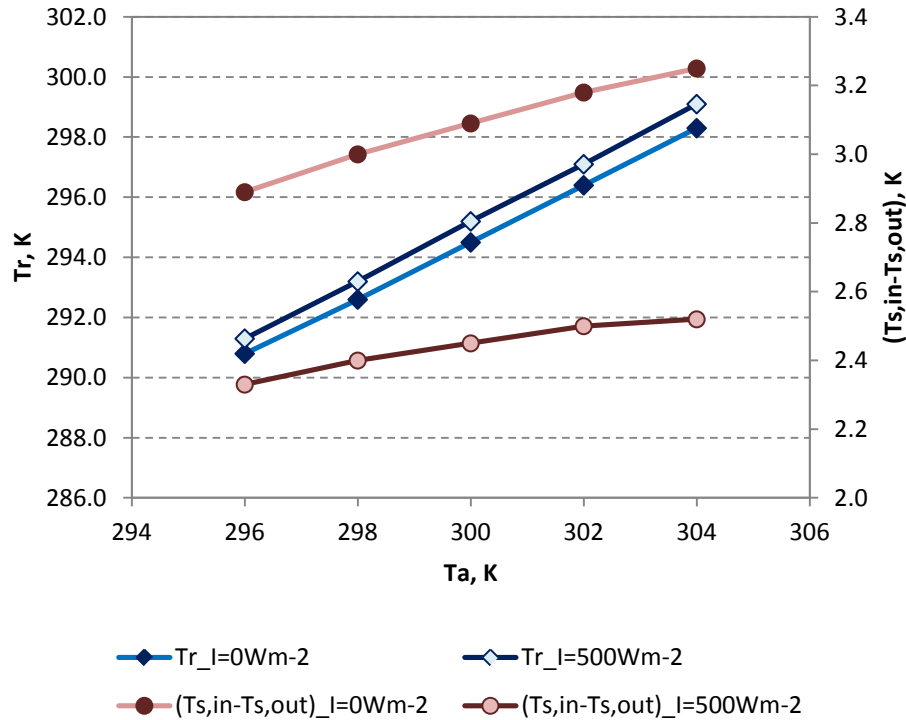


Figure 5-32. Simulated values of  $T_r$  and  $(T_{s,in} - T_{s,out})$  during the day and night time.

## 5.6 Summary and conclusions

In this chapter, two designs, i.e. cooling systems with single plenum and two plenums are discussed according to the measured and modelled results. The main findings of the formal design are as follows:

1) Lower temperature of inlet water results in colder outlet air. However, the system gives adverse results ( $T_{out} > T_a$ ) even if the wall is wetted with chilled water.

2) The low evaporation effect is insufficient to cool the plenum air.

Therefore, this system design is inappropriate to be used for space cooling. On the other hand, the main findings for transpired solar façade with two plenums are as follows:

1) The model for cooling performance gives close results with the experiments.

- 2) Temperature of the water need to be maintained from cycle to cycle to avoid adverse results.
- 3) Lower water temperature results in better cooling effect.
- 4) The water absorbs more heat from Plenum 1 than the Plenum 2.
- 5) Expanding the plate area vertically is able to increase the value of  $(T_{s,in}-T_{s,out})$ , and hence the cooling effectiveness. While expanding the area horizontally does not have significant effect on the cooling effect.
- 6) The cooling efficiency are above 1.0 for solar radiation intensity lower than  $719\text{Wm}^{-2}$ . This indicates that the cooling capacity is greater than the power required for auxiliaries.
- 7) The energy consumption of various types of cooling systems in order to produce is compared with present design. Present design needs 0.52W of auxiliary power to generate 1kW of cooling load, which is similar amount of energy required to some of the solar indirect evaporative cooling and desiccant cooling systems. Though present design consumes more energy to produce the same amount of cooling loads than the conventional refrigerators and absorption systems, lower installation cost and building integrated features should be seen as advantages of the system.
- 8) The system is applicable during daytime and night time. The system gives better cooling effect when there is no solar heat gain.

In conclusions, the system with two plenums not only shows better cooling effect compared to system with single plenum, but also applicable during the night.

## **6. Solar facade for the combined heating and cooling system**

### **6.1 Introduction**

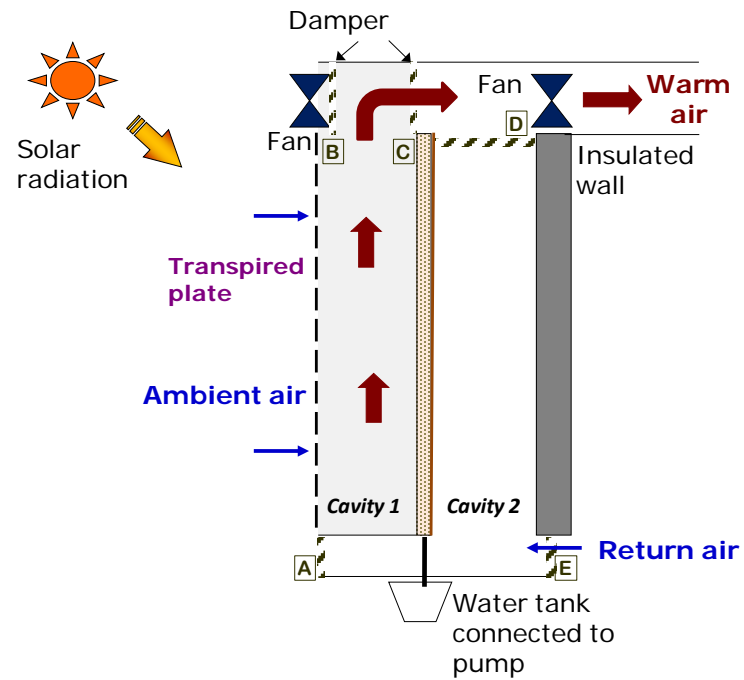
The transpired solar facade has demonstrated a better thermal performance compared to the flat plate (Chapter 4), and it is able to produce cold air with two plenums (Chapter 5). Therefore, in this chapter, this design is selected for further study in a combined system that can be used throughout the year during hot and cold days. The scope of the study includes simulation of the cooling and heating performances, economic analysis and, energy saving, as well as the carbon dioxide reduction potential of the system. The study is carried out in terms of the system being installed as an office building façade in London.

#### **6.1.1 The combined heating and cooling system with controlled dampers**

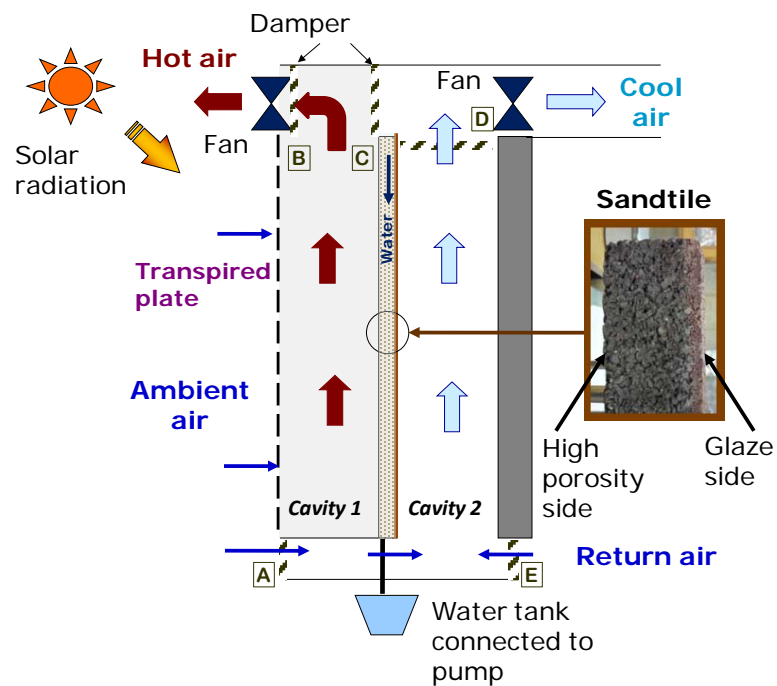
The working mechanisms for the heating and cooling modes are as discussed in Chapters 4 and 5. This section mainly discusses the damper control to shift from one mode to another. Figure 6-1a and 1b show heating and cooling modes of the system respectively.

For the heating mode, Dampers A, B and D are closed, Fan B is switched off, and the sandtile wall is dry. Thus, air is drawn by Fan D through the holes and supplied to the building through Damper C. On the other hand, only Damper C is closed for the cooling mode, and the sandtile wall is wetted with flowing water throughout the operating period. At this time, in Plenum 1, the ambient air is drawn by Fan B through the holes on the plate and exhausted through Damper B. The supply air for Plenum 2 can be drawn from the ambient (through Damper A), from the return air from indoors (through Damper E) or be the mixture of

both. The air is then cooled by the wall and ducted to the building through Damper D.



(a)



(b)

Figure 6-1. (a) Heating and (b) cooling modes with controlled dampers.

## 6.2 Simulation on real building application

### 6.2.1 Building definition

The system installation is assumed to be the south-facing façade of an office building in London. The design and internal gains of the building were adopted from the study of Jenkin and his co-workers (Jenkins, 2008) for the present simulations. In the study, the building was designed as a typical rectangular four-storey office building in an urban environment. The purpose of the study was to simulate climate effects on future UK office heating and cooling energy consumption. Hence, it was deemed appropriate to use the same building design to investigate how the system would aid energy consumption. The building characteristics are detailed in (Jenkins, 2008) and Figure 6-2 shows only the dimensions of the building. The present study assumed that the solar façade was to be installed as a south-facing façade with plate area of  $40\text{m}^2$  ( $H=2\text{m}$ ,  $L=20\text{m}$ ). The installation was assumed to provide heating and cooling for a floor area of the building. In addition, the study also included equipment interventions, lighting, occupant gains and the HVAC system for a future office scenario. The study provided a baseline energy consumption in 2005 and projected for the year 2030. Therefore, the energy saving in the present simulation could be calculated according to the findings of the previous research.

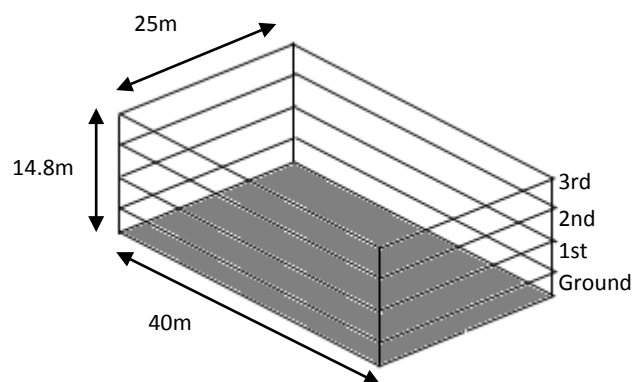


Figure 6-2. Diagram of the building design for present simulation with total height of 14.8m, length of 40m and breadth of 25m.

### 6.2.2 Weather data of London

The weather data for London was obtained from the EnergyPlus Energy Simulation Software's database (U.S. Department of Energy). The data includes the monthly average daily global horizontal irradiance, air temperature and air humidity (Figure 6-3). According to the weather data on cooling degree days (CDD) with a baseline of 291K, cooling is needed during the months of June, July and August. Hence, the present simulation would take the remaining months as cold seasons when heating is needed.

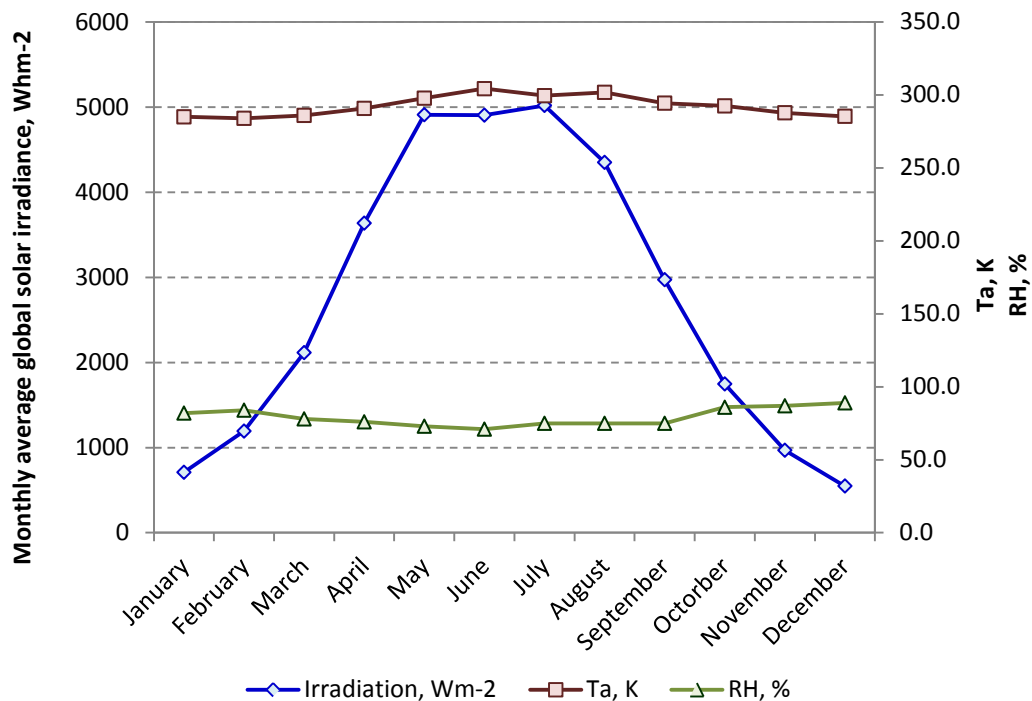


Figure 6-3. Monthly average global solar irradiances and ambient temperatures of London (N51°9') (W0°10').

### 6.3 Heating and cooling performances

Apart from the weather conditions, other input parameters for the model such as suction velocity in Plenum 1 and airflow rate in Plenum 2 are  $0.042\text{ms}^{-1}$  and  $2000\text{m}^3\text{hr}^{-1}$  respectively. In addition, the system is assumed to use return air from the room as the supply air in Plenum 2. As indoor temperature is maintained

at 294 to 296K (Jenkins, 2008), the return air is set to 295K in the present simulation. Whereas, inlet water temperature is set to 285K which is approximately the tap water temperature in the UK during the summer.

Figure 6-4 shows the outlet temperatures and temperature changes of the air throughout the year. During the cold months, the values of rise in air temperature are low especially during the winter, i.e. November to February when the ambient air temperatures and the solar radiation intensities are low. Consequently, the outlet temperatures of these months are below 290K. In contrast, in the month of May, where the outlet temperature is about 303K, higher suction velocity might need to be applied to get a lower air temperature; this depends on the thermal comfort requirement of the occupants. On the other hand, during the summer, the air temperature can be reduced to about 294K. All the outlet temperatures that are shown here are the temperatures of the air leaving the plenums. The mixture of air temperature after entering the room is beyond the focus of present study. Nonetheless, even if the warm or cold air entering the room cannot meet the occupants' thermal comfort, the system is able to reduce the heating or cooling loads of the building by increasing or reducing the indoor air temperature.

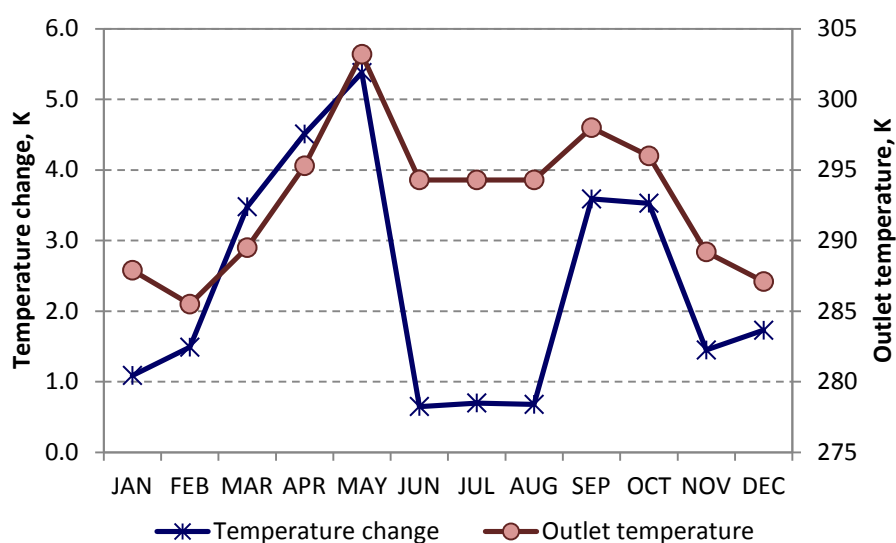


Figure 6-4. Outlet temperatures and temperature changes of the air throughout the year.

#### 6.4 Energy and carbon savings

The annual heating and cooling requirements of the building are  $30.1\text{kWhm}^{-2}$  and  $14.3\text{kWhm}^{-2}$  respectively. Apart from that, the building was assumed to have two units of 147kW non-condensing boilers with load independent flow and return temperatures of  $82^{\circ}\text{C}$  and  $71^{\circ}\text{C}$  respectively, for heating loads; two units of 194kW chillers with  $12^{\circ}\text{C}$  flow and  $7^{\circ}\text{C}$  return temperatures, for cooling loads (Jenkins, 2008). Present system is able to generate warm or cold air and hence reduce the energy requirement in heating and cooling for the building, and thus the energy savings. Table 6-2 shows the energy and  $\text{CO}_2$  savings throughout the year with the present system installed as one of the floor of the building façade. With 2% of total external wall installed with solar façade, the system is able to meet 9% of the building heating load and 1% of the cooling load. This gives an annual energy saving as 10877kWh, which is equivalent to 5874kg $\text{CO}_2$  of emission reduction. Furthermore, if the warm air in the Plenum 1 is not exhausted but is used for other heating purposes, e.g. desiccant cooling or heat recovery, an amount of 8875kWh/year can be added into net energy saving during the hot days. Therefore, the energy saving from the cooling system can be increased to 2% of the cooling requirement of the building.

Table 6-2. Energy and  $\text{CO}_2$  savings from present system.

Energy and $\text{CO}_2$ savings	Amount
Heat delivered by the system, kWh/year	10,401
Cooling capacity, kWh/year	476
Total energy saving per year, kWh	10,877
$\text{CO}_2$ reduction during cold days, kg/year	5,617
$\text{CO}_2$ reduction during hot days, kg/year	257
Total $\text{CO}_2$ reduction per year, kg	5,874

## 6.5 Economic analysis

A similar system has been reported to have a lifetime of 40 years (Cali, 1999). However, the lifetime of present system is assumed to be 30 years for safe judgement. The estimated unit prices and breakdown costs for the whole system installation as well as the energy cost saving are as shown in Table 6-3. The total initial installation cost of present design is estimated to be £2,800 which is about £70/m<sup>2</sup>. This installation cost is less than half of the price of the conventional solar active glaze-covered flat plat air heater (Table 6-4). Hence, this proves that technologies that integrate passive and active solar features are able to reduce the initial cost. Furthermore, the total cost reduction might be greater if the cost saving in building integration is included.

Table 6-3. Initial installation and maintenance costs of the combined heating and cooling system.

	Unit price, £	Sub-total cost, £
Aluminium transpired plate <sup>1</sup>	25/m <sup>2</sup>	800
Santiles <sup>1</sup>	10/m <sup>2</sup>	200
Auxiliaries <sup>1</sup> :	30/m <sup>2</sup>	1,000
Fans, pump, dampers, water tank and ducting		
Others	10/m <sup>2</sup>	400
<i>Total initial installation</i>		<i>2,800</i>
Maintenance (per year)	5% of total initial installation cost	140
Energy cost saving <sup>2</sup>	0.06/kWh	653

<sup>1</sup>The unit prices are based on per unit area of the façade.

<sup>2</sup> Electricity price for non-domestic sector (Department of Energy and Climate Change, 2010).

Table 6-4. Comparisons of initial installation cost of solar glazed-covered flat plate air heater with present design.

Solar collector application	Areas, m <sup>2</sup>	Total initial cost, £	Cost per m <sup>2</sup> , £/m <sup>2</sup>	References
Building ventilation	40	2,800	70	Present
Fruits drying	46	7,500	163	(Sreekumar, 2010)
Solar still	2	325	163	(Kumar, 2009)
Silk cocoon drying	16	2,000	125	(Singh, 2011)

The payback period is estimated by using Equation 6-2.

$$\text{Payback period} = \frac{(\text{Initial installation \& maintenance costs})}{\text{Expected returns per year}} \quad (6-1)$$

The cost effectiveness of the system is determined by the expected savings in heating and cooling costs over the life of the system. By taking into account that money has a time value and a given amount of money will be worth less in the future than it is today, the total energy cost savings and total maintenance costs are reduced to their present value (*PV*) using the present worth factor at an assumed discount rate. In this study, a discount rate of 5% is assumed. The *PV* can be calculated from Equation (6-3) (Kreider, 1975).

$$PV = P_{ann} \{ [(1 + i_{ann})^t - 1] / [i_{ann}(1 + i_{ann})^t] \}, \quad (6-2)$$

where  $P_{ann}$  is the constant annual payments,  $i_{ann}$  is the annual discount rate and  $t$  is the lifetime of the system. The payback period calculation of the system investment is as shown in Table 6-5. The payback period of the combined heating and cooling system for 30 years of lifetime is less than a year, compared to other solar cooling technologies that the payback periods are 7 years and above (Beccali, 2009; Huang, 2011; Tsoutsos 2010).

Table 6-5. Payback period of the system investment with 5% discount rate and 30 year system lifetime.

	Cost, £
Initial investment	2,800
Maintenance in <i>PV</i>	2,152
Total system cost	4,952
Total energy cost saving in <i>PV</i>	10038
<i>Payback period</i>	<i>0.5 years</i>

## 6.6 Conclusions and recommendations

In this chapter, the performance of a combined heating and cooling system has been simulated based on the weather conditions of London. The building characteristics and energy consumptions of a typical building in an urban environment are adopted from previous research. The installation is assumed to be a south-facing façade of the building with an area of 40m<sup>2</sup>, providing heating and cooling for a floor area of the building. Spacing heating is needed for most of the months, however cooling is more favourable for the months of June, July and August. The system is able to give a maximum rise in air temperature of 5.4K and an outlet temperature of 303K in May. During hot days, however, the system is able to cool the indoor air by about 1K. In terms of energy saving, while the cooling system is operating, it is suggested that the warm air in the Plenum 1 should be used for other heating purposes e.g. desiccant cooling or heat recovery to make the cooling system more economically feasible. A simulation study of previous research shows that using the transpired plate heating system to regenerate the desiccant is possible if the plate area is large (Pesaran, 1994). It is estimated that present system is able to give an annual energy saving of 10,877kWh, equivalent to 5,874kgCO<sub>2</sub>/year of emission avoidance. In terms of initial installation cost, the design is estimated to cost for about £70/m<sup>2</sup> and this is cheaper than the conventional solar flat plate air heaters which cost from £125/m<sup>2</sup> to £163/m<sup>2</sup>. Moreover, economic analysis found that the total system

cost is approximately £4,952 for a discount rate of 5% and 30 years of lifetime. The payback period for this system would be less than a year. The auxiliaries cost plays as major part of total installation cost especially in large scale installation. Therefore, future investigations could be done to obtain higher net energy saving. For instance, the experience from the project at the General Motors Battery Plant in Canada (Cali, 1999) shows that fan system modification not only gives better airflow but also reduces the power consumption of the fans. In addition, the study also pointed out that the heating façade is able to reduce building heat loss. Hence, if the data on total avoided heat loss is available, this should be taken into consideration when calculating the energy saving. Heat loss avoidance could reduce the heating energy requirement and thus give more energy saving and shorten the payback period for large scale installation.

## 7. Conclusions

### 7.1 Overview of chapter

This chapter includes the summary and conclusions of the thesis, contributions to the knowledge and recommendations for future work.

### 7.2 Summary and conclusions of the thesis

Two types of facades, i.e. flat and transpired black painted aluminium plates were used as solar collectors for air heating and cooling in buildings. The main findings regarding the heating systems are:

- 1) The transpired façade shows better heat transfer compared to the flat plate. This is mainly due to the transpired design being able to reduce heat loss and hence give better thermal performance. For instance, a system that operates at  $500\text{Wm}^{-2}$  of solar radiation intensity,  $300\text{m}^3\text{hr}^{-1}$  of airflow rate and with an inlet air temperature of 293K gives 8K in air temperature rise for the transpired plate, but only 3K for the flat plate.
- 2) The system efficiency for the flat plate is only about 30%, whereas it is over 85% for the transpired plate. Moreover, the transpired plate shows the highest system efficiency among various types of solar air heaters.
- 3) System efficiency is relatively more sensitive to airflow rate compared to solar radiation intensity. At various solar radiation intensities, the efficiencies for both plates are almost constant. On the other hand, increasing the airflow rate from 100 to  $500\text{m}^3\text{hr}^{-1}$  would increase the system efficiencies by about 6% and 17% respectively, for flat and transpired plates.
- 4) Heat transfer of transpired design was analysed in terms of normal and vertical flows. The vertical flow heat transfer accounted for about 40 to 50% of the total useful energy delivered.

5) Two Nu correlations were developed in the present study, i.e. heat transfer coefficients for the normal and vertical flows. These correlations were developed for a transpired plate with 0.084% of porosity, a triangular array of holes and 2m of height.

6) Normal flow Nu correlation for transpired plate was found to be:

$$Nu_{c,trans} = 0.0004Re_{c,trans}^{1.33} \quad \text{for } 260 \leq Re_{c,trans} \leq 470$$

7) Vertical flow Nu correlation for laminar and turbulent flows are as follows:

Laminar flow:

$$Nu_{f,L,trans} = 0.158Re_{f,trans}^{1.25} \quad \text{for } 1100 < Re_{f,trans} < 2000$$

Turbulent flow:

$$Nu_{f,T,trans} = 0.0023Re_{f,trans}^{1.7} \quad \text{for } Re_{f,trans} \geq 2300$$

8) Though the present study has simplified the heat transfer concept between the back-of-plate and vertical airflow, the values of simulated heat exchange effectiveness of the system are close to the previous study model. Hence, this simplified method, in terms of theoretical calculation and experiment measurements, can be used as an alternative method to evaluate the thermal performance of transpired plate solar collectors, even when the uniformity of the flow is uncertain.

For the cooling system, the air is cooled by the wet sandtile wall and the main findings are:

1) A cooling system with flat plate façade and single plenum gives adverse results ( $T_{out} > T_a$ ) even if the wall is wetted with chilled water at a low solar radiation intensity. Though results show that the wet-wall system is able to reduce solar gain for the building to control overheating, nonetheless due to the low evaporation effect, the overall cooling effect is insignificant.

- 2) Therefore, instead of cooling the air through direct evaporative cooling, the design of the system was modified from single to double plenums, and thus utilised the wet surface to cool the air in the second plenum.
- 3) The heat exchange effectiveness ( $Exh_H$ ) at the heating plenum (Plenum 1) and cooling effectiveness ( $Exh_C$ ) at the cooling plenum (Plenum 2) were calculated from the experimental and the model results. Thus, the mathematical model for transpired façade with two plenums is verified by comparing the ratios of  $Exh_C$  to  $Exh_H$  between these two methods. They have similar results with all the modelled results fall between the acceptance ranges.
- 4) The cooling efficiencies were above 1.0 for a solar radiation intensity lower than  $719Wm^{-2}$ . This indicates that the cooling capacity is greater than the power required for auxiliaries.
- 5) The energy consumption of various types of cooling systems were compared with the present design. The present design needs 0.52W of auxiliary power to generate 1kW of cooling load, which is a similar amount of energy required to some of the solar indirect evaporative cooling and desiccant cooling systems. Though the present design consumes more energy to produce the same amount of cooling loads than conventional refrigerators and absorption systems, lower installation cost and building integrated features should be seen as advantages of the system.
- 6) It was found that inlet water temperature is the key factor that influences the overall cooling effect. Lower water temperature results in better cooling effect, however the temperature of the water need to be maintained from cycle to cycle to avoid adverse results.
- 7) Simulation results show that expanding the plate area vertically will increase the cooling effectiveness. While expanding the area horizontally does not have a significant effect on the cooling effect.

- 8) The system is applicable for both conditions, i.e. with and without solar radiation. In the evening, the system gives better cooling effects compared to the daytime, when there is no solar heat gain.

The transpired solar facade has demonstrated a better thermal performance compared to the flat plate, and it is able to produce cold dry air with two plenums. Therefore, this design is selected for use as a combined system that can be used throughout the year for heating and cooling. Simulation study was carried out based on the weather conditions of London by assuming the façade was installed on an office building with an area of 40m<sup>2</sup>. The main findings are summarised as follows:

- 1) The system is able to deliver 10,401kWh/year of heating load and 476kWh/year of cooling capacity.
- 2) In terms of energy saving, while the cooling mode is operating, it is suggested that the warm air in the heating plenum (Plenum 1) should be used for other heating purposes e.g. desiccant regeneration or heat recovery in order to have more economically feasible investment. With that an additional of 8,875kWh/year of energy can be saved.
- 3) The yearly energy saving was estimated as 10,877kWh, which is equivalent to 5,874kgCO<sub>2</sub>/year of emission avoidance.
- 4) In terms of initial installation cost, the design is estimated to cost about £2,800 in total, or £70/m<sup>2</sup>, and this is only about half the cost of a conventional active solar flat plate air heater. This low cost investment is important to promote and raise the awareness of building integrated solar technologies. If the technologies are affordable by the public, this will open the market for most income groups, and hence lower the price when the technologies are mature.

- 5) Economic analysis found that the total system cost is approximately £4,952 for a discount rate of 5% and 30 years of lifetime. The payback period for such a system would be less than a year.

### **7.3 Contributions**

Followings briefly describe the contributions from the present research:

- 1) The heat transfer comparison between the flat and transpired plates strengthens our knowledge of the ability of transpired design to reduce heat loss. Though transpired design systems have been installed as facades for air heating since the 1990's, no experiment and simulation studies had compared the thermal performance between these two designs. The present study has demonstrated the thermal performances experimentally and heat losses have been analysed for both designs.
- 2) Most of the studies on transpired solar collectors assumed that flow distribution is uniform and hence the air temperatures of the normal and vertical flows are assumed to be the same. One of the reasons for this assumption was the lack of knowledge of vertical flow in the plenum. There were some simulation studies on vertical flow but these had not yet been verified through experiment. In the present study, the heat transfer for transpired plate solar collector was analysed through the normal and vertical flows experimentally. Our experimental results prove that the previous simulation study on the non-uniformity of vertical flow was correct.
- 3) Instead of assuming the flow distribution is uniform, the present study has simplified the heat transfer concept and the experimental measurement method, giving compatible results with the model developed by a previous study. Therefore, these can be used as alternative methods to simulate or measure the plenum air temperature of a transpired solar collector when the uniformity of the flow is uncertain.

- 4) Two Nu correlations, i.e. for normal and vertical heat transfers, have been developed for the system under the condition of uncertainty of flow distribution. Though the correlations have only been tested for the present plate design (e.g. porosity, geometrical distribution of hole, diameter of hole and plate dimension), these findings can serve as a foundation for future research on correlations that correlate with plate design parameters.
- 5) Though the cooling effectiveness of the present design is not high, this study has presented an alternative option for building integrated cooling systems. Since the combined heating and cooling system with two plenums had not yet been examined, the results from the present work can be used as reference for future improvement.
- 6) The low initial investment cost of the system provides information that solar technologies can be affordable and could open the market to different income groups and hence promote and raise the awareness of such a system.
- 7) In terms of contribution to the academic community, the present study has been published in 4 conference proceedings and one review paper in an international journal (Appendix V). In addition, this project has been presented during the SET (Early-Stage Research Scientists, Engineers and Technologists) for Britain event at the House of Commons on 8 March 2010. The project was one of sixty posters displayed during the Engineering poster session and was shortlisted for the SET for Britain Award from hundreds of entries which represent the best engineering research from UK Universities.

#### **7.4 Future work**

A laboratory scale research on solar façade for heating and cooling has been constructed. However, there are a number of aspects that are worthy of further investigations to enhance the knowledge of heat transfer, to improve the system performance and to ensure the economic feasibility of such technology. The suggestions for future work are as follows:

1. Confirmed by Computational Fluid Dynamic (CFD) programme. The heat transfer of the system could be studied by using 2D CFD programme to have better understanding in heat distribution in the plenums.
2. More precise Nu correlations for transpired plate. The developed heat transfer coefficients for transpired plate under the condition of uncertainty of flow distribution were not tested with other plate designs. Further research on more precise correlations with the plate design parameters is needed.
3. System testing on real buildings. This combined heating and cooling system was tested in a laboratory; outdoor testing on real building is important to provide more promising results.
4. Optimisation of water consumption for cooling mode. For the cooling system, the water consumption in the present study was not been optimised. The ability of the sandtile wall to retain water is an advantage to reduce water consumption. At the optimum stage, no pump or tank would be needed to recycle the water, and this hence would avoid the problem of water temperature rise, save the power consumption of the pump, simplify the system construction and lower the initial investment cost.
5. Heat recovery for cooling mode. During the summer, the hot air from the Plenum 1 can be recovered or used for other heating purposes. For instance, previous research (Pesaran 1994) carried out simulation study on desiccant cooling ventilation integrated with a transpired solar collector; doing this would not only being benefit in terms of energy saving, thus making the technology more economically feasible, but it would also improve the cooling effect by integrating passive and solar technologies. Therefore, more research on integrating this system with other heating purposes is needed.
6. Enhancing heat transfer in Plenum 2. The heat transfer in Plenum 2 between the cold air and the wall is poor. Heat transfer enhancement attempts might improve the overall cooling effect, for example, through fins, jet impingement cooling or psychrometric energy cooler (PEC).

7. Alternative facades. Besides the black painted aluminium plate, other types of panels could be installed as alternative options. This would very much depend on the need for thermal comfort and the weather conditions of particular countries. Countries which need more heating might need to install a transpired design panel, but since the heating effectiveness is high, the flexibility in terms of colours is wide. On the other hand, in countries that need more cooling, the panel could be replaced with a photovoltaic (PV) panel. This would have dual benefits. The air flowing behind the PV panel would cool the panel and thus improving the PV efficiency. Secondly, the electricity generated by the PV could be used for the fans and pumps; and hence this would reduce the auxiliaries energy consumption, CO<sub>2</sub> emissions, system cost, payback period and making the green technology economically feasible.

## References

- Abreu, M.I., Corvacho, H., Dias, R.P. 2011. "Passive systems for buildings using buoyancy-driven airflows." *Recent Patents on Engineering* 5:23-31.
- Aldabbagh, L.B.Y., Egelioglu, F., Ilkan, M. 2010. "Single and double pass solar air heaters with wire mesh as packing bed " *Energy and Buildings* 35(9):3783-3787.
- Amer, Emad H. 2006. "Passive options for solar cooling of buildings in arid areas." *Energy* 31(8-9):1332-1344.
- Andrews G.E., Alikhanizadeh M., Asere A.A., Khoshkbar Azari M.S., Mkpadi M.C. 1986. "Small diameter film cooling holes: wall convection heat transfer." *Journal of Turbomachinery* 108:283-289.
- Andrews G.E., Bazdidi-Tehrani F. 1989. "Small diameter film cooling hole heat transfer: the influence of the number of holes." In *Gas Turbine and Aeroengine Congress and Exposition*. Toronto, Ontario, Canada: ASME.
- Andrews, G.E., Bazdidi-Tehrani, F. 1989. "Small diameter film cooling hole heat transfer: the influence of the number of holes." In *Gas Turbine and Aeroengine Congress and Exposition*. Toronto, Ontario, Canada: ASME.
- Andrews G.E., Durance J., Hussain C.I., Ojabor S.N. 1987. "Full coverage impingement heat transfer: influence of the number of holes." *Journal of Turbomachinery* 109:557-563.
- Angioletti, M., Di Tommaso, R. M., Nino, E., Ruocco, G. 2003. "Simultaneous visualization of flow field and evaluation of local heat transfer by transitional impinging jets." *International Journal of Heat and Mass Transfer* 46(10):1703-1713.
- Arulanandam, S.J., Hollands, K. G. T, Brundrett, E. 1999. "A CFD heat transfer analysis of the transpired solar collector under no-wind conditions." *Solar Energy* 67(1-3):93-100.
- ASHRAE. 2009. *ASHRAE Handbook: Fundamentals*. SI Edition. Atlanta: American Society of Heating, Refrigerating and Air-Conditioning Engineers, Inc.
- Augustus, L. M., Kumar S. 2007. "Mathematical modeling and thermal performance analysis of unglazed transpired solar collectors." *Solar Energy* 81(1):62-75.
- Awbi, Hazim B. 1998. "Chapter 7—Ventilation." *Renewable and Sustainable Energy Reviews* 2(1-2):157-188.

- Bazdidi-Tehrani F. , Andrews G.E. . 1994. "Full-coverage discrete hole film cooling: investigation of the effect of variable density ratio." *Journal of Engineering for Gas Turbines and Power* 116:587-596.
- Beccali, M., Finocchiaro, P., Nocke, B. 2009. "Energy and economic assessment of desiccant cooling systems coupled with single glazed air and hybrid PV/thermal solar collectors for applications in hot and humid climate." *Solar Energy* 83(10):1828-1846.
- Bejan, Adrian. 1993. *Heat Transfer* John Wiley & Sons, Inc.
- Bejan, A. 2003. "Porous Media." In *Heat Transfer handbook*, ed. Bejan A., Kraus A.D. : John Wiley & Sons, Inc.
- Belusko, M., Saman, W., Bruno, F. 2008. "Performance of jet impingement in unglazed air collectors " *Solar Energy* 82(5):389-398.
- Bourdoukan, P., Wurtz, E., Joubert, P 2009. "Experimental investigation of a solar desiccant cooling installation " *Solar Energy* 83(11).
- Cali, A., Kutscher, C.F. , Dymond, C.S., Pfluger, R., Hollick, J., Kokko, J., McClenahan, D. 1999. "A report of Task 14 Air Systems Working Group: Low cost, high performance solar air-heating systems using perforated absorbers." In *IEA Solar Heating and Cooling Program, Task 14: Advanced Active Solar Systems* ed. Alfred P. Brunger. Washington: International Energy Agency (IEA).
- Casals, X.G. 2006. "Solar absorption cooling in Spain: Perspectives and outcomes from the simulation of recent installations " *Renewable Energy* 31(9):1371-1389.
- Chandel, S.S., Aggarwal, R.K. 2008. "Performance evaluation of a passive solar building in Western Himalayas." *Renewable Energy* 33(10):2166-2173.
- Cheikh, H.B., Bouchair, A. 2004. "Passive cooling by evapo-reflective roof for hot dry climates " *Renewable Energy* 29(11):1877-1886.
- Choudhury, C., Garg, H.P. 1991. "Evaluation of a jet plate solar air heater." *Solar Energy* 46(4):199-209.
- Chungloo, S., Limmeechokchai, B. 2007. "Application of passive cooling systems in the hot and humid climate: The case study of solar chimney and wetted roof in Thailand." *Building and Environment* 42(9):3341-3351.
- Cooperative Extension Service. 2006. "Passive Solar Heating: an energy factsheet." Alaska: The University of Alaska Fairbanks.
- Dabagh A.M., Andrews G.E., Abdul Husain R.A.A., Husain C.I., Nazari A., Wu J. 1990. "Impingement/effusion cooling: the influence of the number of

- impingement holes and pressure loss on the heat transfer coefficient." *Journal of Turbomachinery* 112:467-476.
- Daou, K., Wang, R.Z., Xia, Z.Z. 2006. "Desiccant cooling air conditioning: a review." *Renewable and Sustainable Energy Reviews* 10(2):55-77.
- Department of Energy and Climate Change. 2010. "Quarterly Energy Prices December 2010."
- Devotta, S., Waghmare, A. V., Sawant, N. N., Domkundwar, B. M. . 2001. "Alternatives to HCFC-22 for air conditioners " *Applied Thermal Engineering* 21(6):703-715.
- Dimoudi, A. Androutsopoulos, S. Lykoudis. 2006a. "Summer performance of a ventilated roof component." *Energy and Buildings* 38(6):610-617.
- Dimoudi, S. Lykoudis, A. Androutsopoulos. 2006b. "Thermal performance of an innovative roof component." *Renewable Energy* 31(14):2257-2271.
- Dymond, C., Kutscher, C. 1997. "Development of a flow distribution and design model for transpired solar collectors." *Solar Energy* 60(5): 291-300.
- Dymond, Christopher. 2007. "When Solar Cookies Beat Conservation Veggies." In *Green+Solar Building Oregon*. Oregon.
- Eicker, U. 2003. *Solar Technologies for Buildings*. West Sussex: John Wiley & Sons Ltd.
- Eicker, U., Pietruschka, D. 2009. "Design and performance of solar powered absorption cooling systems in office buildings " *Energy and Buildings* 41(1):81-91.
- Eicker, U., Schneider, D., Schumacher, J., Ge, T., Dai, Y. . 2010. "Operational experiences with solar air collector driven desiccant cooling systems " *Applied Energy* 87(12):3735-3747.
- El-Dessouky, H. T., Ettouney, H. M., Bouhamra, W. . 2000. "A Novel Air Conditioning System: Membrane Air Drying and Evaporative Cooling." *Chemical Engineering Research and Design* 78(7):999-1009.
- El-Sebaili, A.A., Aboul-Enein, S., Ramadan, M.R.I., Shalaby, S.M., Moharram, B.M. . 2011. "Thermal performance investigation of double pass-finned plate solar air heater " *Applied Energy* 88(5):1727-1739.
- Ellis, M. W., Mathews, E. H. 2002. "Needs and trends in building and HVAC system design tools." *Building and Environment* 37(5):461-470.
- Ellis, M. W., Mathews, E.H. 2001. "A new simplified thermal design tool for architects." *Building and Environment* 36(9):1009-1021.

- Elsayed, S.S., Hamamoto, Y., Akisawa, A., Kashiwagi T. . 2006. "Analysis of an air cycle refrigerator driving air conditioning system integrated desiccant system." *International Journal of Refrigeration* 29(2):219-228.
- Enteria, N., Yoshino, H., Mochida, A., Takaki, R., Satake, A., Yoshie, R., Mitamura, T., Baba, S. . 2009. "Construction and initial operation of the combined solar thermal and electric desiccant cooling system " *Solar Energy* 83(8):1300-1311.
- Fan, Y., Luo, L., Souyri, B. 2007. "Review of solar sorption refrigeration technologies: Development and applications." *Renewable and Sustainable Energy Reviews* 11(8):1758-1775.
- Fleck, B. A., Meier, R. M., Matovic, M. D. 2002. "A field study of the wind effects on the performance of an unglazed transpired solar collector." *Solar Energy* 73(3):209-216.
- Florides, G.A. , Tassou, S.A., Kalogirou, S.A., Wrobel, L.C. 2002. "Review of solar and low energy cooling technologies for buildings." *Renewable and Sustainable Energy Reviews* 6(6):557-572.
- Fong, K.F., Chow, T.T., Lee, C.K., Lin, Z., Chan, L.S. 2010. "Advancement of solar desiccant cooling system for building use in subtropical Hong Kong " *Energy and Buildings* 42(12):2386-2399.
- Forson, F. K., Nazha, M. A. A., Rajakaruna, H. 2003. "Experimental and simulation studies on a single pass, double duct solar air heater." *Energy Conversion and Management* 44(8):1209-1227.
- Forsythe, William Elmer. 2003. *Smithsonian Physical Table*. 9th Edition. New York: Knovel.
- Gan, G. 2006. "Simulation of buoyancy-induced flow in open cavities for natural ventilation." *Energy and Buildings* 38(5):410-420.
- Gan, G. 1998. "A parametric study of Trombe wall for passive cooling of buildings." *Energy and Buildings* 27(1):37-43.
- Gan, G. 2011. "General expressions for the calculation of air flow and heat transfer rates in tall ventilation cavities." *Building and Environment* 46(10):2069-2080.
- Gao, W., Lin, W., Liu, T., Xia, C. 2007. "Analytical and experimental studies on the thermal performance of cross-corrugated and flat-plate solar air heaters " *Applied Energy* 84(4):425-441.
- Gawlik, K., Christensen, C., Kutscher, C. 2005. "A numerical and experimental investigation of low-conductivity unglazed, transpired solar air heaters." *Journal of solar energy engineering* 127:153.

- Ghiabaklou, Z. 2003. "Thermal comfort prediction for a new passive cooling system " *Building and Environment* 38(7):883-891.
- Giabaklou, Z., Ballinger, J.A. 1996. "A passive evaporative cooling system by natural ventilation " *Building and Environment* 31(6):503-507.
- Gunnewiek, L. H., Brundrett, E., Hollands, K.G.T. 1996. "Flow distribution in unglazed transpired plate solar air heaters of large area." *Solar Energy* 58(4-6):227-237.
- Gunnewiek, L.H., Hollands, K.G.T., Brundrett, E. 2002. "Effect of wind on flow distribution in unglazed transpired plate collectors." *Solar Energy* 72(4): 317-325.
- Hajidavalloo, E., Eghtedari, H. . 2010. "Performance improvement of air-cooled refrigeration system by using evaporatively cooled air condenser " *International Journal of Refrigeration* 33(5):982-988.
- Harris, D.J., Helwig, N 2007. "Solar chimney and building ventilation." *Applied Energy* 84(2):135-146.
- Hatami, N., Bahadorinejad, M 2008. "Experimental determination of natural convection heat transfer coefficient in a vertical flat-plate solar air heater " *Solar Energy* 82(10):903-910.
- He, J. , Hoyano, A. 2010. "Experimental study of cooling effects of a passive evaporative cooling wall constructed of porous ceramics with high water soaking-up ability " *Building and Environment* 45(2):461-472.
- Henning, H-M. 2007a. "Solar assisted air conditioning of buildings – an overview." *Applied Thermal Engineering* 27(10):1734-1749.
- Henning, H-M. 2007b. *Solar-Assisted Air-Conditioning in Buildings, A Handbook for Planners*. 2nd Edition. New York: Springer, Wien.
- Hestnes, A.G. 1999. "Building Integration Of Solar Energy Systems." *Solar Energy* 67(4-6):181-187.
- Hirunlabh, J., Kongduang, W., Namprakai, P., Khedari, J. 1999. "Study of natural ventilation of houses by a metallic solar wall under tropical climate." *Renewable Energy* 18(1):109-119.
- HM Government. 2009. "The UK Low Carbon Transition Plan: National strategy for climate and energy." The Stationery Office.
- Hollick, J. C. 1996. "World's largest and tallest solar recladding." *Renewable Energy* 9(1-4):703-707.
- Hollick, J. C. 1998. "Solar cogeneration panels." *Renewable Energy* 15(1-4):5-200.

- Hollworth B.R., Cole G.H. 1987. "Heat transfer to arrays of impinging jets in a crossflow " *Journal of Turbomachinery* 109:564-571.
- Huang, B.J., Wu, J.H. , Hsu, H.Y., Wang, J.H. 2010. "Development of hybrid solar-assisted cooling/heating system " *Energy Conversion and Management* 51(8):1643-1650.
- Huang, B.J., Wu, J.H., Yen, R.H., Wang, J.H., Hsu, H.Y., Hsia, C.J., Yen, C.W., Chang, J.M. "System performance and economic analysis of solar-assisted cooling/heating system." *Solar Energy*, In Press, Corrected Proof, Available online 13 September 2011.
- IEA. 2007a. *Energy Use in the New Millennium: Trends in IEA Countries*. France: OECD/IEA.
- IEA. 2007b. *World Energy outlook 2007: China and India Insights*. France: OECD/IEA.
- IEA. 2008a. "Energy technology perspectives 2008: scenarios and strategies to 2050." France: International Energy Agency.
- IEA. 2008b. *Worldwide Trends in Energy Use and Efficiency: Key Insights from IEA Indicator Analysis*. France: OECD/IEA.
- IEA. 2009. "World energy outlook 2009." France: International Energy Agency.
- IEA. 2010. "IEA Policy pathway: energy performance certification of buildings." France: International Energy Agency.
- Incropera, F.P., Dewitt, D. P. 2002. *Fundamentals of heat and mass transfer*. 5th Edition: John Wiley & Sons Inc.
- Jain, S. , Dhar, P. L., Kaushik, S. C. 1995. "Evaluation of solid-desiccant-based evaporative cooling cycles for typical hot and humid climates." *International Journal of Refrigeration* 18(5):287-296.
- Jaluria, Yogesh. 2003. "Natural Convection." In *Heat Transfer Handbook*, ed. Adrian Bejan, Allan D. Kraus. New Jersey: John Wiley & Sons, Inc.
- Jenkins, D., Liu, Y., Peacock, A.D. 2008. "Climatic and internal factors affecting future UK office heating and cooling energy consumptions " *Energy and Buildings* 40(5):874-881.
- Jie, J., Hua, Y., Gang, P., Bin, J., Wei, H. 2007. "Study of PV-Trombe wall assisted with DC fan." *Building and Environment* 42(10):3529-3539.
- Joseph Khedari, Weerapong Mansirisub, Sompong Chaima, Naris Pratinthong, Jongjit Hirunlabh. 2000. "Field measurements of performance of roof solar collector." *Energy and Buildings* 31(3):171-178.
- Joshi, Y., Nakayama, W. 2003. "Forced Convection: External Flows." In *Heat Transfer Handbook*, ed. Bejan A., Kraus A.D. : John Wiley & Sons, Inc.

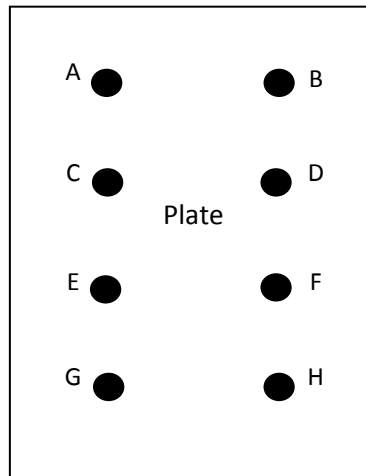
- Joudi, K.A. , Mehdi, S.M. . 2000. "Application of indirect evaporative cooling to variable domestic cooling load " *Energy Conversion and Management* 41(17):1931-1951.
- Juanico, L. 2008. "A new design of roof-integrated water solar collector for domestic heating and cooling." *Solar Energy* 82(6): 481-492.
- Khalid A. Joudi, Salah M. Mehdi. 2000. "Application of indirect evaporative cooling to variable domestic cooling load." *Energy Conversion and Management* 41(17):1931-1951.
- Khedari, J., Mansirisub, W., Chaima, S., Pratinthong, N., Hirunlabh, J 2000. "Field measurements of performance of roof solar collector." *Energy and Buildings* 31(3):171-178.
- Kolokotroni, M., Davies, M., Croxford, B., Bhuiyan, S., Mavrogianni, A. 2010. "A validated methodology for the prediction of heating and cooling energy demand for buildings within the Urban Heat Island: Case-study of London " *Solar Energy* 84(12):2246-2255.
- Kreider, J.F., Kreith, F. 1975. *Solar heating and cooling: engineering, practical design, and economics*. New York: Scripta Book Company.
- Kumar, S., Tiwari, G.N. 2009. "Life cycle cost analysis of single slope hybrid (PV/T) active solar still " *Applied Energy* 86(10):1995-2004.
- Kutscher, C. F. 1994. "Heat exchange effectiveness and pressure drop for air flow through perforated plates with and without crosswinds." *J. Heat Transfer* 116: 391–399.
- Kutscher, C.F., Christensen, C.B., Barker, G.M. 1993. "Unglazed transpired solar collectors: heat loss theory." *ASME Journal of Solar Engineering* 115(3):182–188.
- Kutscher, C.F. 1992. "An investigation of heat transfer for air flow through low porosity perforated plates." In *Department of Mechanical Engineering*. Colorado: University of Colorado.
- Li, A., Jones, P., Zhao, P., Wang, L. 2004. "Heat transfer and natural ventilation airflow rates from single-sided heated solar chimney for buildings." *Journal of Asian Architecture and Building Engineering* 3(2):233-238.
- Maerefat, M., Haghghi, A.P. 2010. "Natural cooling of stand-alone houses using solar chimney and evaporative cooling cavity " *Renewable Energy* 35(9):2040-2052.
- Mattsson, Einar. 2001. *Basic Corrosion Technology for Scientists and Engineers* Second Edition: Institute of Materials Communications Ltd.

- Matuska, T., Sourek, B. 2006. "Façade solar collectors." *Solar Energy* 80(11):1443-1452.
- Miyazaki, T., Akisawa, A., Kashiwagi, T. 2006. "The effects of solar chimneys on thermal load mitigation of office buildings under the Japanese climate." *Renewable Energy* 31(7):987-1010.
- Na-pompet, K., Boonsupthip, W. . 2011. "Effect of a narrow channel on heat transfer enhancement of a slot-jet impingement system." *Journal of Food Engineering* 103(4):366-376.
- Nakayama, Y. 2000. "Flow of viscous fluid." In *Introduction to Fluid Mechanics*, ed. R. F. Boucher. Oxford: Butterworth-Heinemann.
- Nasr, M.M. , Salah Hassan, M. . 2009. "Experimental and theoretical investigation of an innovative evaporative condenser for residential refrigerator." *Renewable Energy* 34(11):2447-2454.
- [Nelkon, M., Ogborn, J.M. 1962. Advanced level practical physics. 2<sup>nd</sup> Edition. London: Heinemann Educational Books Ltd.](#)
- Nwachukwu, N.P. , Okonkwo, W. 2008. "Effect of an Absorptive Coating on Solar Energy Storage in a Trombe wall system." *Energy and Buildings* 40(3):371-374.
- Onbasioglu, H., Egrican, A. N 2002. "Experimental approach to the thermal response of passive systems." *Energy Conversion and Management* 43(15):2053-2065.
- Ong, K. S., Chow, C. C. 2003. "Performance of a solar chimney." *Solar Energy* 74(1):1-17.
- Onishi, J., Soeda, H., Mizuno, M. 2001. "Numerical study on a low energy architecture based upon distributed heat storage system." *Renewable Energy* 22(13):61-66.
- Orel, Z.C., Klanjek, M., Gunde, Hutchins, M. G. 2005. "Spectrally selective solar absorbers in different non-black colours." *Solar Energy Materials and Solar Cells* 85(1):41-50.
- Ozgen, F., Esen, M., Esen, H. 2009. "Experimental investigation of thermal performance of a double-flow solar air heater having aluminium cans " *Renewable Energy* 34(11):2391-2398.
- Park, K-J, Seo,T., Jung,D. 2007. "Performance of alternative refrigerants for residential air-conditioning applications." *Applied Energy* 84(10):985-991.
- Pesaran, A.A., Wipke, K.B. 1994. "Use of unglazed transpired solar collectors for desiccant cooling." *Solar Energy* 52(5):419-427.

- Prasad, S.B., Saini, J.S., Singh, K.M. . 2009. "Investigation of heat transfer and friction characteristics of packed bed solar air heater using wire mesh as packing material " *Solar Energy* 83(5):773-783.
- Probst, M.M., Roecker, C. 2007. "Towards an improved architectural quality of building integrated solar thermal systems (BIST)." *Solar Energy* 81(9):1104-1116.
- Raman, P., Mande S., Kishore, V.V.N. 2001. "A passive solar system for thermal comfort conditioning of buildings in composite climates." *Solar Energy* 70(4):319-329.
- Richman, R.C. , Pressnail, K.D. 2009. "A more sustainable curtain wall system: Analytical modeling of the solar dynamic buffer zone (SDBZ) curtain wall." *Building and Environment* 40(1):1-10.
- Sagot, B. Antonini, G., Christgen,A., Buron,F. . 2008. "Jet impingement heat transfer on a flat plate at a constant wall temperature " *International Journal of Thermal Sciences* 47(12):1610-1619.
- Shen, J, Lassue, S., Zalewski, L., Huang, D. 2007. "Numerical study on thermal behavior of classical or composite Trombe solar walls Classical Trombe wall." *Energy and Buildings* 39(8):962–974.
- Singh, P.L. 2011. "Silk cocoon drying in forced convection type solar dryer " *Applied Energy* 88(5):1720-1726.
- Sodha, M.S., Govind, Bansal, P.K., Kaushik, S.C. . 1980. "Reduction of heat flux by a flowing water layer over an insulated roof." *Building and Environment* 15(2):133-140.
- SolarWall. How SolarWall Technology Works to Provide Fresh Air and Free Heat. 2010 [Cited October 2010]. Available from <http://solarwall.com/en/products/solarwall-air-heating/how-it-works.php>.
- Soteris, A. Kalogirou ed. 2009. *Solar energy engineering: process and systems*. 1st Edition: Elsevier Inc.
- Sparrow, E.M. and Ortiz, M. Carranco. 1982. "Heat transfer coefficients for the upstream face of a perforated plate positioned normal to an oncoming flow." *J. Heat Mass Transfer* 25(1):127-135.
- Specht, Brian *Solar Energy in Canada*. 2009 [Cited July 2009]. Available from <http://www.cansia.ca/Content/Documents/Document.aspx?DocId=12401>.
- Splading, D.B. 1963. *Convection mass transfer*. London: Edward Arnold (Publishers) Ltd.

- Sreekumar, A. 2010. "Techno-economic analysis of a roof-integrated solar air heating system for drying fruit and vegetables " *Energy Conversion and Management* 51(11):2230-2238.
- Stritih, U. 2003. "Heat transfer enhancement in latent heat thermal storage system for buildings." *Energy and Buildings* 35(11):1097-1104.
- Togrul, I.T., Pehlvan, D., Akosman, C. 2004. "Development and testing of a solar air-heater with conical concentrator " *Renewable Energy* 29(2):263-275.
- Tripanagnostopoulos, Y., Souliotis, M., Nousia, T. 2000. "Solar collectors with colored absorbers." *Solar Energy* 68(4):343-356.
- Tsoutsos, T., Aloumpi, E., Gkouskos, Z., Karagiorgas, M. 2010. "Design of a solar absorption cooling system in a Greek hospital " *Energy and Buildings* 42(2):265-272.
- Tyagi, V.V., Buddhi, D. 2007. "PCM thermal storage in buildings: A state of art." *Renewable and Sustainable Energy Reviews* 11(6):1146-1166.
- U.S. Department of Energy, Energy Efficiency and Renewable Energy Office. "EnergyPlus: weather data."
- Van, D.G.W.E., Hollands, K.G.T., Brunger, A. P. 2001. "Heat-exchange relations for unglazed transpired solar collectors with circular holes on a square or triangular pitch." *Solar Energy* 71(1):33-45.
- Wanphen, S., Nagano, K. 2009. "Experimental study of the performance of porous materials to moderate the roof surface temperature by its evaporative cooling effect." *Building and Environment* 44(2):338-351.
- Zamora, B., Kaiser, A.S. 2006. "Optimum wall-to-wall spacing in solar chimney shaped channels in natural convection by numerical investigation." *Applied Thermal Engineering* 29(4): 762-769.
- Zhai, X.Q., Dai, Y.J., Wang, R.Z. 2005. "Comparison of heating and natural ventilation in a solar house induced by two roof solar collectors." *Applied Thermal Engineering* 25(5-6):741-757.
- Zhao, X., Liu, S., Riffat, S. 2008. "Comparative study of heat and mass exchanging materials for indirect evaporative cooling systems." *Building and Environment* 43(11):1902-1911.

## Appendix I: Distribution of solar radiation intensities



Point	Radiation intensity, $Wm^{-2}$				
A	316	507	621	730	837
B	313	512	611	717	820
C	311	511	614	711	822
D	314	508	625	737	827
E	301	493	610	720	825
F	306	488	622	721	811
G	296	486	603	708	807
H	299	491	606	705	809
Average	307	500	614	719	820

## Appendix II: Matlab Programme

### II-1 Heating system with flat plate facade

```
clear all

T= [320; 300];
Tp=320;
Tf=300;

T_S(:,1)=T;

i=2;
for i=2:20

    TAm=290;
    Tin=TAm;
    Tout=2*Tf-Tin;
    Vfan=202/3600; %m3/s
    I=500; %W/m2
    H=2; %height of wall, m
    D=0.25; %width of channel, m
    L=1; %length of wall,
    rol_f=(-0.0047*Tf) + 2.5612 %kg/m3
    cp_f=((2E-5)*Tf) + 1.001*1E3;%J/kgK
    nu_f =((0.0942*Tf)-11.822)*1E-6; %m2/s
    Pr=0.72;
    M=Vfan*rol_f*cp_f/H*L;

    Tsur=TAm;
    hr=0.9*(5.67E-8)*(Tp+Tsur)*((Tp^2)+(Tsur^2));

    TpAm=(Tp+TAm)/2;
    k_pAm=((0.0782*TpAm)+2.64)*1E-3 ;
    nu_pAm =((0.0942*TpAm)-11.822)*1E-6; %m2/s
    alfa_pAm =((0.14*TpAm)-18.62)*1E-6;
    Ra=9.807*(1/TpAm)*(H^3)*abs(Tp-TAm)/(alfa_pAm*nu_pAm);
    Nu_c=(0.825+((0.387*Ra^(1/6))/(1+(0.492/Pr)^(9/16)))^(8/27)))^2;
    hc=Nu_c*k_pAm/H;

    Gr=9.807*(1/Tf)*(H^3)*abs(Tf-((Tp+Tf)/2))/nu_f^2;
    Re_free=(Gr/2.5)^0.5;
    Re_for=Vfan*H/(nu_f*D*L)
    Re=((Re_free^2)+(Re_for^2))^0.5;
    Nu_lam=0.664*(Re^0.5)*(Pr^(1/3))
    Tpf=(Tp+Tf)/2;
    k_pf=((0.0782*Tpf)+2.64)*1E-3 ;
    hf=Nu_lam*k_pf/H;

    S=I*0.95;

    A=[(hr+hc+hf) -hf; hf -(hf+2*M)];
    B=[S+hr*TAm+hc*TAm; -2*M*TAm];

    T=inv(A)*B;
    T_S(:,i)=T
end
```

```
    Tp=T(1,1);
    Tf=T(2,1);
    a=(T_S(1,i)-T_S(1,i-1));
    b=(T_S(2,i)-T_S(2,i-1));

    Eff=100*Vfan*rol_f*cp_f*(Tout-Tin)/(H*L*I);
    Exh=(Tout-Tin)/(Tp-Tin)*100;
    q=M*(Tout-Tin);
    dT=Tout-TAm

    Qr=hr*(Tp-TAm);
    Qc=hc*(Tp-TAm);
    Qf=hf*(Tp-Tf);
    Qd=M*(Tout-Tin);

    i=i+1;

end
```

## II-2 Heating system with transpired plate facade

```

clear all

T= [308; 303; 306];
Tp=308;
Ti=303;
Tout=306;

T_S(:,1)=T;

i=2;
for i=2:20

Ta=298.9;
I=820; %W/m2
vs=0.032; %m/s
vf=0.19; %m/s
D=0.30; %width of channel, m
H=2; %height of wall, m
L=1; %length of wall, m
d=0.0012; %m
P=0.0084;%
Tf=(Tout+Ti)/2;
rol_a=(-0.0047*Ta) + 2.5612 %kg/m3
cp_a=((2E-5)*Ta) + 1.001)*1E3;
cp_f=((2E-5)*Tf) + 1.001)*1E3;%J/kgK
G=vs*rol_a

Tsur=Ta;
hr=0.9*(5.67E-8)*(Tp+Tsur)*((Tp^2)+(Tsur^2))

nu_a =((0.0942*Ta)-11.822)*1E-6; %m2/s
Rec=vs/P*d/nu_a;
Nuc=0.0007*(Rec^1.33);
k_a=((0.0782*Ta)+2.64)*1E-3 ;
hc=Nuc*k_a/d;

nu_f =((0.0942*Tf)-11.822)*1E-6; %m2/s
Ref=vf/P*d/nu_f;
Nuf=0.158*(Ref^1.25);%Laminar
Nuf=0.0026*Ref^1.7;
k_f=((0.0782*Tf)+2.64)*1E-3 ;
hf=Nuf*k_f/H

S=I*0.95;

A=[(hc+hr+hf) (-hc-hf/2) -hf/2; hf G*cp_f-hf/2 -(G*cp_f+hf/2); hc
- (G*cp_a+hc) 0];
B=[S+hr*Ta; 0; -G*cp_a*Ta];

T=inv(A)*B
T_S(:,i)=T
Tp=T(1,1);
Ti=T(2,1);
Tout=T(3,1);
a=(T_S(1,i)-T_S(1,i-1));
b=(T_S(2,i)-T_S(2,i-1));

```

```
c=(T_S(3,i)-T_S(3,i-1));

Eff=100*G*cp_f*(Tout-Ta)/I
Exh=(Tout-Ta)/(Tp-Ta)*100
dT=Tout-Ta
q=G*cp_f*(Tout-Ta)*H*L;

Qr=hr*(Tp-Ta);
Qc=hc*(Tp-Ti);
Qf=hf*(Tp-Tf);
G*cp_a*(Tout-Ta);
Q1=Qf+Qc+Qr-S;
Q2=G*cp_f*(Tout-Ti)-Qf;
Q3=G*cp_a*(Ti-Ta)-Qc;

i=i+1;

end
```

### II-3 Heating system for transpired façade with Kutsher's model

```

clear all

T= [308; 303; 306];
Tp=308;
Ti=303;
Tout=306;

T_S(:,1)=T;

i=2;
for i=2:20

Ta=298.9;
I=820; %W/m2
vs=0.032; %m/s
vf=0.19; %m/s
D=0.3; %width of channel, m
H=2; %height of wall, m
L=1; %length of wall, m
d=0.0012; %m
P=0.0084;%
Tf=(Tout+Ti)/2;
rol_a=(-0.0047*Ta) + 2.5612 ;%kg/m3
cp_a=((2E-5)*Ta) + 1.001)*1E3;
cp_f=((2E-5)*Tf) + 1.001)*1E3;%J/kgK
G=vs*rol_a;
Tsur=Ta;
hr=0.9*(5.67E-8)*(Tp+Tsur)*((Tp^2)+(Tsur^2));

nu_a =((0.0942*Ta)-11.822)*1E-6; %m2/s
Rec=vs/P*d/nu_a;
Nuc=0.0004*(Rec^1.33);
k_a=((0.0782*Ta)+2.64)*1E-3 ;
hc=Nuc*k_a/d;

nu_f =((0.0942*Tf)-11.822)*1E-6; %m2/s
Ref=vf/P*d/nu_f;
Nuf=0.182*(Ref^1.25);%Laminar
%Nuf=0.0026*Ref^1.7;
k_f=((0.0782*Tf)+2.64)*1E-3 ;
hf=Nuf*k_f/H;

S=I*0.95;

A=[(hc+hr) -hc 0; hf G*cp_f-hf/2 -(G*cp_f+hf/2); hc -(G*cp_a+hc)
0];
B=[S+hr*Ta; 0; -G*cp_a*Ta]

T=inv(A)*B
T_S(:,i)=T
Tp=T(1,1);
Ti=T(2,1);
Tout=T(3,1);

a=(T_S(1,i)-T_S(1,i-1));
b=(T_S(2,i)-T_S(2,i-1));
c=(T_S(3,i)-T_S(3,i-1));

```

```
Eff=100*G*cp_f*(Tout-Ta)/I
Exh=(Tout-Ta)/(Tp-Ta)*100
q=G*cp_f*(Tout-Ta)
```

```
Qc=hc*(Tp-Ti);
Qr=hr*(Tp-Ta);
Qf=hf*(Tp-Tf);
Q1=Qc+Qr-S
Q2=G*cp_f*(Tout-Ti)-Qf
Q3=G*cp_a*(Ti-Ta)-Qc
```

```
i=i+1;
```

```
end
```

## II-4 Cooling system with flat plate and single plenum

```

clear all

T= [339; 299; 295];
Tp=339;
Tf=299;
Tw=295;

T_S(:,1)=T;

i=2;
for i=2:20

I=0; %W/m2
Ta=293.2;
Tw1=285.2;
Vfan=100/3600; %m3/s
RH=34.6; %%
Tin=Ta;
Tout=(2*Tf-Tin);
Tw2=2*Tw-Tw1;
Vwater=1.2/1000/60;
H=2; %height of wall, m
D=0.20; %width of channel, m
L=1; %length of wall, m
Ap=H*L;
rol_water=-0.2016*Tw + 1057.1; %kg/m3
rol_f=(-0.0047*Tf) + 2.5612 %kg/m3
cp_f=((2E-5)*Tf) + 1.001)*1E3;%J/kgK
Tfw=(Tw+Tf)/2;
cp_v=(1E-5*Tfw^2-0.0048*Tfw+2.4615)*1E3; %J/kgK
cp_w=(3E-5*Tw^2-0.0195*Tw+7.1425)*1E3;%J/kgK
cp_w1=(3E-5*Tw1^2-0.0195*Tw1+7.1425)*1E3;%J/kgK
cp_w2=(3E-5*Tw2^2-0.0195*Tw2+7.1425)*1E3;%J/kgK
nu_f =((0.0942*Tf)-11.822)*1E-6; %m2/s
Pr=0.72
mf=Vfan*rol_f;
mwl=Vwater*rol_water; %kg/s
wet=0.83; %wettability=1.75/2*26.5/28=0.83;
Hfg=(-2.3571*Tfw+3144.8)*1E3; %(280-310K), Hw=cp_w*Tw+Hfg;J/kg
Hout=(1.9118*Tout+1973.6)*1E3; %(283-323K),J/kg
Hin=(1.9118*Tin+1973.6)*1E3 ; %(283-323K),J/kg
ps=exp(-6069.9385*(1/Tin)+21.2409642-2.711193E-2*Tin+1.673952E-5*Tin^2+2.433502*log(Tin));
p=ps*(RH/100);
win=0.622*p/(101325-p)

Tsur=Ta;
hr=0.9*(5.67E-8)*(Tp+Tsur)*((Tp^2)+(Tsur^2));

Tpa=(Tp+Ta)/2;
k_pa=((0.0782*Tpa)+2.64)*1E-3 ;
nu_pa =((0.0942*Tpa)-11.822)*1E-6; %m2/s
alfa_pa =((0.14*Tpa)-18.62)*1E-6;
Ra=9.807*(1/Tpa)*(H^3)*abs(Tp-Ta)/(alfa_pa*nu_pa);
Nu_c=(0.825+((0.387*Ra^(1/6))/(1+(0.492/Pr)^(9/16)))^(8/27))^2;
hc=Nu_c*k_pa/H;

Gr=9.807*(1/Tf)*(H^3)*abs(Tf-((Tp+Tw)/2))/nu_f^2;

```

```

Re_free=(Gr/2.5)^0.5;
Re_for=Vfan*H/(nu_f*D*L);
Re=((Re_free^2)+(Re_for^2))^0.5;
Nu_lam=0.664*(Re^0.5)*(Pr^(1/3));
Tpf=(Tp+Tf)/2;
k_pf=((0.0782*Tpf)+2.64)*1E-3 ;
hf=Nu_lam*k_pf/H;

k_fw=(0.0579*Tfw + 2.417)*1E-3;
mu_v=(0.04*Tfw-2.91)*1E-6; %Ns/m2
rol_sat=1000; %kg/m3
rol_v=0.0012*Tfw - 0.3281;
rol_Tw=4E-45*Tfw^17; %kg/m3
Pr_v=0.0016*Tfw + 0.377;
%pw=4.4014*Tfw^2-2425.7*Tfw+335167;
pw= 171.12*Tfw - 47427;
pw_out= 171.12*Tout - 47427;
Rew=mw1/H/mu_v;
Le=1;
g_heat=2.1565E-5*Pr_v^(-2/3)*(mw1*1000^2*9.81/H)^(1/3);%kg/m2s
%Nuw=1.207E-3*H*(rol_v^2*9.8/(mw1/H)/mu_v)^(1/3);
Nuw1=g_heat*H/(k_fw/cp_v);
hw1=Nuw1*k_fw/H;
hw2=Nu*k_fw/H;
hw=0.7*hw1+0.3*hw2;
hm=hw/cp_f/Le;
wTw=0.622*pw/(101325-pw);
wout=hm*(wTw-win)*Ap/mf+win
dmw=mf*(wout-win)
mw=(mw1+(mw1+dmw))/2;

Hw=cp_w*Tw;
Hw1=cp_w1*Tw1;
Hw2=cp_w2*(2*Tw-Tw1);

S=I*0.95;

A=[(hc+hr+hf) -hf 0; -hf 2*mf*cp_f/Ap+hf+hw -(dmw*cp_v/Ap+hw); 0
-hw (hw+2*mw*cp_w/Ap+dmw*cp_v/Ap+cp_w*dmw/Ap)];
B=[S+(hc+hr)*Ta; 2*mf*cp_f*Ta/Ap-mf*(wout*Hout-
win*Hin)/Ap+dmw*Hfg/Ap; 2*mw*cp_w*Tw1/Ap-dmw*Hfg/Ap];

T=inv(A)*B;
T_S(:,i)=T
Tp=T(1,1);
Tf=T(2,1);
Tw=T(3,1);
a=(T_S(1,i)-T_S(1,i-1));
b=(T_S(2,i)-T_S(2,i-1));
c=(T_S(3,i)-T_S(3,i-1));

Qr=hr*(Tp-Ta);
Qc=hc*(Tp-Ta);
Qf=hf*(Tp-Tf);
Qw=hw*(Tf-Tw)
Qf-Qw;
QL=dmw*(cp_v*Tw+Hfg)/Ap
mf*cp_f*(Tin-Tout)/Ap+mf*(win*Hin-wout*Hout)/Ap;
Q1=S-Qc-Qr-Qf;

```

```

Q2=mf*cp_f*(Tin-Tout)/Ap+mf*(win*Hin-wout*Hout)/Ap+Qf+QL-Qw;
Q3=mw*(cp_w*Tw2-cp_w*Tw1)/Ap+dmw*cp_w*Tw/Ap+QL-Qw;

ps_out=exp(-6069.9385*(1/Tout)+21.2409642-2.711193E-
  2*Tout+1.673952E-5*Tout^2+2.433502*log(Tout));
p_out=wout*101352/(0.622+wout);
RH_out=p_out*100/ps_out

q=mf*cp_f*(Tin-Tout);
Eff=mf*cp_f*(Tin-Tout)/(H*L*I)*100 ;
dT=Tin-Tout
dw=wout-win

i=i+1;

end

```

## II-5 Cooling system with transpired plate and single plenum

```
clear all

T= [327.8; 296.5; 287.6];

Tp=54.8+273;
Tf=19.5+273;
Tw=14.6+273;
Tr=287;
Ts=286;

T_S(:,1)=T;

i=2;
for i=2:20

I=500; %W/m2
Ta=300;
Tw1=283;
Vfan=100/3600; %m3/s
RH=50; %%
vs=0.1;
vf=0.20;
D2=0.2;
d=0.0012; %m
P=0.0084;%
rol_a=(-0.0047*Ta) + 2.5612 ;%kg/m3
cp_a(((2E-5)*Ta) + 1.001)*1E3;
G=vs*rol_a
Tw2=2*Tw-Tw1;
Tins=298;
Vwater=1.4/1000/60; %m3/s
H=2; %height of wall, m
D=0.25; %width of channel, m
L=1; %length of wall, m
Ap=H*L;
rol_water=-0.2016*Tw + 1057.1; %kg/m3
rol_f=(-0.0047*Tf) + 2.5612 ;%kg/m3
rol_s=(-0.0047*Ts) + 2.5612 ;%kg/m3
cp_f(((2E-5)*Tf) + 1.001)*1E3;%J/kgK
cp_fa(((2E-5)*Ta) + 1.001)*1E3;%J/kgK
cp_fs(((2E-5)*Ts) + 1.001)*1E3;%J/kgK
Tfw=(Tw+Tf)/2;
cp_v=(1E-5*Tfw^2-0.0048*Tfw+2.4615)*1E3;%J/kgK
cp_w=(3E-5*Tw^2-0.0195*Tw+7.1425)*1E3;%J/kgK
cp_w1=(3E-5*Tw1^2-0.0195*Tw1+7.1425)*1E3;%J/kgK
cp_w2=(3E-5*Tw2^2-0.0195*Tw2+7.1425)*1E3;%J/kgK
nu_f =((0.0942*Tf)-11.822)*1E-6; %m2/s
Pr=0.72;
mw1=Vwater*rol_water; %kg/s
wet=0.83; %wetability=1.75/2*26.5/28=0.83;
vf2=Vfan/(L*D2);
ms=Vfan*rol_s

Tsur=Ta;
hr1=0.9*(5.67E-8)*(Tp+Tsur)*((Tp^2)+(Tsur^2));
hr2=0;

nu_a =((0.0942*Ta)-11.822)*1E-6; %m2/s
```

```

Rec=vs/P*d/nu_a;
Nuc=0.0004*(Rec^1.33);
k_a=((0.0782*Ta)+2.64)*1E-3 ;
hc=Nuc*k_a/d;

B=G*cp_fa+hc;
Ti=hc/B*Tp+G*cp_fa/B*Ta;
Tout=2*Tf-Ti;

Hfg=(-2.3571*Tfw+3144.8)*1E3 %(280-310K), Hw=cp_w*Tw+Hfg;J/kg
Hout=(1.9118*Tout+1973.6)*1E3; %(283-323K),J/kg
Hin=(1.9118*Ti+1973.6)*1E3 ; %(283-323K),J/kg

ps=exp(-6069.9385*(1/Ti)+21.2409642-2.711193E-2*Ti+1.673952E-
5*Ti^2+2.433502*log(Ti));
p=ps*(RH/100);
win=0.622*p/(101325-p);

Gr=9.807*(1/Tf)*(H^3)*abs(Tf-((Tp+Tw)/2))/nu_f^2;
Re_free=(Gr/2.5)^0.5;
Re_for=vf*H/(nu_f);
Re=((Re_free^2)+(Re_for^2))^0.5;
Nu_lam=0.664*(Re^0.5)*(Pr^(1/3));
k_fw=((0.0782*Tfw)+2.64)*1E-3 ;
k_s=((0.0782*Ts)+2.64)*1E-3 ;
hw2=Nu_lam*k_fw/H;

nu_s =((0.0942*Ts)-11.822)*1E-6; %m2/s
Gr3=9.807*(1/Ts)*(H^3)*abs(Ts-((Tr+Ts)/2))/nu_s^2;
Re_free3=(Gr/2.5)^0.5;
Re_for3=vf2*H/(nu_s);
Re3=((Re_free3^2)+(Re_for3^2))^0.5;
Nu_lam3=0.664*(Re3^0.5)*(Pr^(1/3));
hf3=0;

Ref=vf/P*d/nu_f;
Nuf=0.158*(Ref^1.25);%Laminar
k_f=((0.0782*Tf)+2.64)*1E-3 ;
hf1=Nuf*k_f/H

k_fw=(0.0579*Tfw + 2.417)*1E-3;
mu_v=(0.04*Tfw-2.91)*1E-6; %Ns/m2
rol_sat=1000; %kg/m3
rol_v=0.0012*Tfw - 0.3281;
rol_Tw=4E-45*Tw^17; %kg/m3
Pr_v=0.0016*Tfw + 0.377;
%pw=4.4014*Tw^2-2425.7*Tw+335167;
pw= 171.12*Tw - 47427;
pw_out= 171.12*Tout - 47427;
Rew=mw1/H/mu_v;
Le=1;
g_heat=2.1565E-5*Pr_v^(-2/3)*(mw1*1000^2*9.81/H)^(1/3);%kg/m2s
%Nuw=1.207E-3*H*(rol_v^2*9.8/(mw1/H)/mu_v)^(1/3);
Nuw1=g_heat*H/(k_fw/cp_f);
hw1=Nuw1*k_fw/H;

hw=0.7*hw1+0.3*hw2;
hm=hw/cp_f/Le;
wTw=0.622*pw/(101325-pw);
wout=hm*(wTw-win)/G+win;

```

```

dmw=G*(wout-win)*Ap; %Tw2-Tw1
mw=(mw1+(mw1+dmw))/2;
Hw=cp_w*Tw;
Hw1=cp_w1*Tw1;
Uw=0;

S=I*0.95;

A=[(hc+hr1+hf1+hr2-hc^2/B) -hf1 -hr2; hf1+2*G*cp_f*hc/B -
    (2*G*cp_f+hf1+hw) (dmw*cp_v/Ap+hw); hr2 hw -
    (hw+2*mw*cp_w/Ap+dmw*cp_v/Ap+cp_w*dmw/Ap+hr2+Uw)];
B=[S+(hc*G*cp_fa/B*Ta+hr1*Ta); G*(wout*Hout-win*Hin)-
    2*G^2*cp_f*cp_fa*Ta/B-dmw*Hfg/Ap; -
    2*mw*cp_w*Tw1/Ap+dmw*Hfg/Ap];

T=inv(A)*B;
T_S(:,i)=T
Tp=T(1,1);
Tf=T(2,1);
Tw=T(3,1);
a=(T_S(1,i)-T_S(1,i-1));
b=(T_S(2,i)-T_S(2,i-1));
c=(T_S(3,i)-T_S(3,i-1));

Qr1=hr1*(Tp-Ta);
Qr2=hr2*(Tp-Tw);
Qc=hc*(Tp-Ti);
Qf1=hf1*(Tp-Tf);
Qf3=hf3*(Ts-Tr);
Qsand=Uw*(Tr-Tw);
Qw=hw*(Tf-Tw);
QL=dmw*(cp_v*Tw+Hfg)/Ap;
G*cp_f*(Tout-Ti);
G*(wout*Hout-win*Hin);
dT=Tout-Ta
Q1=S-Qc-Qr1-Qf1-Qr2;
Q2=G*cp_f*(Tout-Ti)+G*(wout*Hout-win*Hin)-Qf1-QL+Qw;
Q3=mw*(cp_w*Tw2-cp_w*Tw1)/Ap+dmw*cp_w*Tw/Ap+QL-Qw-Qr2-Qsand;

ps_out=exp(-6069.9385*(1/Tout)+21.2409642-2.711193E-
    2*Tout+1.673952E-5*Tout^2+2.433502*log(Tout));
p_out=wout*101352/(0.622+wout);
RH_out=p_out*100/ps_out;

i=i+1;
end

```

## II-6 Cooling system with transpired plate and two plenums

```

clear all

T= [327.8; 296.5; 287.6; 287.0; 286];
Tp=54.8+273;
Tf=19.5+273;
Tw=14.6+273;
Tr=287;
Ts=286;

T_S(:,1)=T;

i=2;
for i=2:20

I=500; %W/m2
Ta=300;
Tw1=293;
Vfan=100/3600; %m3/s
RH=50; %%
vs=0.042;
vf=0.20;
Td=(Ta-273)-((100-RH)/5);
D2=0.2;
d=0.0012; %m
P=0.0084;%
rol_a=(-0.0047*Ta) + 2.5612 ;%kg/m3
cp_a=((2E-5)*Ta) + 1.001)*1E3;
G=vs*rol_a
Tw2=2*Tw-Tw1;
Tins=298;
Vwater=1.4/1000/60; %m3/s
H=12; %height of wall, m
D=0.25; %width of channel, m
L=1; %length of wall, m
Ap=H*L;
rol_water=-0.2016*Tw + 1057.1; %kg/m3
rol_f=(-0.0047*Tf) + 2.5612 ;%kg/m3
rol_s=(-0.0047*Ts) + 2.5612 ;%kg/m3
cp_f=((2E-5)*Tf) + 1.001)*1E3;%J/kgK
cp_fa=((2E-5)*Ta) + 1.001)*1E3;%J/kgK
cp_fs=((2E-5)*Ts) + 1.001)*1E3;%J/kgK
Tfw=(Tw+Tf)/2;
cp_v=(1E-5*Tfw^2-0.0048*Tfw+2.4615)*1E3;%J/kgK
cp_w=(3E-5*Tw^2-0.0195*Tw+7.1425)*1E3;%J/kgK
cp_w1=(3E-5*Tw1^2-0.0195*Tw1+7.1425)*1E3;%J/kgK
cp_w2=(3E-5*Tw2^2-0.0195*Tw2+7.1425)*1E3;%J/kgK
nu_f =((0.0942*Tf)-11.822)*1E-6; %m2/s
Pr=0.72;
mw1=Vwater*rol_water; %kg/s
wet=0.83; %wetability=1.75/2*26.5/28=0.83;
vf2=Vfan/(L*D2);
ms=Vfan*rol_s

Tsur=Ta;
hr1=0.9*(5.67E-8)*(Tp+Tsur)*((Tp^2)+(Tsur^2));
hr2=1.13E-9*(Tp^2+Tw^2)*(Tp+Tw);
%Tsky=Ta*(0.741 +0.0062*Td)^0.25; %Paul Berdahl,The thermal
radiance of clear skies

```

```

%hr1=0.9*(5.67E-8)*(Tp+Tsky)*((Tp^2)+(Tsky^2));

nu_a =((0.0942*Ta)-11.822)*1E-6; %m2/s
Rec=vs/P*d/nu_a;
Nuc=0.0004*(Rec^1.33);
k_a=((0.0782*Ta)+2.64)*1E-3 ;
hc=Nuc*k_a/d;

B=G*cp_fa+hc;
Ti=hc/B*Tp+G*cp_fa/B*Ta;
Tout=2*Tf-Ti;

Hfg=(-2.3571*Tfw+3144.8)*1E3 ;%(280-310K), Hw=cp_w*Tw+Hfg;J/kg
Hout=(1.9118*Tout+1973.6)*1E3; %(283-323K),J/kg
Hin=(1.9118*Ti+1973.6)*1E3 ; %(283-323K),J/kg
ps=exp(-6069.9385*(1/Ti)+21.2409642-2.711193E-2*Ti+1.673952E-
5*Ti^2+2.433502*log(Ti));
p=ps*(RH/100);
win=0.622*p/(101325-p);

Gr=9.807*(1/Tf)*(H^3)*abs(Tf-((Tp+Tw)/2))/nu_f^2;
Re_free=(Gr/2.5)^0.5;
Re_for=vf*H/(nu_f);
Re=((Re_free^2)+(Re_for^2))^0.5;
Nu_lam=0.664*(Re^0.5)*(Pr^(1/3));
k_fw=((0.0782*Tfw)+2.64)*1E-3 ;
k_s=((0.0782*Ts)+2.64)*1E-3 ;
hw2=Nu_lam*k_fw/H;

nu_s =((0.0942*Ts)-11.822)*1E-6; %m2/s
Gr3=9.807*(1/Ts)*(H^3)*abs(Ts-((Tr+Ts)/2))/nu_s^2;
Re_free3=(Gr/2.5)^0.5;
Re_for3=vf2*H/(nu_s);
Re3=((Re_free3^2)+(Re_for3^2))^0.5;
Nu_lam3=0.664*(Re3^0.5)*(Pr^(1/3));
hf3=Nu_lam3*k_s/H;

Ref=vf/P*d/nu_f;
Nuf=0.158*(Ref^1.25);%Laminar
%Nuf=0.0026*Ref^1.7;
k_f=((0.0782*Tf)+2.64)*1E-3 ;
hf1=Nuf*k_f/H;

k_fw=(0.0579*Tfw + 2.417)*1E-3;
mu_v=(0.04*Tfw-2.91)*1E-6; %Ns/m2
rol_sat=1000; %kg/m3
rol_v=0.0012*Tfw - 0.3281;
rol_Tw=4E-45*Tw^17; %kg/m3
Pr_v=0.0016*Tfw + 0.377;
%pw=4.4014*Tw^2-2425.7*Tw+335167;
pw= 171.12*Tw - 47427;
pw_out= 171.12*Tout - 47427;
Rew=mw1/H/mu_v;
Le=1;
g_heat=2.1565E-5*Pr_v^(-2/3)*(mw1*1000^2*9.81/H)^(1/3);%kg/m2s
Nuwl=g_heat*H/(k_fw/cp_f);
hw1=Nuwl*k_fw/H;

hw=0.7*hw1+0.3*hw2;
hm=hw/cp_f/Le;

```

```

wTw=0.622*pw/(101325-pw);
wout=hm*(wTw-win)/G+win;
dmw=G*(wout-win)*Ap; %Tw2-Tw1
mw=(mw1+(mw1+dmw))/2;
Hw=cp_w*Tw;
Hw1=cp_w1*Tw1;
Uw=1/(0.055/1.01);
S=I*0.95;

A=[(hc+hr1+hf1+hr2-hc^2/B) -hf1 -hr2 0 0; hf1+2*G*cp_f*hc/B -
(2*G*cp_f+hf1+hw) (dmw*cp_v/Ap+hw) 0 0; hr2 hw -
(hw+2*mw*cp_w/Ap+dmw*cp_v/Ap+cp_w*dmw/Ap+hr2+Uw) Uw 0; 0 0 Uw
-(Uw+hf3) hf3; 0 0 0 -hf3 2*ms*cp_fs/Ap+hf3];
B=[S+(hc*G*cp_fa/B*Ta+hr1*Ta); G*(wout*Hout-win*Hin)-
2*G^2*cp_f*cp_fa*Ta/B-dmw*Hfg/Ap; -2*mw*cp_w*Tw1/Ap+dmw*Hfg/Ap;
0; 2*ms*cp_fs/Ap*Tins];

T=inv(A)*B;
T_S(:,i)=T
Tp=T(1,1);
Tf=T(2,1);
Tw=T(3,1);
Tr=T(4,1);
Ts=T(5,1);
a=(T_S(1,i)-T_S(1,i-1));
b=(T_S(2,i)-T_S(2,i-1));
c=(T_S(3,i)-T_S(3,i-1));
d=(T_S(4,i)-T_S(4,i-1));
e=(T_S(5,i)-T_S(5,i-1));

Qr1=hr1*(Tp-Ta);
Qr2=hr2*(Tp-Tw);
Qc=hc*(Tp-Ti);
Qf1=hf1*(Tp-Tf);
Qf3=hf3*(Ts-Tr);
Qsand=Uw*(Tr-Tw);
Qw=hw*(Tf-Tw);
QL=dmw*(cp_v*Tw+Hfg)/Ap;
G*cp_f*(Tout-Ti);
G*(wout*Hout-win*Hin);

dT=Tout-Ta;
Q=G*cp_f*(Tout-Ta)*H*L;
Touts=2*Ts-Tins
dt=Tins-Touts
q=ms*cp_fs*(Tins-Touts);
Q1=S-Qc-Qr1-Qf1-Qr2;
Q2=G*cp_f*(Tout-Ti)+G*(wout*Hout-win*Hin)-Qf1-QL+Qw;
Q3=mw*(cp_w*Tw2-cp_w*Tw1)/Ap+dmw*cp_w*Tw/Ap+QL-Qw-Qr2-Qsand;
Q4=Qsand-Qf3;
Q5=ms/Ap*cp_fs*(Tins-Touts)-Qf3;

ps_out=exp(-6069.9385*(1/Tout)+21.2409642-2.711193E-
2*Tout+1.673952E-5*Tout^2+2.433502*log(Tout));
p_out=wout*101352/(0.622+wout);
RH_out=p_out*100/ps_out;
Exh_c=dt/(Tins-Tr)*100

i=i+1;
end

```

## Appendix III

### Experiment and simulation results for heating systems

#### III-1 Heating system with flat plate facade

Experiment results for heating system with flat plate

$I, \text{Wm}^{-2}$	$V_{fan}, \text{m}^3/\text{hr}$	$D, \text{m}$	$T_a, \text{K}$	$T_p, \text{K}$	$T_f, \text{K}$	$T_w, \text{K}$	$T_r, \text{K}$
223	67	0.20	296.5	321.4	296.9	296.5	295.9
223	67	0.20	295.1	315.0	295.4	295.1	294.4
223	134	0.20	295.7	315.4	295.9	295.6	296.4
223	202	0.20	295.4	312.2	295.8	295.7	295.9
223	269	0.20	295.4	312.2	295.8	295.7	295.9
223	331	0.20	295.3	313.0	295.7	295.3	296.0
307	67	0.20	297.4	323.2	297.8	297.1	297.0
307	67	0.20	293.7	319.7	293.9	293.2	293.2
307	67	0.20	294.7	320.6	295.1	294.5	294.3
307	134	0.20	296.0	321.4	296.4	295.9	296.5
307	134	0.20	294.8	319.9	295.1	295.0	294.9
307	202	0.20	294.9	319.7	295.4	295.4	294.6
307	202	0.20	295.4	312.2	295.8	295.7	295.9
307	202	0.20	292.5	317.7	292.6	292.0	292.4
307	202	0.20	291.3	317.2	291.1	290.3	291.9
307	269	0.20	296.1	320.0	296.7	296.6	296.4
307	331	0.20	295.5	318.6	296.1	295.9	296.1
307	331	0.20	293.6	317.3	293.9	293.6	294.0
385	202	0.20	296.2	331.0	296.9	296.9	296.6
385	202	0.20	292.5	326.5	293.0	292.5	293.5
385	202	0.20	294.9	329.4	295.4	295.3	294.6
500	202	0.20	295.9	332.8	296.5	296.5	297.2
500	202	0.20	295.5	332.5	296.0	296.0	295.1
614	202	0.20	296.2	339.0	297.0	297.1	297.9
614	202	0.20	295.8	333.4	296.4	296.1	295.8
719	202	0.20	293.5	341.2	294.4	294.3	294.0
820	202	0.20	296.5	350.4	297.5	297.5	296.5
820	202	0.20	293.7	347.2	294.7	294.8	293.7
820	202	0.20	294.2	346.8	294.9	294.4	293.7
223	67	0.25	295.3	316.0	295.5	294.9	297.3
223	67	0.25	296.8	316.8	297.0	296.9	296.3
223	134	0.25	295.3	316.0	295.5	294.9	297.3
223	134	0.25	296.8	317.0	297.2	297.2	297.0
223	202	0.25	295.3	316.0	295.5	294.9	297.3
223	202	0.25	296.5	314.0	296.9	296.8	296.3
223	269	0.25	296.8	314.0	296.8	295.9	296.8
223	269	0.25	296.5	313.8	296.7	296.5	296.5
223	331	0.25	296.7	314.6	296.9	296.6	297.0
223	331	0.25	296.1	313.0	296.2	295.9	296.4

307	67	0.25	297.9	323.5	298.5	298.4	297.3
307	134	0.25	296.9	322.7	297.3	297.4	297.3
307	202	0.25	297.4	322.8	297.9	298.1	297.1
307	269	0.25	297.5	322.5	297.8	297.8	297.9
307	331	0.25	297.3	321.8	297.5	297.4	297.8
500	202	0.25	297.9	335.6	298.6	298.5	297.9
614	202	0.25	296.9	340.0	297.6	297.7	296.7
719	202	0.25	296.4	340.8	297.1	296.8	296.4
719	202	0.25	296.4	345.1	297.1	296.7	296.3
820	202	0.25	296.8	349.9	297.7	297.6	296.4
223	67	0.30	294.5	314.5	294.9	294.9	297.2
223	67	0.30	294.2	314.1	294.6	295.2	297.5
223	67	0.30	294.1	313.9	294.5	294.3	297.0
223	134	0.30	293.7	313.5	294.0	293.7	296.1
223	134	0.30	292.8	311.9	293.0	292.9	295.5
223	202	0.30	293.5	312.3	293.7	293.2	295.1
223	202	0.30	293.5	312.6	293.8	293.7	295.6
223	202	0.30	295.2	314.0	295.6	295.5	296.8
223	269	0.30	293.9	312.3	294.2	294.0	295.8
223	269	0.30	295.7	313.9	296.6	297.7	298.2
223	269	0.30	294.1	312.5	294.4	294.3	295.8
223	331	0.30	293.9	312.4	294.1	294.4	295.5
223	331	0.30	294.3	311.9	294.3	293.7	295.7
307	67	0.30	293.3	319.3	293.8	294.0	297.3
307	67	0.30	293.8	318.9	294.0	293.4	296.3
307	134	0.30	293.7	319.2	294.1	294.4	296.5
307	134	0.30	294.7	320.0	295.0	294.6	297.1
307	202	0.30	294.0	318.9	294.6	294.9	296.8
307	202	0.30	295.0	319.9	295.5	295.3	297.3
307	269	0.30	293.9	317.8	294.3	294.0	296.0
307	269	0.30	295.5	319.6	296.0	295.8	297.4
307	331	0.30	294.6	318.6	295.0	294.8	296.7
307	331	0.30	295.0	318.2	295.3	294.9	296.6
307	202	0.30	294.0	318.9	294.6	294.9	296.8
307	202	0.30	295.0	319.9	295.5	295.3	297.3
500	202	0.30	294.8	331.5	295.5	295.4	298.2
500	202	0.30	295.9	331.9	296.7	296.4	298.9
614	202	0.30	295.5	337.3	296.3	296.5	299.7
614	202	0.30	296.1	338.1	297.1	296.9	299.7
719	202	0.30	295.9	342.4	296.9	297.3	300.3
719	202	0.30	295.9	342.0	296.7	296.3	299.7
800	202	0.30	296.1	347.5	297.3	297.8	301.1

Simulation results for heating system with flat plate

$I, \text{Wm}^{-2}$	$V_{\text{fan}}, \text{m}^3/\text{hr}$	$D, \text{m}$	$T_a, \text{K}$	$T_p, \text{K}$	$T_f, \text{K}$
223	67	0.20	296.5	313.7	298.1
223	67	0.20	295.1	312.4	296.7
223	134	0.20	295.7	312.5	296.6
223	202	0.20	295.4	311.7	296.0

223	269	0.20	295.4	311.2	295.9
223	331	0.20	295.3	310.7	295.7
307	67	0.20	297.4	319.9	299.7
307	67	0.20	293.7	316.4	296.0
307	67	0.20	294.7	317.3	297.0
307	134	0.20	296.0	317.9	297.2
307	134	0.20	294.8	316.8	296.0
307	202	0.20	294.9	316.3	295.8
307	202	0.20	295.4	316.3	295.8
307	202	0.20	292.5	314.1	293.4
307	202	0.20	291.3	312.9	292.2
307	269	0.20	296.1	316.9	296.8
307	331	0.20	295.5	315.7	296.1
307	331	0.20	293.6	313.9	294.2
385	202	0.20	296.2	322.0	297.3
385	202	0.20	292.5	318.5	293.6
385	202	0.20	294.9	320.8	296.0
500	202	0.20	295.9	327.9	297.4
500	202	0.20	295.5	327.5	297.0
614	202	0.20	296.2	333.9	298.0
614	202	0.20	295.8	333.5	297.6
719	202	0.20	293.5	336.5	295.7
820	202	0.20	296.5	343.9	299.0
820	202	0.20	293.7	341.4	296.2
820	202	0.20	294.2	341.9	296.7
223	67	0.25	295.3	312.7	296.9
223	67	0.25	296.8	314.1	298.4
223	134	0.25	295.3	312.2	296.2
223	134	0.25	296.8	313.7	297.7
223	202	0.25	295.3	311.9	295.9
223	202	0.25	296.5	313.0	297.1
223	269	0.25	296.8	312.9	297.3
223	269	0.25	296.5	312.7	297.0
223	331	0.25	296.7	312.5	297.0
223	331	0.25	296.1	311.9	296.5
307	67	0.25	297.9	320.4	300.2
307	134	0.25	296.9	318.9	298.1
307	202	0.25	297.4	318.9	298.3
307	269	0.25	297.5	318.6	298.2
307	331	0.25	297.3	318.0	297.8
500	202	0.25	297.9	330.0	299.3
614	202	0.25	296.9	334.9	298.7
719	202	0.25	296.4	339.5	298.5
719	202	0.25	296.4	339.5	298.5
820	202	0.25	296.8	344.5	299.2
223	67	0.30	294.5	311.9	296.1
223	67	0.30	294.2	311.6	295.8
223	67	0.30	294.1	311.5	295.7
223	134	0.30	293.7	310.8	294.6
223	134	0.30	292.8	309.9	293.7

223	202	0.30	293.5	310.3	294.1
223	202	0.30	295.2	311.9	295.8
223	269	0.30	293.9	310.4	294.4
223	269	0.30	295.7	312.1	296.2
223	269	0.30	294.1	310.6	294.6
223	331	0.30	293.9	310.1	294.3
223	331	0.30	294.3	310.5	294.7
307	67	0.30	293.3	316.1	295.6
307	67	0.30	293.8	316.5	296.1
307	134	0.30	293.7	316.0	295.0
307	134	0.30	294.7	316.9	295.9
307	202	0.30	294.0	315.9	294.8
307	202	0.30	295.0	316.8	295.8
307	269	0.30	293.9	315.5	294.6
307	269	0.30	295.5	317.0	296.1
307	331	0.30	294.6	315.8	295.2
307	331	0.30	295.0	316.1	295.6
307	202	0.30	294.0	315.9	294.8
307	202	0.30	295.0	316.8	295.8
500	202	0.30	294.8	327.3	296.2
500	202	0.30	295.9	328.3	297.3
614	202	0.30	295.5	333.7	297.3
614	202	0.30	296.1	334.3	297.9
719	202	0.30	295.9	339.2	298.0
719	202	0.30	295.9	339.2	298.0
800	202	0.30	296.1	344.1	298.5

### III-2 Heating system with transpired plate facade

Experiment results for heating system with transpired plate

$I, \text{Wm}^{-2}$	$G, \text{kg/s-m}^2$	$v_f, \text{m/s}$	$D, \text{m}$	$T_a, \text{K}$	$T_p, \text{K}$	$T_i, \text{K}$	$T_f, \text{K}$	$T_w, \text{K}$	$T_r, \text{K}$
223	0.051	0.30	0.20	299.3	305.7	301.1	301.7	300.5	299.6
307	0.049	0.29	0.20	300.2	309.1	302.6	303.8	302.1	300.9
307	0.054	0.28	0.20	300.7	309.6	303.5	304.5	303.2	301.6
307	0.052	0.26	0.20	301.3	310.3	303.7	304.9	303.3	302.1
307	0.050	0.28	0.20	301.9	310.3	304.4	305.4	304.3	302.2
385	0.047	0.32	0.20	299.6	311.3	302.5	304.4	301.9	300.2
385	0.052	0.27	0.20	300.0	311.5	304.0	305.4	304.0	301.2
500	0.052	0.30	0.20	300.5	315.4	305.3	307.5	305.6	301.9
500	0.049	0.29	0.20	300.2	315.1	304.6	306.9	304.6	301.1
614	0.062	0.33	0.20	299.2	315.4	304.3	306.4	304.2	301.4
614	0.058	0.33	0.20	299.8	317.1	305.5	307.9	306.0	301.7
614	0.047	0.30	0.20	300.1	318.1	306.3	309.1	307.2	301.3
614	0.052	0.31	0.20	299.5	317.3	305.0	307.6	305.0	301.1
614	0.062	0.31	0.20	300.6	317.3	306.0	308.3	306.5	303.0
614	0.047	0.33	0.20	301.2	319.9	306.9	310.1	306.9	302.5
719	0.049	0.32	0.20	300.0	321.5	306.2	310.1	307.0	301.7
719	0.052	0.32	0.20	300.5	321.5	306.8	310.5	307.6	301.9
719	0.049	0.32	0.20	301.1	322.5	307.5	311.4	308.6	302.6
719	0.049	0.32	0.20	301.1	322.4	308.1	311.8	309.7	303.0
820	0.053	0.37	0.20	299.6	324.2	306.3	311.3	308.2	301.9
820	0.048	0.37	0.20	299.6	324.9	306.9	312.0	309.3	301.8
223	0.039	0.18	0.25	301.0	308.5	303.1	304.4	302.8	301.6
223	0.050	0.27	0.25	299.6	306.0	301.1	302.0	300.8	300.2
223	0.048	0.13	0.25	301.3	307.7	303.3	304.0	303.1	301.9
307	0.040	0.15	0.25	301.8	311.8	304.6	306.5	304.4	302.2
307	0.052	0.20	0.25	300.2	308.9	303.1	304.2	303.1	301.0
385	0.040	0.20	0.25	301.7	315.3	306.2	308.6	305.9	302.6
385	0.050	0.20	0.25	301.5	313.3	305.1	307.1	305.5	302.1
500	0.040	0.19	0.25	301.8	319.3	307.8	311.1	307.7	302.9
500	0.050	0.17	0.25	300.8	316.1	305.7	308.2	306.1	301.8
614	0.062	0.22	0.25	300.9	317.6	306.6	309.1	307.1	303.6
614	0.052	0.18	0.25	301.4	319.5	307.8	310.8	308.7	303.1
614	0.046	0.15	0.25	301.9	320.4	307.6	311.3	307.5	303.6
614	0.039	0.17	0.25	301.4	321.7	308.1	312.5	308.6	303.0
719	0.039	0.20	0.25	300.9	326.7	307.7	313.8	308.6	303.6
719	0.039	0.20	0.25	301.0	324.9	309.1	314.6	310.6	303.2
719	0.051	0.22	0.25	299.2	320.3	305.7	310.0	306.0	300.9
820	0.046	0.18	0.25	300.7	326.3	308.0	314.0	310.1	303.1
820	0.038	0.24	0.25	300.4	328.5	308.0	315.3	309.5	303.3
820	0.053	0.29	0.25	299.1	323.9	305.6	311.2	307.0	301.7
223	0.039	0.17	0.30	300.2	307.3	302.2	303.4	301.5	300.8
230	0.040	0.18	0.30	299.8	306.7	301.9	302.9	301.4	300.3
230	0.042	0.20	0.30	299.1	306.1	301.2	302.2	300.3	299.7
307	0.039	0.14	0.30	298.9	308.6	301.9	303.5	300.8	299.3
385	0.037	0.16	0.30	299.3	312.8	303.8	306.2	302.7	300.3
500	0.038	0.17	0.30	301.3	318.1	307.5	310.5	307.5	302.4

614	0.037	0.19	0.30	300.3	319.1	306.3	310.4	305.7	302.0
614	0.051	0.17	0.30	300.4	318.0	307.3	309.8	308.1	302.1
614	0.043	0.14	0.30	299.5	318.0	306.1	309.3	306.4	301.1
614	0.061	0.20	0.30	299.9	315.6	305.0	307.1	304.7	302.2
614	0.056	0.19	0.30	299.8	316.6	305.9	308.2	306.3	302.2
614	0.051	0.18	0.30	300.0	317.4	306.4	308.9	307.0	301.7
719	0.035	0.20	0.30	299.9	323.5	308.4	313.5	309.0	301.3
820	0.033	0.18	0.30	300.1	327.6	308.1	315.0	308.5	303.1
820	0.036	0.24	0.30	299.0	327.0	308.3	314.9	309.1	302.1
820	0.036	0.15	0.30	299.7	327.8	309.2	315.9	310.5	302.9
820	0.037	0.19	0.30	298.9	324.5	307.7	314.7	308.1	301.8

Simulation results for heating system with transpired plate by present model

$I, \text{Wm}^{-2}$	$G, \text{kg/s-m}^2$	$v_f, \text{m/s}$	$D, \text{m}$	$T_a, \text{K}$	$T_p, \text{K}$	$T_i, \text{K}$	$T_f, \text{K}$
307	0.049	0.29	0.20	300.2	309.1	303.0	304.0
307	0.054	0.28	0.20	300.7	309.2	303.4	304.3
307	0.052	0.26	0.20	301.3	310.4	304.2	305.1
307	0.050	0.28	0.20	301.9	310.8	304.7	305.7
385	0.047	0.32	0.20	299.6	310.5	303.0	304.5
385	0.052	0.27	0.20	300.0	311.2	303.6	190.9
500	0.052	0.30	0.20	300.5	314.3	304.9	306.5
500	0.049	0.29	0.20	300.2	314.6	304.8	306.4
614	0.062	0.33	0.20	299.2	313.6	304.0	305.6
614	0.058	0.33	0.20	299.8	315.0	304.7	306.5
614	0.047	0.30	0.20	300.1	318.0	305.7	307.9
614	0.052	0.31	0.20	299.5	316.2	304.8	306.8
614	0.062	0.31	0.20	300.6	315.5	305.5	307.0
614	0.047	0.33	0.20	301.2	318.3	306.5	308.9
719	0.049	0.32	0.20	300.0	319.8	306.2	308.8
719	0.052	0.32	0.20	300.5	319.8	306.6	309.0
719	0.049	0.32	0.20	301.1	320.9	307.3	309.9
719	0.049	0.32	0.20	301.1	320.9	307.3	309.9
820	0.053	0.37	0.20	299.6	319.7	306.0	309.0
820	0.048	0.37	0.20	299.6	320.8	306.2	309.6
307	0.040	0.15	0.25	301.8	312.1	304.9	306.2
307	0.052	0.20	0.25	300.2	308.2	302.7	303.8
385	0.040	0.20	0.25	301.7	313.2	305.2	307.2
385	0.050	0.20	0.25	301.5	311.6	304.7	306.1
500	0.040	0.19	0.25	301.8	317.1	306.4	308.9
500	0.050	0.17	0.25	300.8	314.8	305.2	306.9
614	0.062	0.22	0.25	300.9	314.6	305.5	307.2
614	0.052	0.18	0.25	301.4	318.0	306.7	308.7
614	0.046	0.15	0.25	301.9	320.9	307.8	309.9
614	0.039	0.17	0.25	301.4	321.2	307.3	310.3
719	0.039	0.20	0.25	300.9	322.6	307.4	311.2
719	0.039	0.20	0.25	301.0	321.8	306.6	310.3
719	0.051	0.22	0.25	299.2	317.3	304.9	307.7
820	0.046	0.18	0.25	300.7	324.3	308.0	311.2
820	0.038	0.24	0.25	300.4	323.7	307.3	312.2

820	0.053	0.29	0.25	299.1	317.1	304.9	308.3
307	0.039	0.14	0.30	298.9	309.6	302.1	303.4
385	0.037	0.16	0.30	299.3	312.4	303.2	305.2
500	0.038	0.17	0.30	301.3	317.7	306.2	308.7
614	0.037	0.19	0.30	300.3	319.9	306.1	309.5
614	0.051	0.17	0.30	300.4	317.5	305.8	307.8
614	0.043	0.14	0.30	299.5	319.8	305.7	308.0
614	0.061	0.20	0.30	299.9	314.3	304.6	306.3
614	0.056	0.19	0.30	299.8	315.2	304.8	306.7
614	0.051	0.18	0.30	300.0	316.7	305.3	307.4
719	0.035	0.20	0.30	299.9	323.0	306.6	311.0
820	0.033	0.18	0.30	300.1	328.0	308.1	313.1
820	0.036	0.24	0.30	299.0	323.0	306.0	311.3
820	0.036	0.15	0.30	299.7	328.6	308.2	312.2
820	0.037	0.19	0.30	298.9	324.9	306.6	311.1

Simulation results for heating system with transpired plate by Kutscher's model

<b>I, Wm<sup>-2</sup></b>	<b>G, kg/s-m<sup>2</sup></b>	<b>v<sub>f</sub>, m/s</b>	<b>D, m</b>	<b>T<sub>av</sub>, K</b>	<b>T<sub>pr</sub>, K</b>	<b>T<sub>out</sub>, K</b>
223	0.051	0.30	0.20	299.3	305.3	302.8
307	0.049	0.29	0.20	300.2	308.5	305.1
307	0.054	0.28	0.20	300.7	308.6	305.2
307	0.052	0.26	0.20	301.3	309.4	306.0
307	0.050	0.28	0.20	301.9	310.1	306.7
385	0.047	0.32	0.20	299.6	310.2	306.0
385	0.052	0.27	0.20	300.0	310.1	305.9
500	0.052	0.30	0.20	300.5	313.6	308.1
500	0.049	0.29	0.20	300.2	313.6	308.1
614	0.062	0.33	0.20	299.2	313.8	307.1
614	0.058	0.33	0.20	299.8	315.0	308.3
614	0.047	0.30	0.20	300.1	317.0	310.2
614	0.052	0.31	0.20	299.5	315.6	308.8
614	0.062	0.31	0.20	300.6	315.2	308.5
614	0.047	0.33	0.20	301.2	318.1	311.4
719	0.049	0.32	0.20	300.0	319.2	311.4
719	0.052	0.32	0.20	300.5	319.3	311.4
719	0.049	0.32	0.20	301.1	320.3	312.5
719	0.049	0.32	0.20	301.1	320.3	312.5
820	0.053	0.37	0.20	299.6	320.7	311.8
820	0.048	0.37	0.20	299.6	321.8	312.8
223	0.039	0.18	0.25	301.0	307.8	305.4
223	0.050	0.27	0.25	299.6	305.6	303.2
223	0.048	0.13	0.25	301.3	307.4	304.9
307	0.040	0.15	0.25	301.8	310.5	307.2
307	0.052	0.20	0.25	300.2	308.3	304.9
385	0.040	0.20	0.25	301.7	313.3	309.1
385	0.050	0.20	0.25	301.5	311.7	307.5
500	0.040	0.19	0.25	301.8	316.8	311.3
500	0.050	0.17	0.25	300.8	314.1	308.6
614	0.062	0.22	0.25	300.9	315.5	308.9

614	0.052	0.18	0.25	301.4	317.4	310.8
614	0.046	0.15	0.25	301.9	319.0	312.3
614	0.039	0.17	0.25	301.4	320.0	313.4
719	0.039	0.20	0.25	300.9	323.6	315.9
719	0.039	0.20	0.25	301.0	322.7	315.0
719	0.051	0.22	0.25	299.2	318.2	310.3
820	0.046	0.18	0.25	300.7	323.4	314.5
820	0.038	0.24	0.25	300.4	325.5	316.7
820	0.053	0.29	0.25	299.1	320.2	311.3
223	0.039	0.17	0.30	300.2	307.0	304.6
307	0.039	0.14	0.30	298.9	308.3	304.9
385	0.037	0.16	0.30	299.3	311.5	307.2
500	0.038	0.17	0.30	301.3	316.8	311.3
614	0.037	0.19	0.30	300.3	319.6	312.9
614	0.051	0.17	0.30	300.4	316.7	309.9
614	0.043	0.14	0.30	299.5	317.3	310.6
614	0.061	0.20	0.30	299.9	314.6	308.0
614	0.056	0.19	0.30	299.8	315.2	308.5
614	0.051	0.18	0.30	300.0	316.3	309.5
719	0.035	0.20	0.30	299.9	323.2	315.4
820	0.033	0.18	0.30	300.1	327.0	318.2
820	0.036	0.24	0.30	299.0	325.0	316.1
820	0.036	0.15	0.30	299.7	325.7	316.8
820	0.037	0.19	0.30	298.9	324.5	315.6

### III-3 Cooling systems with flat plate and single plenum

Experiment results for cooling system with flat plate, single plenum and wet sandtile wall

$I, \text{Wm}^{-2}$	$V_{\text{fan}}, \text{m}^3/\text{hr}$	$D, \text{m}$	$\text{RH}_{\text{in}}, \%$	$\text{RH}_{\text{out}}, \%$	$T_{\text{ar}}, \text{K}$	$T_{\text{pr}}, \text{K}$	$T_{\text{fr}}, \text{K}$	$T_{\text{wr}}, \text{K}$
307	331	0.20	33.8	34.0	288.9	313.8	289.5	285.2
307	269	0.20	33.8	39.9	289.4	315.1	289.8	285.7
307	202	0.20	32.9	42.5	289.1	314.2	289.5	286.2
307	134	0.20	31.5	41.7	290.5	317.8	291.0	287.6
307	67	0.20	25.2	29.9	290.3	316.8	291.2	287.3
385	331	0.20	31.8	36.5	291.0	321.4	291.6	287.3
385	269	0.20	29.7	35.0	291.2	322.1	291.7	287.2
385	202	0.20	29.8	37.7	290.4	321.5	290.9	287.1
385	134	0.20	27.6	35.3	290.9	322.9	291.5	287.8
385	67	0.20	28.2	31.3	291.6	322.7	292.8	288.3
500	331	0.20	30.0	34.9	291.7	327.8	292.3	287.6
500	269	0.20	30.9	37.1	291.6	328.0	292.2	288.1
500	202	0.20	25.7	32.5	291.5	327.8	292.4	287.2
500	134	0.20	25.9	30.8	291.6	329.0	292.6	287.9
500	67	0.20	22.8	25.8	292.1	330.4	293.5	288.5
614	331	0.20	33.6	41.0	292.6	333.5	293.4	288.5
614	269	0.20	40.7	49.5	292.7	333.9	293.5	289.5
614	202	0.20	17.4	21.6	291.0	334.4	292.1	286.4
614	134	0.20	37.7	46.2	293.5	336.1	294.4	290.8
614	67	0.20	33.3	33.9	294.4	336.4	296.2	291.8
719	331	0.20	39.1	43.1	293.2	338.2	294.3	289.7
719	269	0.20	38.1	42.3	293.3	338.5	294.6	290.0
719	202	0.20	35.6	42.1	293.7	339.3	294.8	290.5
719	134	0.20	34.2	38.4	294.1	340.4	295.2	291.5
719	67	0.20	30.5	28.3	294.0	340.5	296.4	292.0
820	331	0.20	43.6	46.3	292.6	342.9	293.7	289.9
820	269	0.20	38.5	41.6	292.9	342.9	294.0	289.4
820	202	0.20	31.7	32.7	293.2	340.5	294.5	289.6
820	134	0.20	31.6	32.4	291.8	343.0	293.3	289.4
820	67	0.20	34.6	26.1	293.2	344.6	295.9	291.0

Simulation results for cooling system with flat plate, single plenum and wet sandtile wall

$I, \text{Wm}^{-2}$	$V_{\text{fan}}, \text{m}^3/\text{hr}$	$D, \text{m}$	$\text{RH}_{\text{in}}, \%$	$\text{RH}_{\text{out}}, \%$	$T_{\text{ar}}, \text{K}$	$T_{\text{pr}}, \text{K}$	$T_{\text{fr}}, \text{K}$	$T_{\text{wr}}, \text{K}$
307	331	0.20	33.8	30.4	288.9	309.6	289.5	285.1
307	269	0.20	33.8	32.4	289.4	310.7	290.1	285.5
307	202	0.20	32.9	31.9	289.1	311.1	289.9	285.9
307	134	0.20	31.5	30.7	290.5	313.0	291.6	287.1
307	67	0.20	25.2	25.5	290.3	313.5	292.3	286.8
385	331	0.20	31.8	28.8	291.0	316.0	291.7	286.9
385	269	0.20	29.7	28.7	291.2	316.9	292.0	286.8
385	202	0.20	29.8	28.7	290.4	316.8	291.4	286.7
385	134	0.20	27.6	26.2	290.9	318.0	292.4	287.2
385	67	0.20	28.2	26.3	291.6	319.4	294.1	287.8
500	331	0.20	30.0	28.3	291.7	322.8	292.6	287.0
500	269	0.20	30.9	28.9	291.6	323.4	292.7	287.5

500	202	0.20	25.7	24.2	291.5	324.1	292.8	286.7
500	134	0.20	25.9	23.8	291.6	325.0	293.5	287.4
500	67	0.20	22.8	21.6	292.1	326.4	295.5	287.7
614	331	0.20	33.6	30.9	292.6	329.3	293.7	287.9
614	269	0.20	40.7	35.9	292.7	330.2	294.1	288.9
614	202	0.20	17.4	16.5	291.0	329.6	292.7	285.9
614	134	0.20	37.7	32.8	293.5	332.6	295.9	290.0
614	67	0.20	33.3	26.4	294.4	334.6	298.7	291.0
719	331	0.20	39.1	34.9	293.2	334.9	294.5	289.1
719	269	0.20	38.1	33.2	293.3	335.8	294.9	289.3
719	202	0.20	35.6	30.3	293.7	337.0	295.7	289.8
719	134	0.20	34.2	28.5	294.1	338.3	297.0	290.7
719	67	0.20	30.5	23.5	294.0	339.5	299.1	291.1
820	331	0.20	43.6	37.2	292.6	338.9	294.2	289.3
820	269	0.20	38.5	32.6	292.9	340.2	294.7	288.8
820	202	0.20	31.7	26.8	293.2	341.4	295.5	288.8
820	134	0.20	31.6	25.4	291.8	341.0	295.1	288.7
820	67	0.20	34.6	23.8	293.2	343.8	299.0	290.2

### III-4 Cooling systems with transpired plate and two plenums

Experiment results for cooling system with transpired plate, two plenums and wet sandtile wall

I, Wm <sup>-2</sup>	G, kg/s-m <sup>2</sup>	v <sub>f</sub> , m/s	V <sub>fan</sub> , m <sup>3</sup> /hr	D, m	RH <sub>in</sub> , %	RH <sub>out</sub> , %	T <sub>a</sub> , K	T <sub>s,in</sub> , K	T <sub>w,in</sub> , K	T <sub>p</sub> , K	T <sub>i</sub> , K	T <sub>f</sub> , K	T <sub>w</sub> , K	T <sub>r</sub> , K	T <sub>s</sub> , K
307	0.053	0.18	82	0.25	43.6	30.0	296.7	293.1	284.7	306.2	296.1	298.9	286.2	290.2	292.7
307	0.053	0.17	67	0.25	26.7	20.2	296.8	292.9	284.8	306.5	295.6	298.6	286.2	290.2	292.6
385	0.053	0.17	77	0.25	42.2	26.1	297.7	294.2	285.9	309.6	297.6	301.3	287.2	291.2	293.8
385	0.052	0.15	86	0.25	25.4	16.6	297.6	293.2	284.9	309.8	296.2	300.2	286.2	290.2	292.8
500	0.052	0.16	86	0.25	35.6	19.2	299.5	294.3	286.6	314.5	298.7	303.2	288.0	292.0	294.0
614	0.052	0.22	72	0.25	30.6	14.5	299.1	293.8	286.3	316.8	298.6	304.1	287.6	291.6	293.5
614	0.053	0.18	86	0.25	32.9	14.8	297.8	292.9	286.1	316.7	297.7	303.6	287.3	291.3	292.7
614	0.052	0.23	139	0.25	29.3	13.7	297.4	292.8	285.2	317.1	297.7	303.7	287.0	291.0	292.6
614	0.053	0.22	202	0.25	28.7	13.2	296.5	291.9	285.6	316.7	296.9	303.2	286.6	290.6	291.7
614	0.052	0.21	274	0.25	28.5	13.6	297.7	293.4	286.4	317.3	297.6	304.4	287.3	291.3	293.2
614	0.053	0.21	317	0.25	25.7	12.6	297.5	292.6	284.4	316.5	296.9	302.5	286.1	290.1	292.3
614	0.052	0.28	331	0.25	25.9	12.8	297.1	293.1	285.8	317.3	297.4	304.1	287.2	291.2	292.9
719	0.053	0.22	110	0.25	42.5	17.6	296.1	293.4	286.5	321.2	299.3	306.3	287.8	291.8	293.1
719	0.052	0.16	82	0.25	27.9	12.7	298.0	293.4	286.1	321.6	298.5	305.6	287.2	291.2	293.1
820	0.053	0.24	77	0.25	43.3	15.4	296.9	293.5	286.5	325.5	299.6	308.0	287.7	291.7	293.3
820	0.054	0.23	82	0.25	25.1	10.4	296.2	292.6	285.2	326.1	298.3	306.4	286.5	290.5	292.3

Simulation results for cooling system with transpired plate, two plenums and wet sandtile wall

I, Wm <sup>-2</sup>	G, kg/s-m <sup>2</sup>	v <sub>f</sub> , m/s	V <sub>fan</sub> , m <sup>3</sup> /hr	D, m	RH <sub>in</sub> , %	RH <sub>out</sub> , %	T <sub>a</sub> , K	T <sub>s,in</sub> , K	T <sub>w,in</sub> , K	T <sub>p</sub> , K	T <sub>i</sub> , K	T <sub>f</sub> , K	T <sub>w</sub> , K	T <sub>r</sub> , K	T <sub>s</sub> , K
307	0.053	0.18	82	0.25	43.6	39.7	296.7	293.1	284.7	304.7	299.3	300.0	285.2	285.8	292.8
307	0.053	0.17	67	0.25	26.7	24.9	296.8	292.9	284.8	304.9	299.4	300.2	285.0	285.6	292.2
385	0.053	0.17	77	0.25	42.2	37.7	297.7	294.2	285.9	308.1	301.0	302.0	286.4	287.0	293.9
385	0.052	0.15	86	0.25	25.4	23.2	297.6	293.2	284.9	308.6	301.1	302.0	285.2	285.8	292.9
500	0.052	0.16	86	0.25	35.6	31.0	299.5	294.3	286.6	313.3	303.9	305.1	287.0	287.1	294.1
614	0.052	0.22	72	0.25	30.6	24.7	299.1	293.8	286.3	314.1	303.9	305.8	286.7	287.3	293.5

614	0.053	0.18	86	0.25	32.9	27.4	297.8	292.9	286.1	313.8	302.9	304.6	286.6	287.4	292.7
614	0.052	0.23	139	0.25	29.3	23.3	297.4	292.8	285.2	312.3	302.1	304.3	285.7	286.8	292.6
614	0.053	0.22	202	0.25	28.7	23.1	296.5	291.9	285.6	311.4	301.3	303.3	286.0	287.0	291.8
614	0.052	0.21	274	0.25	28.5	23.1	297.7	293.4	286.4	313.0	302.6	304.5	286.8	288.0	293.3
614	0.053	0.21	317	0.25	25.7	20.9	297.5	292.6	284.4	312.7	302.4	304.3	284.8	285.4	292.3
614	0.052	0.28	331	0.25	25.9	20.2	297.1	293.1	285.8	310.8	301.4	303.8	286.2	287.5	292.9
719	0.053	0.22	110	0.25	42.5	32.5	296.1	293.4	286.5	313.6	301.7	304.1	287.0	287.5	293.2
719	0.052	0.16	82	0.25	27.9	22.8	298.0	293.4	286.1	317.8	304.3	306.2	286.5	287.0	293.2
820	0.053	0.24	77	0.25	43.3	31.8	296.9	293.5	286.5	315.9	303.0	305.7	287.1	287.6	293.3
820	0.054	0.23	82	0.25	25.1	18.8	296.2	292.6	285.2	315.6	302.4	305.1	285.5	286.1	292.3

Experiment results for system with transpired plate, two plenums and dry sandtile wall

$I, \text{Wm}^{-2}$	$G, \text{kg/s-m}^2$	$v_f, \text{m/s}$	$V_{fan}, \text{m}^3/\text{hr}$	$D, \text{m}$	$RH_{in}, \%$	$RH_{out}, \%$	$T_a, \text{K}$	$T_{s,in}, \text{K}$	$T_p, \text{K}$	$T_i, \text{K}$	$T_f, \text{K}$	$T_w, \text{K}$	$T_r, \text{K}$	$T_s, \text{K}$
307	0.054	0.11	77	0.25	24.7	13.5	296.3	293.1	307.6	297.9	301.5	299.9	298.1	293.2
385	0.053	0.12	82	0.25	22.8	11.5	296.7	293.1	310.9	298.1	302.3	298.0	296.5	293.2
500	0.051	0.12	77	0.25	21.1	10.1	297.5	294.6	316.4	301.0	305.6	300.9	298.5	294.7
614	0.052	0.14	86	0.25	25.1	9.6	297.8	293.3	318.4	299.6	305.7	297.9	296.0	293.3
614	0.051	0.16	139	0.25	23.4	8.4	297.4	294.1	319.0	301.5	307.4	302.1	299.1	294.1
614	0.052	0.17	211	0.25	22.2	8.7	297.2	294.1	319.7	300.6	305.8	300.4	297.6	294.1
614	0.052	0.14	289	0.25	22.1	8.4	297.0	294.0	319.6	300.6	306.8	300.9	297.6	294.0
614	0.052	0.14	321	0.25	21.6	8.2	297.4	294.4	320.2	301.3	307.8	302.4	298.7	294.5
719	0.051	0.16	77	0.25	22.3	7.9	298.1	294.5	323.6	301.2	308.0	299.9	297.3	294.6
820	0.053	0.19	82	0.25	23.8	6.8	297.9	294.8	329.7	302.5	311.3	303.5	299.5	295.1

Simulation results for system with transpired plate, two plenums and dry sandtile wall

<b>I, Wm<sup>-2</sup></b>	<b>G, kg/s-m<sup>2</sup></b>	<b>v<sub>f</sub>, m/s</b>	<b>V<sub>fan</sub>, m<sup>3</sup>/hr</b>	<b>D, m</b>	<b>RH<sub>in</sub>, %</b>	<b>T<sub>a</sub>, K</b>	<b>T<sub>s,in</sub>, K</b>	<b>T<sub>p</sub>, K</b>	<b>T<sub>i</sub>,K</b>	<b>T<sub>f</sub>, K</b>	<b>T<sub>w</sub>, K</b>	<b>T<sub>r</sub>, K</b>	<b>T<sub>s</sub>, K</b>
307	0.054	0.11	77	0.25	24.7	296.3	293.1	304.9	299.3	300.3	297.9	297.6	293.2
385	0.053	0.12	82	0.25	22.8	296.7	293.1	308.2	301.0	302.2	299.7	299.3	294.4
500	0.051	0.12	77	0.25	21.1	297.5	294.6	311.9	303.4	305.2	301.8	301.3	294.5
614	0.052	0.14	86	0.25	25.1	297.8	293.3	314.3	303.9	306.1	302.4	301.8	294.1
614	0.051	0.16	139	0.25	23.4	297.4	294.1	313.9	303.0	304.8	300.7	300.1	293.1
614	0.052	0.17	211	0.25	22.2	297.2	294.1	312.5	302.2	304.5	300.1	299.5	292.9
614	0.052	0.14	289	0.25	22.1	297.0	294.0	311.6	301.3	303.5	298.8	298.1	292.0
614	0.052	0.14	321	0.25	21.6	297.4	294.4	311.0	301.5	304.1	299.6	298.9	293.2
719	0.051	0.16	77	0.25	22.3	298.1	294.5	318.0	304.4	306.4	302.4	301.8	293.7
820	0.053	0.19	82	0.25	23.8	297.9	294.8	315.8	302.5	305.4	301.5	300.9	292.9

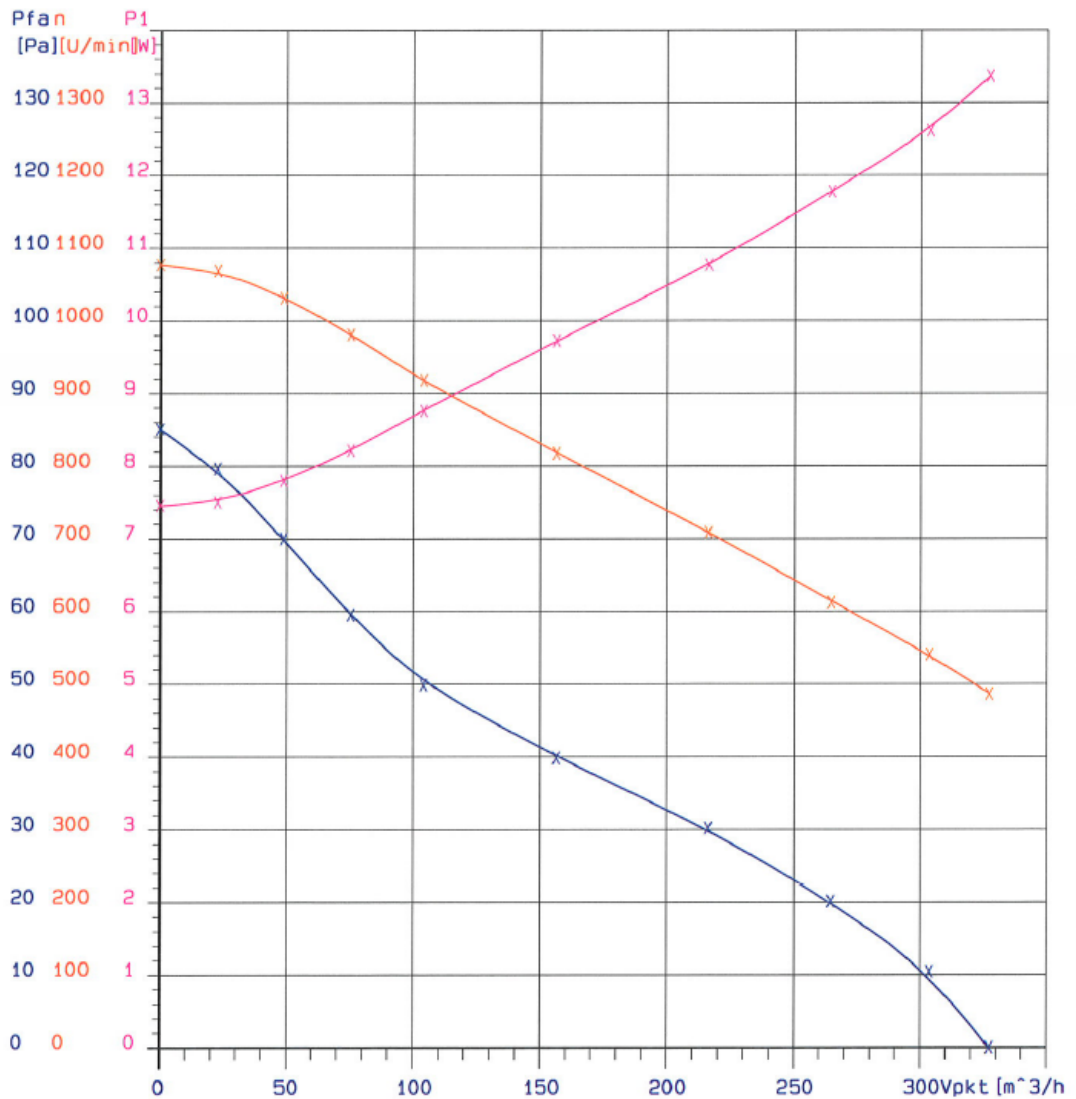
## Appendix IV Power consumption of fan

ebm-papst Mulfingen GmbH & Co. KG

Bachmühle 2 D-74673 Mulfingen Phone +49 (0) 7938 /81-0 Fax +49 (0) 7938/81-110 /26.11.2007

### Luftleistungskennlinien

TYP	MESSNR.	U [V]
D1G146CC07-07 01A	11545	24



## **Appendix V: List of publications**

1. Chan, H-Y, Riffat, S.B., Zhu, J. 2010a. "Review of passive solar heating and cooling technologies." *Renewable and Sustainable Energy Reviews* 14(2): 781-789.
2. Chan, H.Y, Riffat, S., Zhu, J. 2009. "Solar facades for heating and cooling in buildings." In SET2009 - 8th International Conference on Sustainable Energy Technologies. Aachen, Germany.
3. Chan, H.Y, Riffat, S., Zhu, J. 2010b. "An innovative solar façade for heating and cooling in buildings." In SET2010 - 9th International Conference on Sustainable Energy Technologies. Shanghai, China.
4. Chan, H.Y, Riffat, S., Zhu, J. 2010c. "Solar heating facade." In 10th REHVA World Congress Clima 2010: sustainable energy use in buildings Antalya, Turkey.
5. Chan, H.Y, Riffat, S., Zhu, J. 2011. "Experimental performance of unglazed transpired solar collector for air heating." In World Renewable Energy Congress - Sweden. Linköping, Sweden.